

12
USAAVRADCOM-TR-82-D-42

NADC-82268-60



FAA-AM-83-3



U.S. Department of Transportation
Federal Aviation Administration

DESIGN AND TEST CRITERIA FOR INCREASED ENERGY-ABSORBING SEAT EFFECTIVENESS

Joseph W. Coltman
SIMULA, Inc.
2223 S. 48th Street
Tempe, Ariz. 85282

March 1983

Final Report for Period June 1979 - February 1983

Approved for public release;
distribution unlimited.

DTIC
MAY 12 1983

A

Prepared for

APPLIED TECHNOLOGY LABORATORY

U. S. ARMY RESEARCH AND TECHNOLOGY LABORATORIES (AVRADCOM)

Fort Eustis, Va. 23604

00 05 12 004

DTIC FILE COPY

ADA128015

APPLIED TECHNOLOGY LABORATORY POSITION STATEMENT

This report documents one of several efforts the Applied Technology Laboratory, US Army Research and Technology Laboratories (AVRADCOM) has initiated jointly with the Naval Air Development Center (NADC), the FAA Civil Aeromedical Institute (CAMI) and the Air Force Aerospace Medical Research Laboratory (AFAMRL) to define human tolerance levels to vertical crash impact and to optimize crashworthy crewseat design. Results of this program represent a significant advance in the understanding of dynamic/structural/anatomical interactions which affect occupant injury in severe but survivable crashes (over 75 percent of all Army helicopter mishaps are survivable). These findings will be integrated with those of ongoing and future efforts in human tolerance definition and crashworthy seating design with the end objective being a more precise set of design and qualification criteria leading to less costly and more weight-efficient crashworthy seats.

Mr. Kent F. Smith of the Aeronautical Systems Division served as project engineer for this effort.

DISCLAIMERS

The findings in this report are not to be construed as an official Department of the Army position unless so designated by other authorized documents.

When Government drawings, specifications, or other data are used for any purpose other than in connection with a definitely related Government procurement operation, the United States Government thereby incurs no responsibility nor any obligation whatsoever; and the fact that the Government may have formulated, furnished, or in any way supplied the said drawings, specifications, or other data is not to be regarded by implication or otherwise as in any manner licensing the holder or any other person or corporation, or conveying any rights or permission, to manufacture, use, or sell any patented invention that may in any way be related thereto.

Trade names cited in this report do not constitute an official endorsement or approval of the use of such commercial hardware or software.

DISPOSITION INSTRUCTIONS

Destroy this report when no longer needed. Do not return it to the originator.

UNCLASSIFIED

SECURITY CLASSIFICATION OF THIS PAGE (When Data Entered)

REPORT DOCUMENTATION PAGE		READ INSTRUCTIONS BEFORE COMPLETING FORM
1. REPORT NUMBER USAAVRADCOM TR 82-D-42.	2. GOVT ACCESSION NO. AD-A128015	3. RECIPIENT'S CATALOG NUMBER
4. TITLE (and Subtitle) DESIGN AND TEST CRITERIA FOR INCREASED ENERGY-ABSORBING SEAT EFFECTIVENESS		5. TYPE OF REPORT & PERIOD COVERED FINAL REPORT June 1979 - February 1983
		6. PERFORMING ORG. REPORT NUMBER TR-82411 ✓
7. AUTHOR(s) Joseph W. Coltman		8. CONTRACT OR GRANT NUMBER(s) DAAK51-79-C-0026
9. PERFORMING ORGANIZATION NAME AND ADDRESS Simula Inc. 222 S. 48th Street Tempe, Arizona 85282		10. PROGRAM ELEMENT, PROJECT, TASK AREA & WORK UNIT NUMBERS 612209 1L162209AH76 00 271EK
11. CONTROLLING OFFICE NAME AND ADDRESS Applied Technology Laboratory, U.S. Army Research and Technology Laboratories (AVRADCOM) Fort Eustis, Virginia 23604		12. REPORT DATE March 1983
14. MONITORING AGENCY NAME & ADDRESS (if different from Controlling Office)		13. NUMBER OF PAGES 229
		15. SECURITY CLASS. (of this report) Unclassified
		15a. DECLASSIFICATION/DOWNGRADING SCHEDULE
16. DISTRIBUTION STATEMENT (of this Report) Approved for public release; distribution unlimited.		
17. DISTRIBUTION STATEMENT (of the abstract entered in Block 20, if different from Report)		
18. SUPPLEMENTARY NOTES		
19. KEY WORDS (Continue on reverse side if necessary and identify by block number) Aircraft Restraint Systems Crashworthiness Seats Design Criteria Energy Absorption		
20. ABSTRACT (Continue on reverse side if necessary and identify by block number) This report documents a research effort to increase the effectiveness of energy-absorbing seats, through improved design and qualification test criteria. Contained herein are descriptions of a parametric test program and analysis of seat and occupant response sensitivity to design and test variables. Recommendations for improving military specifications and criteria, such as contained in MIL-S-58095(AV), MIL-STD-1290(AV) and USARTL TP-79-22A, to aid in procurement of optimum systems are also provided.		

DD FORM 10/73 1473 EDITION OF 1 NOV 65 IS OBSOLETE

UNCLASSIFIED

SECURITY CLASSIFICATION OF THIS PAGE (When Data Entered)

PREFACE

This report was prepared by Simula Inc. under Contract DAAK51-79-C-0026 for the Safety and Survivability Technical Area of the Applied Technology Laboratory, U.S. Army Research and Technology Laboratories (AVRADCOM), Fort Eustis, Virginia. Mr. Kent Smith of ATL has acted as the Technical Monitor. When the program was initiated in 1979, Mr. George T. Singley III, then of ATL, served in that capacity.

The Program Manager for the Naval Air Development Center contribution to the program has been Mr. Mark Katzeff of the Aircraft and Crew Systems Technology Directorate. Data acquisition and reduction at NADC was conducted under the direction of Mr. Leon Domzalski of the same Directorate. The Federal Aviation Administration effort was managed by Mr. Richard F. Chandler, Chief of the Protection and Survival Laboratory, Civil Aeromedical Institute.

This report has been prepared by Mr. Joseph W. Coltman of Simula Inc., with contributions from Dr. David H. Laananen and Mr. Stanley P. Desjardins.



SEARCHED	INDEXED
SERIALIZED	FILED
APR 1980	
FBI - MEMPHIS	
[Handwritten signature]	

TABLE OF CONTENTS

	<u>Page</u>
PREFACE.	3
LIST OF ILLUSTRATIONS.	8
LIST OF TABLES	14
1.0 INTRODUCTION.	17
2.0 HUMAN TOLERANCE TO ACCELERATIVE LOADING	22
2.1 HUMAN TOLERANCE INVESTIGATIONS	22
2.2 TOLERANCE-BASED CRITERIA FOR SEATS	25
2.3 SEAT/OCCUPANT DYNAMIC RESPONSE	29
3.0 PARAMETRIC STUDY.	32
3.1 VARIABLES EXAMINED	32
3.1.1 Impact Conditions	33
3.1.2 Occupant Characteristics.	33
3.1.3 Seat Design Parameters.	34
3.2 TEST FACILITIES.	36
3.2.1 FAA Civil Aeromedical Institute (CAMI).	36
3.2.2 Naval Air Development Center (NADC)	36
3.2.3 Simula Inc.	36
3.2.4 Wayne State University (WSU).	36
3.3 PARAMETRIC TEST MATRIX	43
3.4 CADAVER TEST PROGRAM	43
3.5 MODIFIED ANTHROPOMORPHIC DUMMY PROGRAM	48
4.0 EQUIPMENT AND TEST PROCEDURES	55
4.1 EQUIPMENT - SEATS.	55
4.1.1 Rigid Seat.	55
4.1.2 Energy-Absorbing Helicopter Seat.	55
4.2 ANTHROPOMORPHIC DUMMIES.	62
4.3 ANALYSIS OF ACCELERATION PULSE	63

TABLE OF CONTENTS (CONTD)

	<u>Page</u>
4.4 STANDARDIZED TEST PROCEDURES	65
4.4.1 Seat Orientation.	65
4.4.2 Seat Preparation.	68
4.4.3 Dummy Positioning	68
4.5 INSTRUMENTATION.	69
5.0 ANALYTICAL METHODS.	72
5.1 CURRENT CRITERION.	72
5.2 PEAK ACCELERATION.	74
5.3 COMPRESSION OF BODY SEGMENTS	75
5.4 DYNAMIC RESPONSE INDEX	75
5.5 INSTRUMENTED ANTHROPOMORPHIC DUMMY	77
5.6 SEAT/OCCUPANT SIMULATION	79
5.7 LINEAR REGRESSION ANALYSIS	95
6.0 RESULTS OF SENSITIVITY ANALYSIS	96
6.1 SENSITIVITY ANALYSES FOR EXPERIMENTAL TEST SERIES	96
6.1.1 Peak Input Acceleration Series	97
6.1.2 Velocity Change Series	98
6.1.3 Rate of Onset Series	106
6.1.4 Energy Absorber Limit-Load Series.	112
6.1.5 Test Facility Impact Conditions.	117
6.1.6 Dummy Type Series.	125
6.1.7 Dummy Percentile Series.	126
6.1.8 Cadavers Versus Anthropomorphic Dummies.	129
6.1.9 Seat Orientation Series.	133
6.1.10 Ramped Energy Absorber Series.	134
6.1.11 Movable Seat Weight Series	136
6.1.12 Seat Frame Spring Rate Series.	141
6.1.13 Seat Cushion Stiffness Series.	142
6.2 ADDITIONAL PERFORMANCE VARIABLES	144
6.2.1 Dummy Performance Degradation	147
6.2.2 Footrest Location and Angle	148
6.2.3 Landing Gear Acceleration Ramp.	150
6.2.4 Test Orientation to Gravity Vector.	152

TABLE OF CONTENTS (CONTD)

	<u>Page</u>
6.2.5 Tolerances on Input Deceleration Pulse Allowed by MIL-S-58095(AV)	154
6.2.6 Method of Transducer Calibration	155
7.0 DISCUSSION OF RESULTS	159
7.1 INPUT ACCELERATION PULSE.	159
7.2 PERFORMANCE CRITERION	159
7.3 SEAT DESIGN PARAMETERS.	160
7.4 TESTING PROCEDURES.	161
8.0 CONCLUSIONS.	163
9.0 RECOMMENDATIONS.	164
9.1 FOLLOW-ON RESEARCH.	164
9.1.1 Energy Absorber Limit-Load Threshold . .	164
9.1.2 Standardized Test Dummy.	164
9.1.3 Refinement of Qualification Test Methods.	165
9.2 SUGGESTED MODIFICATIONS TO CURRENT ENERGY- ABSORBING SEAT SPECIFICATIONS	165
10.0 REFERENCES.	167
APPENDIXES	
A - CAMI TEST A81-121.	170
B - CAMI TEST A81-122.	179
C - CAMI BASELINE TEST A80-053	190
D - NADC BASELINE TEST N-189	201
E - SIMULA BASELINE TEST SEAC-1.	210
F - WAYNE STATE UNIVERSITY TEST 159.	219

LIST OF ILLUSTRATIONS

<u>Figure</u>		<u>Page</u>
1	Overall program elements leading to improved seat design and test criteria.	20
2	Duration and magnitude of spineward acceleration endured by various subjects	23
3	Duration and magnitude of headward acceleration endured by various subjects.	24
4	Maximum acceptable vertical seat acceleration	27
5	Typical response of seat pan, dummy chest, and dummy pelvis to vertical crash loading . .	28
6	Spring-mass representation of seat-occupant system	30
7	Triangular deceleration pulse describing the nominal test condition	35
8	CAMI sled.	37
9	CAMI wire-bending decelerator mechanism. . . .	38
10	Typical baseline deceleration pulses for the four test facilities	39
11	NADC drop tower.	40
12	NADC decelerating mechanism.	41
13	Drop tower used in Simula tests.	42
14	Part 572 pelvic segment with lumbar spine and load cell assembly	52
15	CAMI rigid seat (with VIP-95 dummy in place).	56
16	UH-60A crewseat assembly	57
17	Inverted-tube energy absorber.	59
18	Nominal load-stroke characteristics of ramped energy absorbers used in parametric test program.	60
19	Aircrew restraint system	61

LIST OF ILLUSTRATIONS (CONTD)

<u>Figure</u>		<u>Page</u>
20	Rigid block in Black Hawk crewseat	64
21	Graphic approximation example for rate of onset	65
22	Vertical test, drop tower configuration. . . .	66
23	Vertical test, horizontal sled configuration (CAMI)	67
24	Tensiometer placement on occupant restraint system	70
25	Vertical component of seat pan acceleration measured in two similar tests.	73
26	Seat pan vertical acceleration measured in a qualification test of a production energy- absorbing seat	74
27	Spinal-injury model.	76
28	Probability of spinal injury estimated from laboratory data compared to operational experience	78
29	Eleven-segment (symmetric) occupant model.	80
30	Generalized coordinates for symmetric occupant model	81
31	SOM-LA input properties for Black Hawk seat cushion.	82
32	SOM-LA input properties for polyester restraint system webbing	83
33	Actual sled deceleration pulse for CAMI test A81-124	84
34	Approximate pulse input for SOM-LA simulation of test A81-124	84
35	CAMI test A81-124, dummy pelvis z-acceleration	85
36	CAMI test A81-124, dummy chest z-acceleration	86

LIST OF ILLUSTRATIONS (CONTD)

<u>Figure</u>		<u>Page</u>
37	CAMI test A81-124, dummy head z-acceleration	87
38	CAMI test A81-124, seat z-acceleration	88
39	CAMI test A81-124, seat stroke	89
40	CAMI test A81-124, energy absorber force	90
41	CAMI test A81-124, footrest x-force.	91
42	CAMI test A81-124, footrest z-force.	92
43	CAMI test A81-124, lumbar spine axial load	93
44	CAMI test A81-124, lumbar spine moment	94
45	Rigid seat series parametric test reference.	96
46	Energy-absorbing seat series parametric test reference	97
47	Input acceleration pulses for peak acceleration series.	98
48	Peak input acceleration series, maximum seat stroke.	100
49	Peak input acceleration series, maximum seat pan z-axis acceleration	100
50	Seat pan z-axis acceleration measured in peak input acceleration series	101
51	Pelvic z-axis acceleration measured in peak input acceleration series	102
52	Peak input acceleration series, maximum pelvic z-axis acceleration	103
53	Peak input acceleration series, duration of seat pan z-axis acceleration at 23 G	103
54	Peak input acceleration series, Dynamic Response Index	104
55	Peak input acceleration series, predicted maximum lumbar spine axial load (compression).	104

LIST OF ILLUSTRATIONS (CONTD)

<u>Figure</u>		<u>Page</u>
56	Peak input acceleration series, predicted maximum lumbar spine moment (flexion).	105
57	Comparison of input acceleration pulses for CAMI velocity change series.	105
58	Input velocity change series, maximum seat stroke	107
59	Input velocity change series, maximum seat pan z-axis acceleration.	107
60	Input velocity change series, Dynamic Response Index	108
61	Input velocity change series, predicted maximum lumbar spine axial load (compression).	108
62	Input velocity change series, predicted lumbar spine moment (flexion).	109
63	Rate of onset series, maximum seat stroke. . .	110
64	Comparison of input acceleration pulses for rate of onset series	111
65	Comparison of seat pan z-axis acceleration for rate of onset series	111
66	Energy absorber limit load series, maximum seat stroke.	114
67	Energy absorber limit load series, maximum seat pan z-axis acceleration	114
68	Energy absorber limit load series, Dynamic Response Index	115
69	Energy absorber limit load series, predicted maximum lumbar spine load (compression). . . .	115
70	Energy absorber limit load series, predicted maximum lumbar spine moment (flexion).	116
71	Energy absorber limit load series, maximum lumbar spine moment versus seat stroke	117
72	Nominal baseline input acceleration pulse. . .	118

LIST OF ILLUSTRATIONS (CONTD)

<u>Figure</u>		<u>Page</u>
73	Baseline acceleration pulses for the four test facilities.	119
74	Comparison of pelvis and seat pan z-axis acceleration for baseline test conditions at three facilities.	120
75	Test facility impact condition series, maximum seat stroke.	122
76	Test facility impact condition series, maximum seat pan z-axis acceleration	161
77	Test facility impact condition series, duration of seat pan z-axis acceleration at 23 G.	123
78	Test facility impact condition series, DRI . .	123
79	Test facility impact condition series, maximum lumbar spine axial compressive load	124
80	Test facility impact condition series, maximum lumbar spine y-axis moment (flexion).	124
81	Sled deceleration, rigid seat test A80-026 . .	125
82	Comparison of seat pan force measured in rigid seat tests with three 50th-percentile dummies.	127
83	Seat pan vertical acceleration for a Part 572 dummy and two cadavers measured in vertical mode tests with 14.5-G energy absorbers. . . .	131
84	Seat pan vertical acceleration for a Part 572 dummy and two cadavers measured in combined mode tests with 14.5-G energy absorbers. . . .	131
85	Comparison of normalized seat stroke for cadavers and dummies tested with the Wayne State University input pulse shape	132
86	Seat orientation series, maximum seat stroke	135
87	Comparison of energy absorber force-time histories for ramped E/A series.	136

LIST OF ILLUSTRATIONS (CONTD)

<u>Figure</u>		<u>Page</u>
88	Movable seat weight series, maximum seat stroke.	139
89	Movable seat weight series, maximum seat pan z-axis acceleration.	139
90	Movable seat weight series, Dynamic Response Index.	140
91	Movable seat weight series, maximum lumbar spine axial load (compression)	140
92	Movable seat weight series, maximum lumbar spine moment (flexion)	141
93	Test configuration (for stiffened seat frame test).	142
94	Comparison of response with stiffened seat frame.	143
95	Measurement of seat cushion force-deflection characteristics.	144
96	Load-deflection curves for cushions used in cushion spring rate series	145
97	Comparison of seat pan z-acceleration for various cushion stiffnesses.	146
98	Comparison of pelvic z-acceleration for various cushion stiffnesses.	146
99	Comparison of seat pan z-axis force for dummy performance degradation tests.	147
100	Comparison of pelvic resultant acceleration for dummy performance degradation tests.	148
101	Test conditions for SOM-LA simulations to determine the effect of footrest angle and location	149
102	Input acceleration pulses for simulations examining the effect of landing gear acceleration on seat and occupant response	151
103	Conditions for aircraft orientation simulation	153

LIST OF ILLUSTRATIONS (CONTD)

<u>Figure</u>		<u>Page</u>
104	Dynamic test requirements for Test No. 1 of MIL-S-58095(AV)	155
105	Nominal acceleration pulse for Test No. 1, MIL-S-58095(AV).	156
106	Minimal and maximum rate of onset conditions for simulations of Test No. 1, MIL-S-58095(AV).	156

LIST OF TABLES

<u>Table</u>		
1	Program responsibilities	21
2	Variables examined during parametric study . .	32
3	Test matrix for CAMI rigid seat series	44
4	Dummy identification	45
5	Test matrix for CAMI energy-absorbing seat series.	46
6	Description of cushion types	48
7	Test matrix for NADC energy-absorbing seat series	49
8	Test matrix for Simula energy-absorbing seat series.	49
9	Summary of cadaver test program.	50
10	Test matrix for modified anthropomorphic dummy series.	54
11	Restraint system webbing	62
12	Comparison of test results for peak input acceleration series.	99
13	Comparison of results for velocity change series	106
14	Comparison of results for rate of onset series	110

LIST OF TABLES (CONTD)

<u>Table</u>		<u>Page</u>
15	Comparison of results for energy absorber limit-load series.	113
16	Measured spinal loads and moments for Wayne State University modified dummy test series with combined orientation.	117
17	Comparison of test facility baseline impact conditions	121
18	Average peak accelerations and seat pan loads for rigid seat comparison tests of 50th-percentile dummies (average of three tests). .	126
19	Comparison of response for 95th-percentile dummies in the baseline test configuration . .	127
20	Summary of the effect of anthropomorphic dummy percentile on peak acceleration values	128
21	Summary of the effect of anthropomorphic dummy percentile on spinal loads and moments.	128
22	Comparison of seat and occupant response for dummies and cadavers	130
23	Comparison of seat stroke for cadavers and dummies in the UH-60A crewseat	130
24	Comparison test results for seat orientation series, rigid seat	133
25	Comparison of test results for seat orientation series with energy-absorbing seat	134
26	Effect of seat orientation on lumbar forces and moments.	135
27	Comparison of results for ramped energy absorber load series	137
28	Comparison of test results for seat movable weight series.	138
29	Comparison of test results for stiffened seat frame series	143

LIST OF TABLES (CONTD)

<u>Table</u>		<u>Page</u>
30	Comparison of test results for cushion spring rate series.	145
31	Comparison of SOM-LA simulations to determine the effect of footrest angle and location on seat and occupant response	149
32	Comparison of predicted seat and occupant response for input deceleration pulses with and without landing gear ramp.	152
33	Comparison of seat and occupant response for vertical and horizontal test condition simulations.	153
34	Matrix of SOM-LA simulations for evaluation of sensitivity to test pulse tolerances at 11.5- and 14.5-G energy absorber limit load settings.	157
35	Comparison of predicted seat and occupant response to MIL-S-58095(AV) Dynamic Test 1 with 14.5-G E/A limit load	157
36	Comparison of predicted seat and occupant response to MIL-S-58095(AV) Dynamic Test 1 with 11.5-G E/A limit load	157

1.0 INTRODUCTION

The latest generation of U.S. Army helicopters possesses unprecedented crashworthiness, as pointed out in Reference 1. These aircraft are equipped with many crashworthy features, including seats designed to provide efficient restraint in all loading directions and energy-absorbing stroke in the vertical, or $+G_z$, direction. The seats are designed to comply with existing criteria that were developed and documented in 1971 (References 2, 3, and 4); although these seats are far superior to any prior systems, there are several areas of uncertainty in the design criteria that require additional research to enable further progress to be made in the hardware.

Knowledge concerning human tolerance to $+G_z$ acceleration is extremely limited and constitutes the greatest uncertainty in seat design. In fact, little new information concerning human tolerance to acceleration in this direction has been developed in many years. Although extensive effort has been expended on the critical areas of human head and neck response (U.S. Navy) and the effects of restraint system variables on acceleration loads in the longitudinal and lateral directions (U.S. Air Force), essentially no effort has been directed in this other very critical direction. The need for additional knowledge of $+G_z$ response is affirmed when it is considered that aircraft occupants can withstand the full 95th-percentile survivable crash acceleration conditions in the lateral and longitudinal directions with no energy absorption, only proper restraint (a complex problem when related to the head), but cannot tolerate the 95th-percentile vertical crash pulse without energy absorption.

1. Singley, G. T., III, and Desjardins, S. P., "Crashworthy Helicopter Seats and Occupant Restraint Systems," in Operational Helicopter Aviation Medicine, AGARD Conference Proceedings No. 255, North Atlantic Treaty Organization, Advisory Group for Aerospace Research and Development, Neuilly sur Seine, France, May 1978.
2. Crash Survival Design Guide, Dynamic Science, A Division of Marshall Industries, USAAMRDL Technical Report 71-22, Fort Eustis, Virginia, Eustis Directorate, U.S. Army Air Mobility Research and Development Laboratory, 1971, AD 733358.
3. Military Standard, MIL-STD-1290(AV), Light Fixed - Rotary-Wing Aircraft Crashworthiness, Department of Defense, Washington, D.C., 25 January 1974.
4. Military Specification, MIL-S-58095(AV), Seat System: Crashworthy, Non-Ejection, Aircrew, General Specification For, Department of Defense, Washington, D.C., 27 August 1971.

The last program of significance to investigate the variables associated with vertical (+G_z) acceleration of aircraft occupants was sponsored by the U.S. Army Air Mobility Research and Development Laboratory, Fort Eustis, Virginia (now the Applied Technology Laboratory) in 1969 and 1970. The results of this program are presented in Reference 5. The goal of this earlier program was to evaluate the meager information then available and to develop an achievable criterion to guide the design of crashworthy crewseats for U.S. Army aviation. This task was accomplished, and the resulting criterion has now been in existence for the past ten years.

Techniques used for the design and evaluation of energy-absorbing seating systems are explained in detail in References 1, 2, 4, and 6; however, in summary, the Eiband human tolerance data with upper level ejection seat criteria superimposed (as presented in the Aircraft Crash Survival Design Guide, Reference 7) was taken for the upper limit of tolerable acceleration in the +G_z direction. Tests and analyses were then conducted to establish the force level necessary for the vertical energy-absorption system to limit the acceleration excursions of the seat pan to magnitudes of less than 23 G for time durations in excess of 0.006 sec, as dictated by the tolerance data. The test results indicated that if the energy-absorbing mechanism were set to provide controlled deformation at a force computed using a 14.5-G load factor, the desired result could be achieved. Test data supporting the conclusions of this analysis are presented in Reference 5.

In seat tests conducted during the ensuing years, a characteristic seat pan z-axis acceleration response was observed. In this characteristic curve, the seat pan acceleration rises sharply during the onset of the input pulse, then drops rapidly, sometimes passing through zero. It then rises sharply again and forms a secondary spike before damping out around the load factor used in the

5. Desjardins, S. P., and Harrison, H., The Design, Fabrication, and Testing of an Integrally Armored Crashworthy Crewseat, Dynamic Science, Division of Marshall Industries; USAAMRDL Technical Report 71-54, Eustis Directorate, U.S. Army Air Mobility Research and Development Laboratory, Fort Eustis, Virginia, January 1972, AD 7421733.
6. Desjardins, S. P., and Laananen, D. H., Aircraft Crash Survival Design Guide, Volume IV - Aircraft Seats, Restraints, Litters, and Padding, Simula Inc., USARTL-TR-79-22D, Applied Technology Laboratory, U.S. Army Research and Technology Laboratories (AVRADCOM), Fort Eustis, Virginia, June 1980, AD A088441.
7. Laananen, D. H., Aircraft Crash Survival Design Guide, Volume II - Aircraft Crash Environment and Human Tolerance, Simula Inc., USARTL-TR-79-22B, Applied Technology Laboratory, U.S. Army Research and Technology Laboratories (AVRADCOM), Fort Eustis, Virginia, January 1980, AD A082512.

design of the energy-absorbing system. In most of the tests conducted during the time period between 1971 (when the criteria were established) and the present, the secondary spikes have exceeded the criteria limit of 23 G and have been a source of concern. One question is whether the secondary spike is a natural response of the seat and occupant spring-mass system, or if it is caused by some external source. Also, it is not known whether the acceleration spike is hazardous to the seat occupant.

The need for answering these questions was confirmed in August 1978, during qualification testing of the U.S. Army's Black Hawk helicopter crewseat, when the secondary acceleration spike once again exceeded the criteria limits. At that time it was decided to research the data available and to attempt, through analysis, to determine whether the secondary spike did, in fact, increase the hazard to the occupant. The results of this analysis indicated that the secondary spike is a natural response of the seating system and, in itself, does not increase the hazard to the occupant. However, the analysis also indicated that the crash pulse might be hazardous to the occupant at times other than during the secondary spike. It was further concluded that the criterion based on seat pan acceleration is not sufficiently comprehensive, and that additional research should be immediately initiated to both establish the effects of system variables upon seat and occupant response, and expand knowledge in the area of human tolerance to decelerative loading in the +G_z direction. The data gathered from these programs constitute a necessary prerequisite to establishing a more comprehensive set of criteria controlling the design of crashworthy crewseats.

Under the leadership of the U.S. Army Applied Technology Laboratory (ATL), Fort Eustis, Virginia, and the U.S. Army Aeromedical Research Laboratory (USAARL), Fort Rucker, Alabama, a multi-service effort was initiated with goals of performing the research necessary in these areas. The overall program is illustrated in Figure 1. The research efforts were designed to provide at least a minimum level of information in each area and to meet the following objectives:

- Establish the sensitivity of seat and occupant response to system variables.
- Determine the effect on system performance of the type of dummy being used for testing and establish an appropriate standardized dummy for seat system evaluation.
- Investigate the performance of the seat with an occupant more nearly representative of the operational occupant than are anthropomorphic dummies. Cadavers were to be used for this investigation.
- Establish, through dynamic testing, additional information concerning human tolerance to acceleration loads in the +G_z direction.

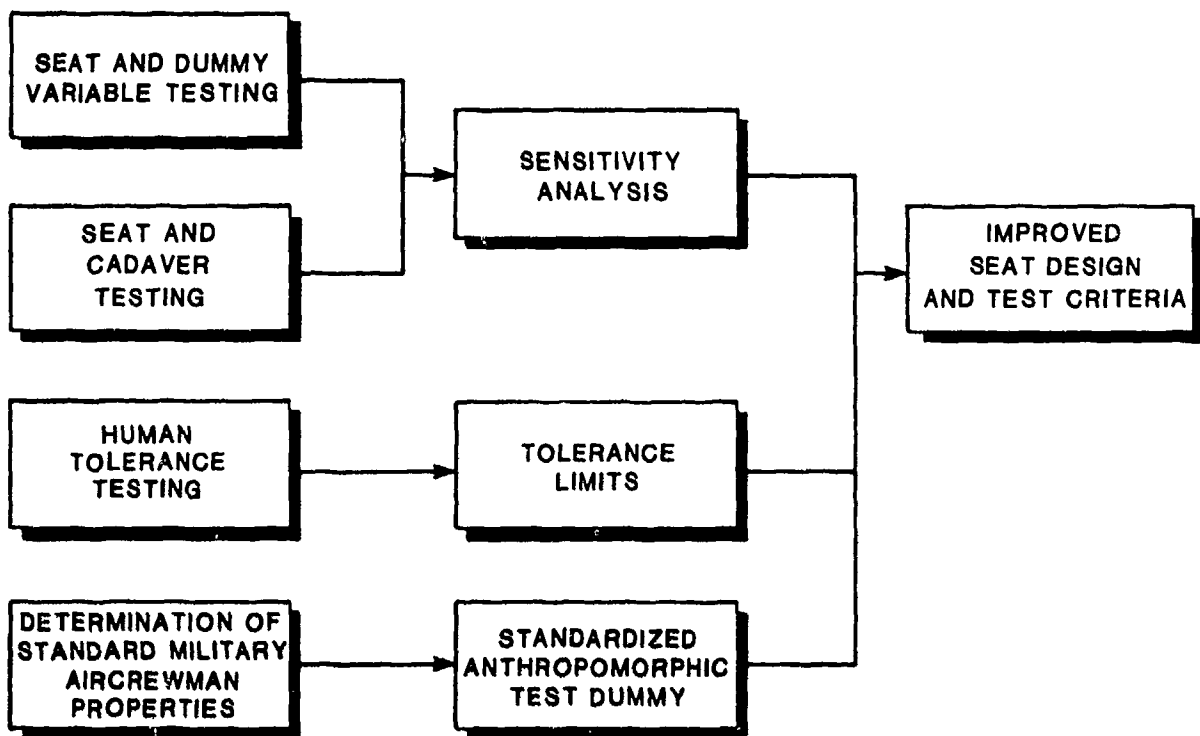


Figure 1. Overall program elements leading to improved seat design and test criteria.

The effort to establish a standardized test dummy is being coordinated by USAARL and involves an ad-hoc committee consisting of representatives from interested Government agencies and the private sector. Research to increase the knowledge of human tolerance to acceleration loads in the +G_x direction is being performed by the Naval Biodynamics Laboratory, Michoud, Louisiana, with support and sponsorship of USAARL. The other research is being coordinated by Simula Inc., Tempe, Arizona, with test and advisory support by many of the other involved organizations, and with the sponsorship primarily of the ATL and USAARL. The overall program is summarized in Table 1.

This report describes the program of seat and dummy testing, as well as subsequent analyses, to establish the sensitivity of the system to a number of variables. Chapter 2 presents background information on the need for energy-absorbing seats and the response of the combined seat/occupant system. Chapter 3 outlines the research program in detail. Procedures for testing and analysis are described in Chapters 4 and 5, respectively. Results of the sensitivity analysis are described in Chapter 6, and conclusions and recommendations, particularly with respect to improvements in seat criteria, are presented in Chapters 8 and 9.

TABLE 1. PROGRAM RESPONSIBILITIES

Program Objective	Agency/Organization	Responsibility	Sponsor
Establish the sensitivity of vertically (z-axis) stroking seating systems and improve the criteria for their design.	Simula Inc., Tempe, Arizona	Overall responsibility for program direction. Provide all seat hardware, data analysis, data synthesis and interpretation, and report results. Also, perform testing, data acquisition, reduction, and analysis.	Applied Technology Laboratory US Army Research and Technology Laboratories (AVRADCOM), Fort Eustis, Virginia
	Civil Aeromedical Institute, Oklahoma City, Oklahoma	Perform dynamic testing support; provide instrumentation and test dummies; record, reduce, and submit data; and advise on other programs.	Federal Aviation Administration
	Naval Air Development Center, Warminster, Pennsylvania	Provide dynamic test support, instrumentation, data acquisition, and reduction.	U.S. Navy
Determine the tolerance threshold limit-load setting for the energy-absorbing mechanism that would not cause spinal injury in cadavers. Also, determine the response of an energy-absorbing crewseat with a human cadaver as an occupant for comparison with the response using an anthropomorphic dummy.	Simula Inc., Tempe, Arizona	Overall program responsibility. Provide test seat hardware, establish instrumentation requirements, perform final analysis of data, interpret and report results.	U.S. Army Applied Technology Laboratory, Fort Eustis, Virginia; U.S. Army Aeromedical Research Laboratory, Fort Rucker, Alabama; Federal Aviation Administration Technical Center, Atlantic City, New Jersey; U.S. Air Force, 6570th Aerospace Medical Research Laboratory, Wright-Patterson Air Force Base, Ohio
	Bioengineering Center, Wayne State University	Acquire cadavers, instrument the cadavers; perform the dynamic tests; acquire, record and reduce test data.	Same as above
Standardize the seat test dummy.	Ad-hoc committee consisting of representatives from industry and Government	Acquire and select pertinent data for use in establishing the physical parameters of the military aircrewman for use in subsequent development of a standardized test dummy.	U.S. Army Aeromedical Research Laboratory, Fort Rucker, Alabama
Improve knowledge of the tolerance of human subjects to $+G_z$ accelerative loading.	U.S. Naval Biodynamics Laboratory, Michoud, Louisiana	Overall program responsibility including performing tests of live human volunteers, followed by surrogates. Acquisition of data, analysis and presentation of results.	U.S. Army Aeromedical Research Laboratory, Fort Rucker, Alabama; U.S. Naval Biodynamics Laboratory, Michoud, Louisiana

2.0 HUMAN TOLERANCE TO ACCELERATIVE LOADING

The tolerance of the human body to impact forces depends on a number of variables, including characteristics of the individual such as age, sex, and general state of health. Military systems can be expected to be used by personnel who are primarily younger and in better physical condition than the general population for which much tolerance data has been obtained. Thus, in some cases, a degree of conservatism may be built into the application of tolerance criteria in designing Army aircraft. However, whole-body tolerance criteria have been based on experiments involving subjects seated with "correct" upright posture. Because a helicopter pilot is unlikely to maintain such posture in flight, particularly when near the ground, tolerable levels of such variables as +G_z acceleration may be significantly reduced under actual crash conditions.

2.1 HUMAN TOLERANCE INVESTIGATIONS

The magnitude and duration of the applied accelerative force have definite effects on human tolerance, as shown in Figure 2. As indicated by this curve, a spineward chest-to-back (-G_x) accelerative force of 45 G has been tolerated voluntarily by some subjects when the pulse duration is less than 0.044 sec. Under similar conditions, when the duration is increased to 0.2 sec, the tolerable magnitude is reduced to about 25 G. Accordingly, Figure 2 (Reference 8) shows that the tolerable limits on acceleration loading are a function of duration.

The whole-body tolerance data displayed in Figure 2 were collected for a variety of full-torso restraints and, in some cases, head restraint. With less optimum restraint, some debilitation and injury will occur at this acceleration level, or, in other words, the tolerable level will be reduced.

The human body is able to withstand a much greater force applied perpendicular to the long axis of the body in a forward or backward (G_y) direction than applied parallel to the long axis (G_x), as demonstrated by a comparison of the curves in Figures 2 and 3. A primary reason for the significantly lower tolerance to headward (+G_z) loading is the susceptibility of the lumbar vertebrae, which must support most of the upper torso load, to compression fracture. Also, the skeletal configuration and mass distribution of the body are such that vertical loads cannot be distributed over as large an area as can loads applied forward or backward (G_y). These vertical loads, therefore, result in greater force per unit area than do sternumward or spineward loads. Finally, along the direction of the long axis, the body configuration allows for greater displacement of the viscera within the body

8. Elband, A. M., Human Tolerance to Rapidly Applied Accelerations: A Summary of the Literature, NASA Memorandum 5-19-59E, National Aeronautics and Space Administration, Washington, D.C., June 1959.

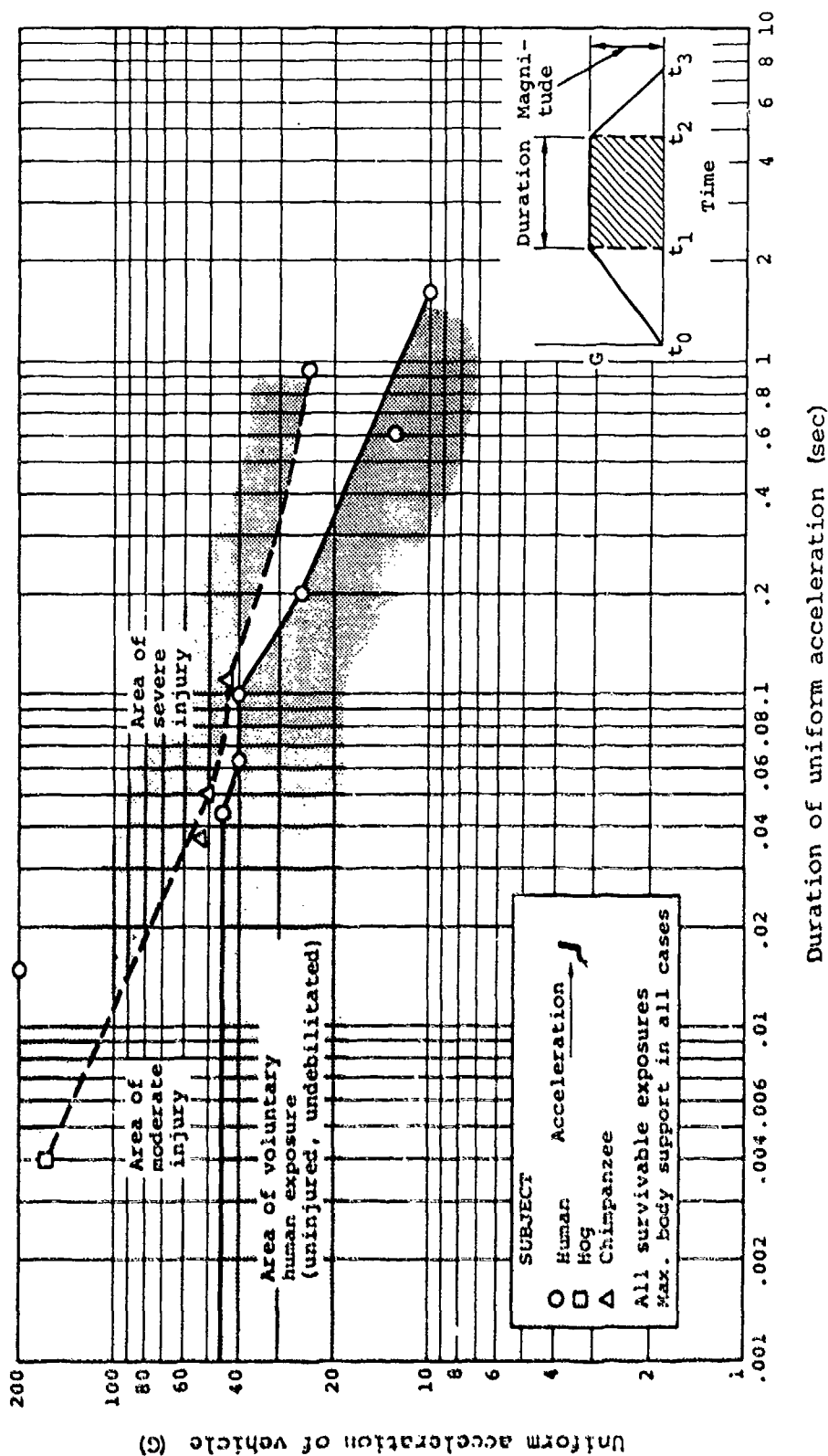


Figure 2. Duration and magnitude of spineward acceleration endured by various subjects (from Reference 8).

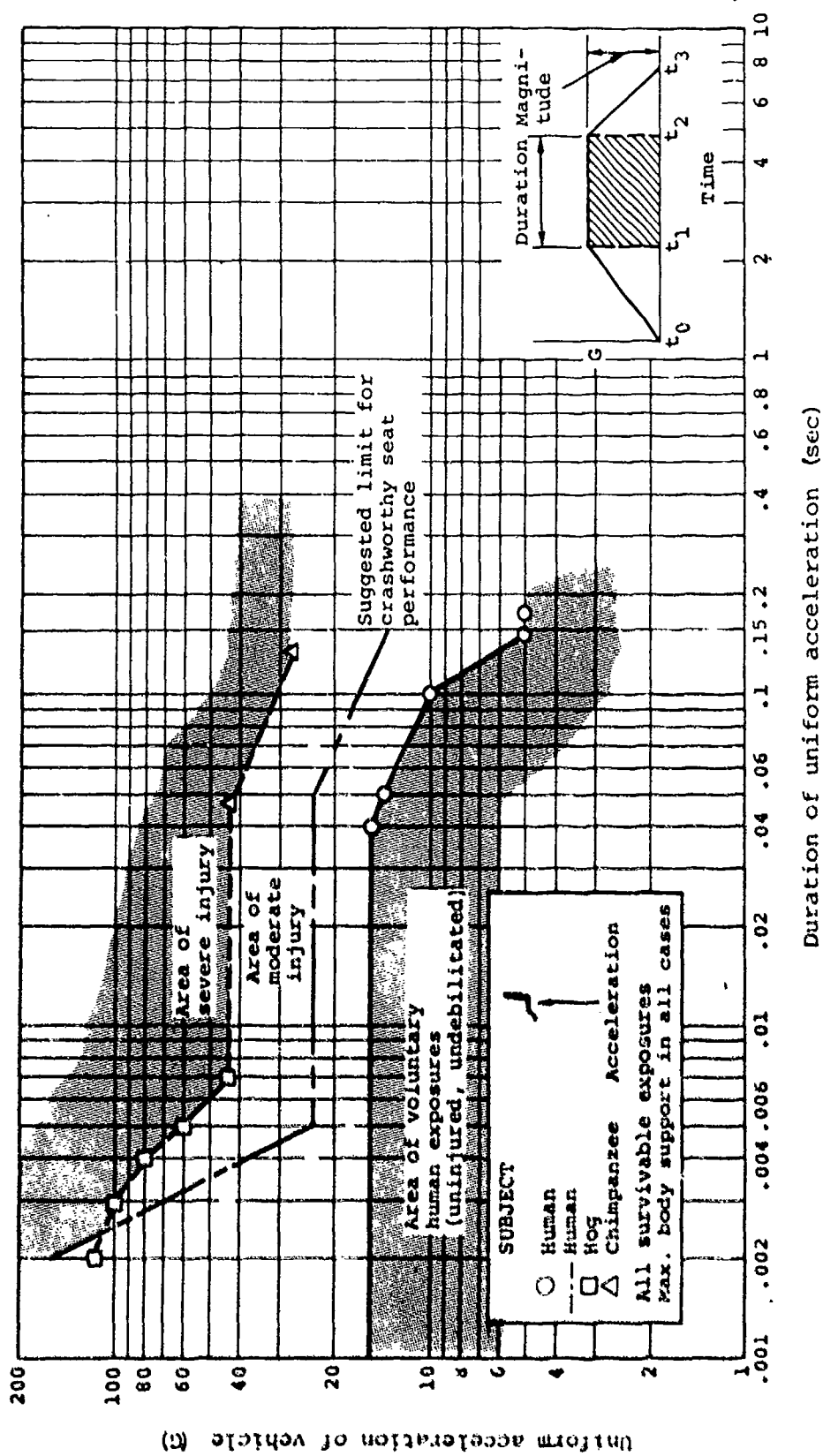


Figure 3. Duration and magnitude of headward acceleration endured by various subjects (from Reference 8).

cavity. Forces applied parallel to the long axis of the body, headward or tailward (G_z), place a greater strain on the suspension system of the viscera than do forces applied sternumward or spineward (G_x), thereby increasing the susceptibility of the viscera to injuries.

Human tolerance to lateral ($\pm G_y$) impact acceleration is not well defined, as a rather narrow range of pulse durations has been explored in tests. The U.S. Air Force conducted a series of tests with human volunteers in which several orientations were used (Reference 9). In 32 tests to evaluate $\pm G_y$ impact vectors, there were no adverse subjective reactions to acceleration magnitudes up to 22 G with a rate of onset of 1350 G/sec and velocity changes to 19.3 ft/sec. Subjects were restrained by lap belts, torso harness, and leg restraints and supported by a contoured pad. In a series of tests conducted by the Royal Air Force (Reference 10), a conventional military aircraft seat and five-point restraint system was used with human subjects tolerating up to 17.1 G without irreversible injury.

No end points for human tolerance to lateral impacts were proposed in the reports of these experiments, but a reasonable conclusion from these data is that the human survival limit with conventional military aircraft restraint is probably on the order of 20 G applied for a duration of 0.1 sec.

2.2 TOLERANCE-BASED CRITERIA FOR SEATS

The desired function of crashworthy crewseats is to protect occupants from the decelerative crash load hazards with severities up to and including those of a 95th-percentile survivable crash pulse. Reference 7 reports that 95 percent of survivable accidents involved average accelerations of less than 15 G in the longitudinal direction, 24 G in the vertical direction, and 16 to 17 G laterally, depending on aircraft type. For a triangular pulse, the peak values would be twice these levels or 30 G longitudinal, 48 G vertical, and 32 to 34 G lateral. Comparing these values with the tolerable levels reported above, it appears that a properly restrained human can withstand the lateral and longitudinal loads associated with the respective 95th-percentile survivable crash pulses. Therefore, no load attenuation is necessary, or desirable for crewseats due to space limitations of most cockpits, in

9. Brinkley, J. W., Weis, E. B., Clarke, N. P., and Temple, W. E., A Study of the Effect of Five Orientations of the Acceleration Vector on Human Response, AMRL Memo M-28, Aerospace Medical Research Laboratory, Wright-Patterson Air Force Base, Ohio, 1963.
10. Reader, D. C., The Restraint Afforded by the USAF and Proposed RAF IAM Seat Harnesses for the F-111 Under High Forward and Lateral Decelerations, IAM Report 421, Institute of Aviation Medicine, Farnborough, Hampshire, United Kingdom, 1967.

those directions. In the vertical direction, however, crash energy absorption and force attenuation are required since the human spine can withstand only a fraction of the load associated with the 95th-percentile survivable vertical crash pulse.

Various criteria for design of the vertical energy absorption system have been established. Basically, they involve establishing the force level at which the energy-absorbing system should stroke to limit the load in the human spine to a tolerable magnitude. This is accomplished by determining some "effective" weight for the occupant (effective weight is less than the total body weight because part of the body weight - the weight of the feet and part of the legs - is carried by the floor of the aircraft rather than by the seat), adding to it the movable weight of the seat, and multiplying the sum by the load factor (G) determined to be tolerable. The criteria included in the 1970 edition of the Crash Survival Design Guide (Reference 11), Paragraph 3.3.3.1, state that "This effective weight plus the weight of the movable portion of the seat should be decelerated at an average level of 18 G or less." Average G is further defined as "The total velocity change of the seat pan (ΔV) divided by the total pulse duration of the seat pan." (Notice that no mention was made of the shape of the deceleration-time history but, rather, only the average deceleration established by dividing the area under the curve by the duration.) However, some researchers felt that perhaps the 18-G average value was too high and would still allow occupant injury. Consequently, in 1969 and 1970, a limited research program was sponsored by the U.S. Army Aviation Materiel Laboratories and conducted by Dynamic Science (AvSER Facility) to try to reevaluate, verify, and refine the criteria for the design of crashworthy armored crewseats. One recommendation of this program, which is documented in Reference 5, was the use of a limit-load factor of 14.5 G for integrally armored crewseats.

Again, the objective of the criteria was to provide design guidance to help in the development of seats that would limit occupant spinal loads to tolerable levels during crash pulses of severities up to, and including, the 95th-percentile survivable vertical crash pulse. The acceptable acceleration levels specified by Reference 4, which had been based on the Eiband tolerance data and the ejection seat design band (Reference 9), were selected for use. As shown in Figure 4, this criterion limits the headward ($+G_z$) acceleration imposed on the occupant to 23 G for time durations in excess of 0.006 sec, where time durations are defined as the length of the plateau between the onset and the offset portions of the acceleration-time histories experienced by the seat pan. The research program was structured to determine and establish the stroke distance and load for the energy-absorbing mechanisms to limit the accelerations imposed on the

11. Crash Survival Design Guide, Dynamic Science, A Division of Marshall Industries, USAAMRDL Technical Report 70-22, Fort Eustis, Virginia, Eustis Directorate, U.S. Army Air Mobility Research and Development Laboratory, 1970, AD 695648.

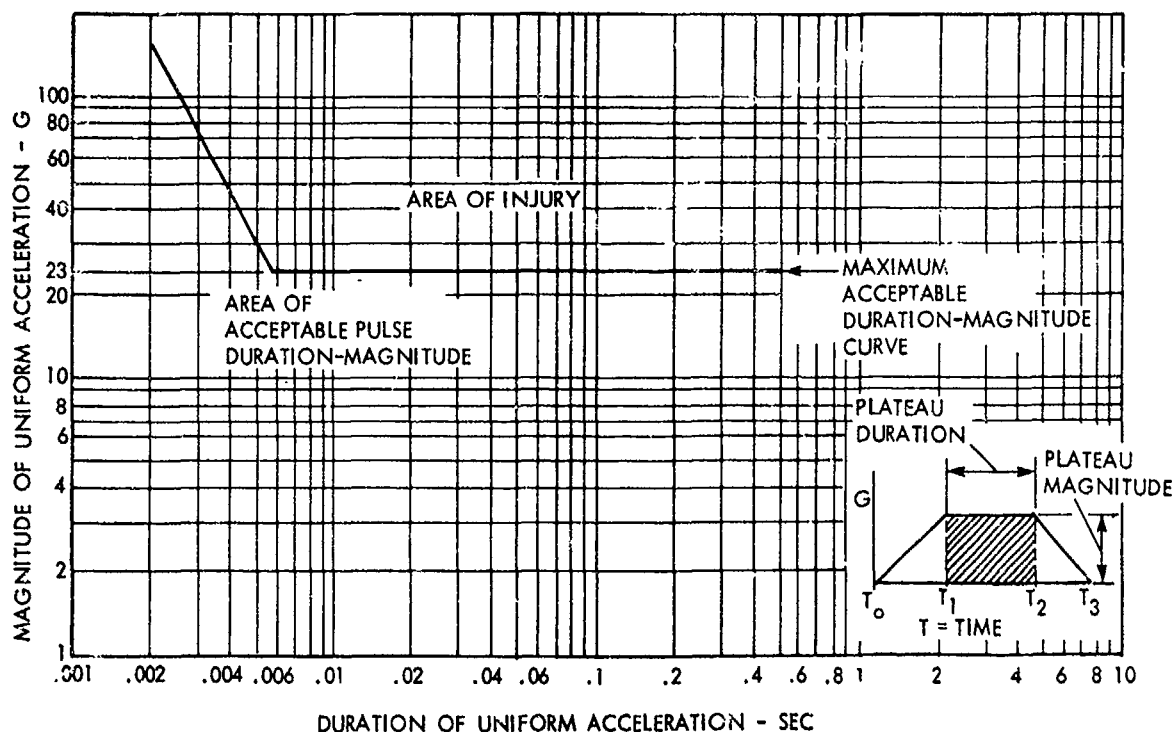


Figure 4. Maximum acceptable vertical seat acceleration (from Reference 4).

occupant to values less than those estimated to produce injury according to this criterion. It was thought that if the load attenuation system on the seat would provide such performance, then, within the limits of the seat stroke, the occupant would have as good a chance of avoiding injury as an individual using an ejection seat.

The 1970 research program consisted of analysis followed by a series of eight dynamic tests to develop the criteria for determining the limit load that would produce the desired performance within the prescribed minimum practical stroking distance of 12 in. Because of funding limitations, the program conducted was not sufficient to include a comprehensive investigation of the influence of many of the variables, such as energy absorber load-versus-deformation characteristics, anthropomorphic dummy variables, input pulse rate of onset and shape, bottom cushion load-deflection characteristics, and seat spring rate. However, the tests that were run indicated that it should be possible to maintain the seat pan acceleration within the limits of the criteria used for ejection seats.

In the years following development of the criteria, several crash-worthy seats were developed. As these seats were dynamically tested, a characteristic acceleration-time history was displayed (see Figure 5). This characteristic shape had been evident in

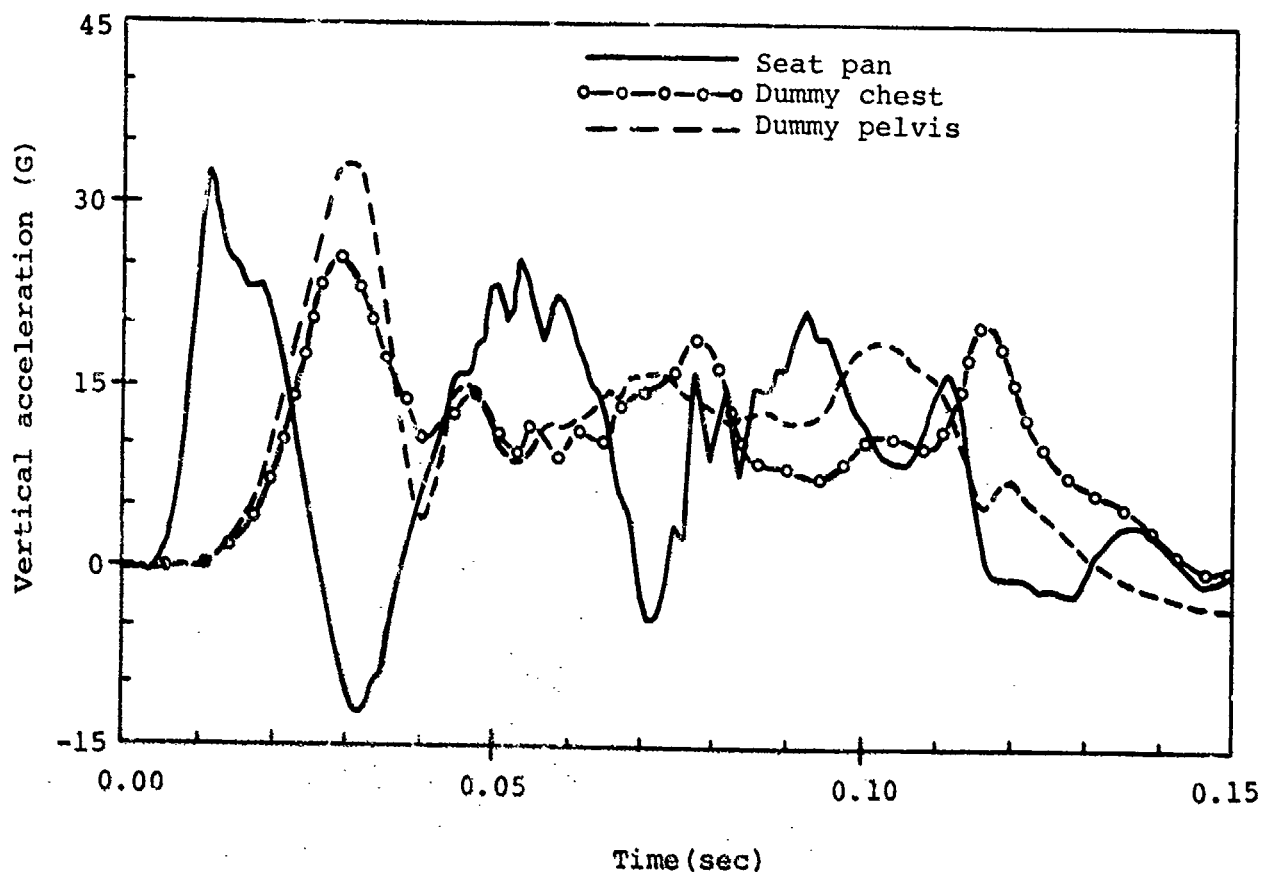


Figure 5. Typical response of seat pan, dummy chest, and dummy pelvis to vertical crash loading.

the criteria development test data as well, but the magnitudes of the peaks and valleys had been lower. As mentioned in the Introduction, the shape of the seat pan acceleration-versus-time history includes a high initial spike followed by a deep notch that sometimes passes through zero, actually changing sign. This notch is followed by a second high peak, followed, in turn, by various waveforms damping out and usually centering around the design limit-load factor of the system. This characteristic shape is apparent in all dynamic tests of the various crashworthy seat designs, including the Dynamic Science criteria development seat (Reference 5), the Simula Inc. UTTAS prototype seat (Reference 12),

12. Domzalski, L., and Singley, G. T., III, Joint Army/Navy Test Program for Black Hawk Seat Systems, Report NADC-79229-60 (Draft), Naval Air Development Center, Warminster, Pennsylvania, 1979.

the Simula Inc./Norton Co. Black Hawk production seat (Reference 13), and the ARA Inc. JA/N SEAT (Reference 14).

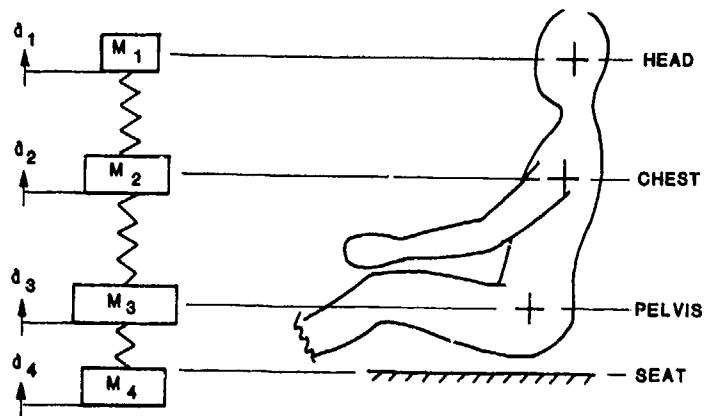
2.3 SEAT/OCCUPANT DYNAMIC RESPONSE

The explanation of the formation of the characteristic acceleration waveform is associated with the inherent dynamic response of the seating system and its occupant. Total coupling of the seat and its occupant is not achieved since the occupant consists of distributed masses connected by nonrigid body members, such as the vertebral column and neck in humans or elastic structural members in anthropomorphic dummies. Further, the interface between the occupant and seat is buttocks flesh and a cushion which do not form a rigid connection between the occupant and the seat pan. While stroking toward the floor, the energy absorber exerts a constant upward force on the moving seat mass. (Reference 4 requires that the energy absorber force be equal to the sum of the effective weight of the occupant and movable part of the seat multiplied by the load factor of 14.5 G.) The acceleration measured on the seat is then determined by the magnitude of the downward force applied by the occupant.

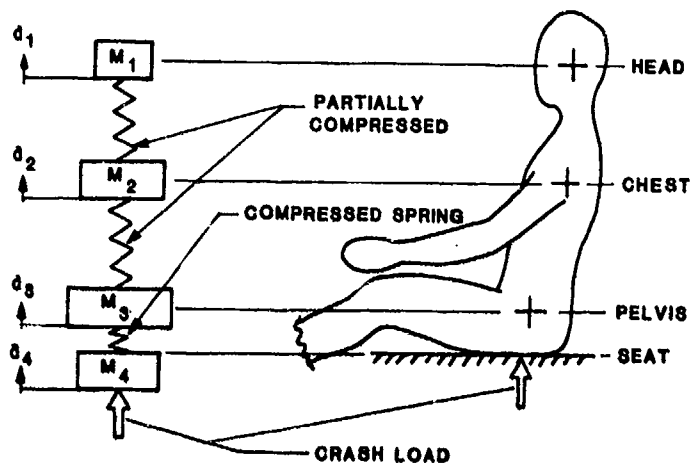
Idealizing the dynamic system of seat and occupant, all springs in the system are initially unloaded prior to impact, as shown in Figure 6(a). During the initial phase of the impact, the downward inertial load applied by the occupant to the seat pan is low. The cushion must be compressed before this load can become significant and a force acts to slow the occupant. It is during this time period that the seat pan acceleration characteristically grows from zero to a relatively large value as the energy-absorbing system acts to slow the small mass of the seat pan. As a result, the seat pan peak acceleration can reach magnitudes as great as the input floor acceleration.

In the second phase, each of the body parts is compressed, applying a downward force on the seat as shown in Figure 6(b). This downward force decreases the seat acceleration while the upward reactive force increases the body acceleration. It is possible that the downward inertial force applied by the body can equal the force required to stroke the energy-absorbing system. The net acceleration on the seat pan can drop to zero, or, in some cases, actually reverse direction.

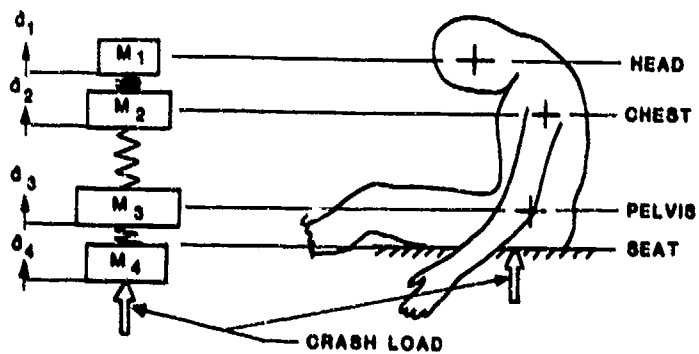
13. Dummer, R. J., Qualification Test Report, 613-1787 C00L Qualification Testing of Armored Crashworthy Aircrew Seat, RA-305252-1, for Sikorsky Aircraft Contract 576344, Norton Company, Worcester, Massachusetts, October 1978.
14. Chandler, R. F., Dynamic Test of Joint Army/Navy Crashworthy Armored Crewseat, Protection and Survival Laboratory, Memorandum Report AAC-119-80-2, Civil Aeromedical Institute, Mike Monroney Aeronautical Center, Federal Aviation Administration, Oklahoma City, Oklahoma, 25 April 1980.



(a) INITIAL CONDITION, UNLOADED



(b) ONSET OF DECELERATION LOAD WHEREIN PELVIS REGION IS RESPONDING TO DECELERATION LOAD BUT UPPER TORSO AND HEAD ARE NOT



(c) HIGH-DECELERATION LOAD, STEADY-STATE CONDITION

Figure 6. Spring-mass representation of seat-occupant system.

The accelerations of all components in the final phase eventually approach a common steady-state level, and the seat and occupant move together at the design acceleration level for the energy absorber setting (Figure 6(c)).

Referring to Figure 5, it is important to note that the peak accelerations of the seat pan do not necessarily coincide with peak accelerations of the occupant pelvis or chest, and thus are not necessarily hazardous to his safety. This deficiency was apparent when the existing criteria were developed, but they were adopted since, from an overall standpoint, the criteria had limited the incidence of injury in ejection seats. However, the Eiband tolerance data used in the criteria do not consider the seat pan acceleration excursions from the average. These data were smoothed in much the same manner as used for calculating average G described in the second paragraph of Section 2.2.

Consequently, the more comprehensive study, described in the Introduction, was undertaken to develop the data necessary to better understand the dynamic response of the seat and occupant systems. This understanding can then be quantified and used to establish more comprehensive design criteria to enable the design of seating systems that will reduce the crash hazard to the occupant.

3.0 PARAMETRIC STUDY

The goal of the program described in this report was to provide the necessary data to more effectively use the available stroking distance for energy-absorbing seats, thus reducing the probability of occupant injury due to vertical decelerative loading. At the initiation of the program, it was determined that the available computer simulation methods were not sufficiently validated for this type of work; therefore a parametric study had to be completed using dynamic impact tests. This chapter describes the development of the parametric test matrix to provide the data base for optimizing energy absorber design.

3.1 VARIABLES EXAMINED

Thirteen variables were chosen to determine their effect on seat and occupant response. These variables were chosen based on results from the original Criteria Development Test Program (Reference 5) and experience gained in the development and testing of the UTTAS prototype armored crewseat (Reference 12). The 13 variables, listed in Table 2, fall into three major categories as described in the following sections.

TABLE 2. VARIABLES EXAMINED DURING
PARAMETRIC STUDY

- Test facility impact conditions
 - Magnitude of input acceleration
 - Velocity change
 - Rate of onset of input acceleration
 - Dummy type
 - Dummy percentile
 - Cadavers versus anthropomorphic dummies
 - Energy absorber limit load
 - Ramped energy absorbers
 - Movable seat weight
 - Seat frame stiffness
 - Seat cushion stiffness
 - Seat orientation to impact vector
-

3.1.1 Impact Conditions

The impact conditions to which the cockpit area of an aircraft is subjected are controlled by the velocity and attitude at impact, as well as the design characteristics of the fuselage section impacting the ground. Seat orientation to the impact vector is a function of the aircraft orientation at impact and the design angle of the seat, which is usually pitched backward in the aircraft to enhance seated comfort. The velocity change is controlled mainly by the input velocity; however, the restitution characteristics of the fuselage sections crushed during impact can allow the aircraft to attain a significant rebound velocity. The velocity change is equal to the sum of the magnitudes of the initial velocity and the velocity achieved during rebound. The load-deformation characteristics of the fuselage sections crushed during impact will also determine the rate of onset, which is a measure of the rate at which the impact loads can build up in the structure, and the maximum impact load in the structure which is characterized by the peak input deceleration.

In a dynamic impact test of an occupant/seat system, crash forces are simulated by inertial loading that is induced either by acceleration from rest or deceleration from an initial velocity. Although it was originally thought that these conditions were equivalent, Hearon, et al. (Reference 15) have recently shown that there is an inherent difference in the two methods due to dynamic preload. In the parametric study, all four test facilities used the deceleration technique to simulate inertial loading. Each facility had a unique method of simulating the load-deformation characteristics of a crushing structure. Seat and occupant response for the various test facilities was the final variable in this area.

3.1.2 Occupant Characteristics

Energy-absorbing seat development and testing is currently conducted using anthropomorphic dummies. The applicable military standards do not specify a standard dummy, and the available test dummy types can differ significantly in their response characteristics depending on the original design goals for the dummy. None of the existing dummies were designed or optimized for vertical impact testing. Therefore, an obvious area of interest in this program was to compare the characteristic responses for anthropomorphic dummies used in dynamic testing. Also of interest was a determination of the effect of dummy weight (described by percentile of the U.S. male population) on seat and occupant response.

15. Hearon, B. F., Raddin, J. H., and Brinkley, J. W., "Guidance for the Utilization of Dynamic Preload in Impact Injury Prevention," in Impact Injury: Mechanisms, Prevention and Cost, North Atlantic Treaty Organization, Advisory Group of Aerospace Research and Development, Neuilly sur Seine, France, April 1982.

The use of anthropomorphic dummies as human surrogates for dynamic testing implies that the response of dummies and humans is similar. However, this is not a commonly held belief among the researchers in crash testing. The U.S. Army has undertaken an effort to examine human occupant response and tolerance to vertical impact loading through the use of cadavers. This work is presently being conducted under Contract DAAK51-79-C-0016 (Reference 16). In the parametric study, preliminary results from the cadaver testing program will be used to compare the effects of cadavers and anthropomorphic dummies on energy-absorbing seat response.

3.1.3 Seat Design Parameters

A number of seat design parameters directly affect response of the occupant and seat. Although development of flight-weight prototype seats has shown some variation in these parameters, this study attempted to examine the anticipated design range to determine the sensitivity of occupant response.

The energy absorber limit load is of particular interest because it directly affects the magnitude of inertial loading in the body. For a constant-load energy-absorbing system, the limit load is normally expressed as a multiple of the effective weight of the occupant and movable seat weight, which is called the limit-load factor. This limit-load factor is set to prevent the accelerative loading in the spine from exceeding tolerable levels. Ideally, the limit load should be set at the highest tolerable level to maximize the use of the available stroke distance in severe crashes. Data gathered from the cadaver test program described earlier and from field experience with production energy-absorbing seats should allow the limit-load factor to be optimized. In this study the effect of energy absorber limit load on seat stroke and occupant response will be examined. Also, analysis has suggested that, under certain conditions, an energy-absorber load that increases throughout the impact may actually reduce the dynamic overshoot in the body. This variable was examined by building special "ramped" energy absorbers with the desired load characteristics.

Three additional seat design parameters were examined to determine their effect on body dynamics during the crash sequence. These parameters were the weight of the stroking portion of the seat, the longitudinal stiffness of a vertically stroking seat, and the load-deflection characteristics of the seat pan cushion.

3.2 TEST FACILITIES

Four test facilities were used to complete the parametric test matrix: the FAA Civil Aeromedical Institute (CAMI), the Naval

16. Contract No. DAAK51-79-C-0016, "Hardware, Test Support, and Engineering Services," Applied Technology Laboratory, U.S. Army Research and Technologies Laboratory (AVRADCOM), May 9, 1979.

Air Development Center (NADC), Simula Inc., and Wayne State University Bioengineering Center (WSU). The majority of tests were conducted at CAMI due to their ability to conduct laboratory-type testing in a controlled, indoor, horizontal decelerator facility. NADC and Simula, both vertical drop tower facilities, were used to repeat key tests to determine the effect of input pulse shape and facility type (horizontal decelerator versus drop tower). Wayne State University conducted the cadaver test program and a series of dummy tests using a horizontal decelerator.

The four test facilities and sample input pulses for the nominal input condition, shown in Figure 7, are described in the following sections.

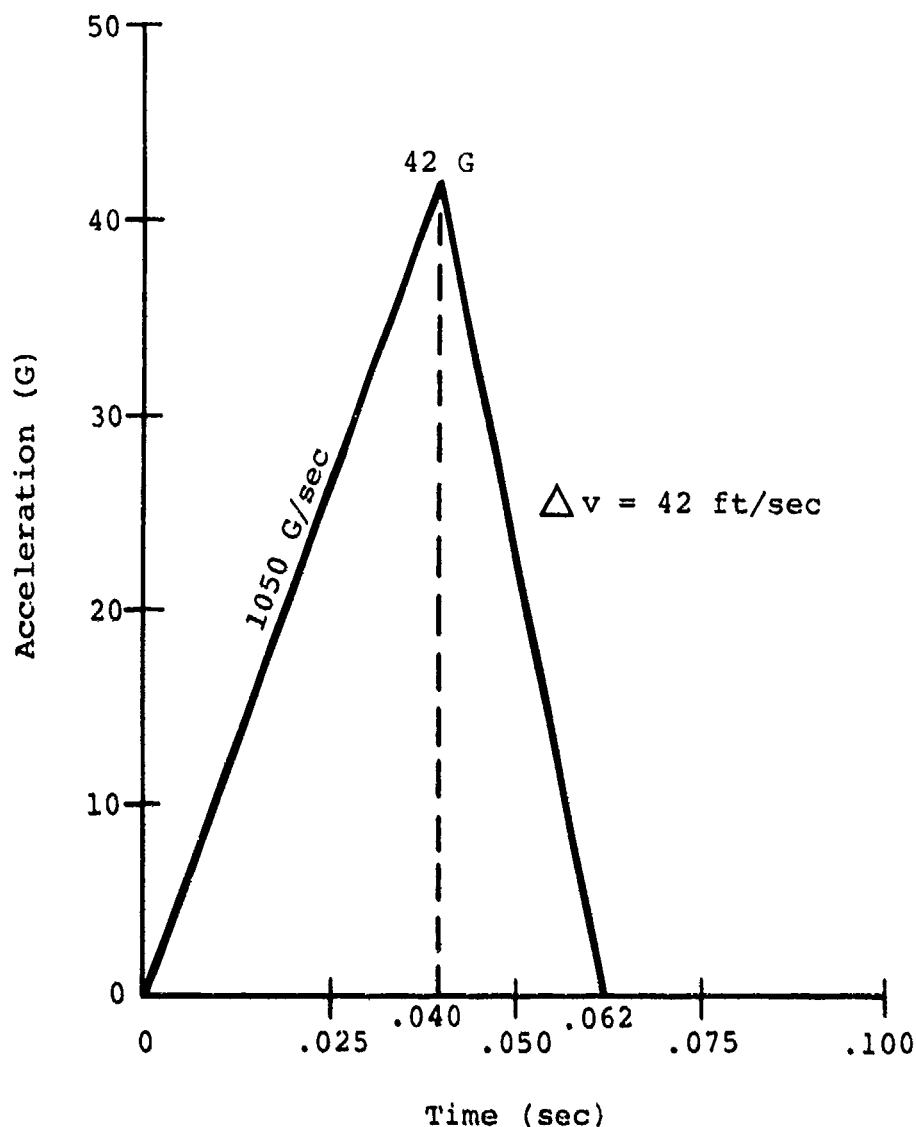


Figure 7. Triangular deceleration pulse describing the nominal test condition.

3.2.1 FAA Civil Aeromedical Institute (CAMI)

The CAMI facility uses a guided sled, shown in Figure 8, pulled along a set of horizontal rails by a falling weight. The sled achieves the desired initial velocity approximately 5 ft from the impact point. During travel through the final 5 ft, the sled moves at a constant velocity and passes through a velocity trap placed 2 to 4 in. before the impact point. At the impact point the sled encounters multiple stages of 1/4-in. steel wires which are plastically deformed as they are pulled between dies. The decelerating mechanism is shown before and after a test in Figure 9. Up to four wires can be placed in 42 successive stations, and the numbers and locations of wires can be varied to obtain a wide range of input pulse shapes.

The CAMI deceleration pulse is shown in Figure 10(a). It is characterized by a smooth shape with only about five percent of the velocity change occurring in rebound.

3.2.2 Naval Air Development Center (NADC)

The NADC facility shown in Figure 11 uses a drop cage, guided in a vertical tower, which is accelerated to the desired velocity by gravity. The initial velocity is measured as the average velocity of the sled during the 6 in. of cage travel prior to impact. The decelerating mechanism is a Van Zelm-type which uses steel straps pulled over rollers to absorb the crash energy, as illustrated in Figure 12.

The baseline input pulse shown in Figure 10(b) has a distinct oscillation with a short duration peak followed by a reduction below zero and then the major deceleration pulse. Approximately ten percent of the velocity change is due to rebound.

3.2.3 Simula Inc.

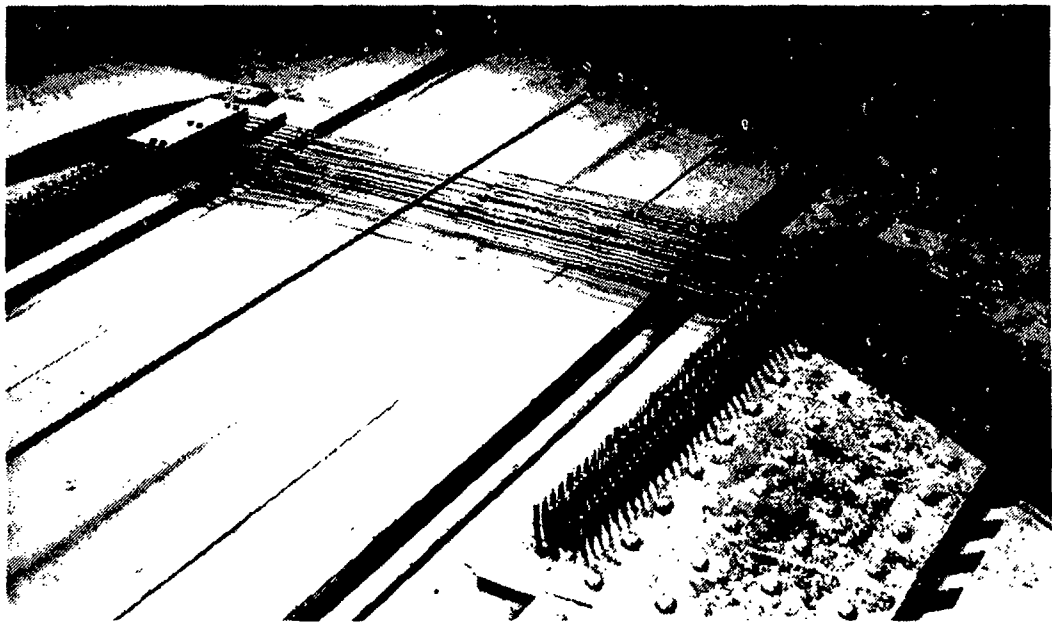
Tests conducted by Simula used the Arizona State University drop tower shown in Figure 13(a). The decelerating mechanism is a pyramid-shaped paper honeycomb stack designed by Simula to provide the necessary deceleration characteristics by varying the shape and qualities of each honeycomb layer, and is shown in Figure 13(b). A comparison of the Simula and CAMI baseline pulses in Figures 10(c) and 10(a), respectively, shows that they have similar features. Inherently, a significant rebound occurs when air is trapped as the honeycomb stack crushes, and in the baseline pulse approximately 25 percent of the velocity change is due to rebound.

3.2.4 Wayne State University (WSU)

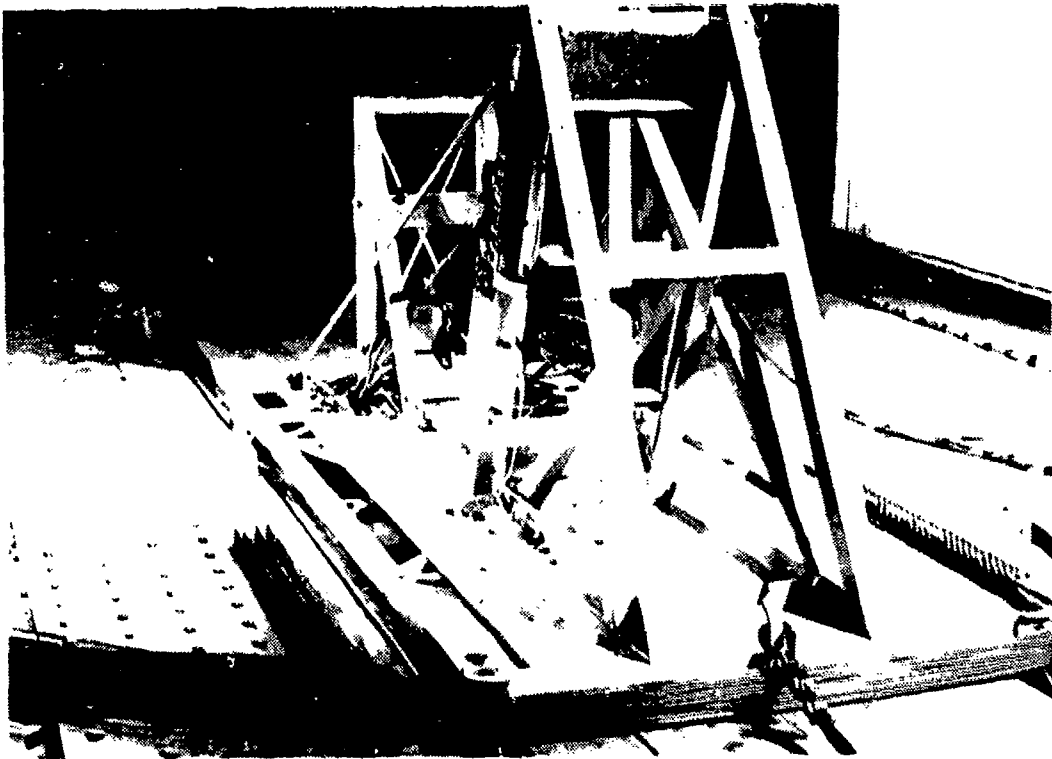
The WSU WHAM IV test facility uses a horizontal sled accelerated by pneumatic pressure to within 5 ft of the impact point. During the ensuing constant-velocity phase and prior to impact, a magnetic proximity sensor is used to estimate average velocity over a 1-ft distance. The decelerating mechanism is a hydraulic cylinder



Figure 8. CAMI sled.

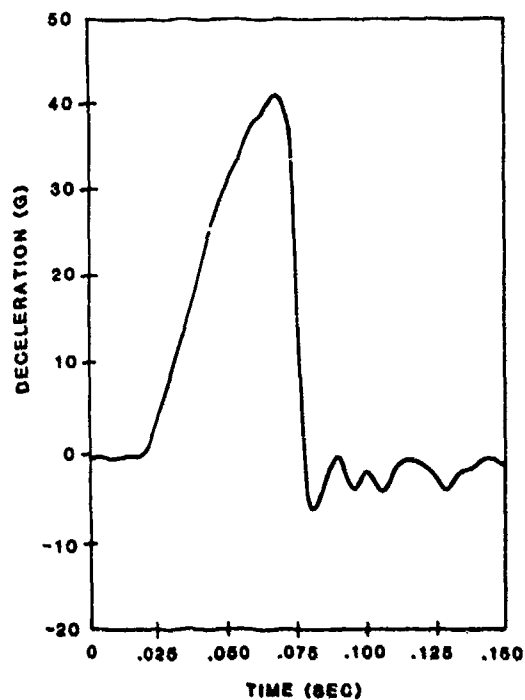


(a) Wires in position prior to test.

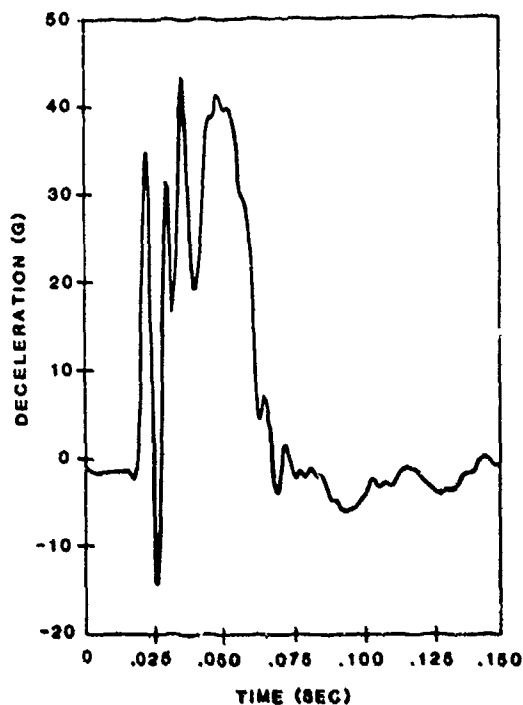


(b) Sled and wires following test.

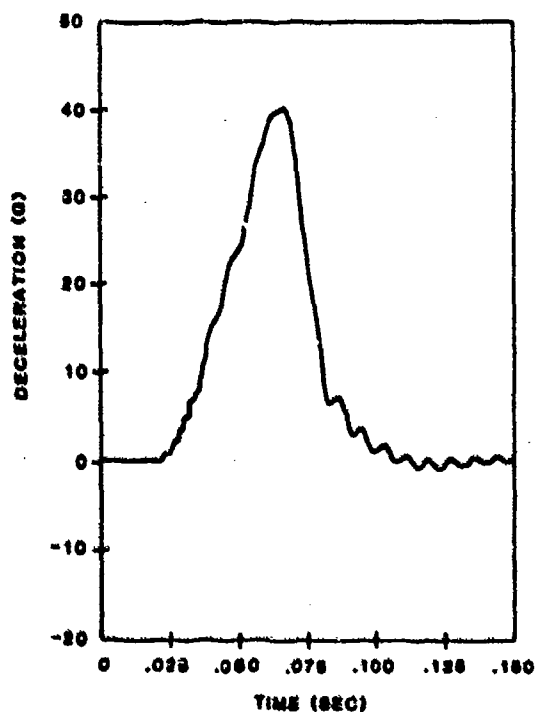
Figure 9. CAMI wire-bending decelerator mechanism.



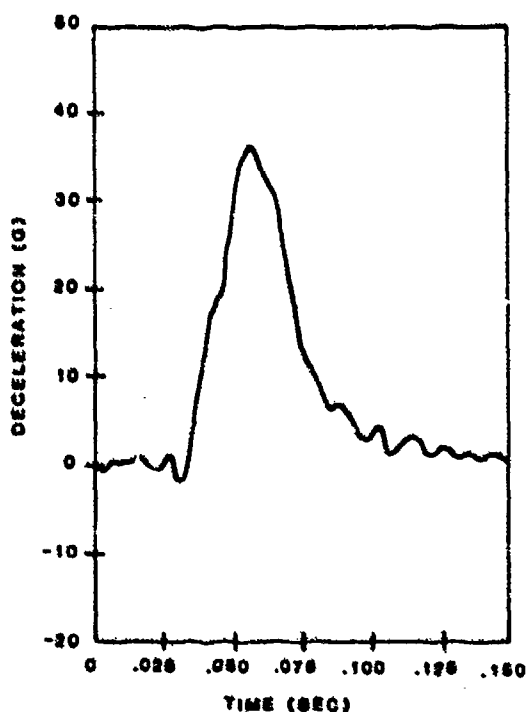
(A) CAMI



(B) NADC



(C) SIMULA



(D) WBU

Figure 10. Typical baseline deceleration pulses for the four test facilities.

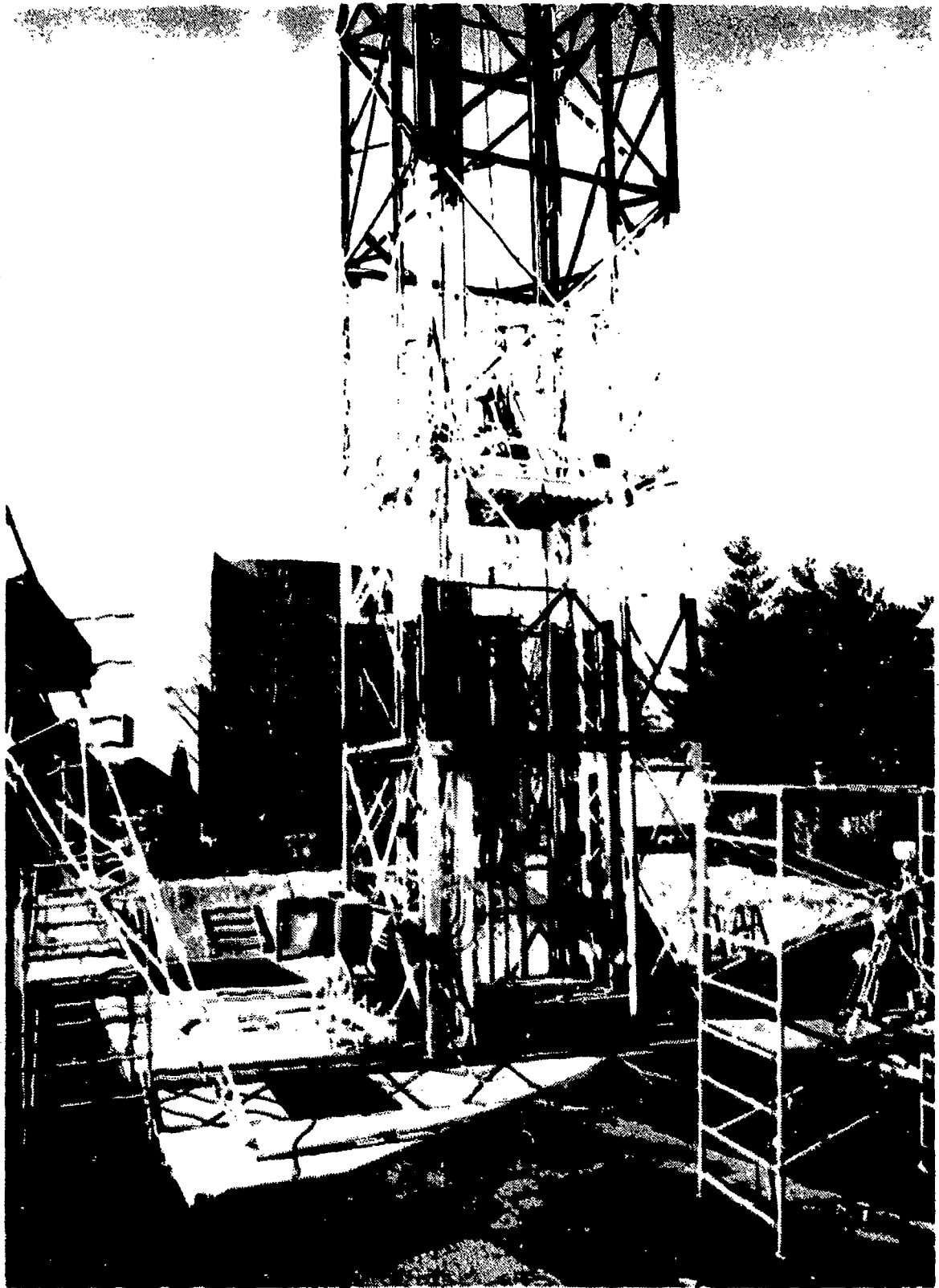


Figure 11. NADC drop tower.



(a) Straps in position prior to test.

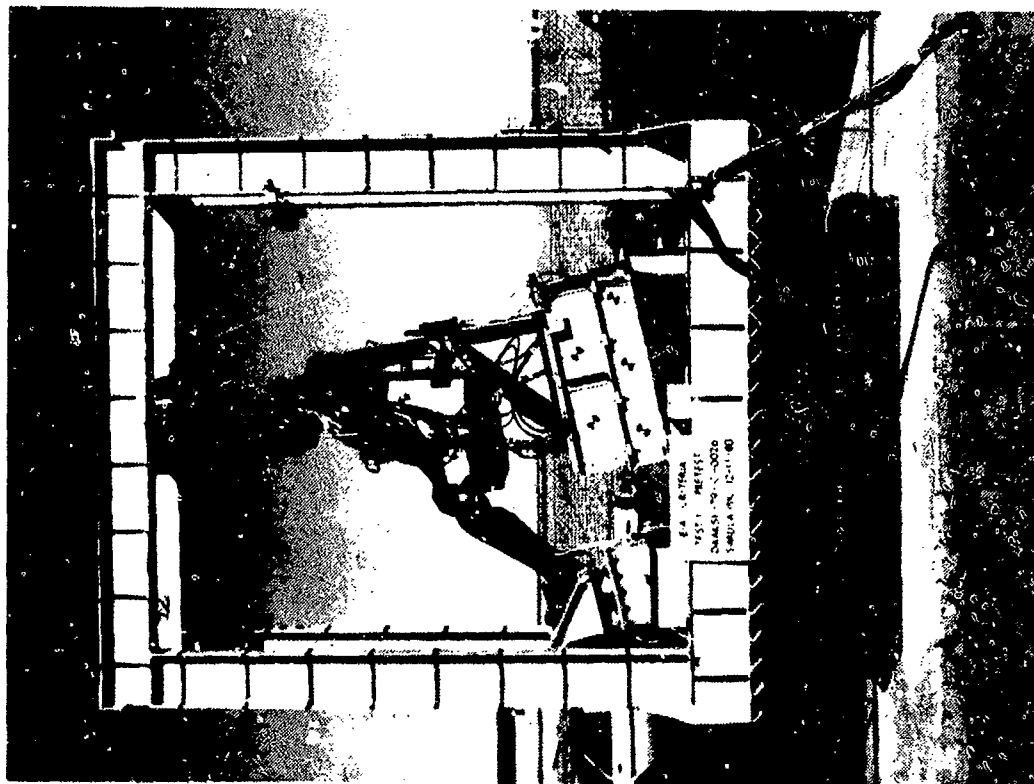


(b) Deformed straps following test.

Figure 12. NADC decelerating mechanism.



(a) Drop tower with seat and dummy prior to test.



(b) Drop platform and paper honeycomb stack prior to test.

Figure 13. Drop tower used in Simula tests.

in which the pressure is controlled by regulating the flow of hydraulic fluid through a series of orifices. Although the deceleration pulse has a smooth shape, it is characterized by a rate of onset significantly higher than the CAMI or Simula facilities. A minimal amount of the velocity change is due to rebound.

3.3 PARAMETRIC TEST MATRIX

A series of 62 dynamic tests was conducted to provide data to determine the effect of the 13 variables. Fifty tests were conducted at CAMI, of which 23 used a rigid seat and 27 used a production energy-absorbing crewseat. NADC and Simula conducted nine and three tests, respectively, all of which utilized the energy-absorbing seat. Tables 3 through 8 describe the test conditions for all of the tests conducted at CAMI, NADC, and Simula.

3.4 CADAVER TEST PROGRAM

The cadaver test program was conceived to provide a design base of human body tolerance data for optimization of energy-absorbing seating systems. The main objective is to determine the highest energy absorber limit-load setting that can be tolerated by the human body. The limit-load threshold is being evaluated by conducting dynamic tests with cadavers and assessing the spinal condition following the test. A major technical difficulty yet to be overcome in the program is to relate spinal fracture threshold between the cadaver and Army aviator populations.

The test program was designed to initiate testing at the operational limit-load setting of 14.5 G and gradually reduce the limit load until a threshold was achieved. Originally, it was planned to conduct a purely vertical dynamic test (+13 degrees pitch of the seat vertical axis) and, if no spinal fracture occurred, then a combined-mode test (+30 degrees pitch) would also be conducted. However, it became apparent after the first test series at 14.5 G that the spinal condition could not be reliably assessed with posttest x-rays. The remainder of the test program followed the protocol of one test per cadaver in the combined mode, which was believed to be more severe, followed by a spinal autopsy to determine condition.

As mentioned above, the test series began with a 14.5-G energy absorber limit-load setting. Subsequent series were conducted at 11.5 G and 8.5 G; the latter level appears to be near the spinal injury threshold for the cadaver population. The typical fracture encountered in this test program was an anterior wedge fracture of the vertebral body due to a combination of compressive loading and bending.

Bone samples were taken from each cadaver to provide a baseline for comparison of bone strength with the aviator population. It is interesting to note that early accident experience in Black Hawk helicopters with the same seat design and 14.5-G energy absorber settings shows that this level provides a significant degree of protection from spinal injury for Army aviators.

TABLE 3. TEST MATRIX FOR CAMI RIGID SEAT SERIES

Primary Variable	Test no.	Rate of Onset (G/sec)	Δv (ft/sec)	G_p	Dummy* Type	Dummy Percentile	Seat Pitch (deg)
<u>Basic Dummy Type</u>							
Hybrid II	A80-025	510	42.1	14.2	1	50	0
	A80-026	510	42.1	14.4	1	50	0
	A80-027	550	41.9	14.4	1	50	0
VIP-50	A80-022	460	42.0	14.0	2	50	0
	A80-023	520	42.3	14.7	2	50	0
	A80-024	510	42.4	14.1	2	50	0
CG-50	A80-032	520	42.0	14.6	3	50	0
	A80-033	510	41.9	14.6	3	50	0
	A80-034	510	41.8	14.5	3	50	0
<u>Dummy Percentile</u>							
95th	A80-028	520	41.6	13.8	4a	95	0
	A80-030	510	41.8	14.0	4a	95	0
	A80-031	540	42.1	14.1	4b	95	0
	A80-029	530	41.8	14.3	5	95	0
5th	A80-035	510	42.2	14.2	6	5	0
<u>Seat Orientation</u>	A80-038	570	42.6	15.6	1	50	+30
	A80-037	580	42.3	14.7	4	95	+30
	A80-036	490	42.7	14.9	6	5	+30
<u>Dummy Performance Verification Tests</u>							
Following CAMI Tests	A80-083	510	41.4	13.8	1	50	0
	A80-084	480	42.0	14.1	1	50	0
	A80-085	510	42.3	14.1	1	50	0
Following NADC and Simula Tests	A81-004	500	42.5	14.4	1	50	0
	A81-005	520	42.5	14.6	1	50	0
	A81-006	500	42.4	14.4	1	50	0

*See Table 4 for description of anthropomorphic dummy types.

TABLE 4. DUMMY IDENTIFICATION

Test Matrix Dummy Code	Dummy Description	Serial Number	Providing Organization
1	Alderson Hybrid II (50th percentile - Part 572)	870	NADC
2	Alderson VIP-50A (50th percentile)	314	CAMI
3	Alderson CG-50 (50th percentile)	501	NADC
4a	Alderson VIP-95 (95th percentile with elastomeric spine)	133*	CAMI
4b		153	ATL
5	Alderson CG-95 (95th percentile)	500	NADC
6	Alderson CG-5 (5th percentile)	719	NADC
7	Rigid Block (50th percentile effective weight, epoxy with seat used as mold and seat cushions removed)	N/A	Simula

*Alderson VIP-95 S/N 133 had been reworked to add an Ensolite pad under pelvis in buttocks flesh.

In addition to the human tolerance data that are being collected, each cadaver test provides information about the characteristics of human body response in energy-absorbing seats for comparison with anthropomorphic dummy response. Although the human body is difficult to instrument, significant comparisons between cadaver and dummy response can be made by examining seat response such as seat pan acceleration histories and seat stroke. The sensitivity analysis discussed in Chapter 6 includes a comparison of seat response for the two occupant types.

Recommendations for an optimal energy absorber limit-load setting will be presented in the final report at the completion of the cadaver testing program under Contract DAAK51-79-C-0016 (Reference 16).

The cadaver testing series is summarized in Table 9.

TABLE 5. TEST MATRIX FOR CAMI ENERGY-ABSORBING SEAT SERIES

Primary Variable	Test No.	Rate of Onset (G/sec)	Δv (ft/sec)	G _p	Dummy* Type	Dummy* Percentile	E/A LL (G)	Movable Weight (lb)	Cushion Type**	Seat Pitch (deg)
Baseline Response with CAMI Pulse Shape	A80-053	980	44.8	40.7	1	50	14.5	65	1	17
	A80-054	1040	44.2	40.2	1	50	14.5	65	1	17
Cushion Stiffness	A80-067	1060	44.0	41.2	1	50	14.5	65	2	17
	A80-068	1130	44.1	41.2	1	50	14.5	65	3	17
Dummy Type	A80-076	980	44.4	40.5	3	50	14.5	65	1	17
Dummy Percentile	A80-073	1070	45.6	40.2	4a	95	14.5	65	1	17
	A80-074	1050	45.0	41.4	6	5	14.5	65	1	17
E/A Limit Load	A80-055	1070	44.1	39.2	1	50	11.5	65	1	17
	A80-075	1120	45.9	42.5	6	5	8.5	65	1	17
Rate of Onset of Input Pulse	A80-057	820	43.6	35.0	1	50	14.5	65	1	17
	A80-058	1750	44.3	44.6	1	50	14.5	65	1	17
Stiffened Seat Frame Stiffness	A80-059	1070	43.7	40.4	1	50	14.5	65	1	17
	A80-079	950	44.1	38.9	1	50	14.5	65	1	34
Movable Seat Weight	A80-060	990	44.5	41.5	1	50	14.5	35	1	17
	A80-061	1060	43.8	40.5	1	50	14.5	120	1	17

*See Table 4 for description of anthropomorphic dummy types.

**See Table 6 for description of cushion types.

TABLE 5. TEST MATRIX FOR CAMI ENERGY-ABSORBING SEAT SERIES (CONTINUED)

Primary Variable	Test No.	Rate of Onset (G/sec)	Δv (ft/sec)	G _p	Dummy*		E/A LL (G)	Movable Weight (lb)	Cushion**		Seat Pitch (deg)
					Type	Percentile			Type		
Peak G of input pulse	A80-063	1840	45.6	50.9	1	50	14.5	65	1	1	17
	A80-062	910	43.3	32.2	1	50	14.5	65	1	1	17
	A80-064	710	42.1	21.9	1	50	14.5	65	1	1	17
Velocity change of input pulse	A80-070	750	33.9	31.2	1	50	14.5	65	1	1	17
	A80-077	1480	34.9	40.9	1	50	14.5	65	1	1	17
	A80-071	560	27.1	23.6	1	50	14.5	65	1	1	17
Ramped E/A load	A80-065	1060	43.4	40.9	1	50	9.5-19.5	65	1	1	17
	A80-066	1050	43.7	41.9	1	50	7.3-21.7	65	1	1	17
Dummy Stiffness	A80-069	1120	44.0	42.0	7	50	14.5	65	1	1	17
Seat orientation	A80-078	950	44.0	39.9	1	50	14.5	65	1	1	34***
	A80-081	1200	53.0	45.2	1	50	14.5	65	1	1	34***

*See Table 4 for description of anthropomorphic dummy types.

**See Table 6 for description of cushion types.

***In addition to 34-degrees pitch, the seat was oriented with 10 degrees roll in the seat coordinate system.

TABLE 6. DESCRIPTION OF CUSHION TYPES

Type Number	Description
1	Simula Black Hawk crewseat cushion designed to minimize rebound
2	Soft polyurethane cushion with same contour and dimensions as Type 1
3	Rigid, volume-controlled density foam cushion with same contour and dimensions as Type 1
4	Three layers of 3-in.-thick soft polyurethane foam without contour

3.5 MODIFIED ANTHROPOMORPHIC DUMMY PROGRAM

Analyses of the data from the sensitivity testing program demonstrated that the current criterion for seat evaluation based on seat pan acceleration is not sufficiently sensitive or repeatable to provide a measure of injury potential. A suggested alternative was to directly measure spinal forces and moments, which are the vertebral injury-causing mechanisms, throughout the crash sequence. The U.S. Army Aeromedical Research Laboratory initiated a program to modify a set of dummies for dynamic testing to assess the feasibility of this method (Reference 17).

Two anthropomorphic dummies, a 50th-percentile Hybrid II (conforming to the Part 572 Specification) and a 95th-percentile Alderson VIP-95 with elastomeric spine, were modified. The modifications consisted of inserting a six-axis load cell at the base of the lumbar spine projecting into the pelvic accelerometer cavity. A schematic drawing of the Hybrid II lower torso is shown in Figure 14 with the installed load cell. The VIP-95 dummy also had sufficient space at the base of the neck segment for installation of a load cell without alteration of existing anthropometry.

The goal of the modified dummy program was to determine the feasibility of measuring spinal loads and moments with simple modifications to an existing anthropomorphic dummy. The performance verification test program consisted of eight tests divided into

17. Laananen, D. H., and Coltman, J. W., Measurement of Spinal Loads in Two Modified Anthropomorphic Dummies, Simula Inc. TR-82405, Final Report, Contract DAMD17-81-C-1175, U.S. Army Aeromedical Research Laboratory, Fort Rucker, Alabama, May 1982.

TABLE 7. TEST MATRIX FOR NADC ENERGY-ABSORBING SEAT SERIES

Primary Variable	Test No.	Rate of Onset (G/sec)	Δv (ft/sec)	G _p	Dummy* Type	Dummy Percentile	E/A LL (G)	Movable Weight (lb)	Cushion Type**	Seat Pitch (deg)
Baseline Response with NADC Pulse Shape	N-189	2530	40.4	44.9	1	50	14.5	65	1	13
	N-190	2620	40.5	45.0	1	50	14.5	65	1	13
Peak G of Input Pulse	N-188	2830	39.2	51.7	1	50	14.5	65	1	13
	N-191	1980	37.9	35.2	1	50	14.5	65	1	13
Velocity Change of Input Pulse	N-192	900	30.0	31.1	1	50	14.5	65	1	13
	N-193	566	22.7	22.9	1	50	14.5	65	1	13
Ramped E/A Load	N-194	2470	41.4	46.6	1	50	9.5-19.5	65	1	13
Seat Orientation	N-195	2335	41.0	42.7	1	50	14.5	65	1	0
	N-196	1650	41.3	46.7	1	50	14.5	65	1	30***

*See Table 4 for description of anthropomorphic dummy types.

**See Table 6 for description of cushion types.

***In addition to 30-degrees pitch, the seat was oriented with 10 degrees roll in the seat coordinate system.

TABLE 8. TEST MATRIX FOR SIMULA ENERGY-ABSORBING SEAT SERIES

Primary Variable	Test No.	Rate of Onset (G/sec)	Δv (ft/sec)	G _p	Dummy* Type	Dummy Percentile	E/A LL (G)	Movable Weight (lb)	Cushion Type**	Seat Pitch (deg)
Baseline Response with Simula pulse shape	SEAC-1	1090	42.4	39.6	1	50	14.5	65	1	13
	SEAC-2	1110	42.2	40.9	1	50	14.5	65	1	13
Cushion Stiffness	SEAC-3	1120	41.8	40.5	1	50	14.5	65	4	13

*See Table 4 for description of anthropomorphic dummy types.

**See Table 6 for description of cushion types.

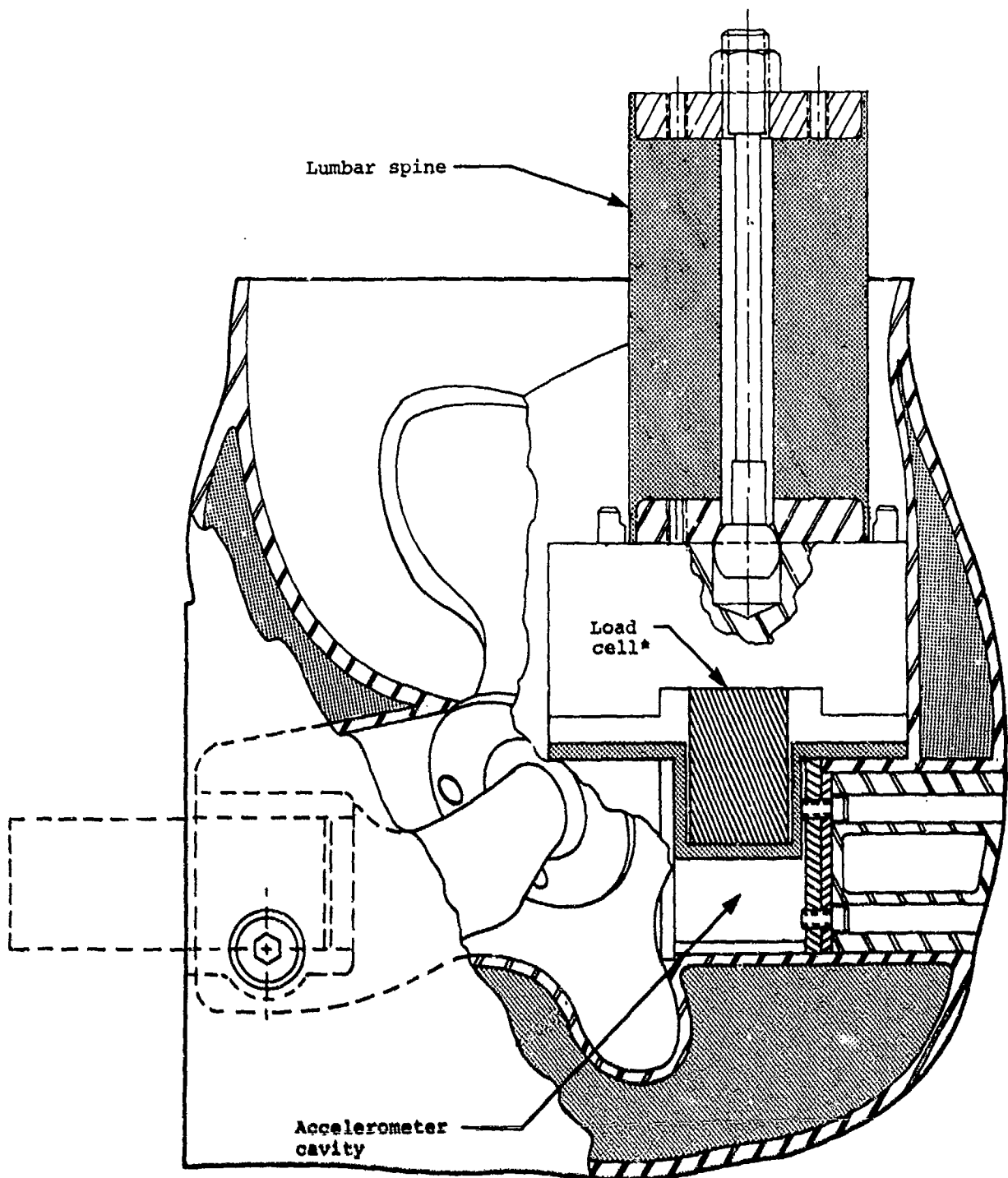
TABLE 9. SUMMARY OF CADAVER TEST PROGRAM

Test No.	Cadaver No.	Sex	Condition*	Age	Height	Weight (lb)	Seat Type	Peak a _z or E/A Limit Load (G)	Seat Stroke (in.)	Fracture Condition
Rigid Seat Series #1 (3 Runs)	4612	M	E	52	5'10"	161	Rigid	4,6,8	N/A	T9 @ 8 G
Rigid Seat Series #2 (11 Runs)	4654	M	E	49	5'7"	202	Rigid	4 to 30	N/A	T10 & T11 @ 30 G, Compression Failure
Rigid Seat Series #3 (8 Runs)	4660	M	E	51	5'7"	216	Rigid	4 to 30	N/A	T8 @ 13 G, Anterior Wedge Fracture
AF020	4784	F	U	44	5'3"	166	Black Hawk	Vertical 14.5 Combined	7.6	None
AF021									5.5	T12, End Plate, C1-C2 Articulation Failure
AF025	4840	M	U	55	5'7"	160	Black Hawk	Vertical 14.5	7.4	L3, Anterior Wedge Fracture
AF028	4850	F	U	61	5'4"	140	Black Hawk	Vertical 14.5 Combined	7.1	None
AF029									4.5	T12, Anterior Wedge Fracture

*E = embalmed; U = unembalmed.

TABLE 9. SUMMARY OF CADAVER TEST PROGRAM (CONTINUED)

Test No.	Cadaver No.	Sex	Condition	Age	Height	Weight (lb)	Seat Type	Peak a _z or E/A Limit Load (G)	Seat Stroke (in.)	Fracture Condition
AF031	4875	F	U	63	5'5½"	148	Black Hawk	Vertical 14.5	7.1	T8, Compression Fracture
AF033	4921	M	U	52	5'9"	218	Black Hawk	Combined 11.5	9.4	L1, Anterior Wedge Fracture
AF035	4975	M	U	63	5'8"	141	Black Hawk	Combined 11.5	7.0	L3, Anterior Wedge Fracture
AF037	4983	F	U	58	5'3"	160	Black Hawk	Combined 11.5	8.3	L1, Anterior Wedge Fracture
AF039	5229	M	U	52	5'10"	201	Black Hawk	Combined 8.5	12.3	None
AF040	5257	M	U	63	5'6"	142	Black Hawk	Combined 8.5	9.7	L2, End Plate Fracture
AF041	5343	M	U	54	5'10"	165	Black Hawk	Combined 8.5	8.9	None
AF042	99	M	U	47	5'10"	155	Black Hawk	Combined 8.5	9.0	L4, Fracture Type Unknown; C1-C2 Separation
AF043	135	M	U	61	5'10"	147	Black Hawk	Combined 8.5	11.2	T6, T10, Fracture Type Unknown; Multiple Anterior Rib Fractures
AF044	140	M	U	54	5'11"	174	Black Hawk	Combined 8.5	12.2	T12, Fracture Type Unknown; Multiple Anterior Rib Fractures



*Robert A. Denton, Inc., Rochester, Michigan, Model 1000

Capacities: F_x , F_y 3000 lb; F_z 5000 lb

M_x , M_y 3000 in.-lb; M_z 6000 in.-lb

Figure 14. Part 572 pelvic segment with lumbar spine and load cell assembly.

two series. The first series repeated four tests from the parametric test matrix conducted at CAMI. In the second series an attempt was made to duplicate test conditions for four cadaver tests conducted at Wayne State University. A summary of the test series is presented in Table 10, and a complete discussion of the research effort can be found in Reference 17.

TABLE 10. TEST MATRIX FOR MODIFIED ANTHROPOMORPHIC DUMMY SERIES

Test Description	Test No.	Comparable Test No.	Rate of Onset (G/sec)	Δv (ft/sec)	G	Modified Dummy Type	Percentile	E/A Seat	
								LL (G)	Pitch (Deg)
CAMI Rigid Seat Series	A81-121	A80-025	530	42.4	14.1	Hybrid II	50	N/A	0
		026							
		027							
	A81-122	A80-028	510	42.5	13.8	VIP-95	95	N/A	0
		030							
		031							
CAMI Energy-Absorbing Seat Series	A81-123	A80-073	1060	44.1	39.7	VIP-95	95	14.5	+17
	A81-124	A80-053	1000	45.0	41.3	Hybrid II	50	14.5	+17
		054							
	A81-127	A80-081	1160	52.4	48.0	Hybrid II	50	14.5	+34
WSU Energy-Absorbing Seat Series	WSU-156	AF021	1990	40.5	36.7	Hybrid II	50	14.5	+34
	WSU-157	AF037	1890	42.1	38.0	Hybrid II	50	11.5	+34
	WSU-159	AF020	1710	41.1	35.7	Hybrid II	50	14.5	+17
		AF025							
	WSU-160	-	1610	40.9	36.4	Hybrid II	50	11.5	+17

4.0 EQUIPMENT AND TEST PROCEDURES

In order to isolate the effects of the variables being tested at various facilities and in different tests at those facilities, standardized equipment and procedures were employed throughout the program. The seats and dummies used in the program are discussed in this chapter, along with procedures for conducting the tests and achieving standard input conditions.

4.1 EQUIPMENT - SEATS

Most of the testing was accomplished using an energy-absorbing helicopter crewseat, but some tests were conducted with a rigid seat, in order to isolate the effects of dummy type and size. Both of these seats and associated hardware are discussed below.

4.1.1 Rigid Seat

In order to provide data for dummy comparison, testing was conducted at the FAA Civil Aeromedical Institute (CAMI) with each of the dummies in a rigid seat. As shown in Figure 15, the seat pan and back form a right angle with respect to each other. No cushions were used, and the 1-in.-thick plywood seat pan was supported by a six-axis load cell. The four-point restraint system used automotive-type nylon webbing. In order to impose a vertical (+G_z) acceleration on the dummy, the vertical (z) axis of the seat was aligned with the velocity vector; in other words, horizontal for the sled impact.

4.1.2 Energy-Absorbing Helicopter Seat

The majority of testing was conducted with a production UH-60A Black Hawk crewseat, which has energy-absorption capability in the vertical direction and is described in Reference 18. As shown in Figure 16, the seat frame includes two vertical guide tubes, which serve as races for the linear bearing, bucket-carrier assemblies. Each bearing assembly contains four contoured rollers located at 90-degree increments to surround the guide tube, thus permitting low-friction translation of the bucket along the axis of the guide tube.

Two energy absorbers that restrain the seat bucket in its vertical position are attached at the upper crossmember of the frame and at the yoke mounted on the vertical adjustment mechanism, which is attached to the seat bucket back. Vertical inertial crash loads force the seat bucket down the guide tubes against the resistance of the energy absorbers, producing an energy-absorbing stroke in that direction. The energy-absorbing devices used on this seat are tensile, inversion-tube type.

18. Desjardins, S. P., et al., Crashworthy Armored Crewseat for the UH-60A Black Hawk, paper presented at 35th Annual National Forum of the American Helicopter Society, Washington, D.C., May 1979.

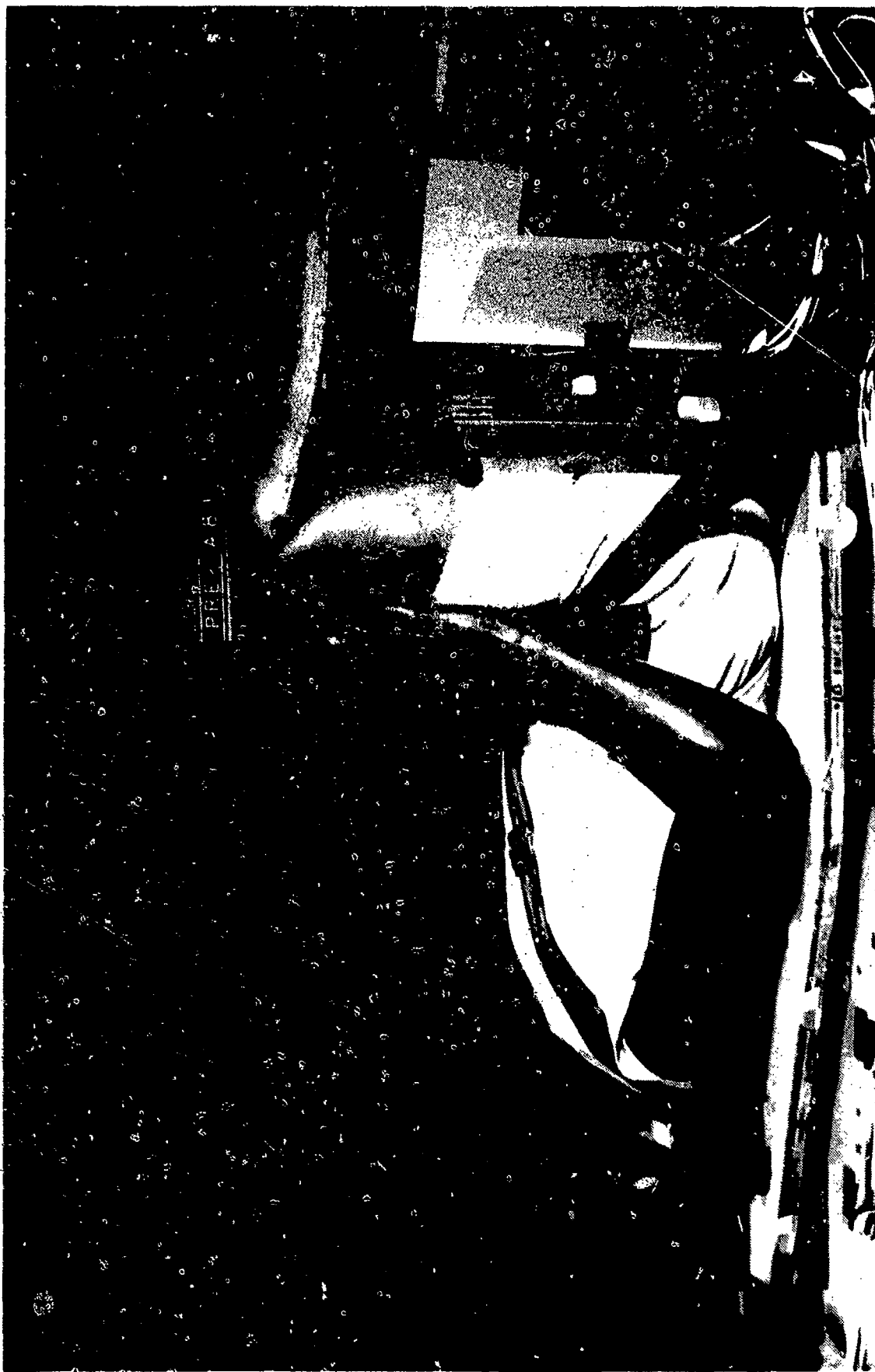


Figure 15. CAMI rigid seat (with VIP-95 dummy in place).

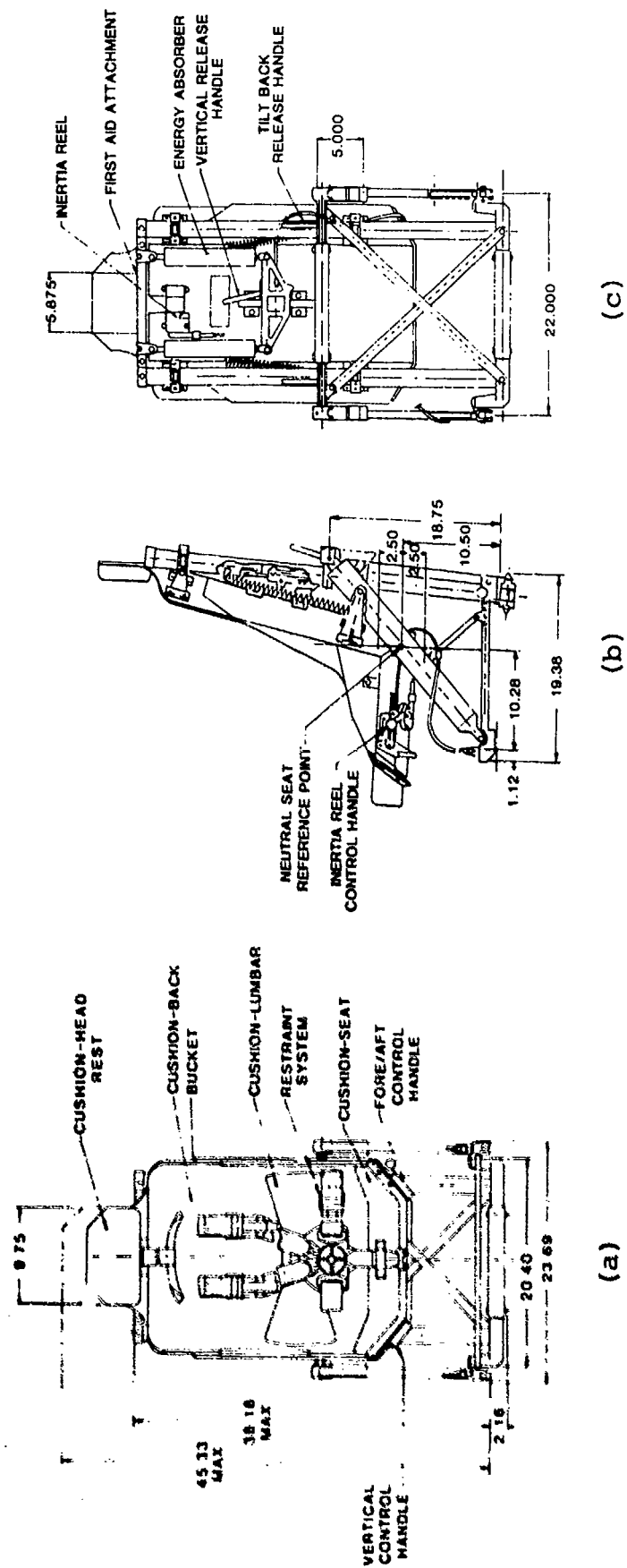


Figure 16. UH-60A crewseat assembly.

The interface between the bucket and the yoke is provided by a T-track mounted on the back of the seat bucket, a sliding fitting with T-slot (through which the T-track passes) attached to the yoke, and a spring-loaded adjustment locking pin. Withdrawal of the pin releases the attachment between the seat bucket and frame so that the seat weight is carried by counterbalance springs, which were removed for all testing on this program. Five inches of vertical position adjustment are provided by this mechanism.

Longitudinal adjustment is achieved by releasing spring-loaded adjustment locking pins in each of the front track fittings, permitting 5 in. of fore and aft adjustment.

The bucket of the production seat, in its operational configuration, provides ballistic protection and structural support for the bottom, back, and sides of the thighs of the occupant. The operational bucket is constructed of a lightweight, 13-ply laminate of Kevlar 49 material faced with extremely hard boron carbide ceramic tile in those areas requiring ballistic protection. A layer of nylon spall shield is used to cover the boron carbide and all cut edges of the Kevlar. Holes for attachment of such items as frame fittings are drilled through the Kevlar, and provisions for attachment are included in the tile. For frame attachment fittings, the boron carbide is cut away, allowing the brackets to be seated directly on the Kevlar. The lap belt anchors, inertia reel, and adjustment handles are seated against aluminum standoffs, bonded to the Kevlar through cutouts in the boron carbide. These support the compressive load of the attachment without increasing the possibility of cracking the brittle ceramic. For the parametric test program steel plates were used instead of the boron carbide ceramic tile on the bucket to permit adjustment of the seat movable weight. Plates were bolted to both the back and bottom of the seat bucket, located so as to maintain the position of the seat center-of-mass at the same point as in the operational configuration with armor.

4.1.2.1 Cushions. The standard bottom cushion used in the UH-60A crewseat bucket is a unique design that maximizes comfort and crash safety. The surface of the cushion is contoured to distribute load over the greatest buttocks area, in order to minimize any local concentration of loading that would cause discomfort. The cushion base is made from foamed polyethylene, and the contour is lined with a thin layer of temperfoam to distribute local loads and maximize comfort. This material is a loading rate sensitive polyurethane foam to help develop a more rigid, but yet comfortable, link between the occupant and the seat bucket. A final layer of reticulated polyurethane foam is provided for both load distribution and thermal comfort. The cushion is enclosed in a protective covering of fire-retardant, open-weave nylon material. Also, provisions are made to allow fore and aft circulation of air that can pass through the open-celled, reticulated foam for cooling purposes. Air circulation is natural, not forced.

The back and lumbar support cushions are of typical design, using standard upholstery foam and open-weave nylon covers. The headrest cushion is formed of temperfoam for cushioning of head impact.

A new bottom cushion core was inserted into the nylon cover for each test. Back cushions and headrest cushions were reused throughout the test series.

In the test matrix, three nonstandard cushions, intended to have force-deflection characteristics substantially different from the production cushion were used. Both a rigid bottom cushion, made of foamed polyurethane, and a soft cushion, contoured from upholstery foam, were sized to produce approximately the same seating position for the dummy as with the production cushion. Also, three slabs of furniture foam having an undeformed thickness of nine inches were used as a cushion to determine the effect of relative motion between the occupant and seat pan allowed by soft, thick cushions.

4.1.2.2 Energy Absorbers. Each of the energy-absorbing devices on the production seat exerts a constant load during stroking. As illustrated in Figure 17, these devices make use of the inversion of a thin-walled ductile aluminum tube. As required by Reference 4, the total energy absorber load is determined by multiplying a given load factor times the total moving weight of seat and occupant. For the UH-60A Black Hawk, the weight of the stroking part of the seat is 60.6 lb. Adding the effective weight of the 50th-percentile Army aviator, 139.0 lb, the total movable weight is 199.6 lb, which when multiplied by a load factor of 14.5 gives a total dynamic stroking load of 2,894 lb. Dividing the dynamic stroking load by a rate sensitivity factor of 1.2 gives a total design static load of 2,412 lb. The static stroking load for each of the two energy absorbers is then 1,206 lb.

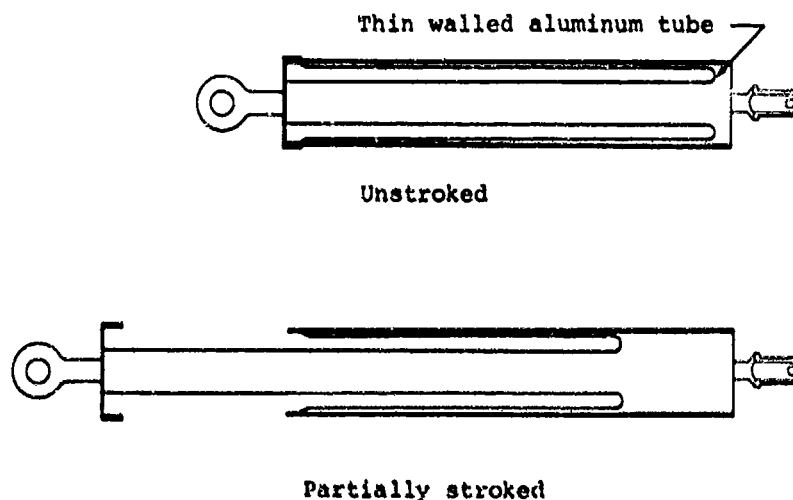


Figure 17. Inverted-tube energy absorber.

For a given aluminum alloy, the stroking load of the energy absorber is determined by the diameter and wall thickness of the inverting tube. For two of the tests conducted at CAMI, energy absorbers with reduced limit loads were needed. Using load factors of 11.5 and 8.5 gave static stroking loads of 956 and 707 lb, respectively. Devices with these limit loads were manufactured and used at CAMI in tests A80-055 and A80-075.

For two of the tests at CAMI and one test at NADC, it was desired to use energy absorbers with an increasing ramp force-deflection characteristic. The desired characteristics shown in Figure 18 were approximated in the energy absorber design by grinding a gradual taper on the outside diameter of the aluminum inversion tube.

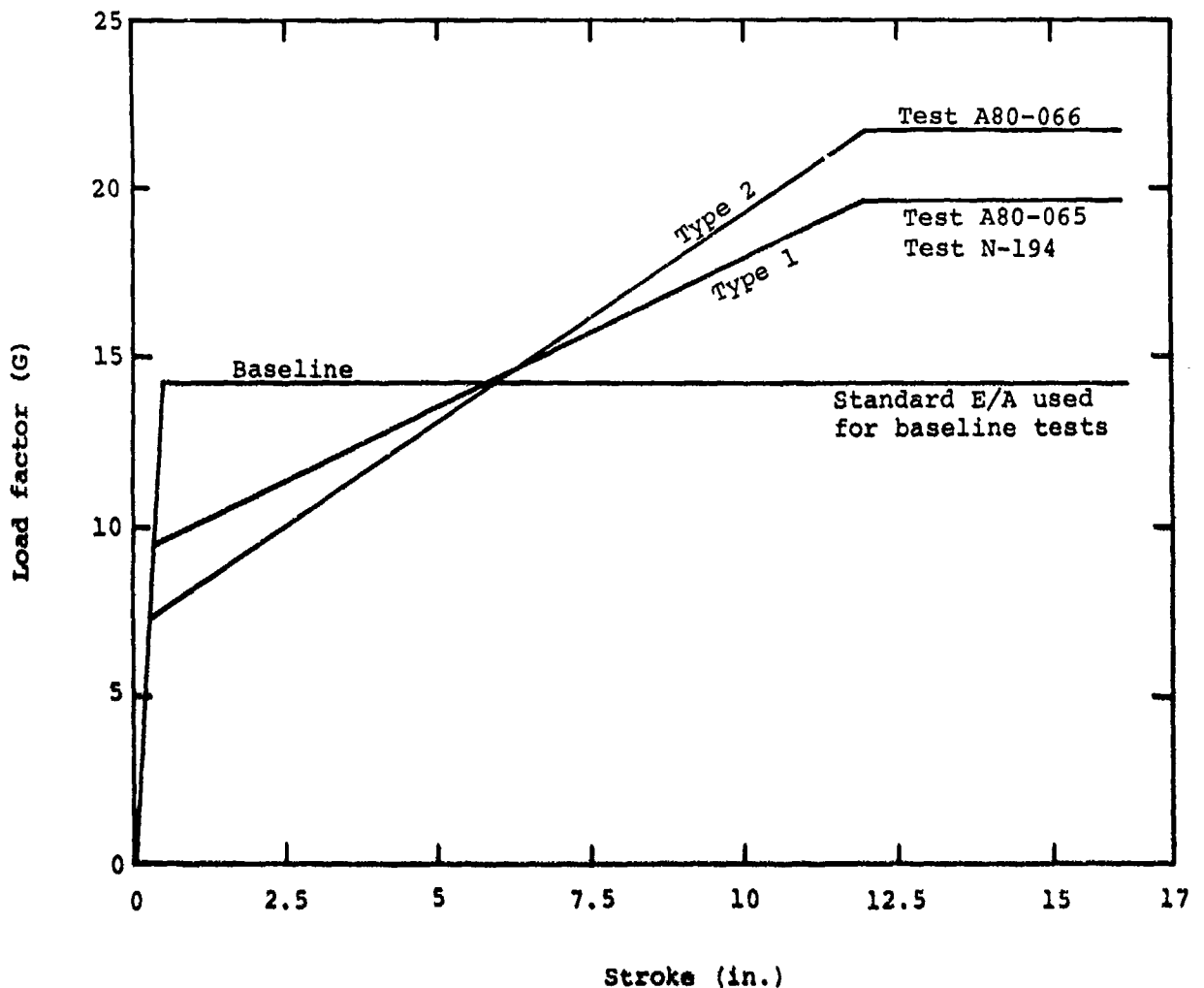


Figure 18. Nominal load-stroke characteristics of ramped energy absorbers used in parametric test program.

4.1.2.3 Restraint System. The restraint system used in the UH-60A Black Hawk crewseat is a five-point system, which includes a lap belt tiedown strap. As illustrated in Figure 19, adjusters are provided in both shoulder straps and both lap belt straps, and the buckle is a rotary-release type, backed by a comfort pad. Characteristics of the low-elongation webbing are presented in Table 11.

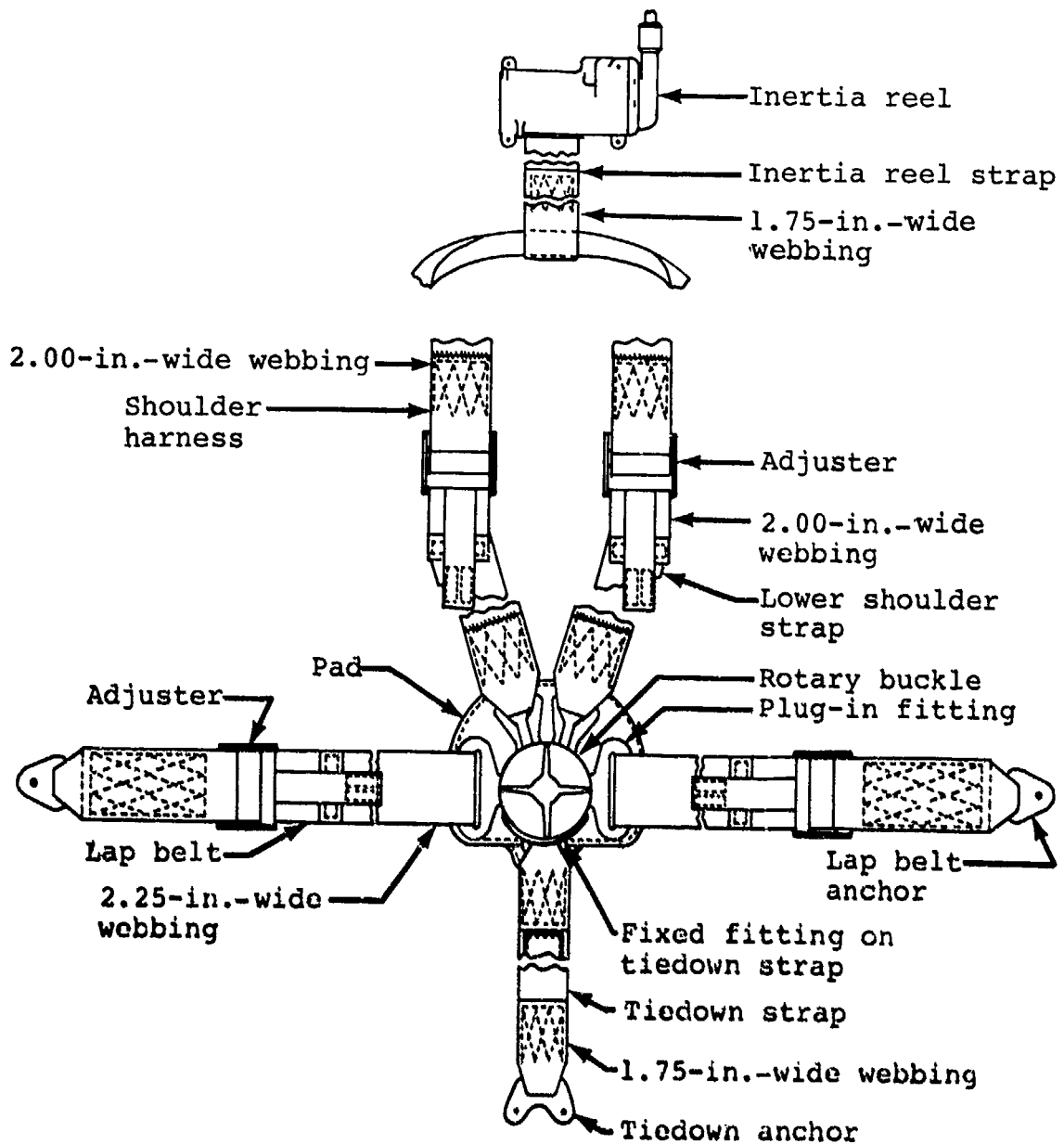


Figure 19. Aircrew restraint system.

TABLE 11. RESTRAINT SYSTEM WEBBING

Component	Thickness (in.)	Width (in.)	Average Elongation at Design Load (Percent)	Ultimate Load (lb)	Design Load (lb)
Lap Belt	0.057	2.25	7.5	8880	4000
Tiedown	0.057	1.78	7.5	6980	3000
Shoulder Straps	0.057	2.03	7.0	7800	4000

4.2 ANTHROPOMORPHIC DUMMIES

The Aircraft Crash Survival Design Guide (Reference 7) recommends that for aircraft seat testing a dummy conforming to Part 572 (Reference 19) specification should be used. All of the modern anthropomorphic dummies have been designed for automotive impact testing and not for accurate response to vertical impact. The spinal column, which is a critical region of human tolerance to aircraft crash loading, has been designed in the Part 572 dummy to simulate response to -G_x loading rather than the more critical +G_z loading seen in aircraft accidents. However, the reinforced rubber cylinder, used as the lumbar spine in this dummy, permits more consistent positioning than the steel ball-and-socket configuration used in some other dummies. Instability in the latter type could affect the response of the upper torso with concomitant penalties on test repeatability. Another advantage of the Part 572 dummy for aircraft seat testing is a humanlike pelvic structure, which should result in load distribution on the cushion close to that for a human. Finally, if the results of tests conducted at different facilities are to be compared, standardization of dummies and test facilities is mandatory, and the Part 572 dummy is the only truly standard dummy.

For these reasons, an Alderson Hybrid II dummy built to the Part 572 specification was selected for use in the baseline test configuration at all facilities, and it was the only dummy used in the NADC and Simula tests. At CAMI, tests were conducted using all six of the dummy designs listed in Table 4. The 95th-percentile dummy most closely resembling the Part 572 design is the Alderson VIP-95 with an elastomeric lumbar spine, shown as dummy code 4 in

19. Code of Federal Regulations, "Anthropomorphic Test Dummy," Title 49, Chapter 5, Part 572, Federal Register, Vol. 38, No. 62, April 2, 1973, pp. 8455-8458.

Table 4. It was one of these 95th-percentile dummies that was selected along with a Hybrid II for installation of a six-axis load cell in the lumbar region for the related modified dummy test program described in Chapter 3.

In order to eliminate the effects of dummy dynamic response, a rigid block weighing approximately 140 lb was fabricated of epoxy with steel weights located to position the center of mass at 10 in. above the seat pan and 10 in. forward of the seat back. This corresponds approximately to that of the seated 50th-percentile dummy. This block, secured by a restraint system, is shown in Figure 20.

4.3 ANALYSIS OF ACCELERATION PULSE

The rate of onset (RO) of the input acceleration pulse at each facility was determined using a procedure illustrated in Figure 21 (Reference 20) and outlined as follows:

- Locate the calibration baseline.
- Determine the maximum acceleration magnitude (G_p).
- Construct a reference line parallel to the calibration baseline at a magnitude equal to 10 percent of the peak acceleration (G_p). The first and last intersections of this line with the acceleration-time plot defines points 1 and 2.
- Construct a second reference line parallel to the calibration baseline at a magnitude equal to 90 percent of the peak acceleration. The first and last intersections of this line with the acceleration-time plot define points 3 and 4.
- Construct a second reference line parallel to the calibration baseline at a magnitude equal to 90 percent of the peak acceleration. The first and last intersections of this line with the acceleration-time plot define points 3 and 4.
- Some logic and practical judgment may be required for selection of the first and last intersections depending on the noise, structural or electronic, apparent in the data. Significant tendencies are important, not noise.
- Construct the onset line defined by a straight line through points 1 and 3.

20. Military Specification, MIL-S-9479, Seat System Upward Ejection, Aircraft, General Specification for, Department of Defense, Washington, D.C.

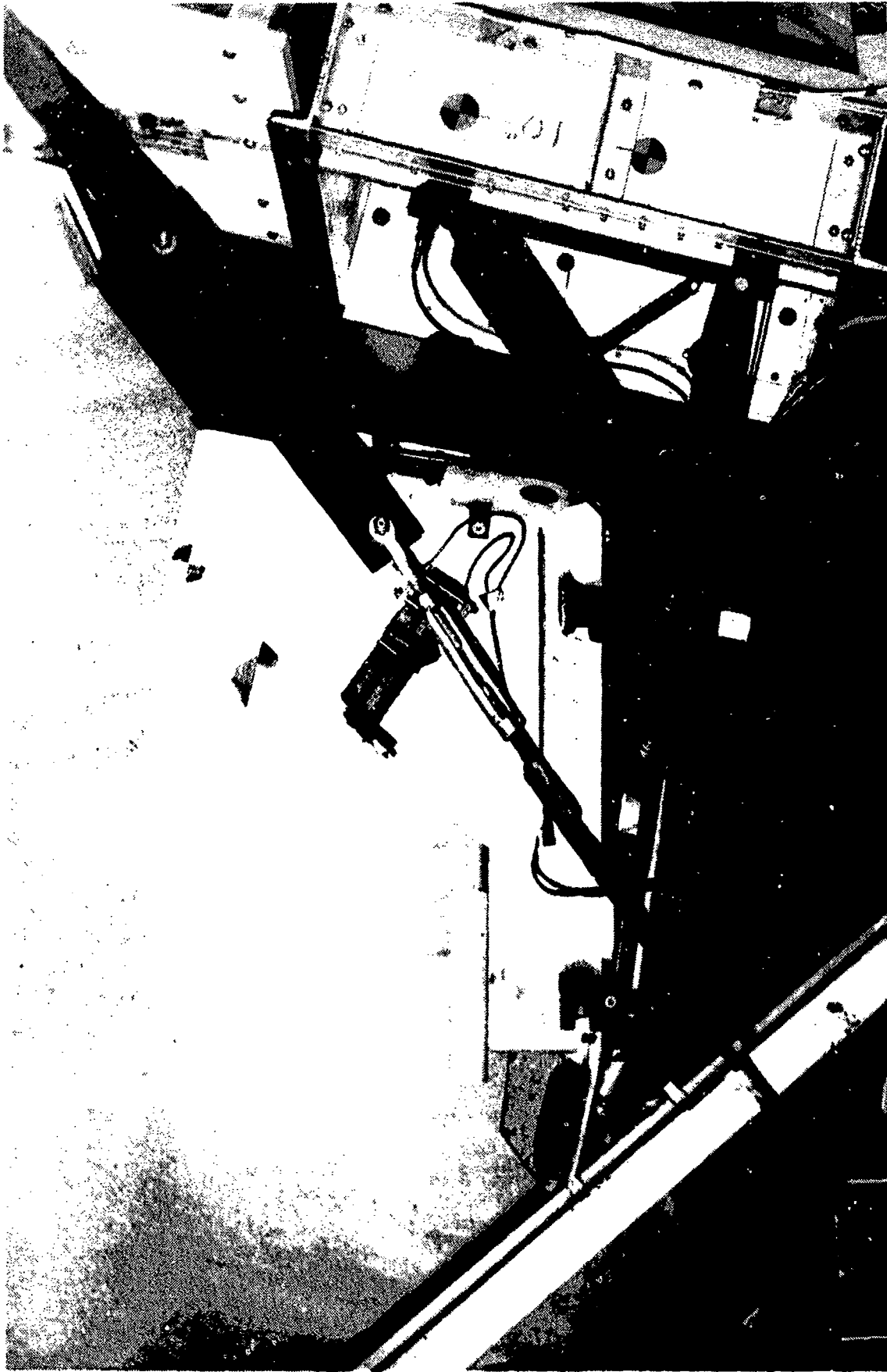


Figure 20. Rigid block in Black Hawk crewseat.

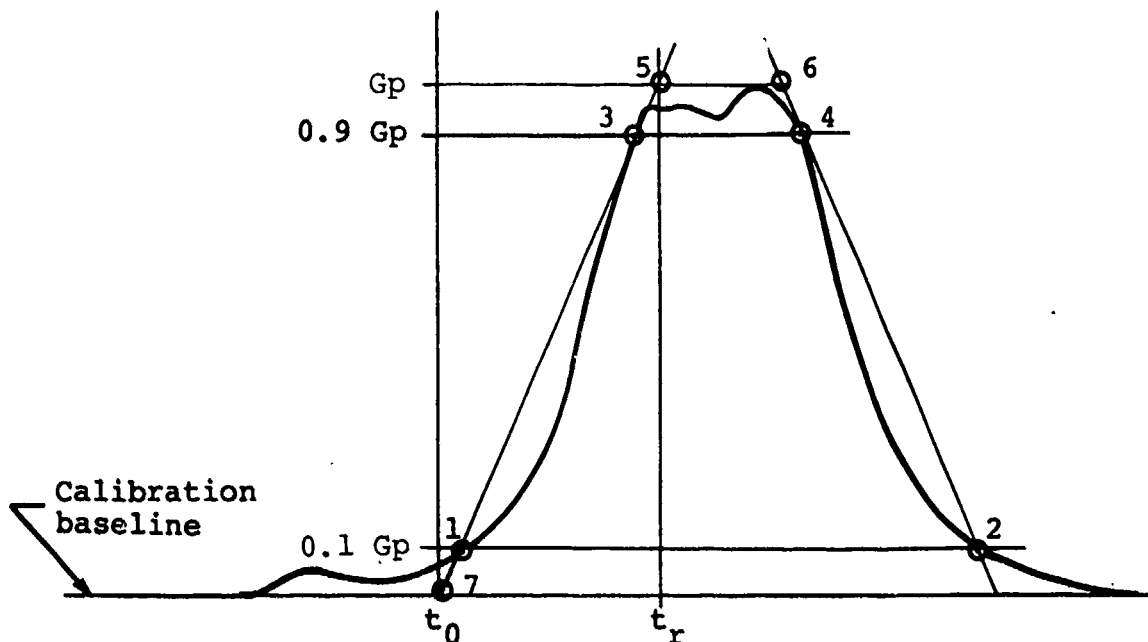


Figure 21. Graphic approximation example for rate of onset (from Reference 20).

- If desired, construct the offset line defined by a straight line through points 2 and 4.
- If desired, construct a line parallel to the calibration baseline, through the peak acceleration. The time interval defined by the intersections of this line with the constructed onset and offset lines (points 5 and 6) is the plateau duration.
- Locate the intersection of the constructed onset line with the calibration baseline (point 7). The time interval defined by points 7 and 5 is the rise time (t_r).
- The rate of onset is the slope of the onset line, G_p/t_r .

4.4 STANDARDIZED TEST PROCEDURES

Standardized procedures for orienting the seat, maintaining the seat, and positioning the dummy were followed at each facility.

4.4.1 Seat Orientation

Seat orientation varied depending on the use of a vertical drop tower or horizontal sled, as described below. The vertical configuration tests conducted by NADC and Simula oriented the seat so that the seat vertical (z) axis was pitched forward 13 degrees, as shown in Figure 22. Because for the Black Hawk crewseat the seat back tangent line is oriented 13 degrees from the vertical

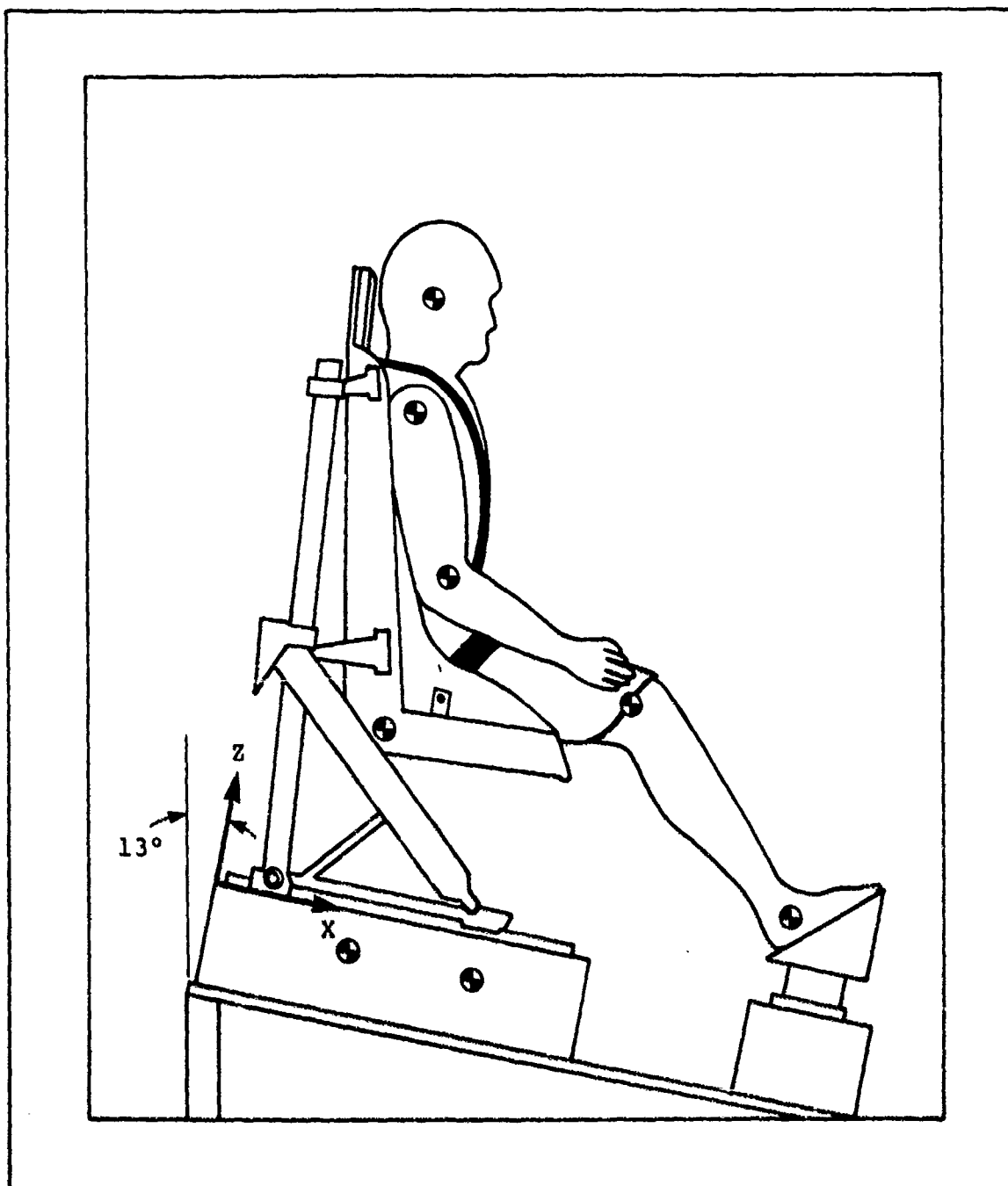


Figure 22. Vertical test, drop tower configuration.

axis of the seat, the seat back was parallel to the impact velocity vector for the vertical tests. At NADC, one test was conducted in a second "vertical" orientation, where the vertical seat axis was parallel to the velocity vector. Also at NADC, one test was conducted in a combined orientation with the seat pitched forward 30 degrees from the velocity vector and rolled 10 degrees.

4.4.1.2 Horizontal Sled Tests. For the tests conducted in the vertical configuration at CAMI and Wayne State University, the seat was pitched forward 17 degrees with respect to the velocity vector. The configuration for CAMI is illustrated in Figure 23. The first 13 degrees of pitch was provided to align the back tangent line with the horizontal surface of the sled, or parallel to the velocity vector. This was done to eliminate initial extension of the elastomeric spine that would be caused by an angle oriented downward to the seat back. The additional 4 degrees of pitch was added to counteract the 1 G of gravity that reduces the overturning moment on the dummy. Since during most of the tests the energy-absorbing mechanism on the seat is set to stroke at 14.5 G, the angle of the resultant acceleration was determined by establishing the tangent of the angle $1/14.5 = 0.069$, which is the arc tangent of 4 degrees. Thus, under stroking loads, the overturning moment on the dummy should be somewhat corrected for the 1 G of gravity, and the response should be similar to that for a seat in the upright-oriented position in a vertical drop. For the combined orientation tests on the horizontal sled facilities, the seat was pitched forward 34 degrees from the velocity vector and rolled 10 degrees in the seat coordinate system. The first 30 degrees of pitch was provided because the present qualification test requirements include a 30-degree forward pitch. The additional 4 degrees of pitch was added to approximately counteract the 1 G of gravity that would reduce the overturning moment on the dummy, as described above.

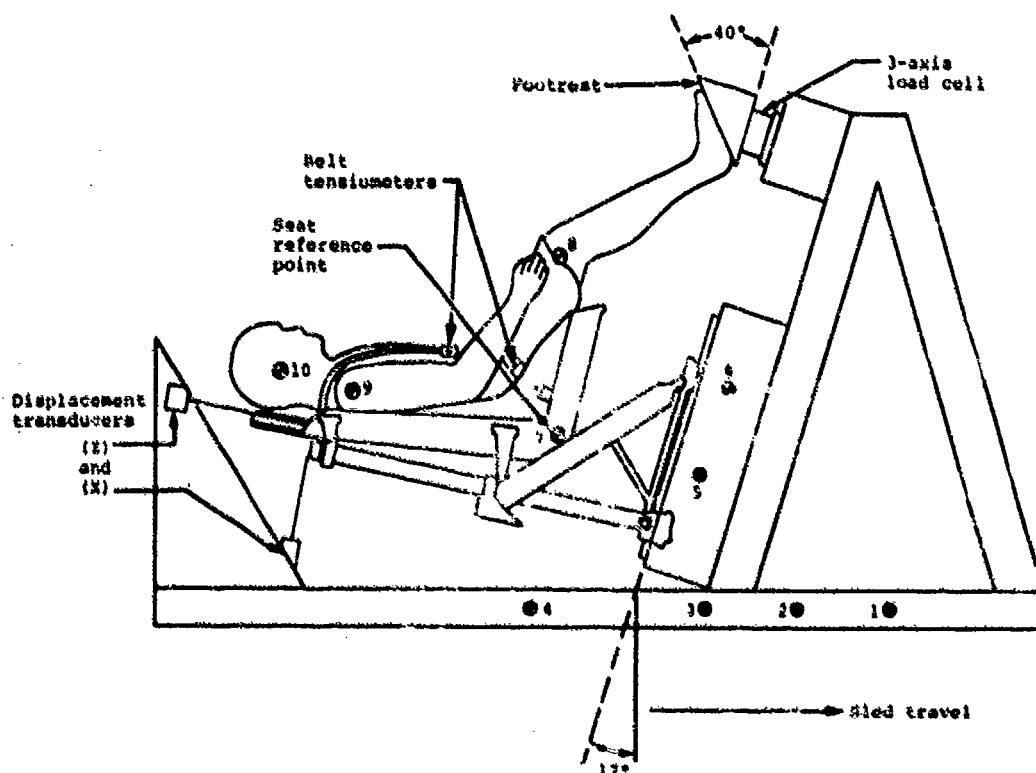


Figure 23. Vertical test, horizontal sled configuration (CAMI).

4.4.2 Seat Preparation

The UH-60A Black Hawk crewseat was locked in the top of the vertical adjustment range for all tests. For the tests using 50th-percentile dummies, the seat was locked in the middle of the fore and aft adjustment range and was moved forward or aftward for tests with a 5th- or 95th-percentile dummy, respectively. The seat was inspected for damage prior to each test, and the four linear bearing assemblies were replaced after every five tests. A new set of energy absorbers and a new seat bottom cushion were installed for each test.

4.4.3 Dummy Positioning

Photographic targets were placed on the outer (lateral) surface of each shoulder and knee and on each side of the head. These targets were used to locate the dummy in the seat and to facilitate analysis of motion picture data. A target was also placed on the side of the seat at the seat reference point. Targets were placed on the sled and floor fixture to assist in film analysis. Prior to each test, the dummy was positioned in the seat described as follows:

- The dummy joints were tightened until the frictional resistance in the joint would support the outstretched limb.
- Actual installation of the dummy in the seat varied somewhat among facilities; however, the following general technique was used:
 - The dummy's upper torso was folded forward around the hip joints until the torso touched or was as close as possible to the thighs.
 - The dummy was placed in the seat and its buttocks were pushed back as far as possible.
 - The dummy's legs were placed against the footrest simulating the rudder pedals and taped to the footrest.
 - The dummy's body was raised by rotating it again around the hip joints and pressing the dummy's back against the back of the seat. The rotation of the dummy's torso tended to push the dummy further back in the seat.
- The restraint system was fastened and adjusted as follows:
 - All fittings were inserted into the buckle with the inertia reel locked.

- The lap belt and shoulder straps were adjusted by pulling the free end of the straps toward the buckle. A 50-lb force was applied to the lap belt straps and a 30-lb force to the shoulder straps.
- A 7/32 Allen wrench was placed in the end of the inertia reel spool and 80 in.-lb of the torque was applied, tightening the inertia reel strap.
- The location of the targets from a selected reference point was measured on the seat for the first test and for each subsequent test using the same dummy. The position of the dummy was adjusted until the target locations were matched.

4.5 INSTRUMENTATION

Instrumentation used in the tests at CAMI is as follows:

	<u>Number of Channels</u>
<u>Accelerometers</u>	
• Seat bucket, triaxial (aircraft axes).*	3 (2)
• Seat bucket, vertical (parallel to the seat back tangent line) 1 channel (redundant).	1
• Chest, triaxial.*	3 (2)
• Pelvis, triaxial.*	3 (2)
• Head, triaxial.*	3 (2)
• Platform, vertical (parallel to velocity vector), 1 channel.	1
• Platform, vertical (parallel to velocity vector), 1 channel (redundant).	1
• Fixture, triaxial (aircraft axes).	3 (2)
<u>Loads</u>	
• Strain-gaged energy absorber clevises. 2 channels.	2
• Restraint system webbing tensiometers, 5 channels (as shown in Figure 24).	5
• Footrest loads (3 channels).*	3 (2)
<u>Displacement</u>	
• Vertical, parallel to guide tubes, attached to bucket on centerline, either below seat reference point for operation in retraction mode or near headrest for operation in extension mode.	1
• Vertical, parallel to guide tubes (redundant).	1

*Lateral measurements were not required for purely vertical (0° pitch, yaw, and roll relative to the velocity vector) tests.

- Longitudinal, perpendicular to guide tubes, attached at center of upper crossmember. 1
- Lateral, perpendicular to guide tubes, attached at top of guide tube.* 1 (0)

Impact Switch

- 1 channel for each data tape.

1

33 (26)

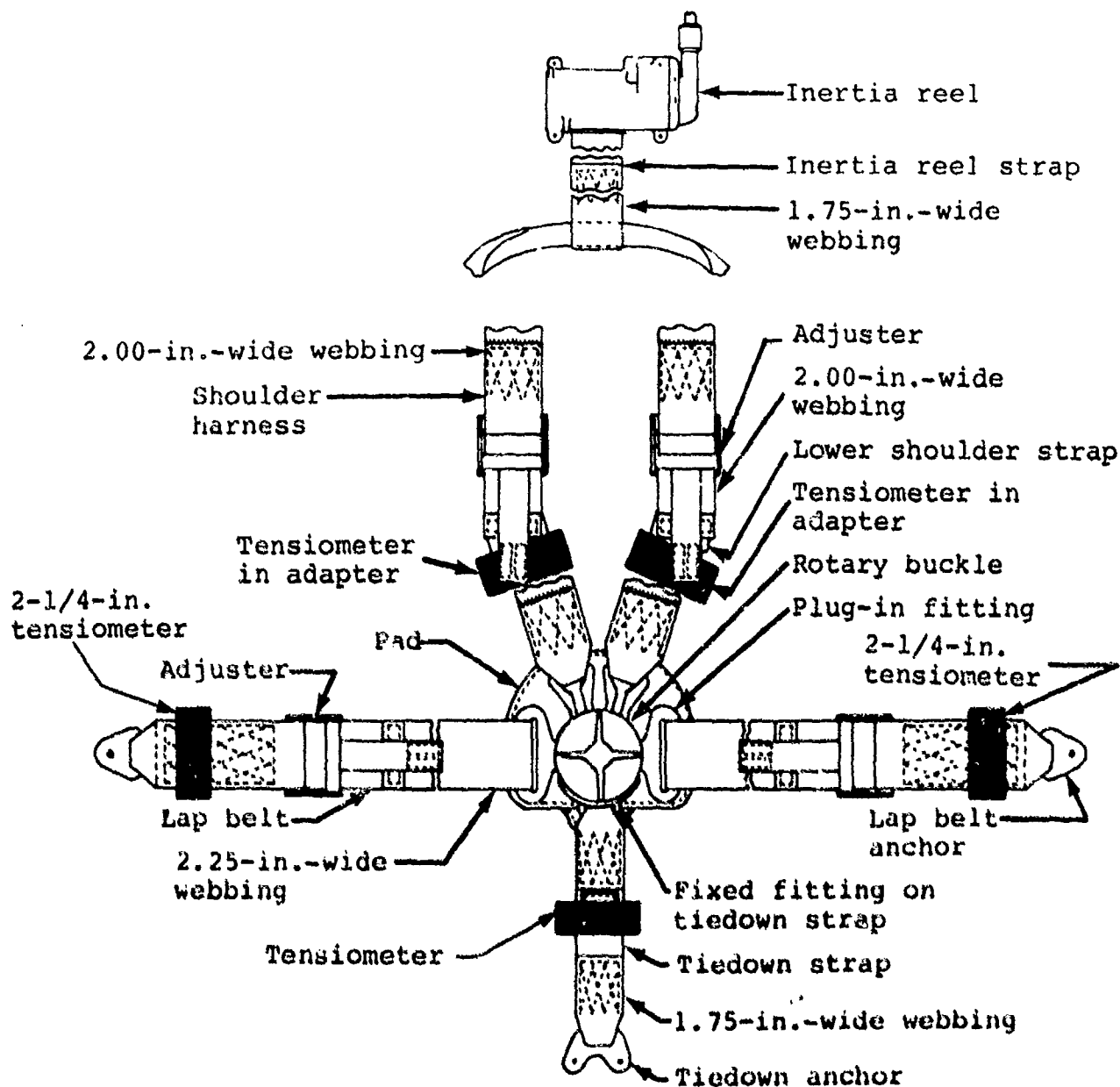


Figure 24. Tensiometer placement on occupant restraint system.

For dummy tests with rigid seats the following instrumentation was used:

Number
of Channels

Accelerometers

- | | |
|--|---|
| ● Chest, biaxial. | 2 |
| ● Pelvis, biaxial. | 2 |
| ● Head (translation and rotation). | 3 |
| ● Platform, vertical (parallel to velocity vector). | 1 |
| ● Platform, vertical (parallel to velocity vector), redundant. | 1 |

Loads

- | | |
|--|---|
| ● Restraint system webbing tensiometers. | 5 |
| ● Seat pan loads, triaxial. | 3 |
| ● Footrest loads, triaxial. | 3 |

Impact Switch

- | | |
|---------------------------------|----------|
| ● 1 channel for each data tape. | <u>1</u> |
| | 21 |

Photographic equipment was as follows:

Cameras

- High-speed 16 mm color, 500 frames/sec (minimum), 4 each (minimum).
- Real-time 16 mm color, 1 each (selected tests as required).
- Pre- and posttest 35 mm color, 1 each.

A triaxial accelerometer mount was located under the seat reference point (SRP) on the bottom of the seat pan. It was mounted so that the vertical transducer was parallel to the seat pan (which was pitched up 3 degrees from the horizontal axis) and so that the vertical transducer was located approximately 1.15 in. forward of the aft edge of the seat pan on its centerline. The redundant mount (vertical acceleration) was located on the seat back, oriented to measure acceleration in the direction of the back tangent line, which is pitched back 13 degrees from the vertical axis.

5.0 ANALYTICAL METHODS

Integral to a research effort to improve energy-absorbing seat design is the development of methods for evaluating those designs with comprehensive test criteria. In order to develop a basis for improving test criteria, a number of parameters were examined to determine their degree of correlation with relative test severity. During the sensitivity analysis, each parameter was used to assess the relative hazard between dynamic tests in a series, such as total velocity change. It is the objective of this research effort to determine which parameter has the greatest potential for reliably predicting relative test severity, and in the future it will be necessary to determine values for this parameter that provide an absolute measure of spinal injury potential.

The parameters examined in the sensitivity analysis are discussed below.

5.1 CURRENT CRITERION

The current seat evaluation criterion is based on the magnitude and duration of the seat pan vertical acceleration. As discussed in Section 2.2, the measure of absolute test severity is based on the work of Eiband (Reference 8). The tolerable region of acceleration magnitude and duration, shown in Figure 4, dictates that the seat pan acceleration not exceed 23 G for a duration greater than 0.006 sec. There are several significant deficiencies with this evaluation method. As noted in Section 2.3 on the interaction of the body and seat pan, the maximum seat pan acceleration occurs when the body is experiencing the least transmitted loads. Also, the seat pan acceleration is totally unrelated to upper torso flexion, which appears to be a major contributor to the typical anterior wedge compression failures of the spine. Finally, the current interpretation of MIL-S-58095(AV), as opposed to the intent of Eiband's work, assesses the pass/fail performance of a seat on the acceleration spike with the greatest duration at the 23-G level; but it is possible that multiple acceleration spikes raise the average acceleration well above the tolerable level. For example, in the parametric test program two baseline tests were conducted at CAMI with nearly identical input conditions. The seat pan accelerations for the two tests are shown in Figure 25. The performance of the seat in Test A80-053 would be judged as a borderline case while the same seat used in test A80-054 would most likely be judged as not meeting the requirements of MIL-S-58095(AV). The seat tested in A80-053 would be evaluated as a safer design because a higher-frequency oscillation occurred at the precise time to allow the seat pan acceleration to drop below 23 G. A seat with a characteristic high frequency seat pan oscillation, shown in Figure 26, can be rated as acceptable even though it is obvious that the average acceleration exceeds 23 G for a long duration.

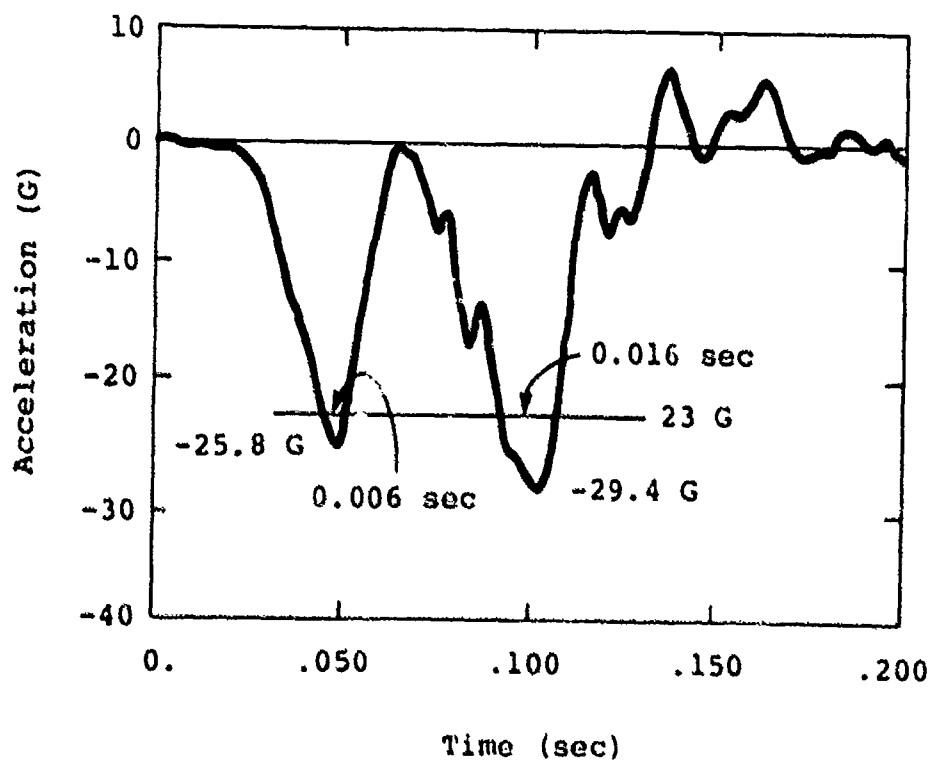
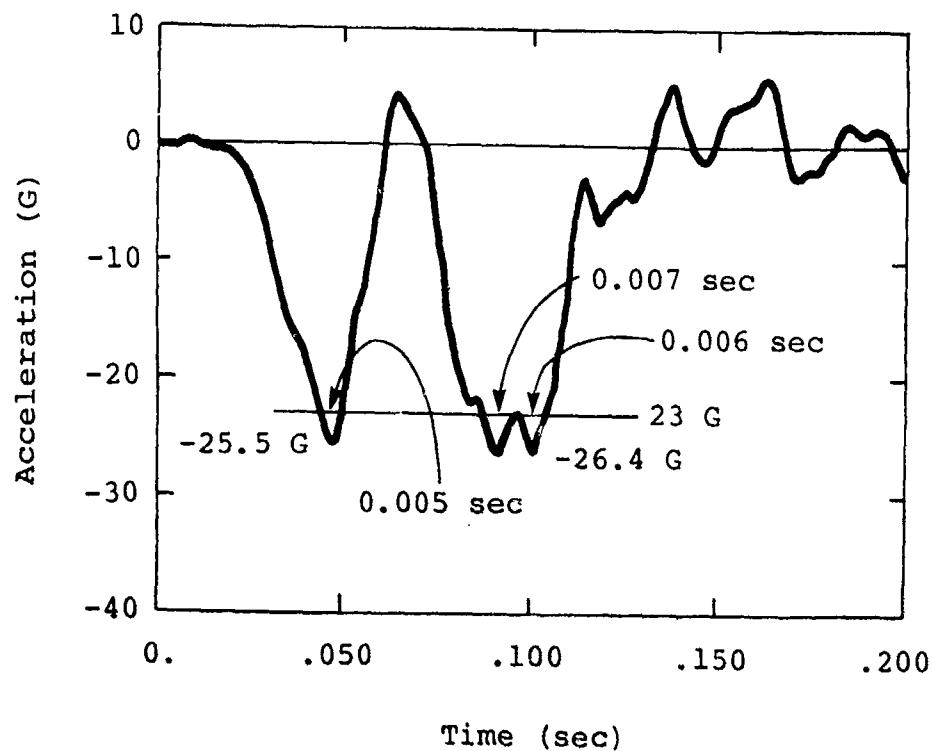


Figure 25. Vertical component of seat pan acceleration measured in two similar tests.

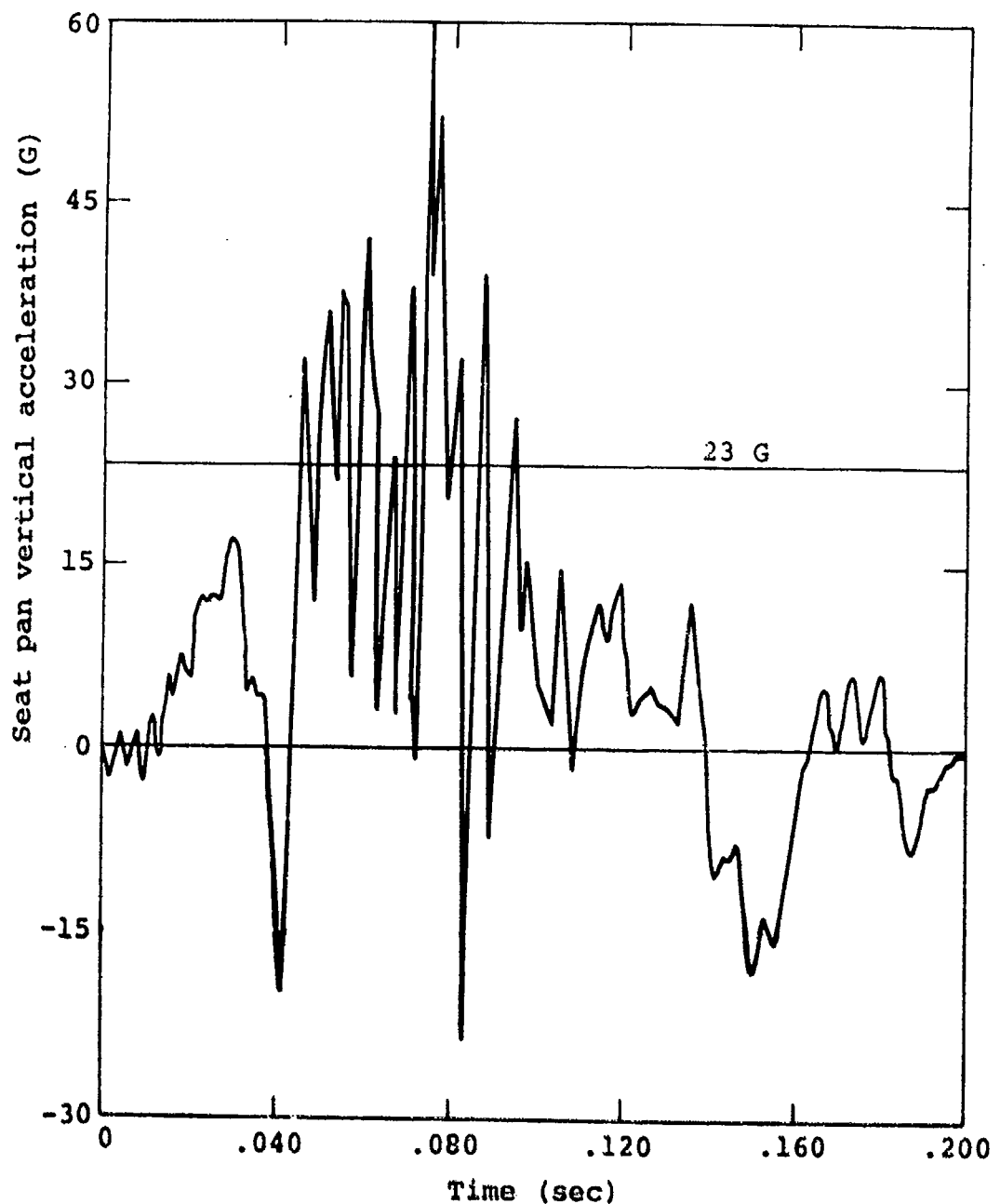


Figure 26. Seat pan vertical acceleration measured in a qualification test of a production energy-absorbing seat.

5.2 PEAK ACCELERATION

The maximum magnitudes of seat and body accelerations were tabulated extensively in the sensitivity analysis. The parameter is easily calculated and provides qualitative comparison between tests. For example, in the peak input acceleration series described in Section 6.1.1, both seat pan and pelvic z-axis acceleration magnitudes show a direct correlation to the peak values

of input acceleration. This example points out the positive and negative aspects of using peak accelerations as indicators of relative test severity. The parameter does show a definite trend in the input acceleration series; however, this may be an inconclusive trend because it fails to include the other very important quantity related to injury, i.e., time duration. It is possible that the measured peak acceleration on the seat pan or in the body occurs during an extremely short duration spike, and that the constant energy absorber limit load produces an average acceleration that is invariant to the magnitude of input deceleration. Without including additional information with this parameter, caution must be exercised in drawing conclusions. However, in combination with other indicators of test severity, as used in the sensitivity analysis, peak acceleration values can be very effective in predicting severity, especially in comparing tests where the input pulse, seat design parameters, and occupant type can be expected to produce similar response characteristics.

5.3 COMPRESSION OF BODY SEGMENTS

Axial loads in the spine are directly related to the amount of compression that occurs during the impact sequence. An attempt was made to calculate lumbar spine deflection by double integration of the relative z-axis accelerations in the pelvis and chest as described in the following equation:

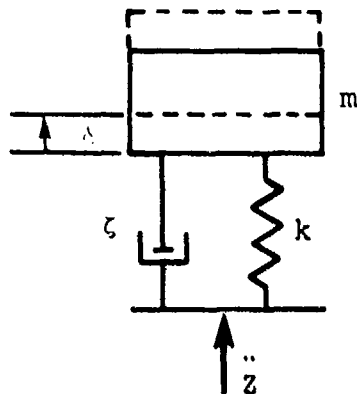
$$\delta \text{ spine} = \int_0^t \left[\int_0^t (a_{z_{\text{chest}}} - a_{z_{\text{pelvis}}}) dt \right] dt$$

Unfortunately, after several trials with the data from the three Simula energy-absorbing seat tests described in Table 8, it was apparent that there were insurmountable problems with this method. Any systematic errors in the data due to transducer calibration and data processing tend to be propagated during the integrations, and rotation of the body segments causes the accelerometer axes to become misaligned, resulting in a rapidly diverging function. Also, the only way to verify this parameter (without instrumenting the dummy to actually measure spinal deflection) was by comparison with film analysis, which has its own set of accuracy problems. Therefore, this parameter was not used in the sensitivity analysis.

5.4 DYNAMIC RESPONSE INDEX

A weighted impulse function of the seat or body segment acceleration was originally suggested as a candidate for determining test severity. This type of function has significant advantages over peak accelerations because it combines the effects of magnitude and duration to a certain degree depending on the weighting function.

The U.S. Air Force has done considerable work in developing a damped, single-degree-of-freedom model of the human upper torso for study of impact applied parallel to the spinal column (Reference 21). The model, shown in Figure 27, represents the spinal column (spring element) and body mass acting on it. The single-degree-of-freedom system is used to predict maximum spinal deflection and associated force within the spinal column for a given impact environment. Properties of model elements have been derived from existing data. Spring stiffness and breaking strength have been determined from cadaver vertebral segments, and the damping ratio has been calculated from measurements of mechanical impedance during vibration tests.



m = mass (lb-sec²/in.)
 δ = deflection (in.)
 ζ = damping ratio
 k = stiffness (lb/in.)
 \ddot{z} = acceleration input (in./sec²)

$$*DRI = \frac{\omega_n^2 \delta_{\max}}{g}$$

ω_n = natural frequency of the analog = $\sqrt{k/m}$ (rad/sec)

*Dynamic Response Index $g = 386 \text{ in./sec}^2$

Figure 27. Spinal-injury model (from Reference 21).

The equation of motion for this system is the second-order differential equation shown below.

$$\frac{d^2\delta}{dt^2} + 2\zeta\omega_n \frac{d\delta}{dt} + \omega_n^2 \delta = \ddot{z}$$

21. Stech, E. L., and Payne, P. R., Dynamic Models of the Human Body, Frost Engineering Development Corp. AMRL Technical Report 66-157, Aerospace Medical Research Laboratory, Wright-Patterson Air Force Base, Ohio, November 1969, AD 701383.

The solution of this equation, δ , is the spinal deflection of the simple, single degree-of-freedom model. This solution is an impulse-type function in that it takes into account the time period in which the acceleration is acting. The Dynamic Response Index (DRI) is proportional to the maximum value of spinal deflection and has the form:

$$DRI = \frac{\omega_n^2 \delta_{\max}}{g}$$

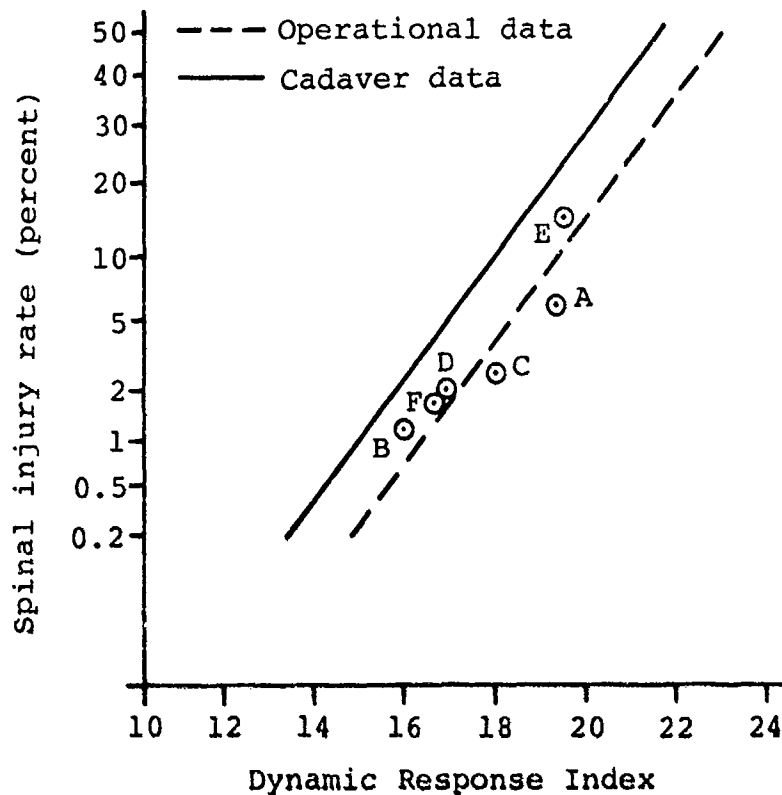
The Air Force has been successful in quantifying the injury potential for ejection seat injuries with the DRI. The probability of injury at various DRI levels is shown in Figure 28 (Reference 22). For evaluation of ejection seat injuries, the seat acceleration is used as input for the DRI equation. In general, ejection seats have an extremely rigid bucket compared with production energy-absorbing seats; therefore, both the seat pan and pelvic acceleration were tried as input to the DRI model for the sensitivity analysis. However, only the seat pan DRI appeared to be a consistent indicator of test severity, and because of the problems associated with instrumenting cadavers it was the only form of the DRI that could be calculated for the cadaver test series.

5.5 INSTRUMENTED ANTHROPOMORPHIC DUMMY

Initial work in the sensitivity analysis indicated that all of the candidate parameters for correlation to test severity and injury potential had significant deficiencies. It was concluded that the only expedient way to determine injury potential would be to actually measure the injury-causing loads and moments during the impact sequence. A test program was undertaken, as described in Section 3.5, to determine the feasibility of instrumenting a test dummy to measure these parameters. During the research effort, six-axis load cells were installed at the base of the lumbar spine of a Hybrid II dummy and the spine and neck of a VIP-95 dummy. The only possible installation scheme, without extensive redesign, placed the load cells in the accelerometer cavity below the spine.

A limited number of test results were collected in the program and proved the validity of this evaluation method. However, a number of technical difficulties were encountered which will have to be overcome before a dedicated test evaluation dummy can be built. Lumbar forces and moments measured in the two dummies differed from those predicted by the mathematical model described

22. Brinkley, J. W., and Shaffer, J. T., Dynamic Simulation Techniques for the Design of Escape Systems: Current Applications and Future Air Force Requirements, AMRL Technical Report 71-29-2, Aerospace Medical Research Laboratory; Wright-Patterson Air Force Base, Ohio, December 1971, AD 740439.



Aircraft type	Nonfatal ejections
A*	64
B*	62
C	65
D*	89
E	33
F	48

*Denotes rocket catapult.

Figure 28. Probability of spinal injury estimated from laboratory data compared to operational experience (from Reference 22).

in Section 5.6, particularly during significant forward bending (flexion) of the torso. A secondary load path, such as the "gut," is suspected to account for the differences.

If the concept of an instrumented anthropomorphic dummy is adopted as the criterion for seat performance, and there are many positive aspects to warrant this choice, two tasks will have to be completed before construction of the test device. A design evaluation of the deflection characteristics of the candidate dummy must be undertaken to ensure that the response imitates the human body, and that the load cell installation does not affect body

dynamics. Also, benchmark dynamic tests must be conducted, comparing cadavers and living human subjects with the standardized test dummy, to provide a quantitative assessment of the levels of loads and moments that represent significant injury potentials.

5.6. SEAT/OCCUPANT SIMULATION

Computer simulations of seat and dummy response were made using the SOM-LA program during the sensitivity analysis. As described in References 23 and 24, SOM-LA (Seat/Occupant Model-Light Aircraft) includes a lumped-parameter model of an aircraft occupant and an optional finite element seat model. Interface between the seat and occupant is provided by seat cushions and a restraint system consisting of a lap belt and, if desired, a single-strap or double-strap shoulder harness. A lap belt tiedown strap, or crotch strap, can be added for simulation of a full, five-point restraint system like that used on the UH-60A Black Hawk crewseat. The response of the occupant and seat can be predicted for any given set of aircraft impact conditions, including the initial velocity and attitude and the input acceleration.

Program SOM-LA includes a three-dimensional occupant model which may, at the option of the user, be restricted to symmetric plane motion. The three-dimensional model is comprised of 12 rigid links, connected by ball-and-socket and hinge joints and has a total of 29 degrees of freedom. The symmetric model was used in the simulations for the sensitivity analysis because it has deformable beam-type elements in the spine and neck, as shown in Figure 29. As illustrated in Figure 30, this model has 11 degrees of freedom, which include both axial and flexural deformation of the two spinal elements.

The same procedures are used in SOM-LA for calculating forces applied to both two-dimensional and three-dimensional occupants. That is, the three-dimensional geometry of the restraint system is used in determining its position and the forces it exerts on the ellipsoidal contact surfaces fixed to the torso segments of the occupant model. Thus, the two-dimensional model is actually

23. Laananen, D. H., Bolukbasi, A. O., and Coltman, J. W., Computer Simulation of an Aircraft Seat and Occupant in a Crash Environment, Volume I - Technical Report, TR-82401, Simula Inc., DOT/FAA/CT-82/33-I, Federal Aviation Administration Technical Center, Atlantic City Airport, New Jersey, September 1982.
24. Laananen, D. H., Coltman, J. W., and Bolukbasi, A. O., Computer Simulation of an Aircraft Seat and Occupant in a Crash Environment, Volume II - Program SOM-LA User Manual, TR-81415, Simula Inc., DOT/FAA/CT-82/3-I, Federal Aviation Administration Technical Center, Atlantic City Airport, New Jersey, September 1982.

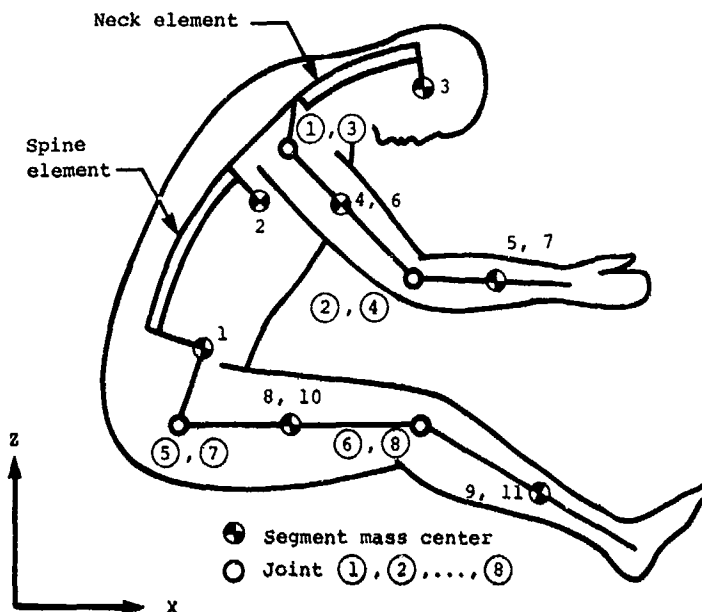


Figure 29. Eleven-segment (symmetric) occupant model.

a three-dimensional model restricted to plane motion, and no penalty is incurred by its use in simulating impacts for which occupant and seat motion is symmetric, as in most testing conducted on this program.

For cases where the finite element seat analysis is not desired, SOM-LA offers two options for modeling the seat. First, a rigid seat consists of two plane surfaces that remain fixed in the aircraft coordinate system; these surfaces support the cushions. A second option is the simulation of a guided energy-absorbing seat like the UH-60A Black Hawk crewseat with a two-degree-of-freedom model. The energy-absorbing stroke and rotational stiffness of the seat are represented. Input parameters for this simplified seat model include energy absorber force-stroke characteristics, movable seat weight, rotational stiffness characteristics, seat moment of inertia, and damping coefficients. For the simulations made on this program, the actual force-stroke characteristics for the energy absorbers were used.

Other input data for SOM-LA include the properties of the cushions and the restraint system webbing. The force-deflection characteristics for the UH-60A Black Hawk seat cushion, combined with the dummy buttocks, are shown in Figure 31. In Figure 32 are shown the approximate force-strain curves for the low-elongation polyester webbing used in the five-point restraint system. Also, the sled deceleration is approximated by up to 16 points in acceleration and time. As an example, the sled deceleration for the CAMI vertical baseline test with the modified 50th-percentile dummy is shown in Figure 33, and the approximate pulse used as SOM-LA input, in Figure 34.

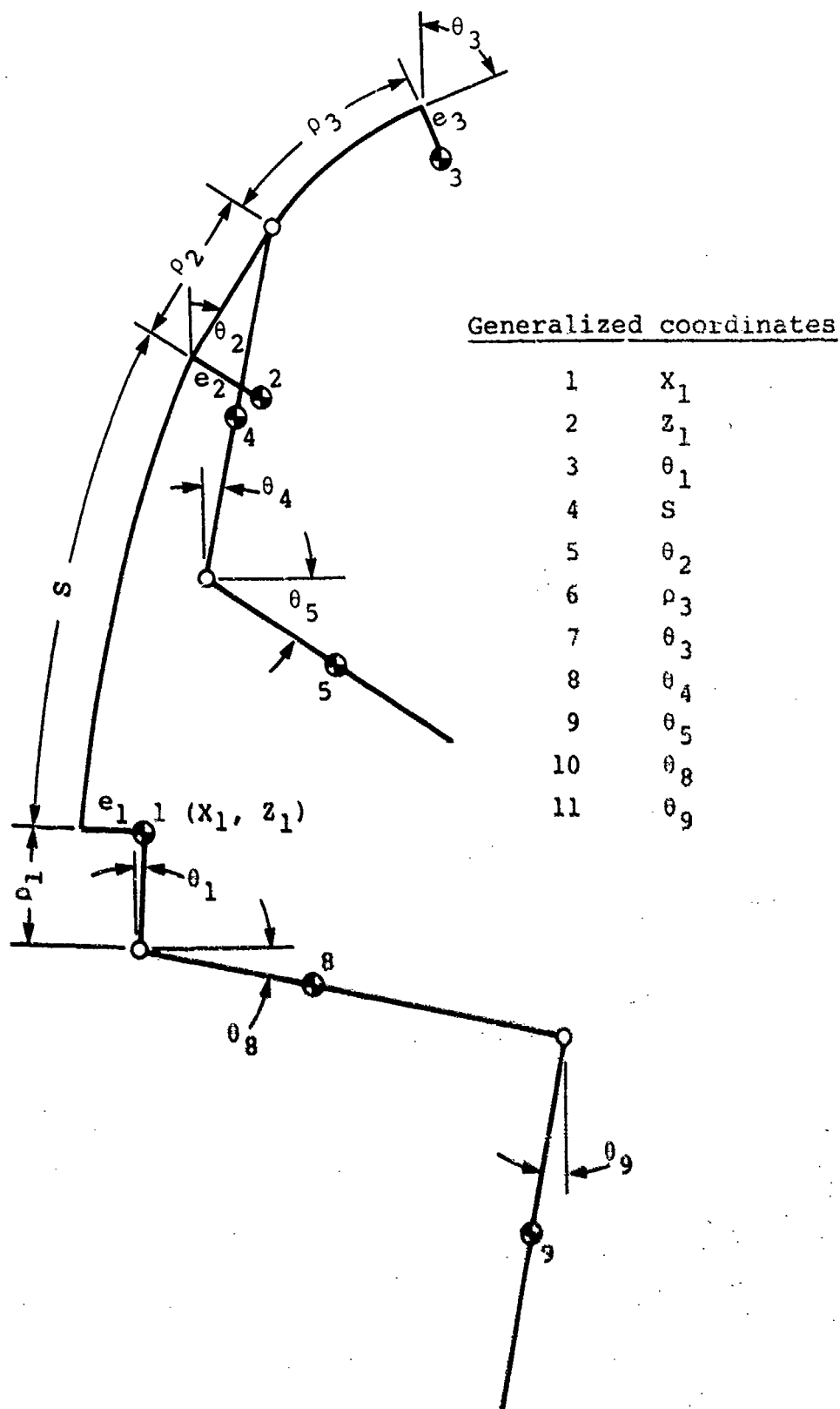


Figure 30. Generalized coordinates for symmetric occupant model.

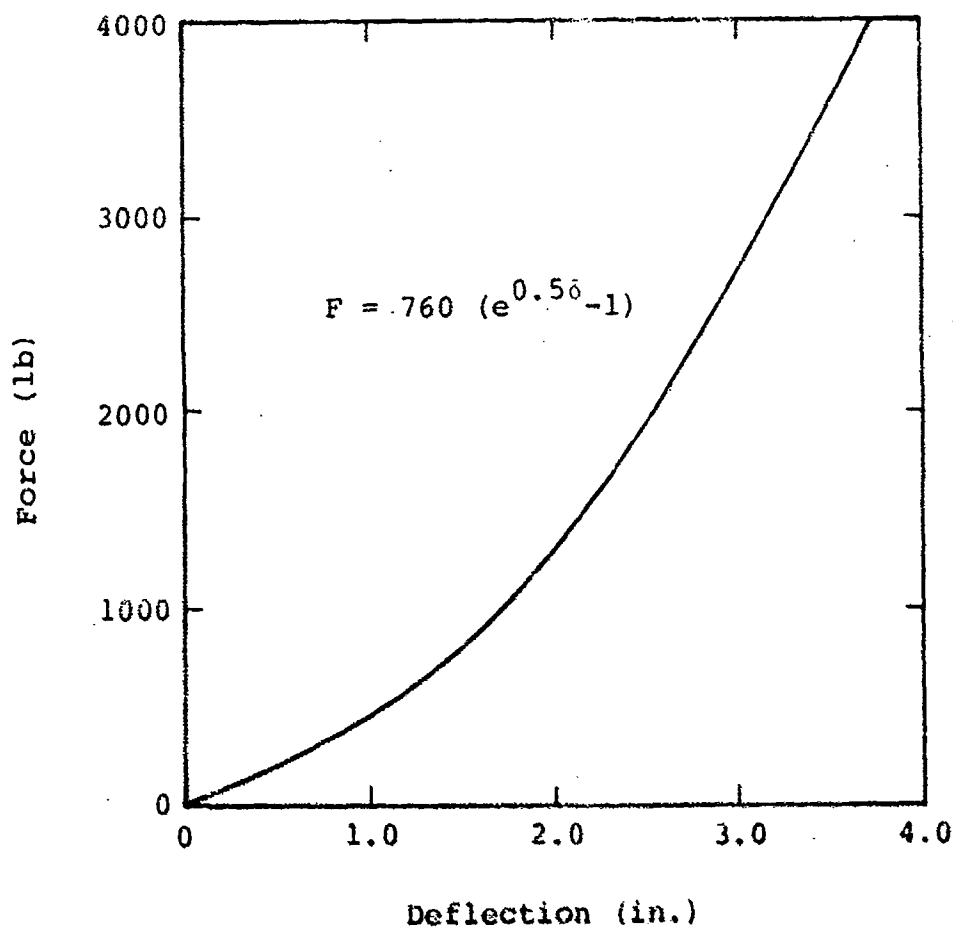


Figure 31. SOM-LA input properties for Black Hawk seat cushion.

Output data from SOM-LA include the following:

- Seat acceleration
- Occupant pelvis, chest, and head acceleration
- Lap belt, shoulder belt, and tiedown strap loads
- Energy absorber force
- Footrest force
- Spinal forces and moments
- Other injury criteria, such as severity indices and the Head Injury Criterion (HIC)
- Seat stroke

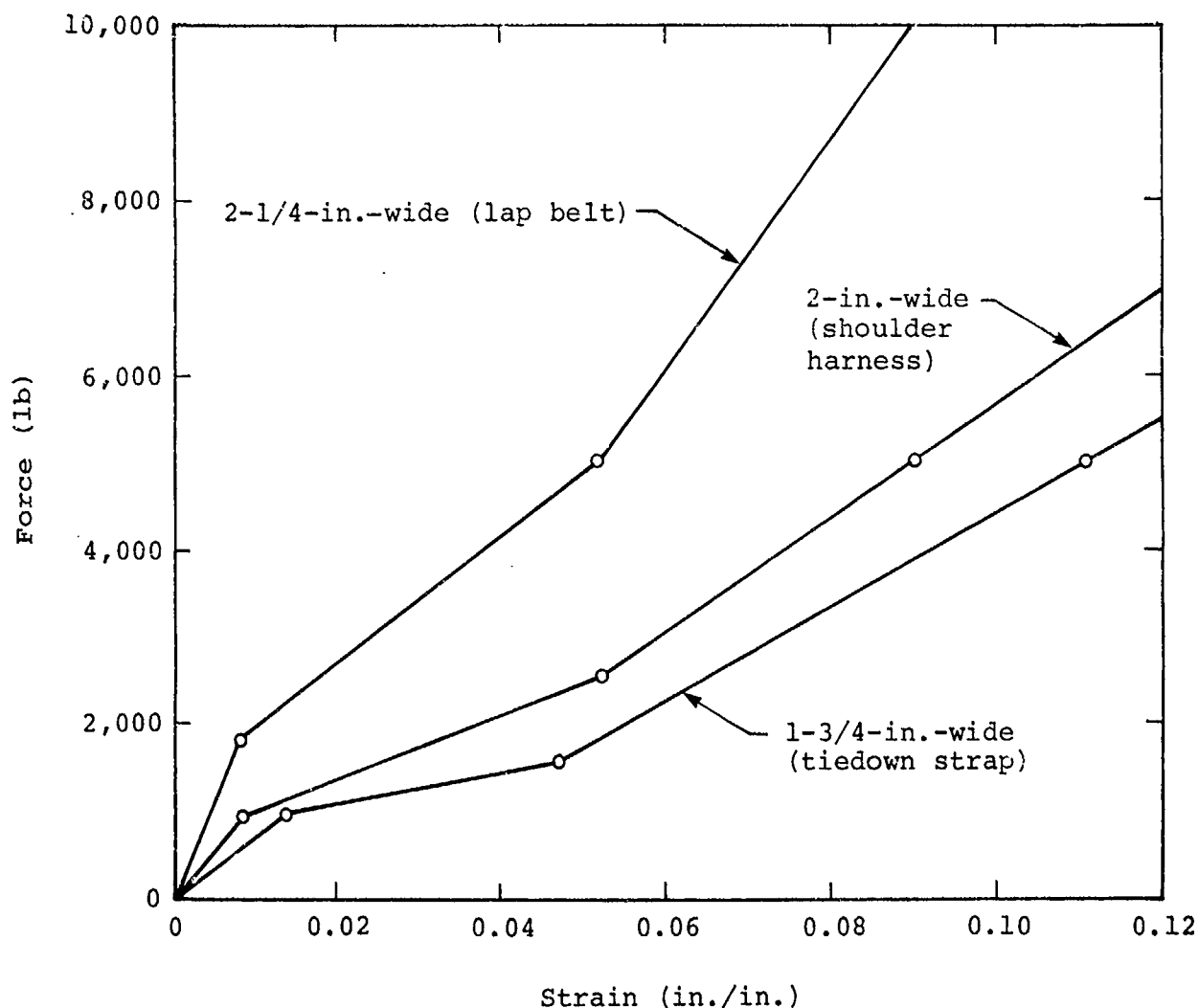


Figure 32. SOM-LA input properties for polyester restraint system webbing.

As an example, output data for SOM-LA simulation of CAMI test A81-124 are compared with test data in Figures 35-44. Computer predictions match the test data rather closely, with the exception of lumbar force and moment. As shown in Figure 43, the axial force predicted by SOM-LA is much higher than that measured in the test. The difference is attributed to a second load path in the dummy which is not present in the mathematical model. When the dummy torso bends significantly in flexion the "gut" segment, which is inserted between the pelvis and thorax, can support a significant compressive load, greatly reducing the axial force carried by the spine. Also, the flexural stiffness of the torso is altered, completely changing the moment carried by the spine, as evident in Figure 44.

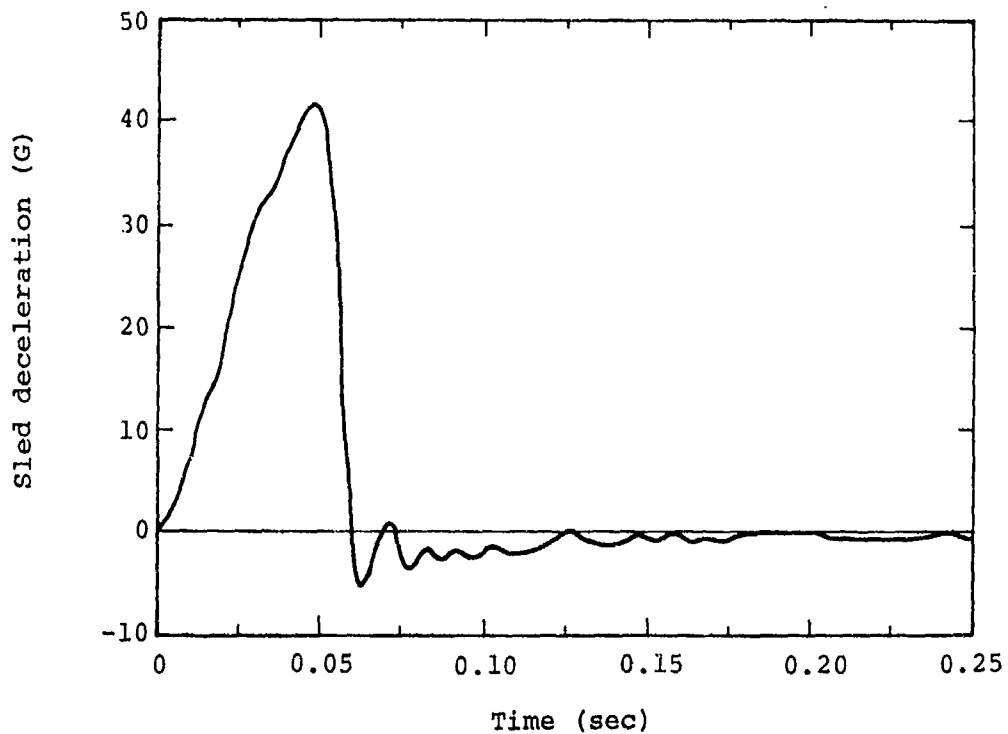


Figure 33. Actual sled deceleration pulse for CAMI test A81-124.

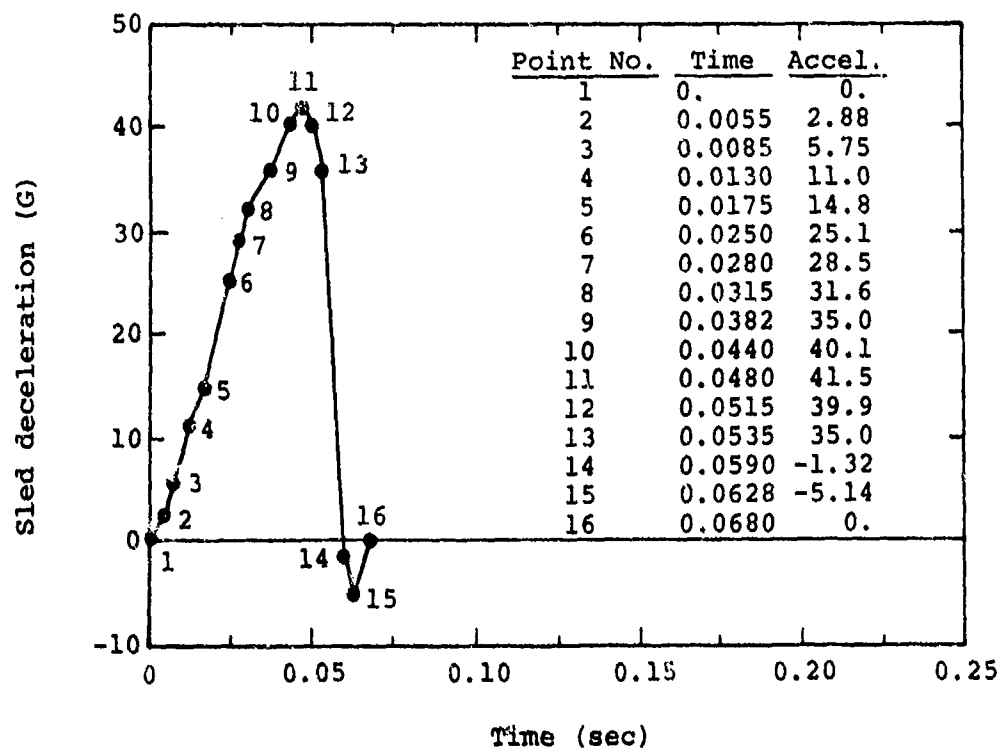


Figure 34. Approximate pulse input for SOM-LA simulation of test A81-124.

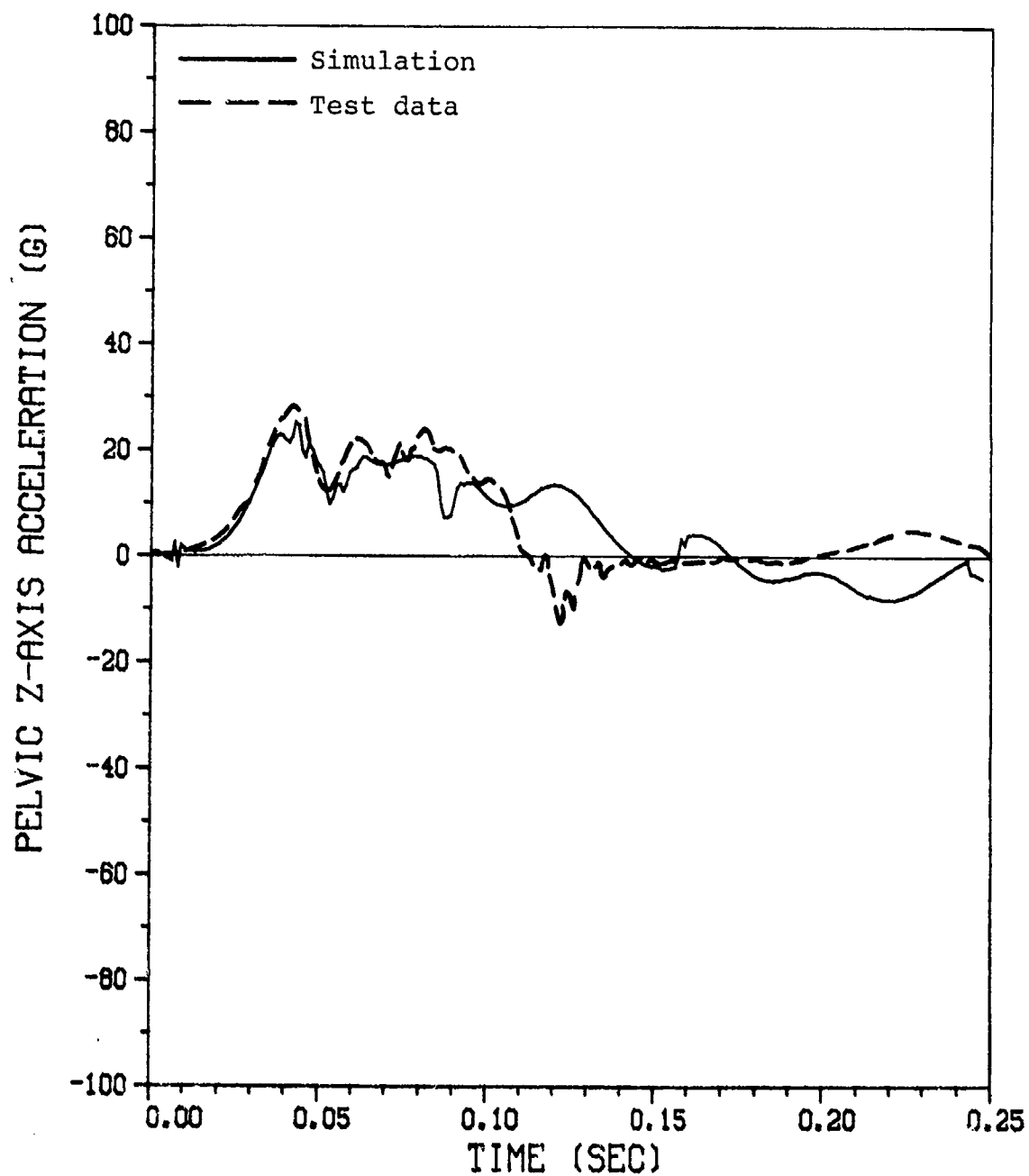


Figure 35. CAMI test A81-124, dummy pelvis z-acceleration.

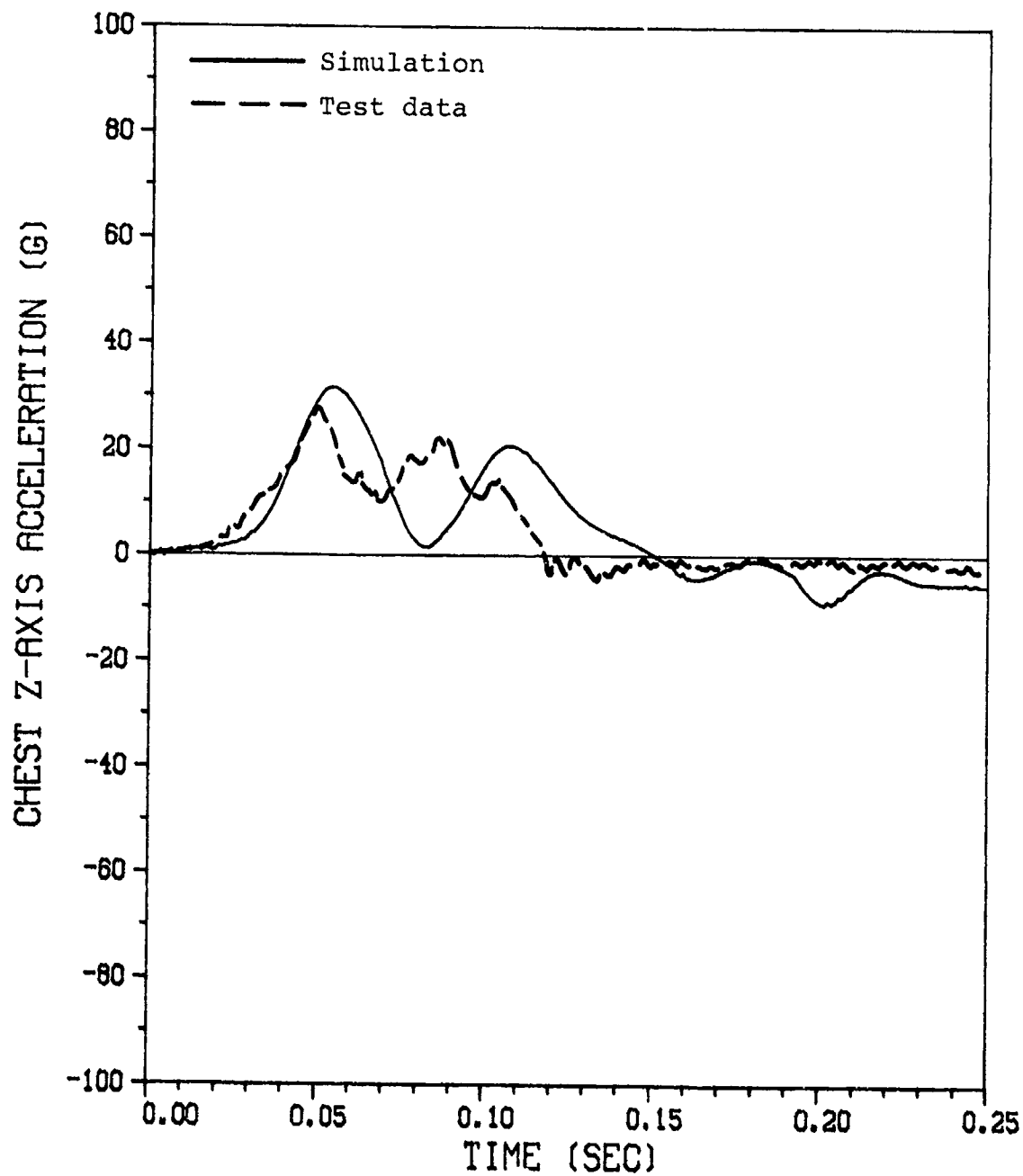


Figure 36. CAMI test A81-124, dummy chest z-acceleration.

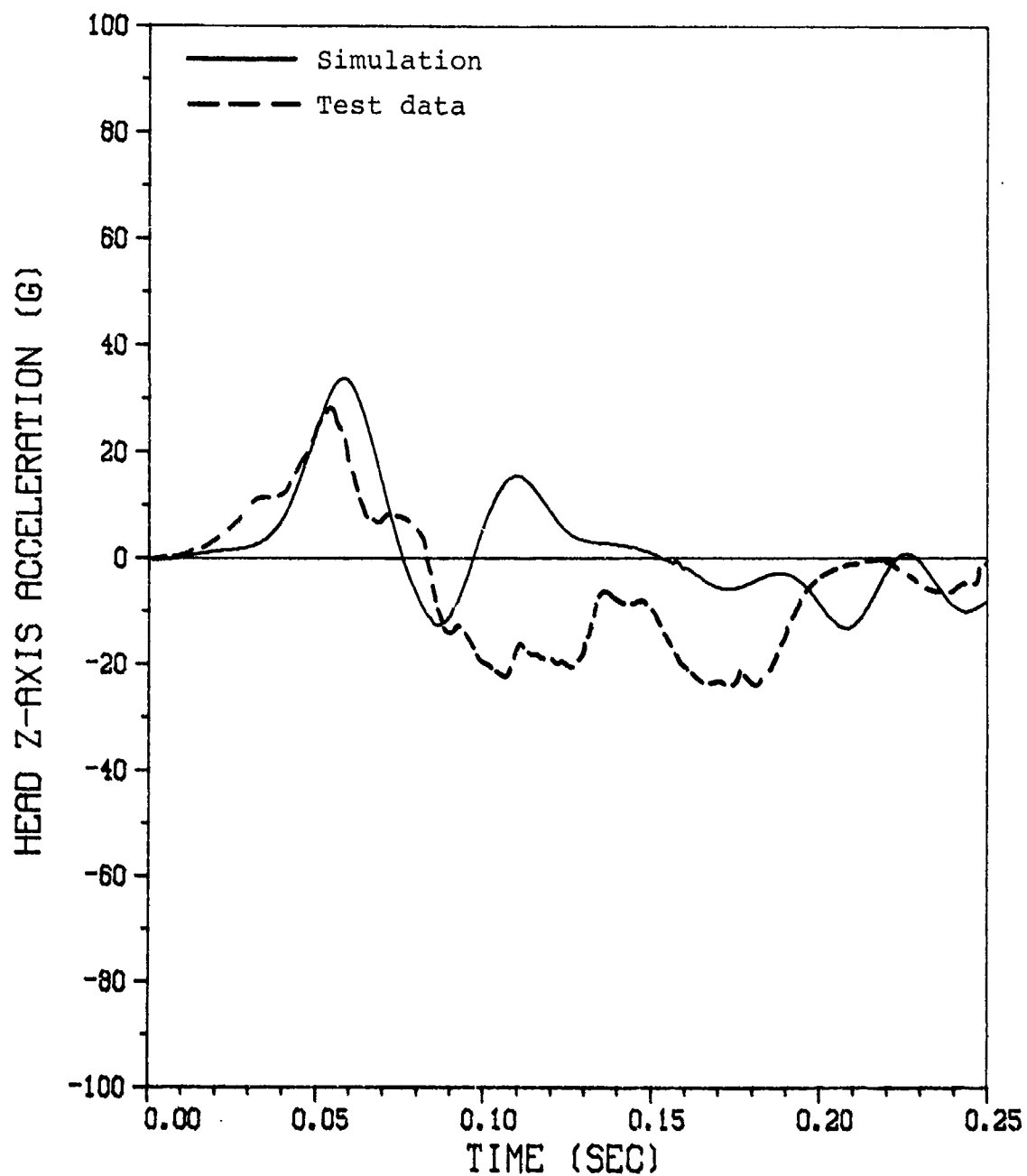


Figure 37. CAMI test A81-124, dummy head z-acceleration.

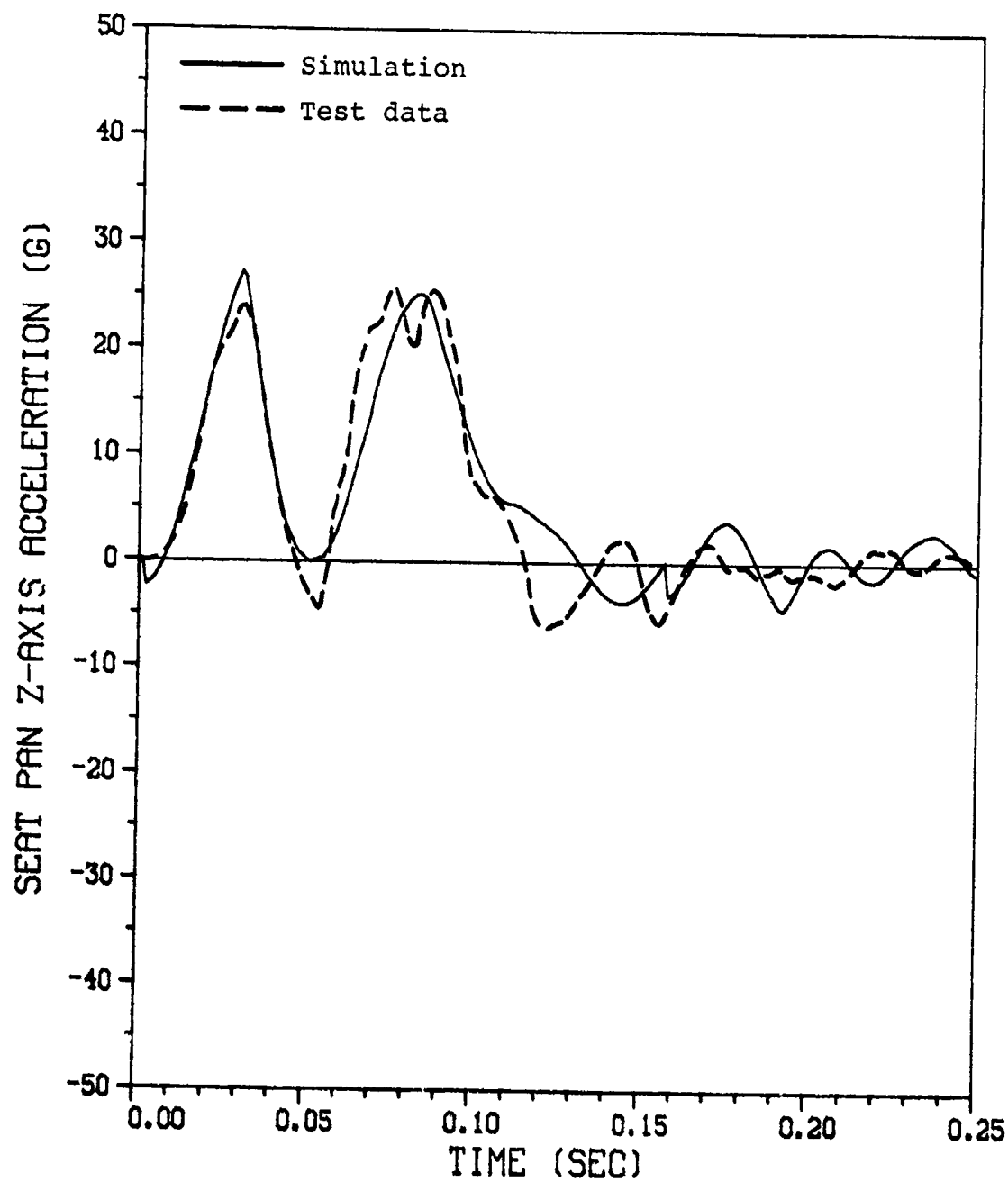


Figure 38. CAMI test A81-124, seat z-acceleration.

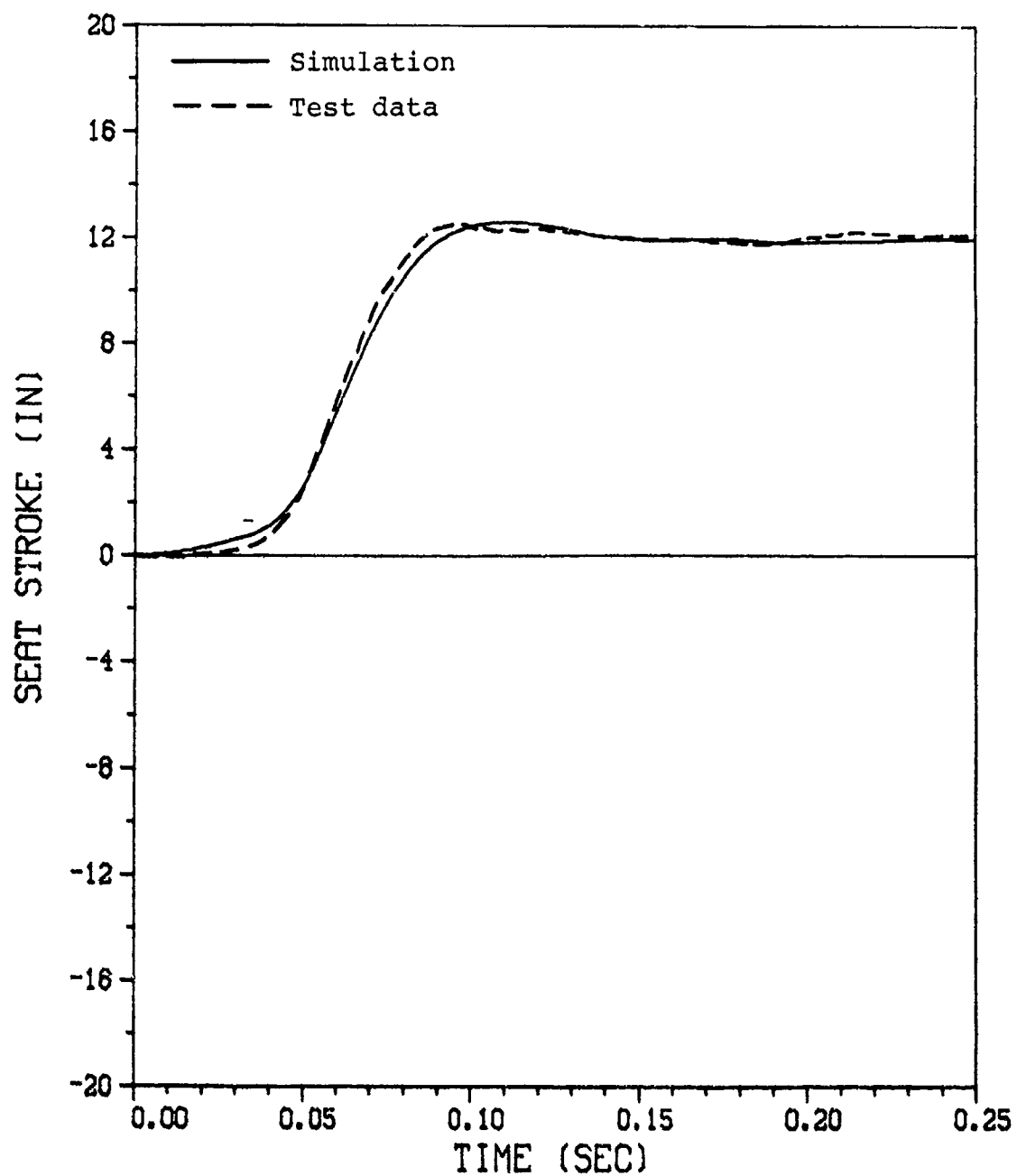


Figure 39. CAMI test A81-124, seat stroke.

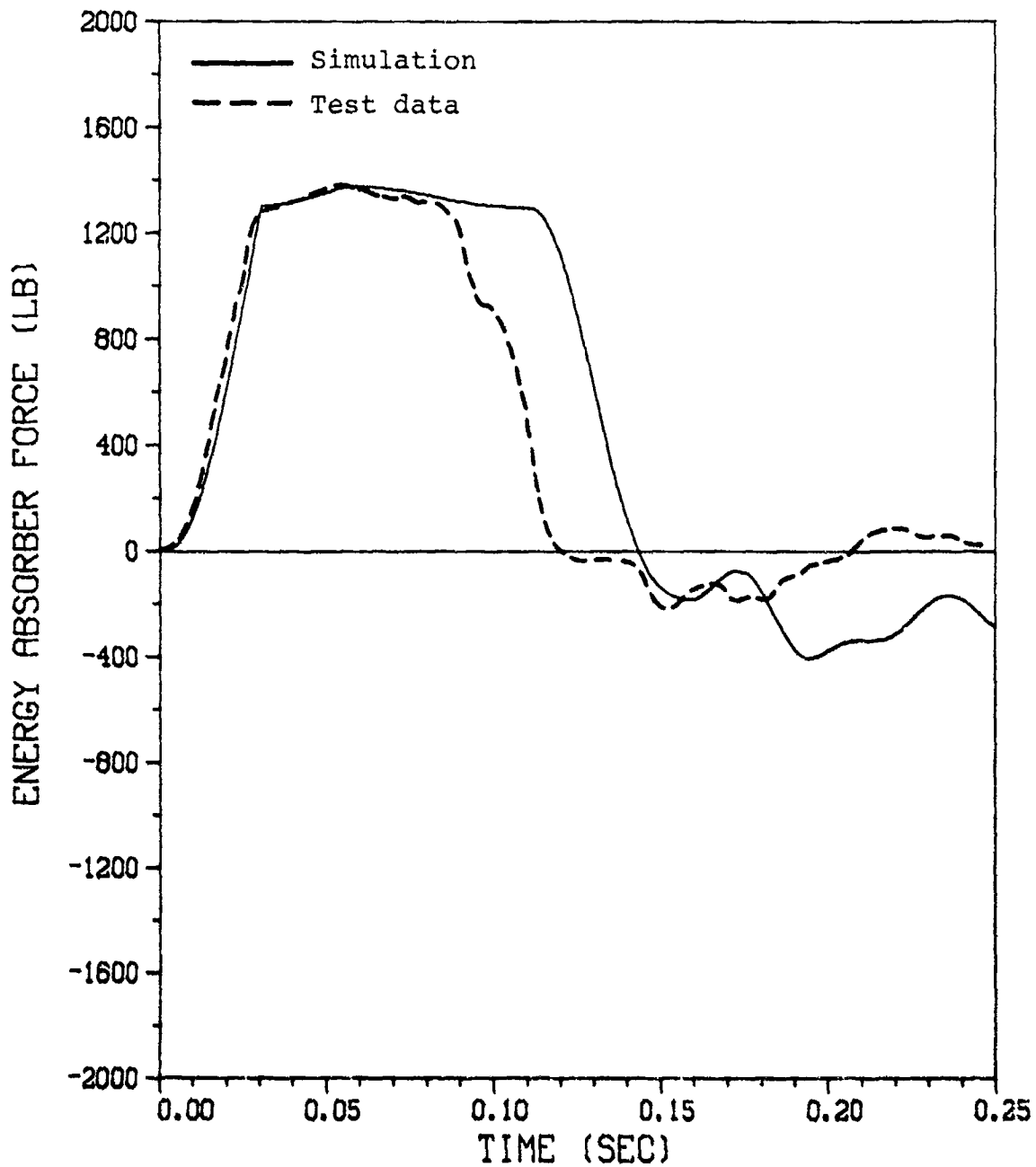


Figure 40. CAMI test A81-124, energy absorber force.

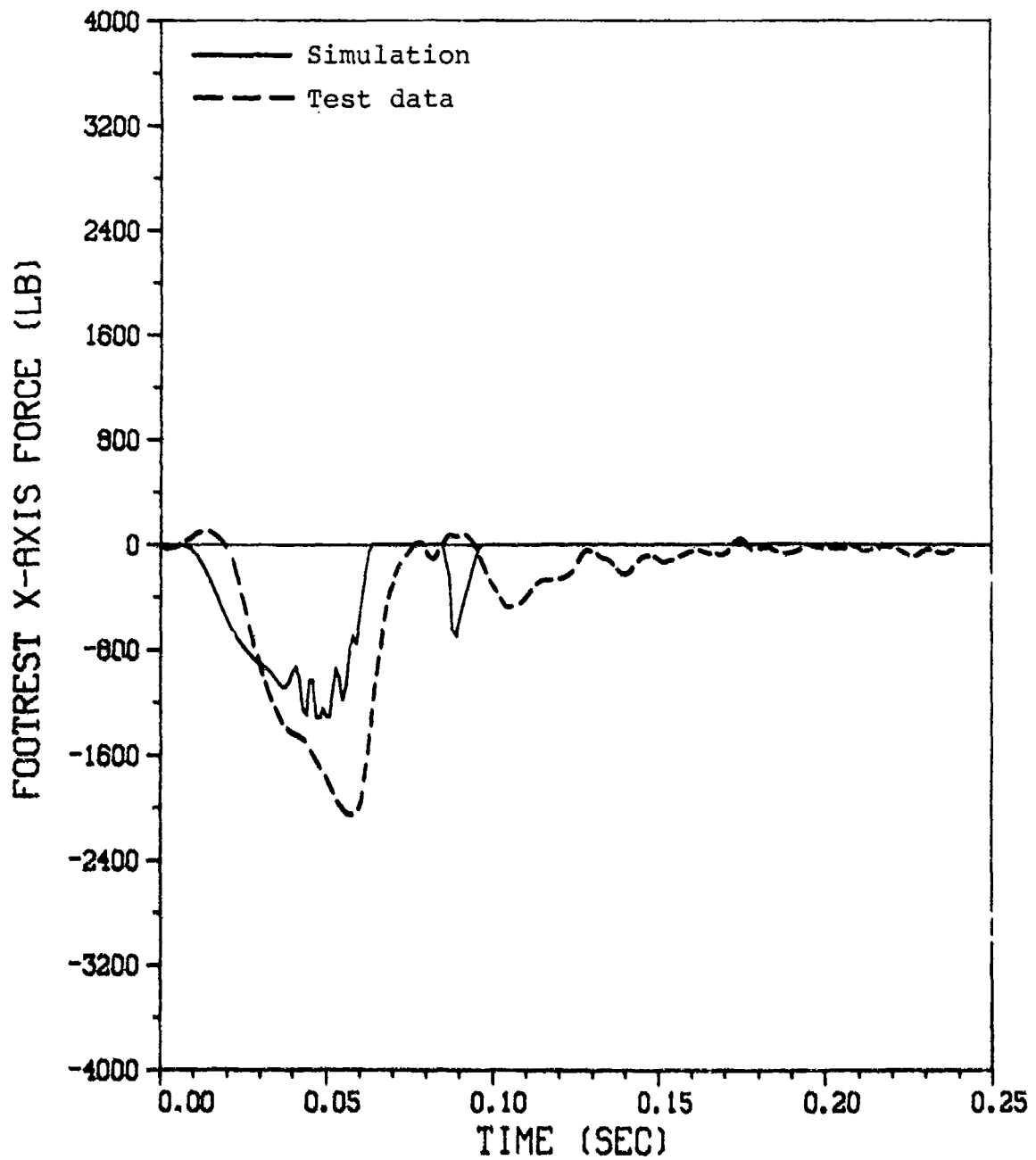


Figure 41. CAMI test A81-124, footrest x-force.

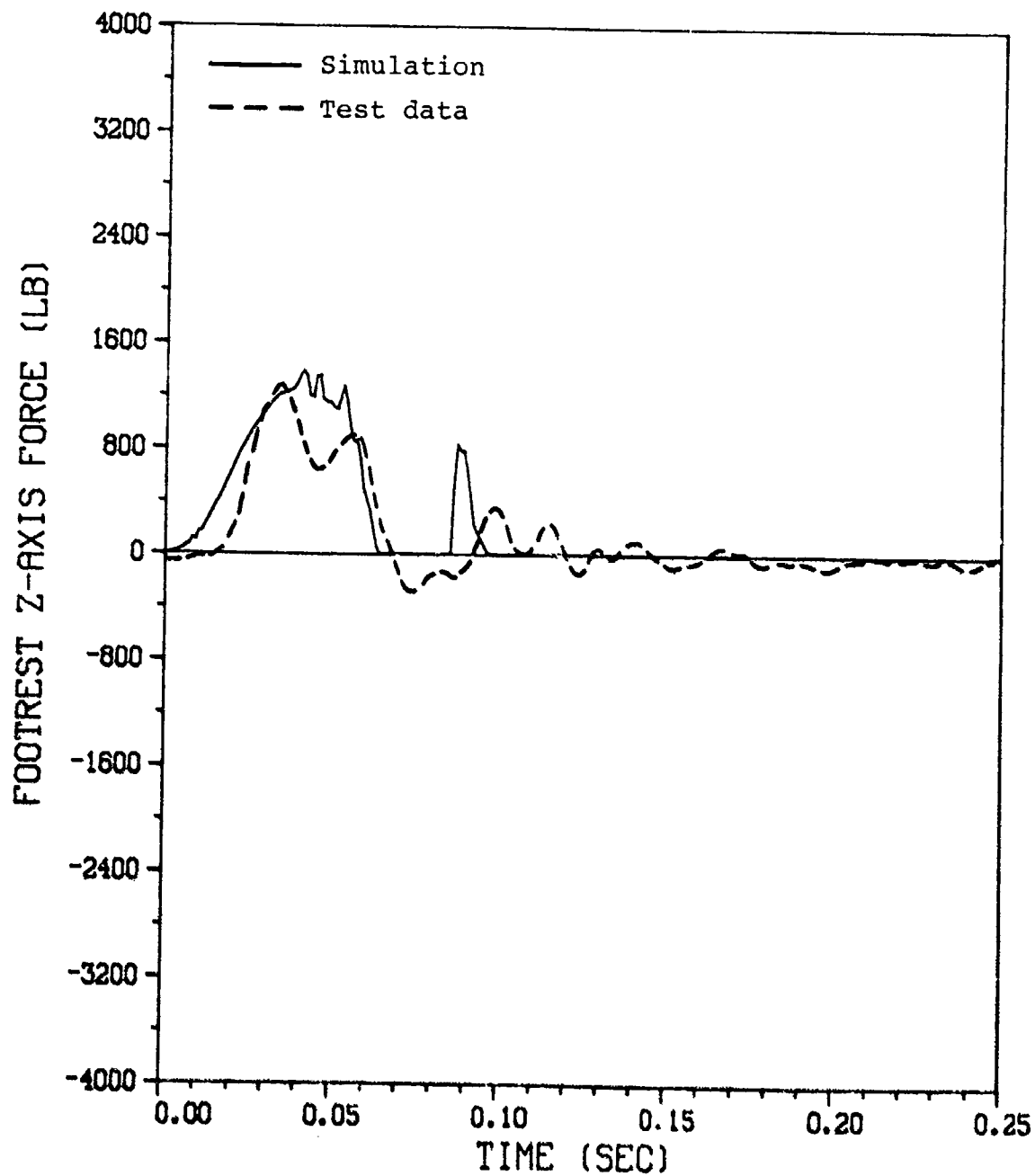


Figure 42. CAMI test A81-124, footrest z-force.

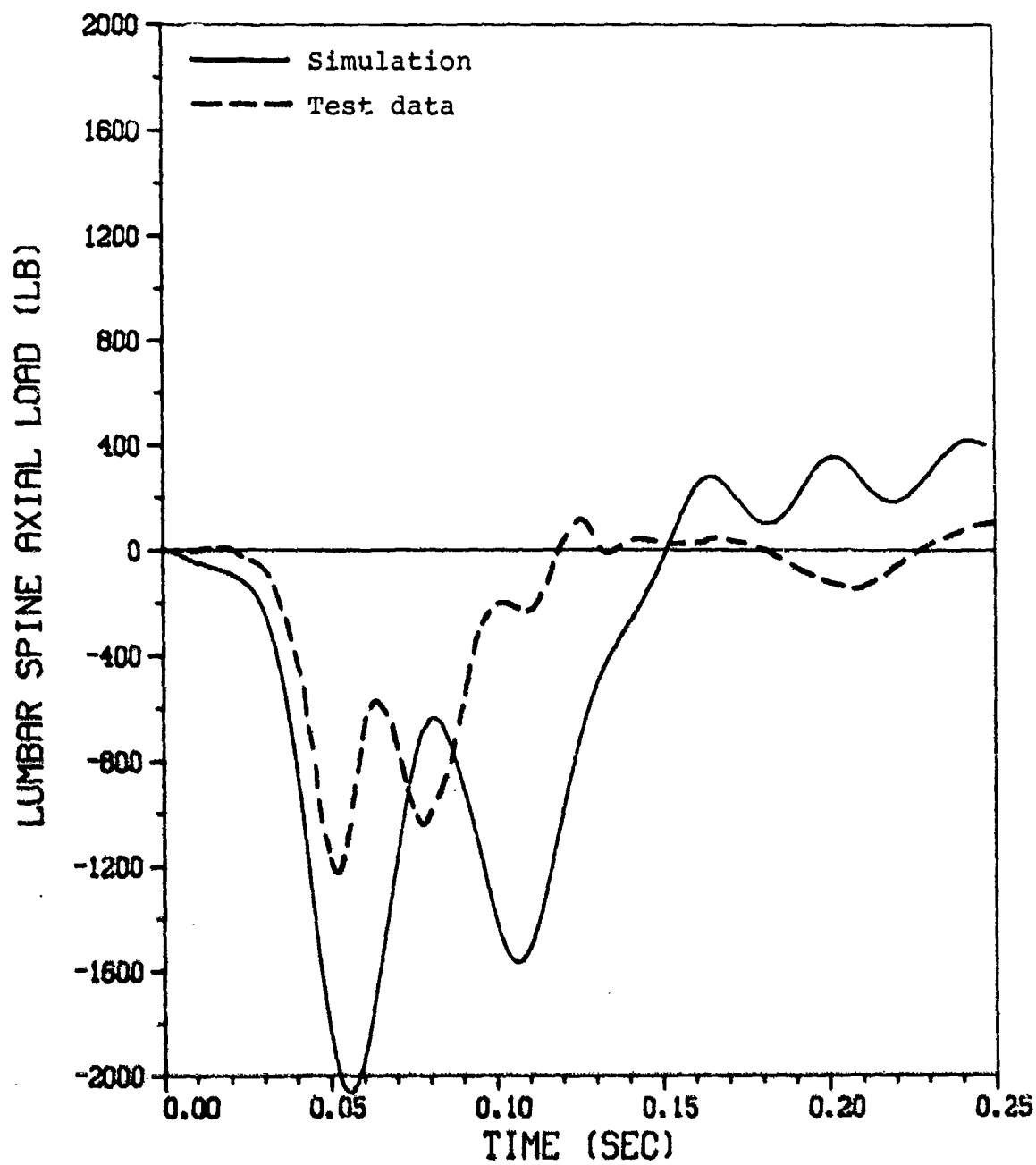


Figure 43. CAMI test A81-124, lumbar spine axial load.

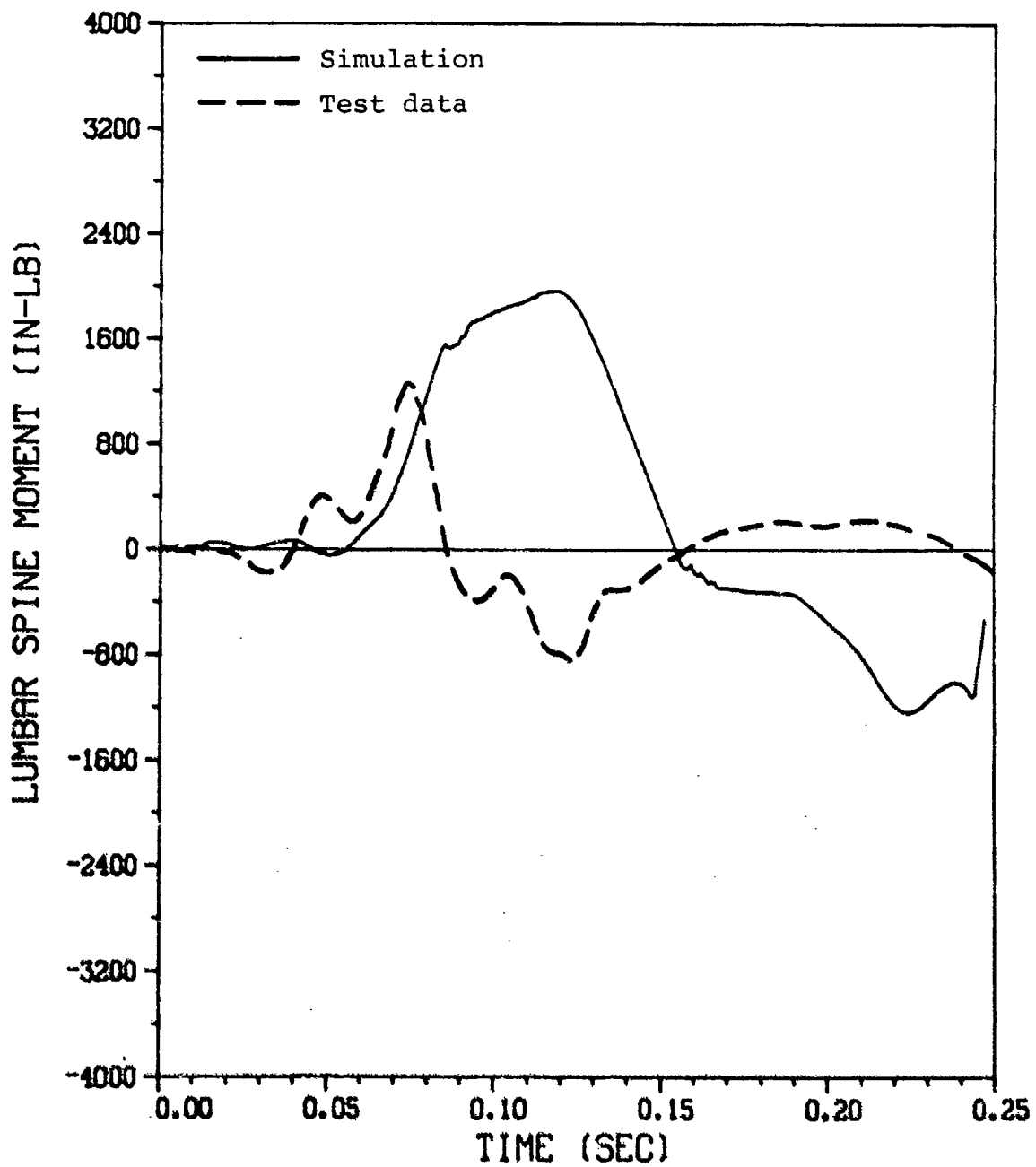


Figure 44. CAMI test A81-124, lumbar spine moment.

5.7 LINEAR REGRESSION ANALYSIS

The least-squares linear regression analysis whose results are presented in Chapter 6 is employed to minimize the sum of the squares of the deviations of the actual data points from the straight line of best fit. In order to approximate a set of n data points (x, y) by a straight line given by

$$y = mx + b$$

the following equations are used:

$$\text{Slope, } m = \frac{\sum_{i=1}^n (x_i y_i) - \left(\sum_{i=1}^n x_i \sum_{i=1}^n y_i \right) / n}{\sum_{i=1}^n (x_i^2) - \left(\sum_{i=1}^n x_i \right)^2 / n}$$

$$\text{y-intercept, } b = \left(\sum_{i=1}^n y_i - m \sum_{i=1}^n x_i \right) / n$$

The correlation coefficient, R , which provides a measure of the quality of the straight-line fit, is given by

$$R = m \sigma_x / \sigma_y$$

where σ_x and σ_y are the standard deviations of the x and y data points.

6.0 RESULTS OF SENSITIVITY ANALYSIS

This chapter presents a discussion of the sensitivity of seat and occupant response to the 13 experimentally examined variables. The sensitivity analysis for the experimental test series consists of a comparison of measured time histories of seat or occupant response, a tabulation of maximum values, and, where possible, graphs of severity indicators showing trends through linear regression of the data. During the course of this research effort, it became apparent that several other variables not included in the original test matrix could have considerable bearing on an updated energy-absorbing seat specification. The system performance sensitivity to these variables was either implied from test data or compared with a test matrix of SOM-LA simulations, since the parametric test series could not be expanded within the budgeted funding.

6.1 SENSITIVITY ANALYSES FOR EXPERIMENTAL TEST SERIES

Sensitivity analyses for each of the 13 variables examined with experimental testing are discussed in this section. The charts included in Figures 45 and 46 provide a reference source for applicable test numbers in both the rigid seat and energy-absorbing seat test series.

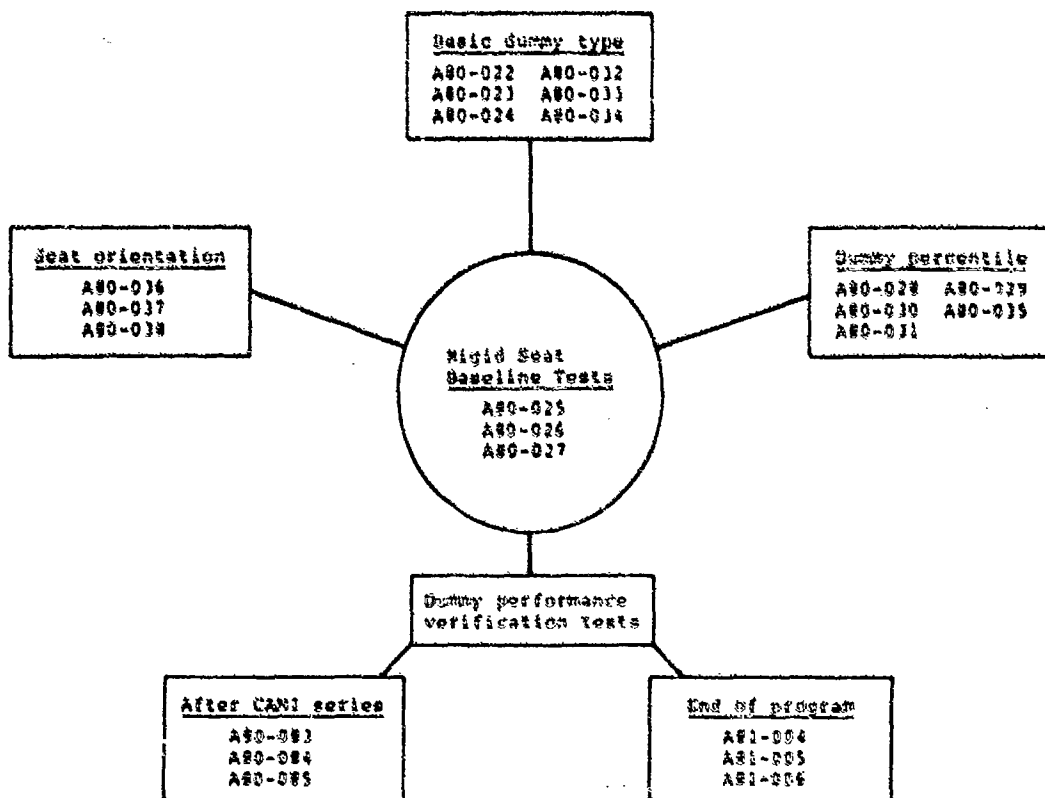


Figure 45. Rigid seat series parametric test reference.

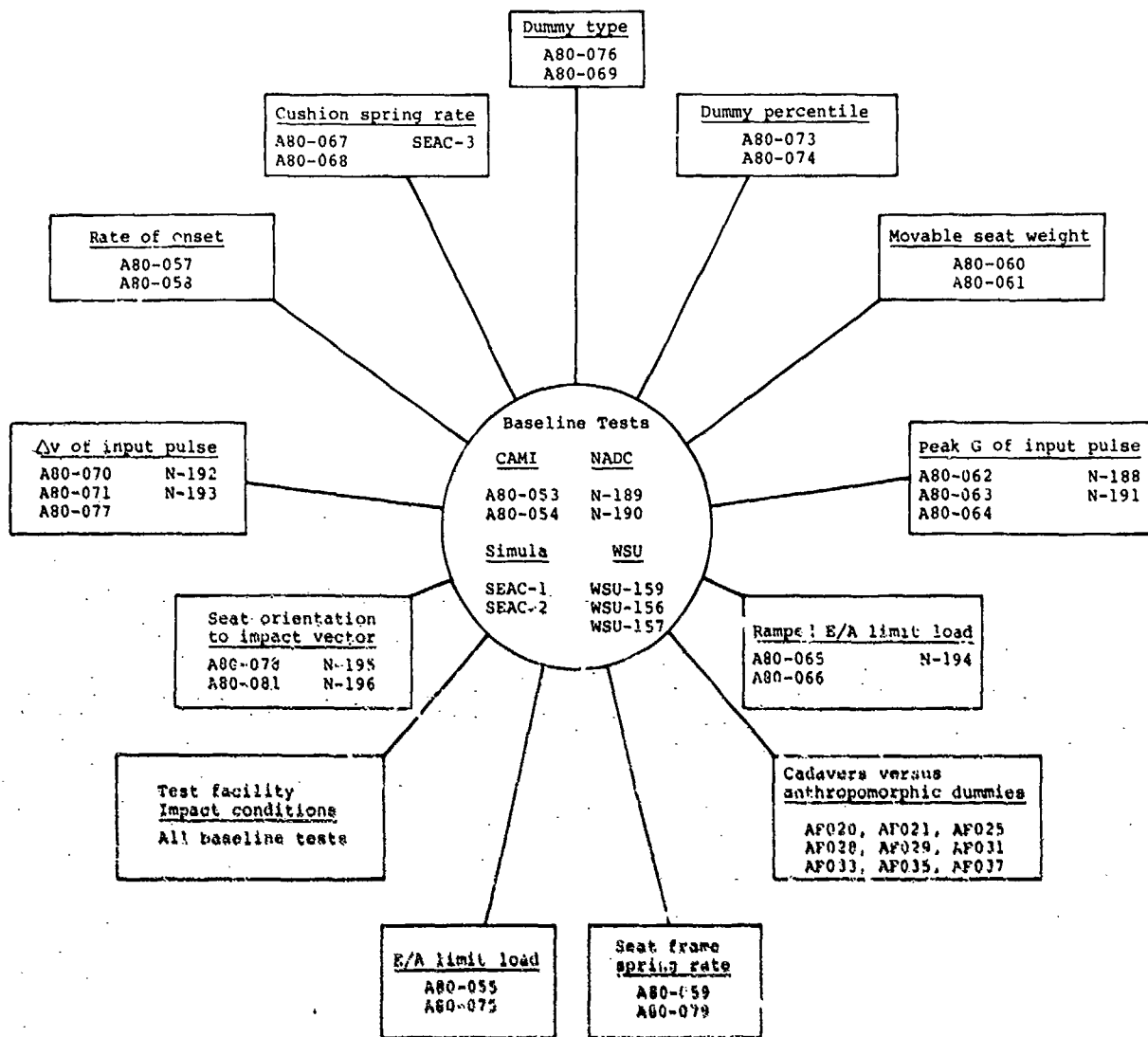


Figure 46. Energy-absorbing seat series parametric test reference.

6.1.1 Peak Input Acceleration Series

The peak input acceleration series was designed to investigate seat and occupant sensitivity to the input pulse shape. The input conditions in an actual crash are a function of the landing gear/fuselage deformation characteristics, impact velocity, and accident site terrain properties. For this series, the velocity change was held constant at 42 ft/sec; the resulting input pulses are shown in Figure 47. Measured peak values for the seat and occupant are summarized in Table 12. There appears to be a definite trend in the vertical response of the seat as determined by the required stroke distance and the maximum seat pan acceleration plotted in Figures 48 and 49. Recorded seat pan z-axis acceleration time histories are shown in Figure 50.

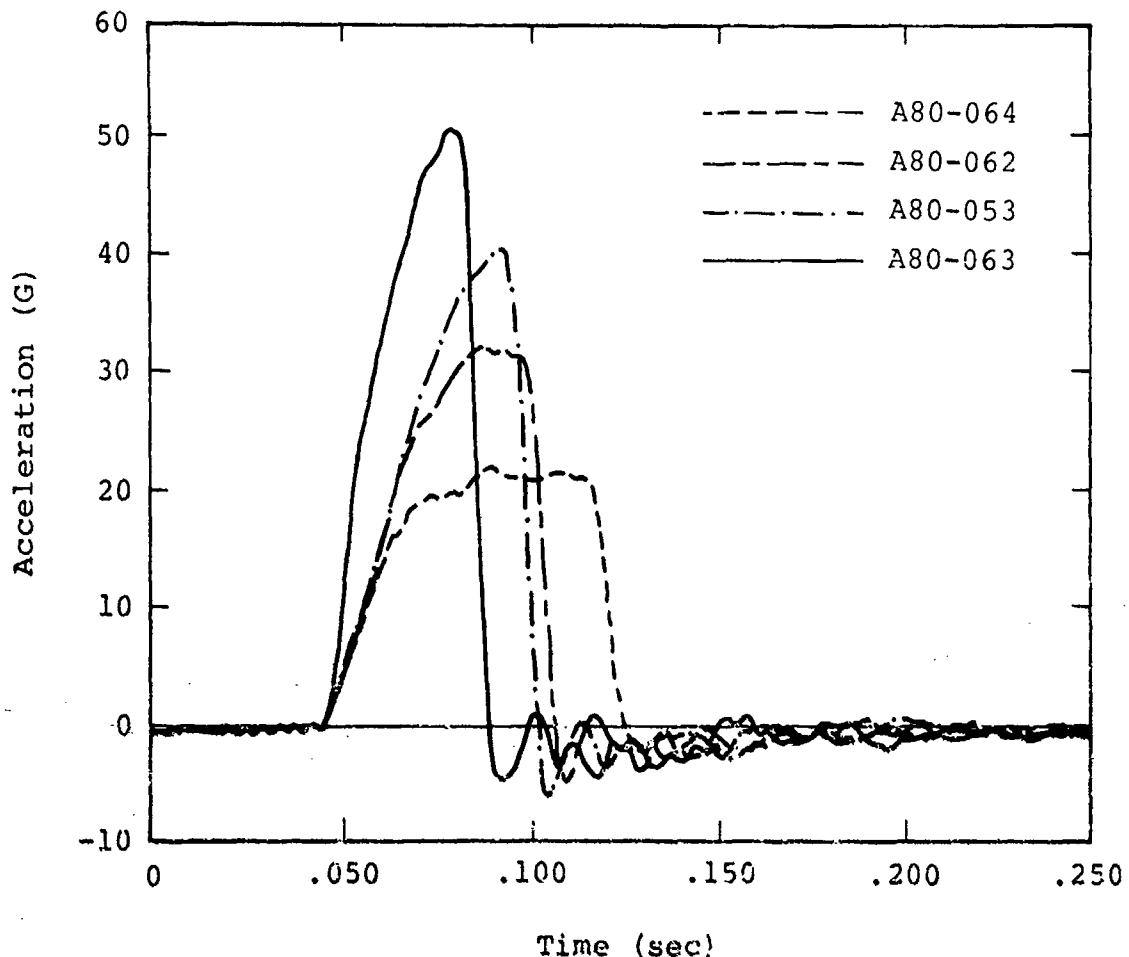


Figure 47. Input acceleration pulses for peak acceleration series.

Vertical accelerations recorded in the anthropomorphic dummy also show an increasing trend with the peak input acceleration. This trend can be seen in the pelvic z-axis time histories shown in Figure 51 and the sensitivity plot of pelvic acceleration versus input (Figure 52).

Several test severity indicators, shown in Figures 53 through 56, were tabulated for this series, and all show the same increasing trend with increasing peak input acceleration. However, there is a significant amount of scatter in the measured seat pan acceleration duration data and the predicted spinal moment. The DRI and predicted lumbar spine axial load both show a strong relationship to peak input acceleration, as demonstrated by correlation coefficients of 0.92 and 0.97, respectively.

6.1.2 Velocity Change Series

Impact energy is proportional to the square of the velocity. Therefore, it would be expected that seat and occupant response

TABLE 12. COMPARISON OF TEST RESULTS FOR PEAK INPUT ACCELERATION SERIES

Peak Input Accel (G)	Test No.	Initial Velocity (ft/sec)	Total Velocity Change (ft/sec)	Seat Stroke (in.)	Peak Acceleration (G)								Duration of Seat Pan z Acceleration at 23 G (sec)	DRI
					Seat Pan x	Seat Pan z	Pelvis x	Pelvis z	Chest x	Chest z	Head x	Head z		
21.9	A80-064	41.3	42.1	7.0	15.4	22.4	10.7	24.4	12.1	24.1	22.4	28.5	0.	17.0
32.2	A80-062	41.8	43.3	9.5	26.0	24.6	9.7	36.8	31.1	26.5	37.8	26.1	0.005	18.9
35.2	N-191	36.8	37.9	9.4	14.1	33.3	14.0	30.8	9.40	31.5	19.1	32.5	0.010	20.9
40.7	A80-053	41.8	44.8	10.6	25.3	26.4	17.1	30.5	18.1	30.4	31.5	36.5	0.007	21.0
40.2	A80-054	42.3	44.2	10.5	22.1	29.4	10.1	30.8	24.1	25.8	38.5	28.2	0.016	19.7
44.9	N-189	36.8	40.4	10.8	16.6	36.3	15.0	38.8	10.0	36.1	24.7	40.8	0.006	20.8
45.0	N-190	36.8	40.5	11.6	16.8	34.6	18.7	40.1	14.7	37.4	22.7	42.8	0.007	20.7
51.7	N-188	36.8	39.2	11.5	20.4	42.0	15.7	40.2	13.4	37.8	23.4	43.2	0.009	23.2
50.9	A80-063	42.1	45.6	11.7	22.3	31.8	36.8	45.9	20.4	26.8	32.5	32.5	0.013	21.4

Peak Input Accel (G)	Test No.	Peak E/A Load (lb)		Peak Lap Belt Load (lb)		Peak Shoulder Belt Load (lb)		Peak -G Strap Load (lb)	Peak Footrest Load (lb)	
		Right	Left	Right	Left	Right	Left		x	z
21.9	A80-064	1350.	1450.	180.	161.	241.	154.	389.	1340.	1640.
32.2	A80-062	1400.	1440.	281.	-	154.	228.	388.	1640.	2220.
35.2	N-191	1430.	1440.	362.	348.	221.	255.	496.	1390.	2040.
40.7	A80-053	1380.	1590.	373.	213.	200.	147.	593.	1760.	2200.
40.2	A80-054	1420.	1550.	300.	233.	87.	250.	560.	1900.	2120.
44.9	N-189	1449.	1457.	342.	335.	188.	221.	476.	1670.	2310.
45.0	N-190	1370.	1415.	361.	508.	181.	355.	515.	1090.	2410.
51.7	N-188	1450.	1400.	274.	488.	94.	100.	963.	1993.	2620.
50.9	A80-063	1400.	1440.	268.	275.	295.	-	690.	2330.	3100.

would be a strong function of this parameter. All of the compiled maximum values listed in Table 13 show an increasing trend with additional velocity change. It should be noted that it was not possible to maintain the same pulse shape and peak input acceleration as the velocity change decreased; these three parameters are not independent of each other and would be expected to vary in a similar manner for an aircraft fuselage. Four input acceleration pulses for the CAMI test series are compared in Figure 57.

Several measured test parameters show a strong correlation to the velocity change variable. These parameters, seat stroke, maximum seat pan z-axis acceleration, and DRI, are plotted in Figures 58, 59, and 60, respectively; and, as would be expected, seat stroke is shown to be highly sensitive to changes in velocity. Program SOM-LA was used to simulate each of the nine tests in this series.

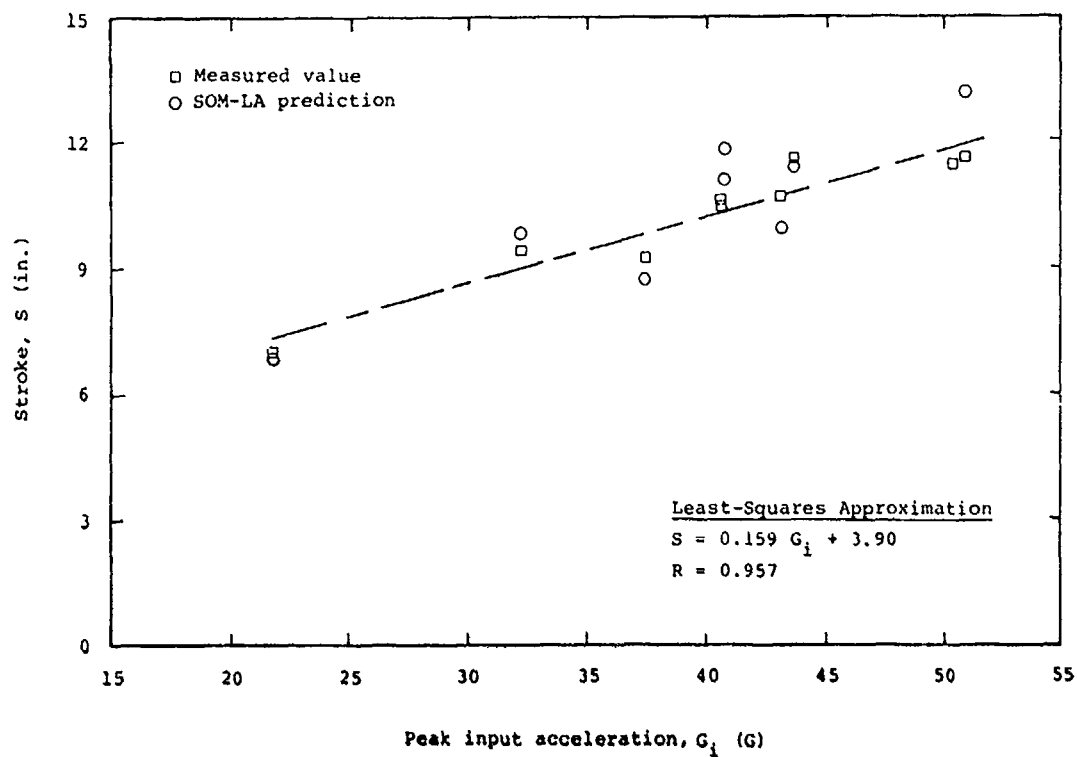


Figure 48. Peak input acceleration series, maximum seat stroke.

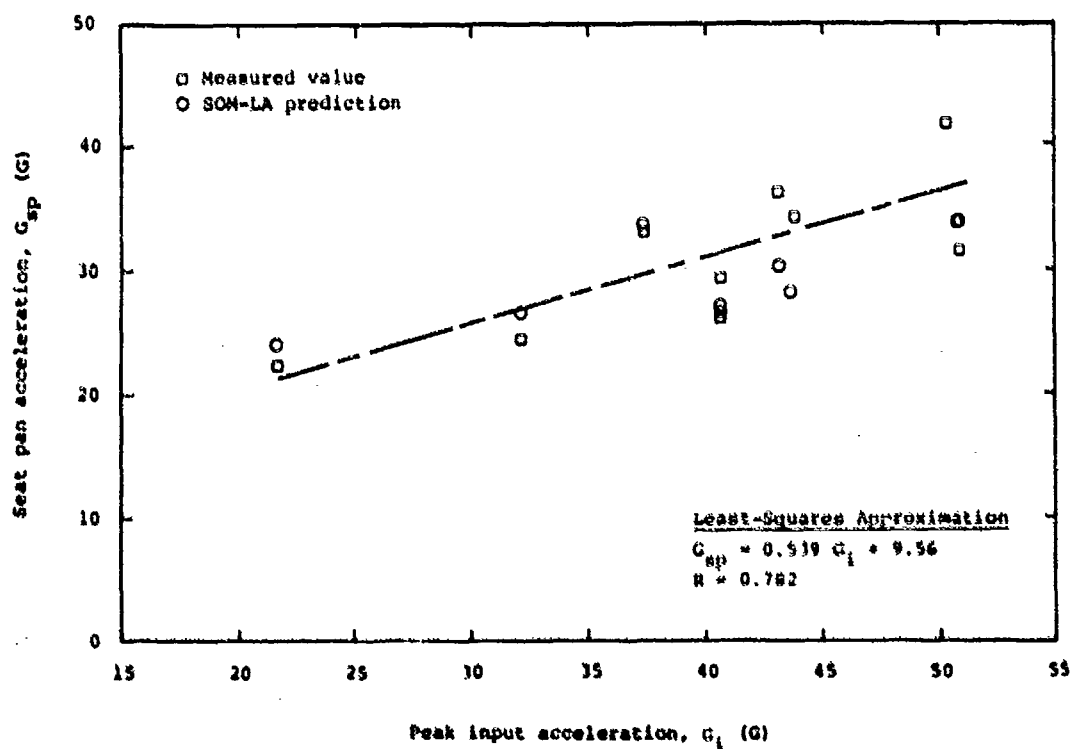


Figure 49. Peak input acceleration series, maximum seat pan z-axis acceleration.

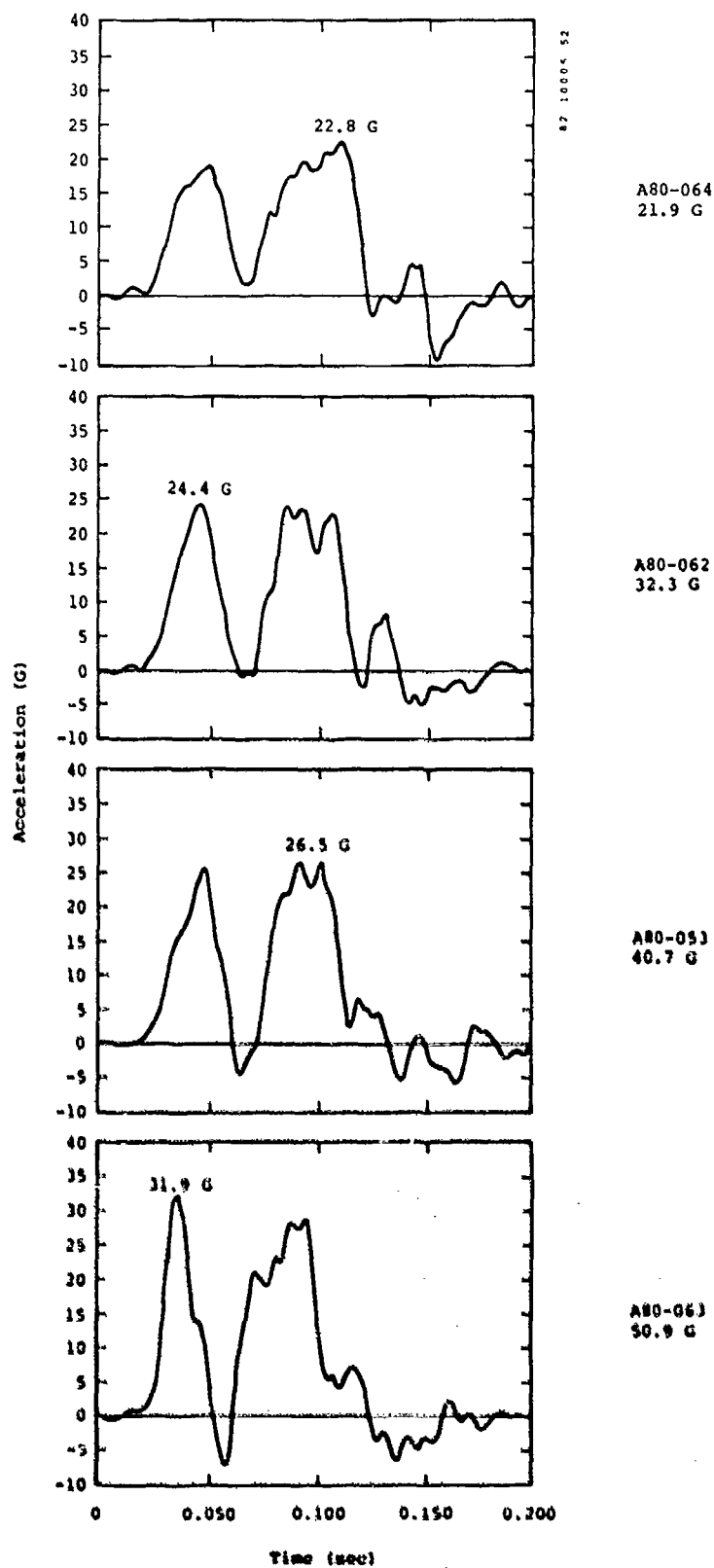


Figure 50. Seat pan z-axis acceleration measured in peak input acceleration series.

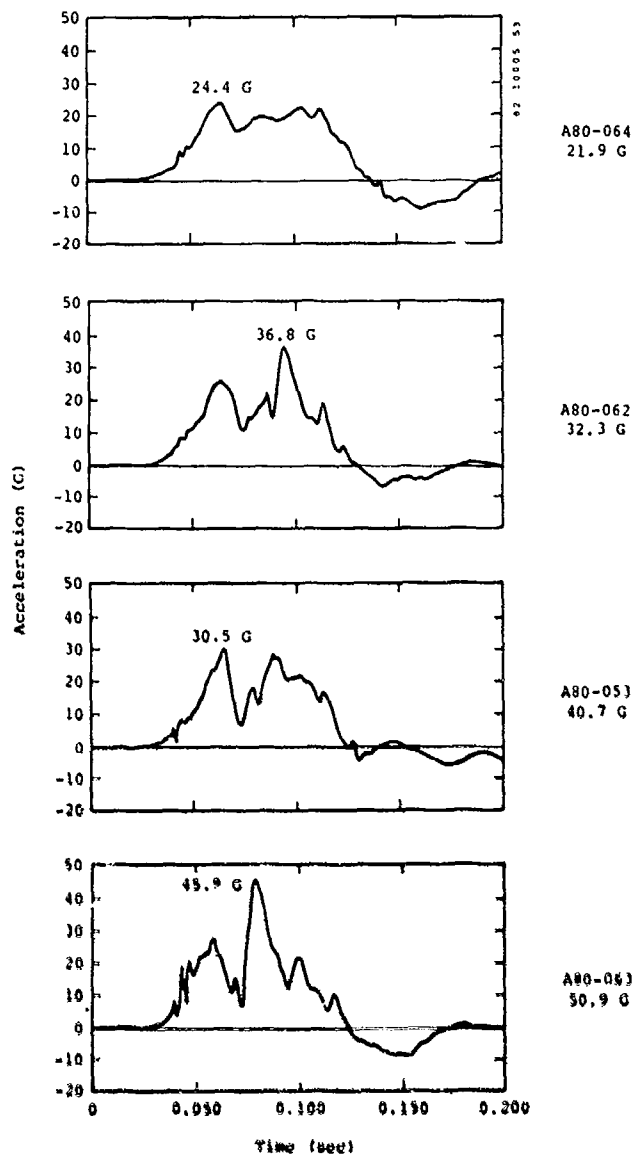


Figure 51. Pelvic z-axis acceleration measured in peak input acceleration series.

Results of the simulations, which compare favorably with measured test data, are also plotted in these figures. Included in this section are predictions of peak spinal load and moments plotted against velocity change, shown in Figures 61 and 62. Sensitivity of the predicted spinal loads and DR₁₀₀ to increasing velocity exhibit similar characteristics in which there is a definite trend, although the velocity does not appear to be a strong influence. This is a predictable trend because both of these parameters, indicating spinal load, should be greatly affected by the magnitude of transmitted crash loads, which are controlled by the energy absorber limit load and are ideally not influenced by the applied load duration, which is a function of the impact energy. Data presented in Section 6.1.4 for the energy absorber limit load

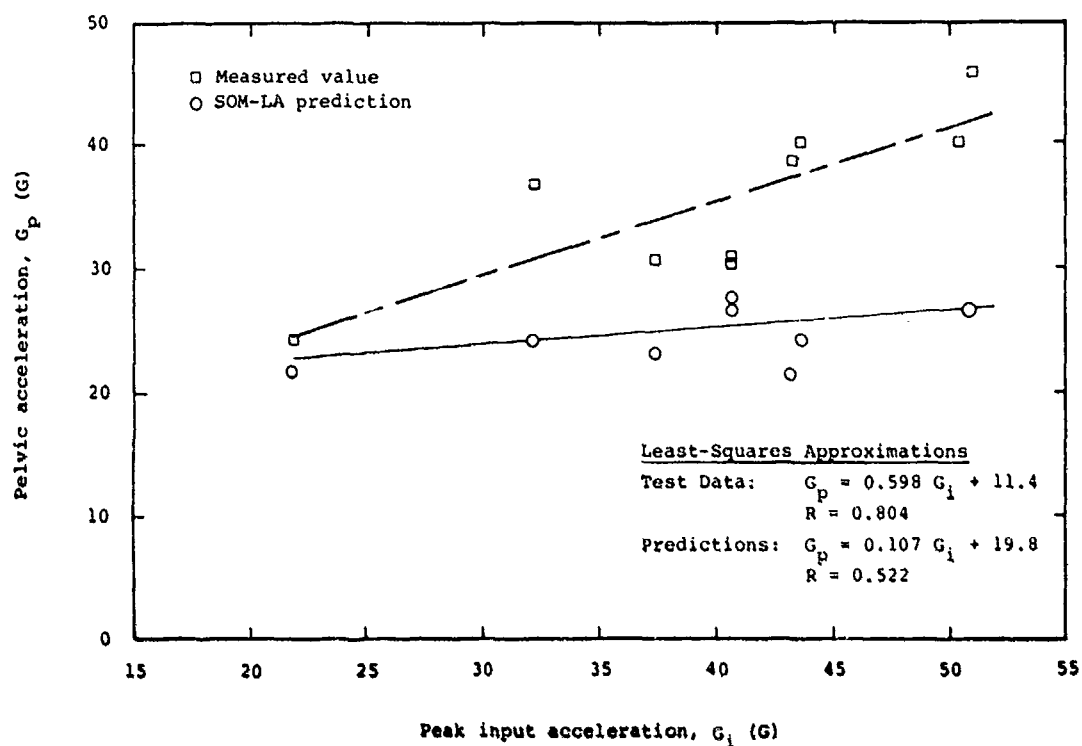


Figure 52. Peak input acceleration series, maximum pelvic z-axis acceleration.

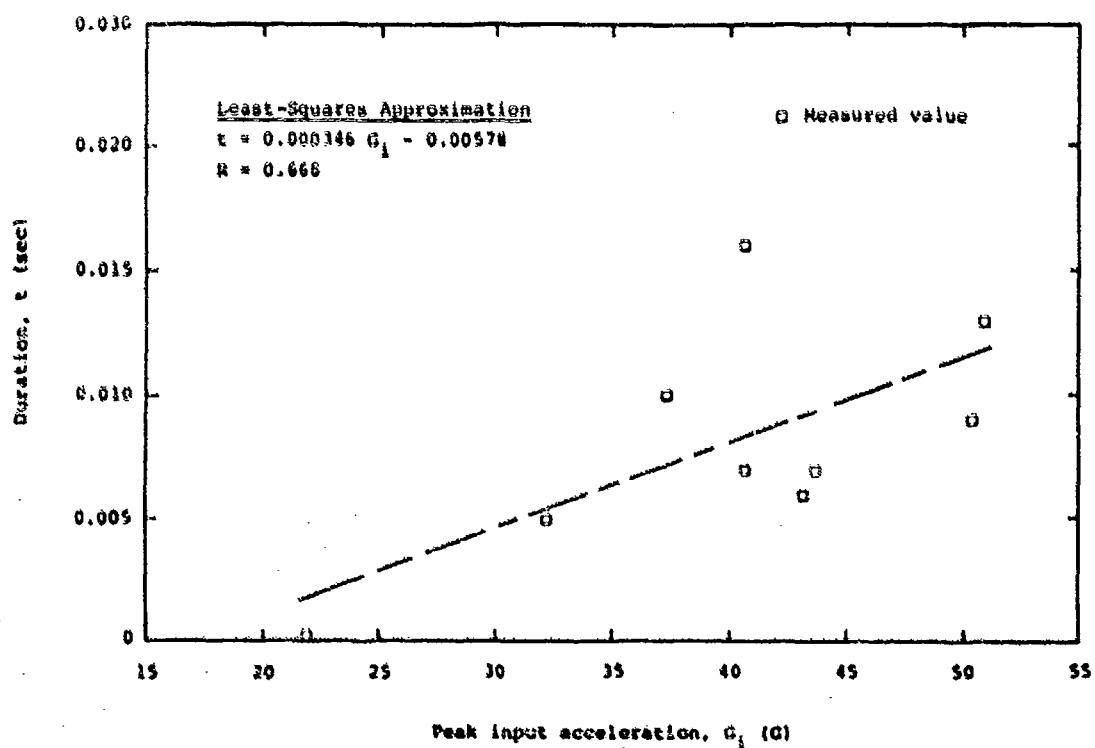


Figure 53. Peak input acceleration series, duration of seat pan z-axis acceleration at 23 G.

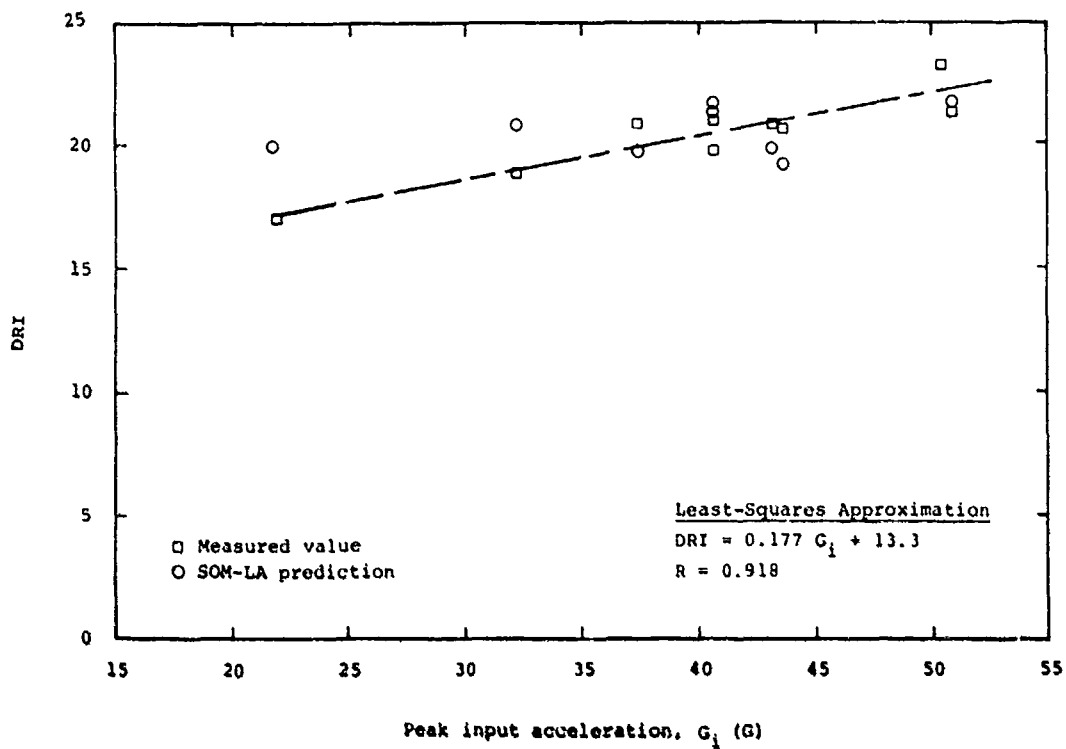


Figure 54. Peak input acceleration series, Dynamic Response Index.

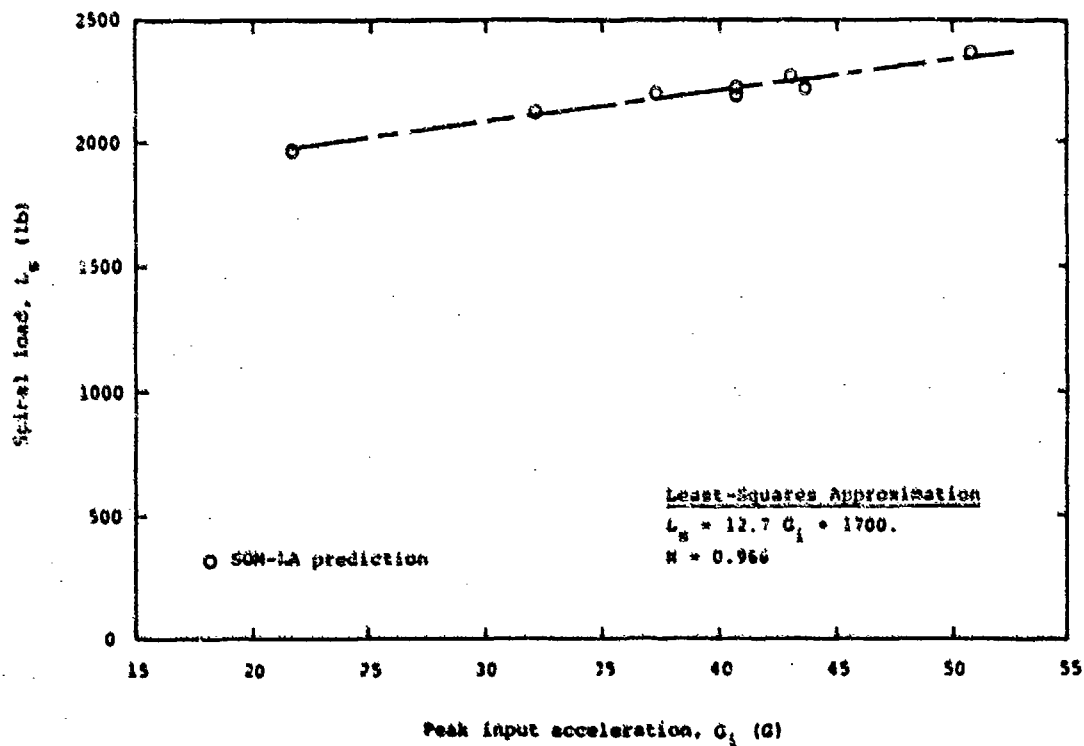


Figure 55. Peak input acceleration series, predicted maximum lumbar spine axial load (compression).

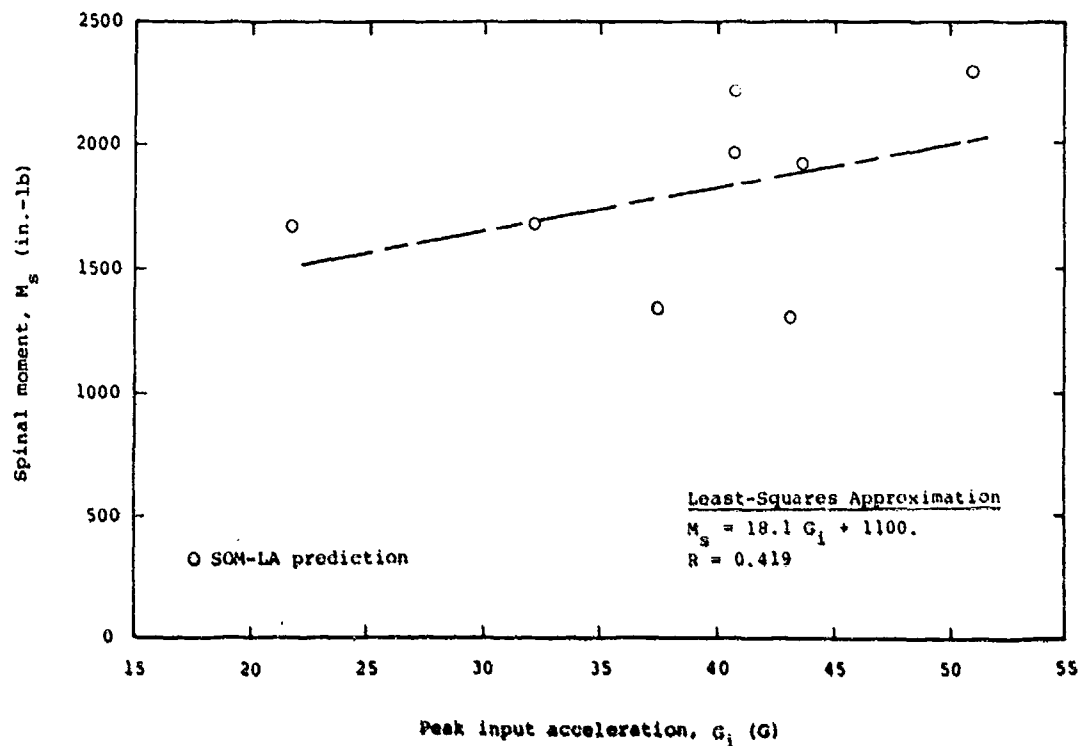


Figure 56. Peak input acceleration series, predicted maximum lumbar spine moment (flexion).

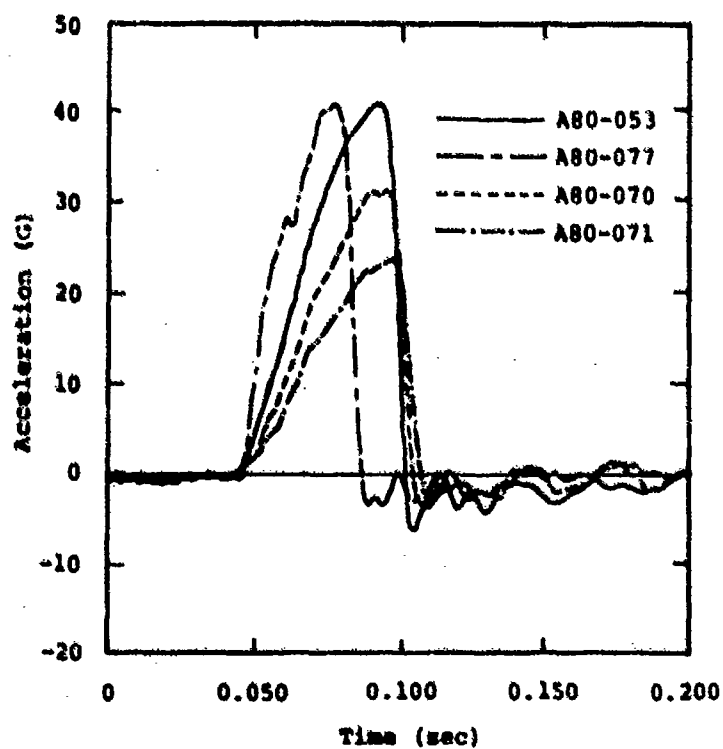


Figure 57. Comparison of input acceleration pulses for CAMI velocity change series.

TABLE 13. COMPARISON OF RESULTS FOR VELOCITY CHANGE SERIES

Total Velocity Change (ft/sec)	Test No.	Initial Velocity (ft/sec)	Peak Input Accel (G)	Seat Stroke (in.)	Peak Acceleration (G)								Duration of Seat Pan z Acceleration at 23 G (sec)	DRI
					Seat Pan x	Seat Pan z	Pelvis x	Pelvis z	Chest x	Chest z	Head x	Head z		
44.8	A80-053	41.8	40.7	10.6	25.3	26.4	17.1	30.5	18.1	30.4	31.5	36.5	0.007	21.0
44.2	A80-054	42.3	40.2	10.5	22.1	29.4	10.1	30.8	24.1	25.8	38.5	28.2	0.016	19.7
40.4	N-189	36.8	44.9	10.8	16.6	36.3	15.0	38.8	10.0	36.1	24.7	40.8	0.006	20.8
40.5	N-190	36.8	45.0	11.6	16.8	34.6	18.7	40.1	14.7	37.4	22.7	42.8	0.007	20.7
34.9	A80-077	32.4	40.9	6.4	22.4	28.3	23.4	29.1	15.4	24.4	23.5	26.8	0.007	20.1
33.9	A80-070	32.3	31.2	5.6	20.4	20.9	13.7	26.8	10.7	24.8	19.8	29.1	0.	17.0
30.0	N-192	25.4	31.1	5.4	12.5	27.1	13.7	32.2	7.4	32.5	13.1	34.5	0.004	17.6
27.1	A80-071	25.6	23.6	2.2	14.9	18.4	9.0	25.1	12.4	25.8	8.4	29.1	0.	18.9
22.7	N-193	18.8	22.9	2.3	10.4	19.1	6.7	26.4	4.3	25.1	10.0	25.8	0.	16.6

Total Velocity Change (ft/sec)	Test No.	Peak E/A Load (lb)		Peak Lap Belt Load (lb)		Peak Shoulder Belt Load (lb)		Peak -G Strap Load (lb)	Peak Footrest Load (lb)	
		Right	Left	Right	Left	Right	Left		x	z
44.8	A80-053	1380.	1590.	373.	213.	200.	147.	593.	1760.	2200.
44.2	A80-054	1420.	1550.	300.	233.	87.	250.	560.	1900.	2120.
40.4	N-189	1450.	1460.	342.	335.	188.	221.	476.	1670.	2310.
40.5	N-190	1370.	1420.	361.	502.	181.	355.	515.	1890.	2410.
34.9	A80-077	1370.	1440.	148.	107.	141.	174.	369.	1950.	2640.
33.9	A80-070	1380.	1470.	120.	74.	154.	174.	361.	1420.	1970.
30.0	N-192	1520.	1540.	255.	281.	248.	295.	461.	1260.	1540.
27.1	A80-071	1370.	1420.	194.	201.	147.	361.	575.	1130.	1390.
22.7	N-193	1380.	1490.	320.	310.	310.	390.	470.	950.	1150.

series do show that the DRI and spinal load are strongly influenced by the transmitted loads. Another significant relationship in the data exists between spinal moment and seat stroke, both of which are strong functions of velocity change. It is theorized that the test procedure of taping the feet to the footrest caused this apparent relationship, because a significant tensile load in the upper legs can be produced as the seat strokes. This load, which increases with stroke due to the load path angle, causes the pelvic section to rotate and that must be resisted by a moment in the lumbar spine which adds to the moment caused by flexion of the upper torso.

6.1.3 Rate of Onset Series

Results from the rate of onset test series indicate that the effect this parameter has on seat and occupant performance must be

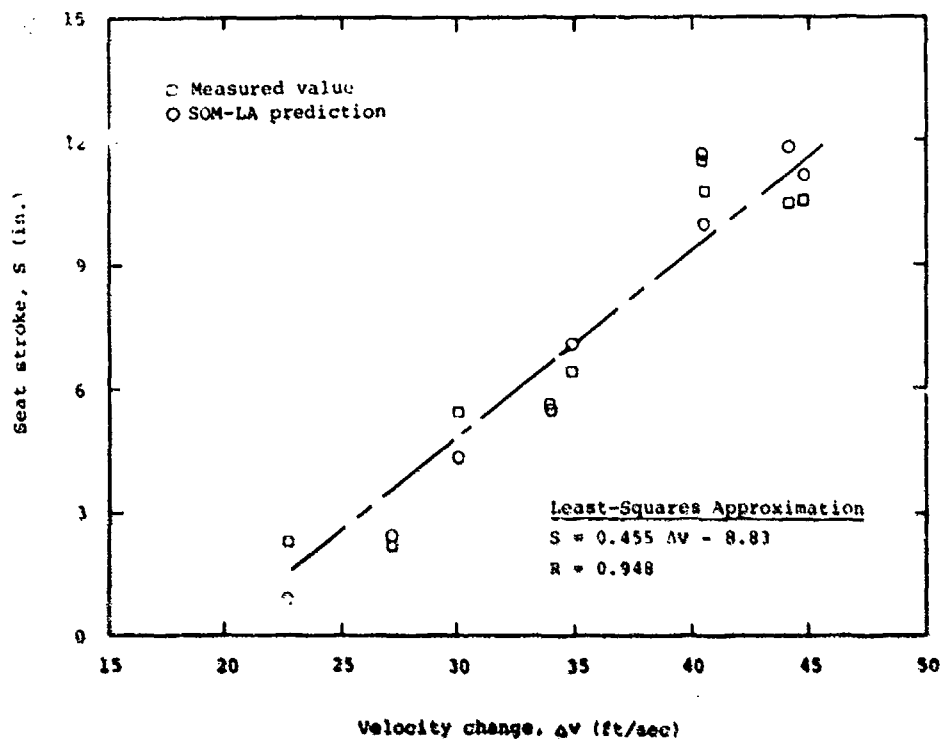


Figure 58. Input velocity change series, maximum seat stroke.

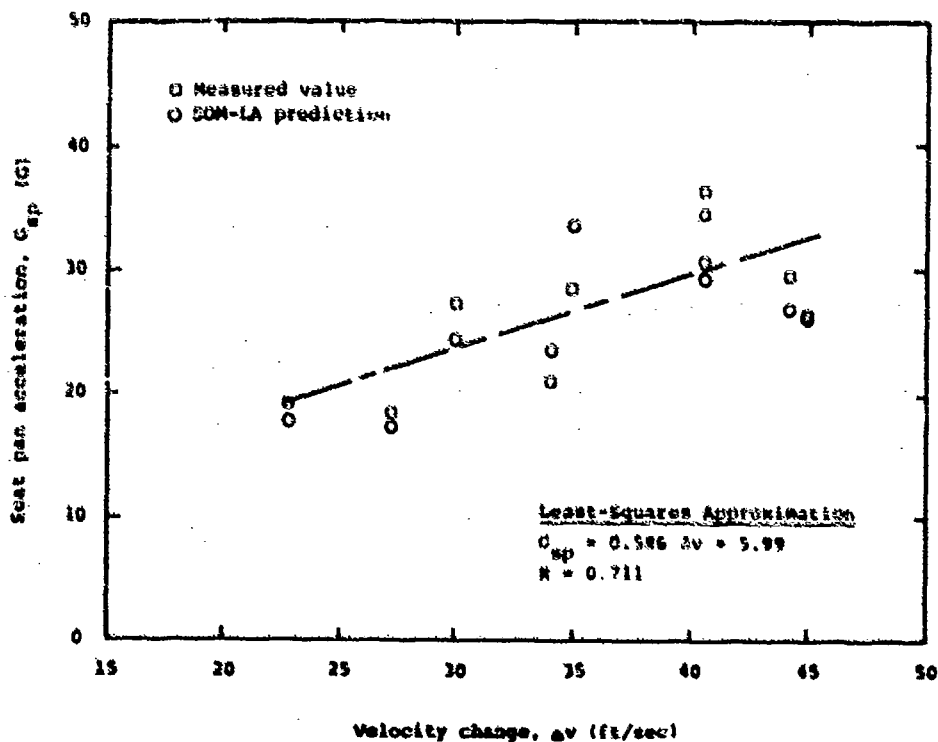


Figure 59. Input velocity change series, maximum seat pan z-axis acceleration.

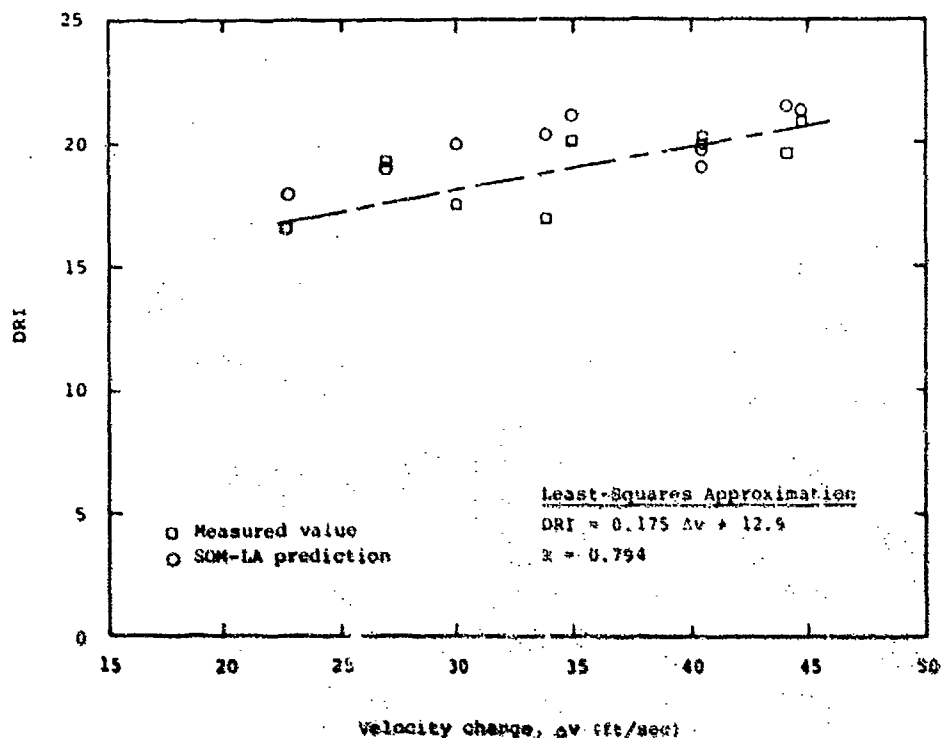


Figure 60. Input velocity change series, Dynamic Response Index.

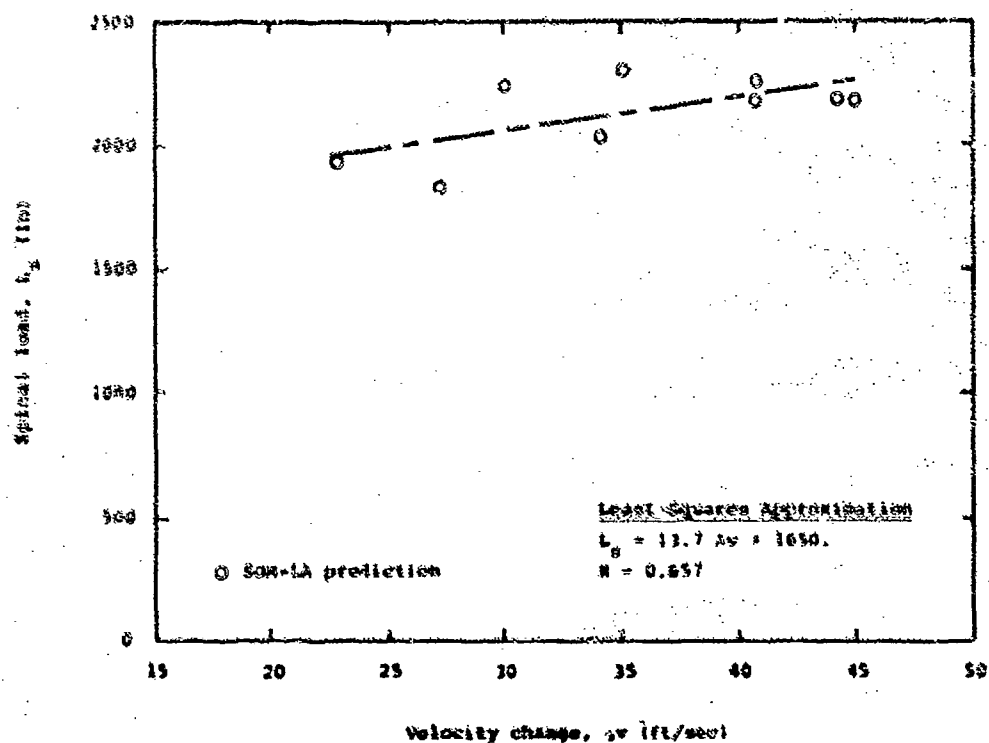


Figure 61. Input velocity change series, predicted maximum lumbar spine axial load (compression).

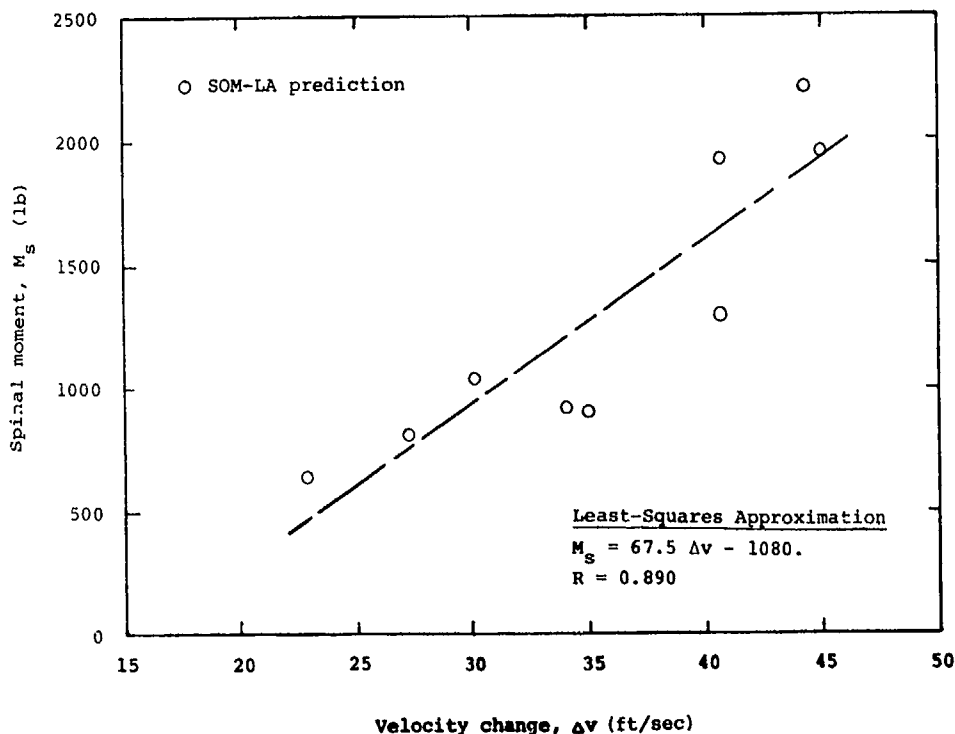


Figure 62. Input velocity change series, predicted lumbar spine moment (flexion).

considered secondary when compared to the effect of peak input acceleration or velocity change. Compiled data shown in Table 14 for the two series, 44 ft/sec and 34 ft/sec, indicate a lack of significant trends although the sample size is small and the range of rate of onset is limited. Only the seat stroke, plotted in Figure 63, can be correlated to rate of onset with any statistical confidence, and it is not certain whether this trend is actually due to the rate of onset or to the peak accelerations for the input pulses, compared in Figure 64, which cannot be independently controlled in an impact test. In fact, if the seat stroke measured in this series is normalized according to the sensitivity curve for peak input acceleration, shown in Figure 48, then the stroke values for the four tests at 44 ft/sec would be 10.4, 10.6, 10.5, and 10.4, indicating that the variation in this series can be explained almost entirely by peak G rather than rate of onset. The vertical acceleration response of the seat pan, shown in Figure 65, does not appear to be greatly influenced by rate of onset of the input pulse. Similar acceleration-time history comparisons for body segment accelerations also exhibit a relative insensitivity to rate of onset changes, compared with the influence of acceleration magnitude and velocity change.

The effects of rate of onset tolerances on seat/occupant response were investigated by computer simulation and are discussed in Section 6.2.5.

TABLE 14. COMPARISON OF RESULTS FOR RATE OF ONSET SERIES

Rate of Onset (G/sec)	Test No.	Peak Input Accel (G)	Total Velocity Change (ft/sec)	Seat Stroke (in.)	Peak Acceleration (G)								Duration of Seat Pan z Acceleration at 23 G (sec)	DRI
					Seat Pan x	Seat Pan z	Pelvis x	Pelvis z	Chest x	Chest z	Head x	Head z		
820.	A80-057	35.0	43.6	9.5	23.1	27.3	16.4	31.2	21.4	24.1	28.5	27.1	0.008	18.4
980.	A80-053	40.7	44.8	10.6	25.3	26.4	17.1	30.5	18.1	30.4	31.5	36.5	0.007	21.0
1040.	A80-054	40.2	44.2	10.5	22.1	29.4	10.1	30.8	24.1	25.8	38.5	28.2	0.016	19.7
1750.	A80-058	44.6	44.3	11.0	24.3	29.8	17.4	37.2	26.8	26.1	32.2	33.5	0.007	20.6
750.	A80-070	31.2	33.9	5.6	20.4	20.9	13.7	26.8	10.7	24.8	19.3	29.1	0.	17.0
1490.	A80-077	40.9	34.9	6.4	22.4	28.3	23.4	29.1	15.4	24.4	23.5	26.3	0.007	20.1

Rate of Onset (G/sec)	Test No.	Peak EA Load (lb)		Peak Lap Belt Load (lb)		Peak Shoulder Belt Load (lb)		Peak -G Strap Load (lb)	Peak Footrest Load (lb)	
		Right	Left	Right	Left	Right	Left		x	z
820.	A80-057	1430.	1380.	348.	181.	147.	201.	590.	1870.	2420.
980.	A80-053	1380.	1590.	373.	213.	200.	147.	593.	1760.	2200.
1040.	A80-054	1420.	1550.	300.	233.	87.	250.	560.	1900.	2120.
1750.	A80-058	1380.	1480.	496.	261.	214.	181.	523.	1950.	3210.
750.	A80-070	1380.	1470.	120.	74.	154.	174.	361.	1420.	1970.
1490.	A80-077	1370.	1440.	148.	107.	141.	174.	389.	950.	2640.

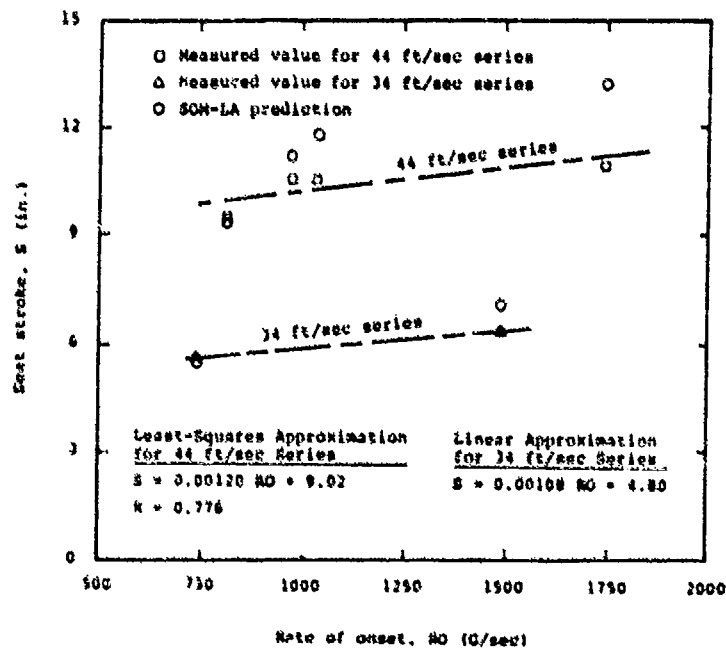


Figure 63. Rate of onset series, maximum seat stroke.

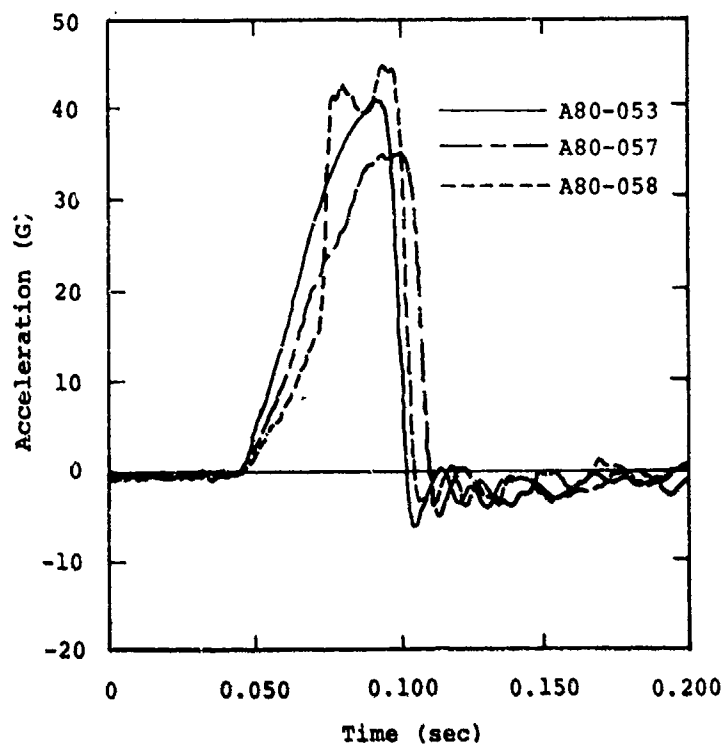


Figure 64. Comparison of input acceleration pulses for rate of onset series.

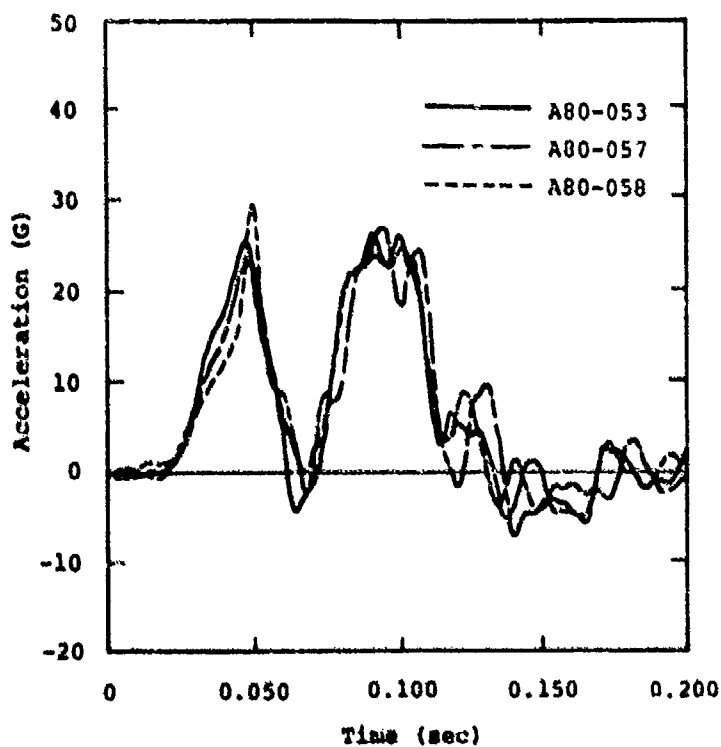


Figure 65. Comparison of seat pan z-axis acceleration for rate of onset series.

6.1.4 Energy Absorber Limit-Load Series

The energy absorber limit load is one of the most important parameters influencing the severity of the environment to which an occupant is subjected. The test series conducted in this program provides only a portion of the data necessary to optimize seat design: i.e., the relationship of seat stroke and transmitted accelerative loads to the energy absorber limit load. The optimal goal in energy-absorbing seat design is a limit load set at the highest possible level for the majority of occupant weights to assure that the available stroke distance can be used to absorb the maximum possible crash energy before the occupant bottoms out. The other information required to achieve this goal, namely the tolerable energy absorber limit load for the Army aviator population, will have to be derived from cadaver testing programs, human volunteer and primate experiments, and accident data from aircraft equipped with energy-absorbing seats.

Several differing types and percentiles of anthropomorphic dummies were used in this test series; however, this does not seem to have obscured important trends in seat performance. An effective limit load factor was calculated for each test from the equation:

$$L_L = \frac{\text{Energy Absorber Load}}{\text{Vertical Effective Occupant Weight} + \text{Movable Seat Weight}}$$

Results from this test series are compared in Table 15. Several of the variables, particularly seat stroke, and seat pan and pelvis z-axis acceleration are greatly influenced by energy absorber limit load. Seat stroke is plotted as a function of limit load in Figure 66. Linear regression was used to provide a least-squares approximation of the data; however, additional data plotted in Figure 66 indicate that the relationship between stroke and limit load may follow a higher order function. These data were calculated from two sources, i.e., the theoretical stroke equation for a triangular pulse derived in Volume IV of the Aircraft Crash Survival Design Guide (Reference 3):

$$\text{Stroke, } S = G_m g t_m^2 \left(\frac{1}{2} + \frac{K}{2} - \frac{K^3}{24} - 1 \right)$$

where G_m = peak input acceleration

t_m = half of the input acceleration pulse duration

K = limit load factor/ G_m .

TABLE 15. COMPARISON OF RESULTS FOR ENERGY ABSORBER LIMIT-LOAD SERIES

Test Parameter	Test No.	Peak Input Accel (G)	Velocity Change (ft/sec)	Total Seat Stroke (in.)	Peak Acceleration (G)								Duration of Seat Pan z Acceleration at 23 G (sec)	DRI	Effective Limit Load Factor (G)
					Seat Pan x	Seat Pan z	Pelvis x	Pelvis z	Chest x	Chest z	Head x	Head z			
50th % 14.5 G	A80-053	40.7	44.8	10.6	25.3	26.4	17.1	30.5	18.1	30.4	31.5	36.5	0.007	21.0	14.6
50th % 14.5 G	A80-054	40.2	44.2	10.5	22.1	29.4	10.1	30.8	24.1	25.8	38.5	28.2	0.016	19.7	14.6
50th % 11.5 G	A80-055	39.2	44.1	14.2	24.6	28.1	17.1	20.7	24.1	20.7	50.5	18.2	0.018	19.4	11.7
5th % 14.5 G	A80-074	41.4	45.0	9.8	25.4	31.1	14.4	30.8	32.2	32.1	69.3*	28.1	0.009	19.7	16.2
5th % 8.5 G	A80-075	42.5	45.9	16.1	26.0	26.6	22.2	34.5	47.6	68.7*	70.4*	70.0*	0.008	17.8	10.5
95th % 14.5 G	A80-073	40.2	45.6	12.0	28.1	25.1	19.4	41.2	15.4	29.8	53.6	20.7	0.004	18.0	12.0

Test Parameter	Test No.	Peak E/A Load (lb)		Peak Lap Belt Load (lb)		Peak Shoulder Belt Load (lb)		Peak -G Strap Load (lb)	Peak Footrest Load (lb)	
		Right	Left	Right	Left	Right	Left		x	z
50th % 14.5 G	A80-053	1380.	1590.	373.	213.	200.	147.	593.	1760.	2200.
50th % 14.5 G	A80-054	1420.	1550.	300.	233.	87.	250.	560.	1900.	2120.
50th % 11.5 G	A80-055	1210.	1170.	174.	107.	221.	255.	517.	2190.	1950.
5th % 14.5 G	A80-074	1360.	1450.	154.	187.	174.	127.	481.	1190.	1820.
5th % 8.5 G	A80-075	888.	930.	201.	107.	94.	101.	436.	1490.	1890.
95th % 14.5 G	A80-073	1390.	1440.	174.	334.	120.	120.	448.	1640.	2620.

*Amplifiers saturated.

and from Program SOM-LA test simulations using the input acceleration from A80-053, with the only variable being the energy absorber limit load. If the relationship between E/A limit load and stroke is not linear, then it becomes even more important to set the limit load at the highest possible level compatible with human tolerance because even a small reduction in load can result in a significant stroke increase with a resulting increase in the hazard of bottoming out. A nonlinear dependence of stroke on E/A limit load would indicate that variable-load systems would be quite beneficial, particularly for retrofit applications where stroke distance is usually restricted.

A definite trend is apparent in the seat pan z-axis acceleration and DRI, presented in Figures 67 and 68, although neither parameter appears to be particularly sensitive to limit load. The SOM-LA simulations described above predict some very interesting and unexpected trends in terms of spinal load and moment. The maximum lumbar spine compressive load, presented in Figure 69, shows a direct relationship to limit load where the spinal load

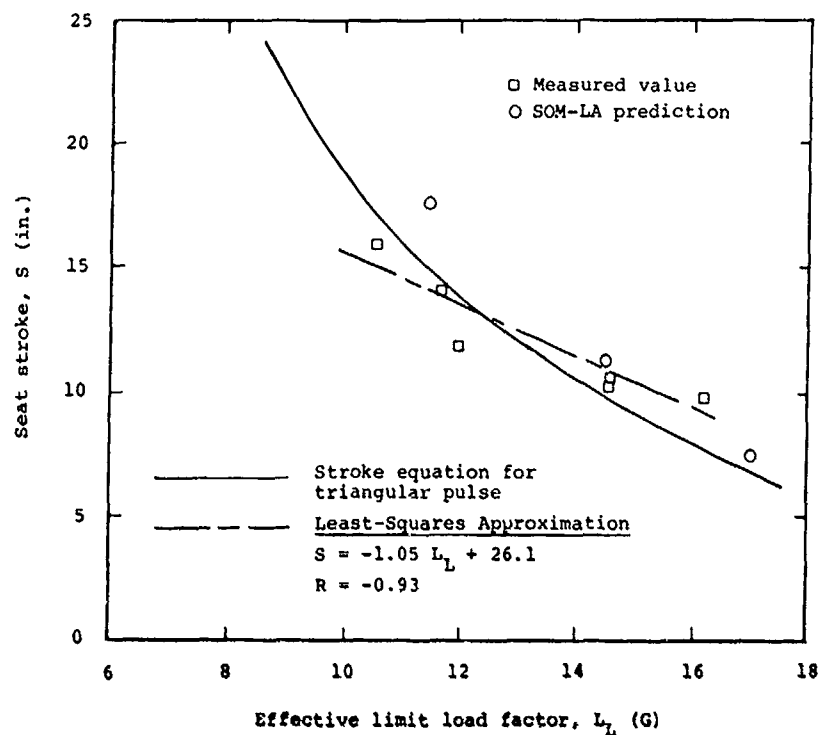


Figure 66. Energy absorber limit load series, maximum seat stroke.

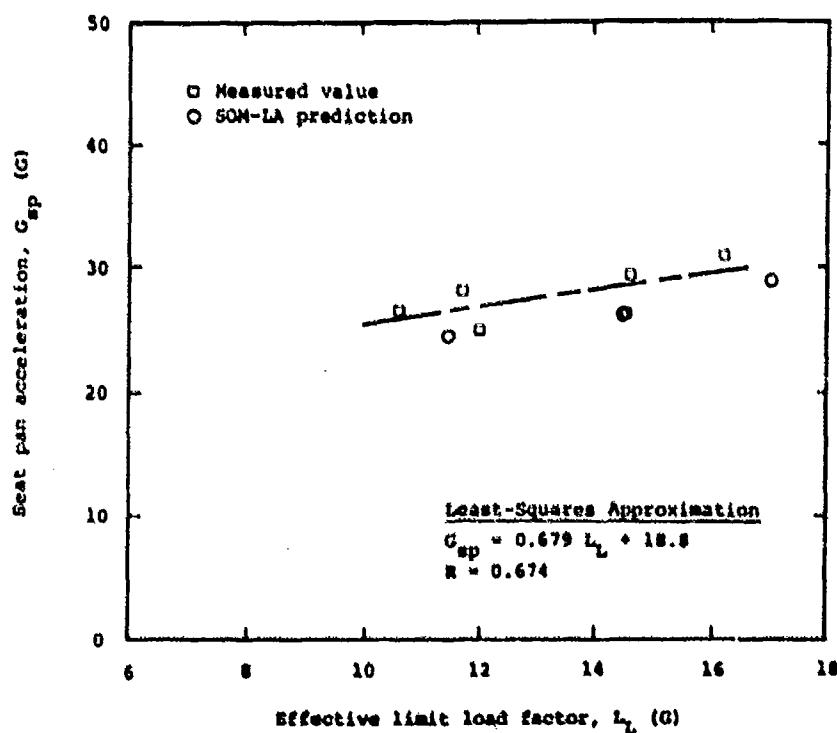


Figure 67. Energy absorber limit load series, maximum seat pan z-axis acceleration.

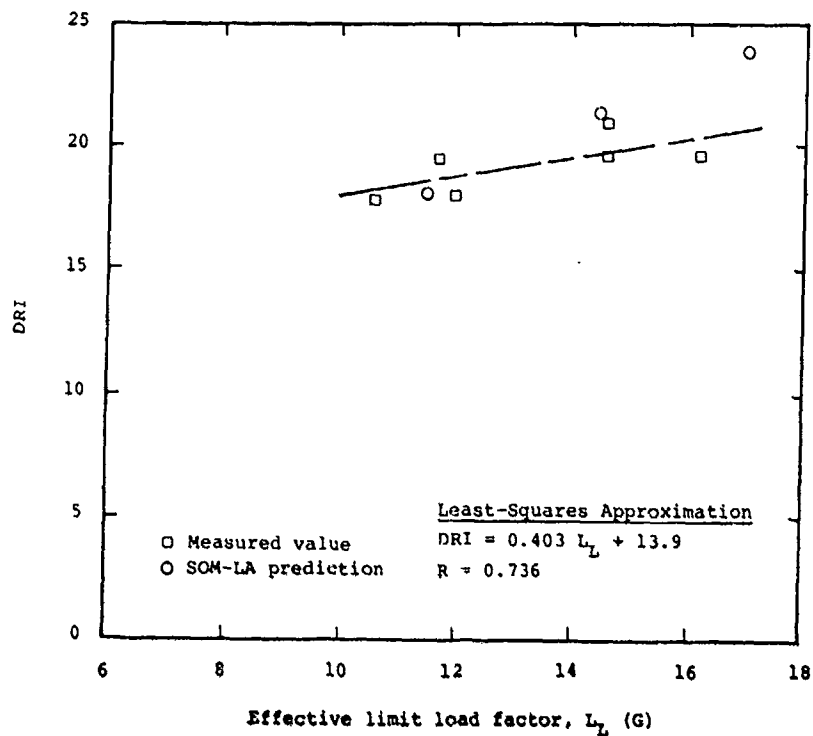


Figure 68. Energy absorber limit load series. Dynamic Response Index.

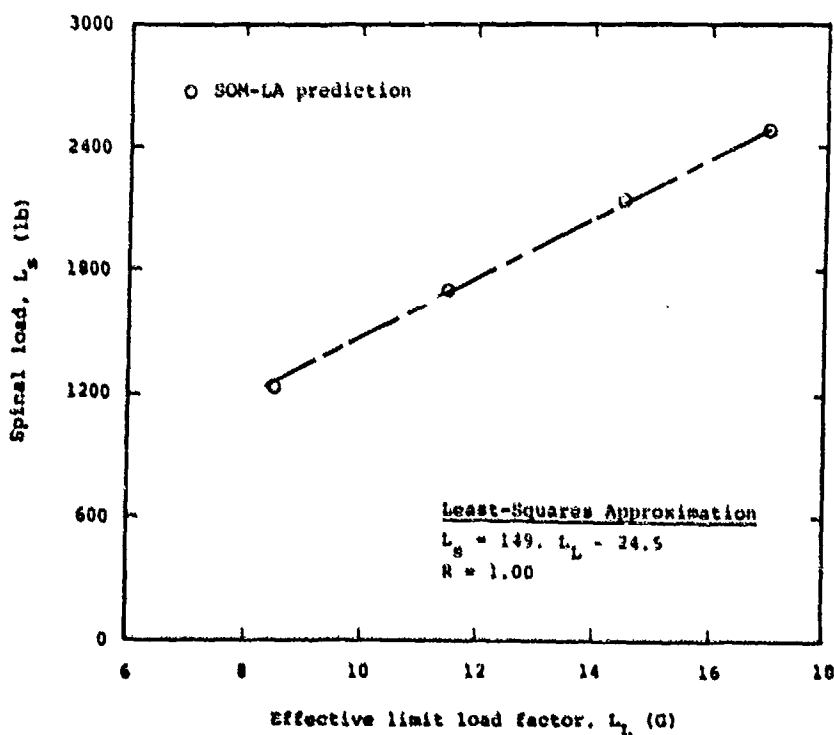


Figure 69. Energy absorber limit load series, predicted maximum lumbar spine load (compression).

doubles from approximately 1200 to 2400 lb while the E/A limit-load factor is increased from 8 G to 16 G. The spinal moment, shown in Figure 70, predicts, unexpectedly, that the moment actually decreases for an increase in limit load and this function is not just linear but rather a higher-order function. After analysis of this trend, it appears that the SOM-LA predictions of maximum spinal load are strongly influenced by the amount of seat stroke that occurs, which in turn is controlled by the energy absorber limit load. Spinal load is plotted against seat stroke in Figure 71.

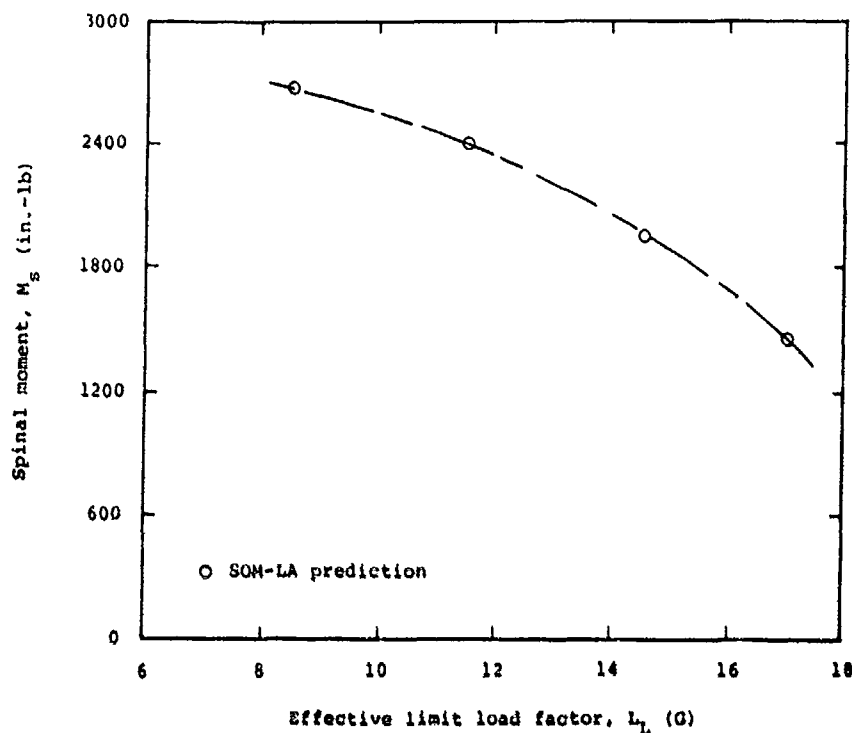


Figure 70. Energy absorber limit load series, predicted maximum lumbar spine moment (flexion).

The only test data available to verify these trends are from the modified dummy test series conducted at Wayne State University. Maximum recorded spinal loads and moments for two combined-mode tests are listed in Table 16. The maximum spinal load is in direct proportion to the energy absorber load as predicted by the SOM-LA simulations; whereas the predicted inverse relationship between spinal moment and E/A limit load is not nearly as obvious in the measured test data. It is apparent that further test work with an instrumented dummy would be beneficial in verifying these trends.

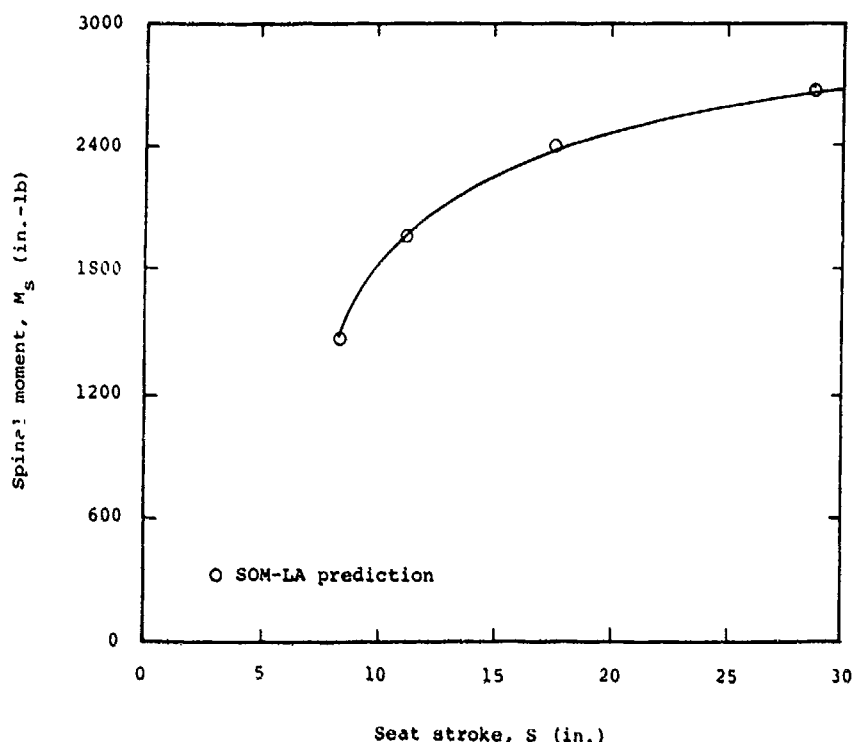


Figure 71. Energy absorber limit load series, maximum lumbar spine moment versus seat stroke.

TABLE 16. MEASURED SPINAL LOADS AND MOMENTS FOR WAYNE STATE UNIVERSITY MODIFIED DUMMY TEST SERIES WITH COMBINED ORIENTATION

Limit Load Factor (G)	Seat Stroke (in.)	Peak Spinal Load (lb)	Peak Spinal Moment (in.-lb)
14.5	4.5	1140.	913.
11.5	6.2	850.	938.

6.1.5 Test Facility Impact Conditions

The sensitivity of seat and occupant response to a particular input pulse shape is an important variable in terms of qualification testing. Each facility evaluating energy-absorbing seating systems will have a characteristically shaped deceleration pulse representative of the type of deceleration mechanism used. All facilities will be attempting to duplicate an idealized triangular test pulse within some set of reasonable tolerances, such as those specified in Reference 6; although MIL-S-58095(AV) does not presently set acceptable deviations for the input pulse. In addition

to the input pulse shape, another factor that can affect seat and occupant response is the decelerator orientation, i.e., the relationship of the deceleration direction to the gravity vector.

The parametric test plan for the input pulse shape test series called for each participating facility to approximate the nominal baseline deceleration pulse shown in Figure 72. The closest approximation of each facility to the prescribed conditions within the constraints imposed by their deceleration mechanism is shown in Figure 73. Seat and occupant response, as represented by the seat pan and pelvis z-axis accelerations, are presented in Figure 74 for the four test facilities.

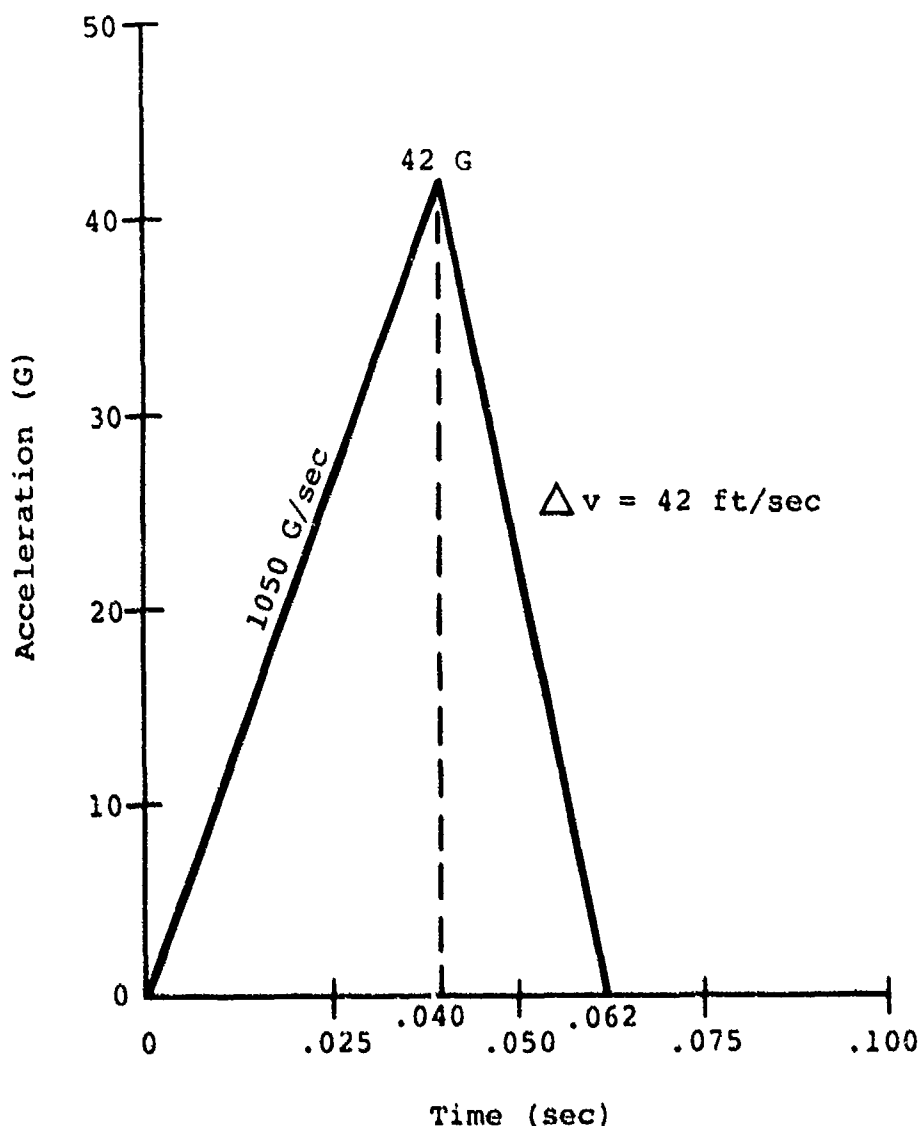


Figure 72. Nominal baseline input acceleration pulse.

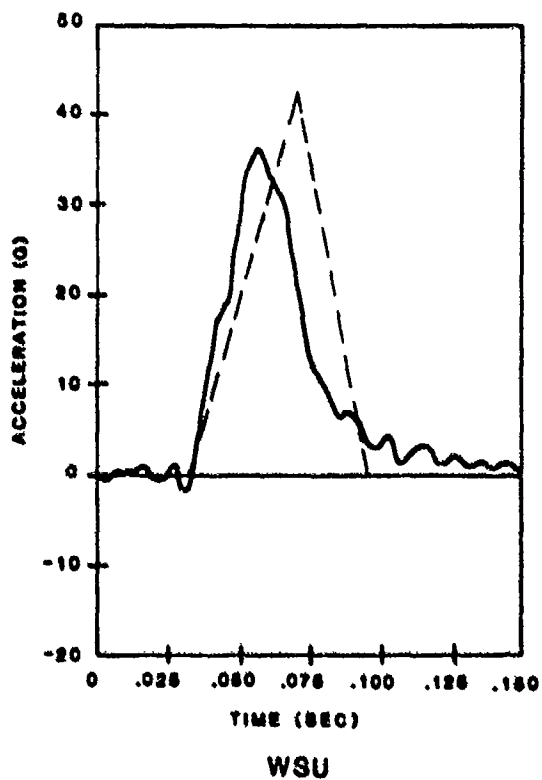
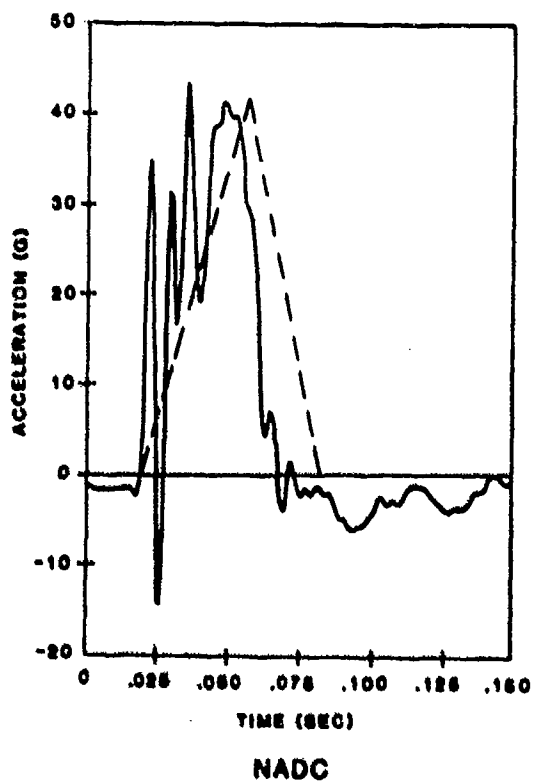
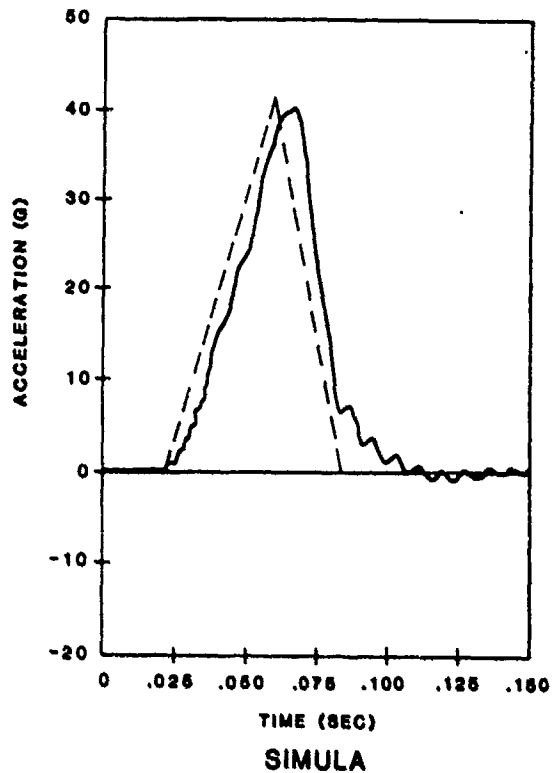
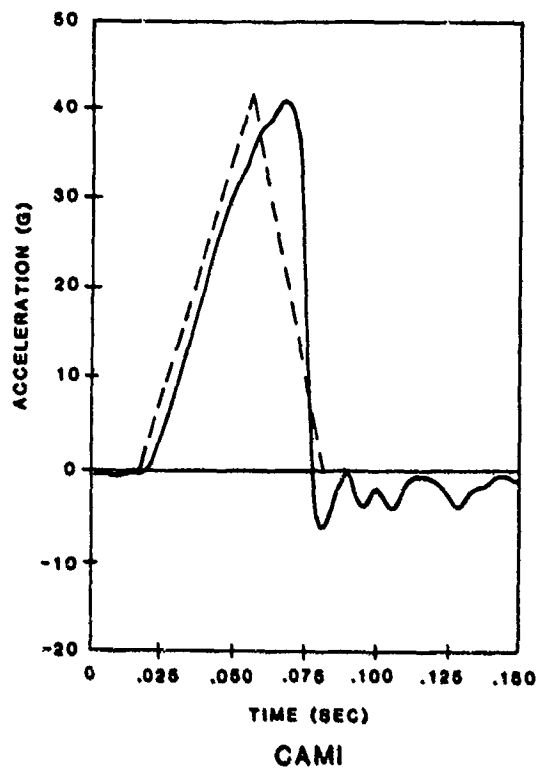
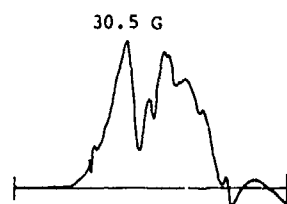


Figure 73. Baseline acceleration pulses for the four test facilities.

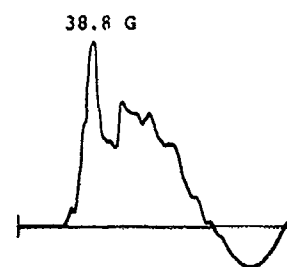


CAMI A80-053

Pelvis z acceleration

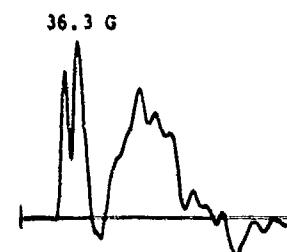


Seat pan z acceleration

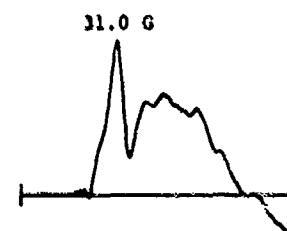


NADC Drop 189

Pelvis z acceleration



Seat pan z acceleration



Simula E/A Criteria Test 1

Pelvis z acceleration



Seat pan z acceleration

Figure 74. Comparison of pelvis and seat pan z-axis acceleration for baseline test conditions at three facilities.

There is often a tendency to conclude that certain test facilities are better able to simulate the crushing characteristics of aircraft by their ability to duplicate the triangular test pulse. The triangular pulse is merely representative of the waveforms that have been observed in the major impact during aircraft crash tests. The repeatability of a test pulse among facilities is far more important than the ability to reproduce a specific crash pulse.

Measured test values for the baseline tests at the four facilities are compared in Table 17. It is important to note that there are significant differences in seat and occupant response among facilities. Six parameters relating to test severity are plotted in Figures 75 through 80 for comparison to baseline tests conducted at the four facilities. There are obvious differences in magnitudes of seat and occupant response that cannot be explained by the sensitivity curves presented in Sections 6.1.1 through 6.1.4. It is sufficient to conclude from this series that facilities differ, that the effect of these differences on seat performance is significant, and that it would be very difficult to adjust test data in order to compare tests conducted at various facilities. If it is important to compare tests, then they must be conducted at the same facility.

TABLE 17. COMPARISON OF TEST FACILITY BASELINE IMPACT CONDITIONS

Test Facility	Test No.	Rate of Onset (G/sec)	Peak Input Accel (G)	Total Initial Velocity (ft/sec)	Velocity Change (ft/sec)	Peak Acceleration (G)								Duration of Seat Pan z Acceleration at 23 G (sec)	DWI
						Seat Pan x	Seat Pan z	Head x	Head z	Chest x	Chest z	Head x	Head z		
CAMI	ABU-053	940	40.7	41.8	44.8	25.3	26.4	17.1	10.5	18.1	30.4	31.5	36.5	0.007	21.0
	ABU-054	1040	40.2	42.3	44.2	22.1	29.4	10.1	10.8	24.1	25.8	38.5	28.2	0.016	19.7
WADC	W-189	2530	44.9	36.8	40.4	16.6	34.3	15.0	18.8	10.0	36.1	24.7	40.8	0.004	20.8
	W-190	2620	45.0	36.8	40.5	16.8	34.6	18.7	40.1	14.7	37.4	22.7	42.8	0.007	20.7
Simula	SEAC-1	1090	39.6	31.1	42.4	12.3	22.1	16.3	31.0	11.3	30.7	17.7	36.3	0.	19.4
	SEAC-2	1110	40.9	31.1	42.2	13.8	25.5	11.7	39.7	11.7	36.0	16.3	43.0	0.003	21.5
MSU	W-159	1710	36.1	41.2	41.2	15.5	28.6	13.2	18.8	7.3	42.1	17.2	39.0	0.011	18.5

Test Facility	Test No.	Seat Strike (in.)	Peak R/A Load (lb)		Peak Lap Belt Load (lb)		Peak Shoulder Belt Load (lb)		Peak -G Strap Load (lb)	Peak Footrest Load (lb)	
			Right	Left	Right	Left	Right	Left		x	z
CAMI	ABU-053	10.4	1280.	1590.	373.	213.	200.	147.	593.	1740.	2200.
	ABU-054	10.5	1420.	1550.	300.	233.	87.	250.	560.	1900.	2120.
WADC	W-189	10.8	1449.	1457.	347.	315.	149.	221.	478.	1670.	2310.
	W-190	11.4	1370.	1415.	361.	508.	181.	355.	515.	1840.	2410.
Simula	SEAC-1	9.5	1281.	1367.	253.*	240.*	246.*	227.*	320.*	1570.	1510.
	SEAC-2	9.4	1310.	1400.	253.	267.	307.	280.	300.*	1610.	2010.
MSU	W-159	6.3	1404.**	1204.**	74.	77.	471.	338.	310.	1045.	2609.

*Load is increasing at end of recorded time history.

**Compatibility problems between transducers and MSU signal conditioning system caused error in R/A load data. Magnitude of error could not be estimated.

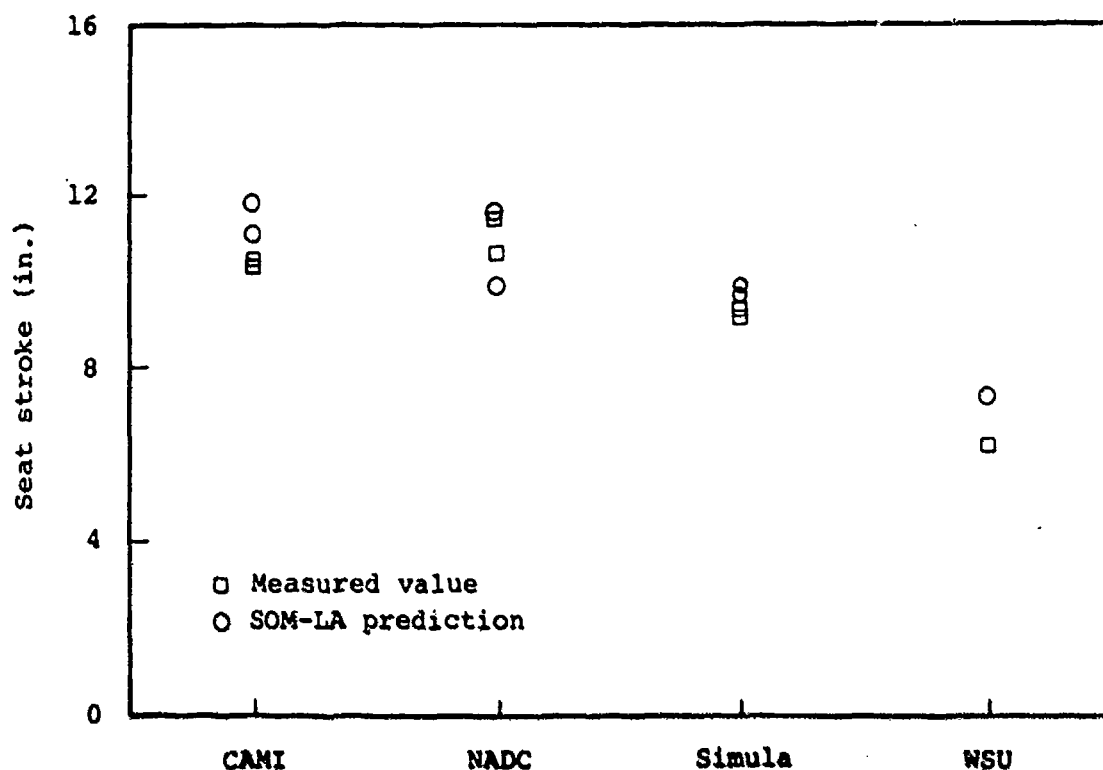


Figure 75. Test facility impact condition series, maximum seat stroke.

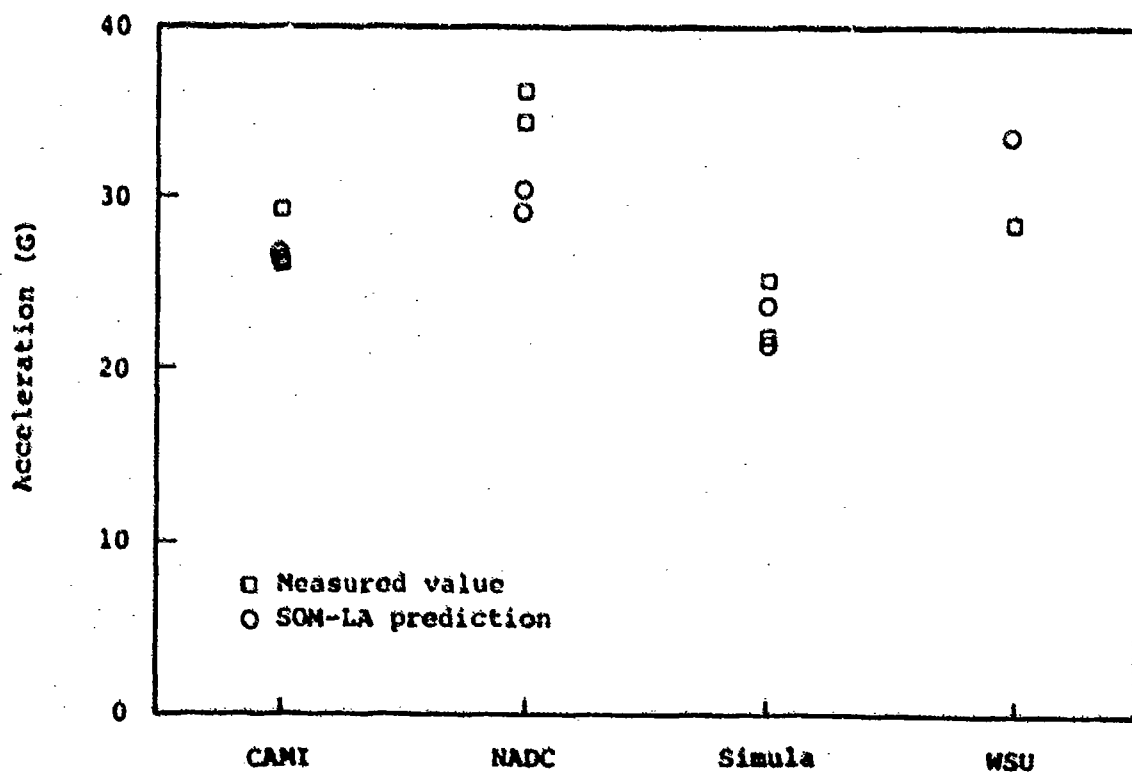


Figure 76. Test facility impact condition series, maximum seat pan z-axis acceleration.

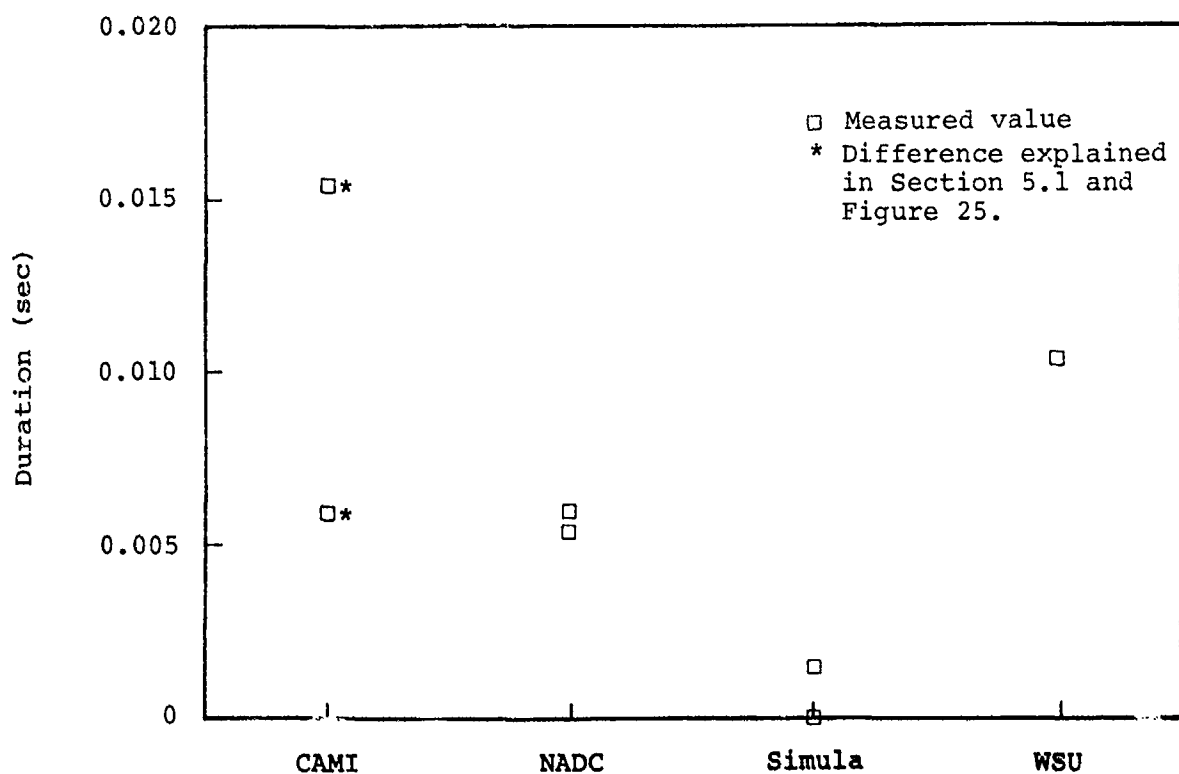


Figure 77. Test facility impact condition series, duration of seat pan z-axis acceleration at 23 G.

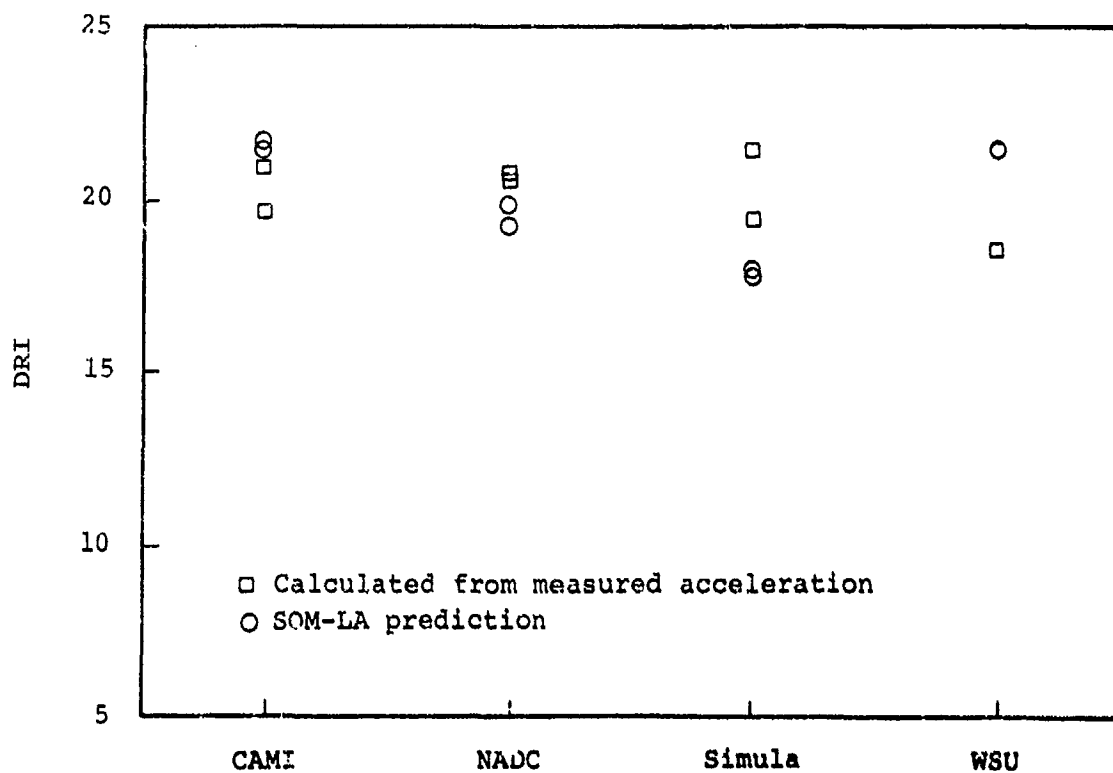


Figure 78. Test facility impact condition series, DRI.

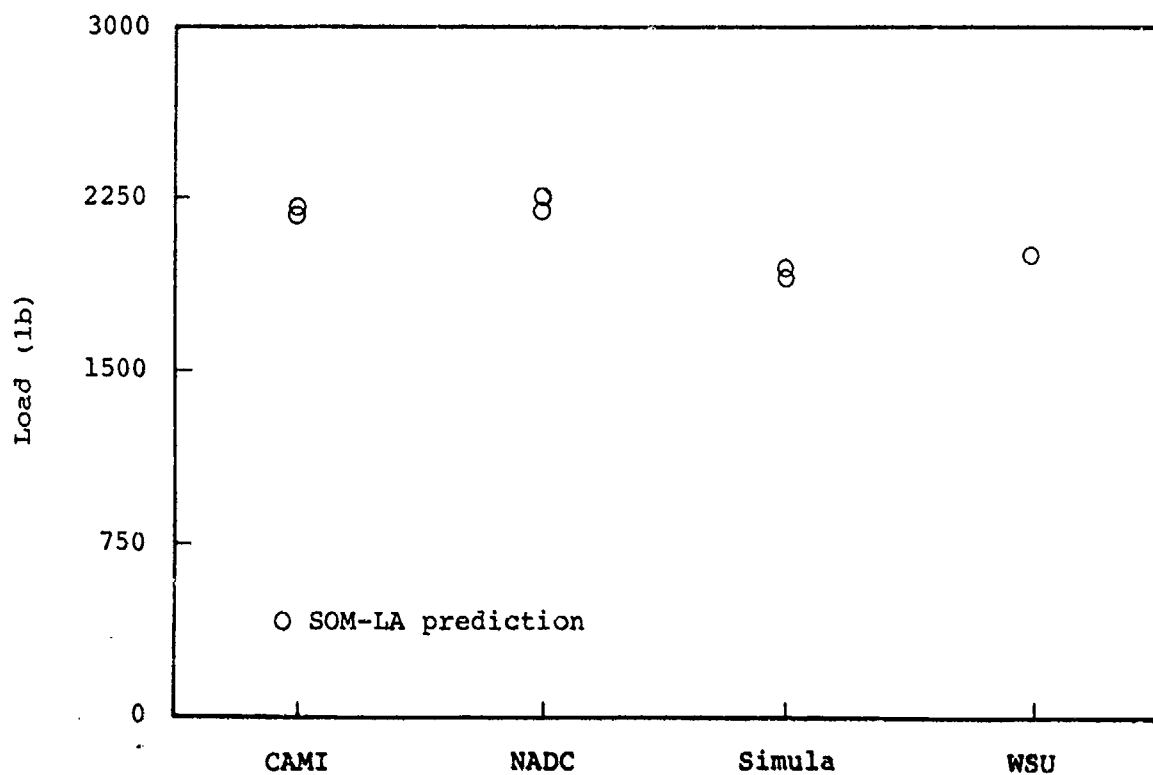


Figure 79. Test facility impact condition series, maximum lumbar spine axial compressive load.

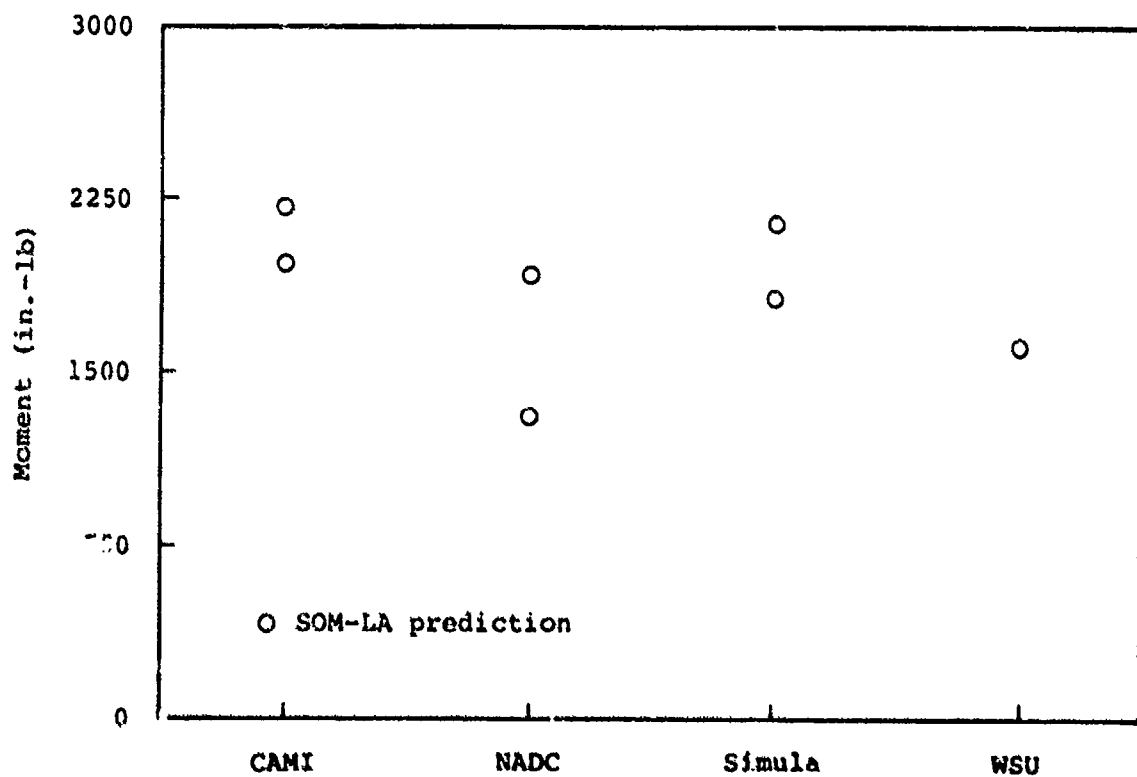


Figure 80. Test facility impact condition series, maximum lumbar spine y-axis moment (flexion).

6.1.6 Dummy Type Series

Most of the testing for response comparisons of various dummy models was accomplished using a rigid seat. As described in Section 4.1.1, the seat back was horizontal for all tests, thereby aligned with the impact velocity vector on the CAMI sled facility. No cushions were used, and the seat pan was mounted on a six-axis load cell. In order to remove the dynamic effects of the stroking seat and the interaction between the occupant and seat, a 14.5-G trapezoidal-shaped input pulse was used. The actual pulse from Test A80-026, which used the baseline Hybrid II dummy, is shown in Figure 81; others were nearly identical.

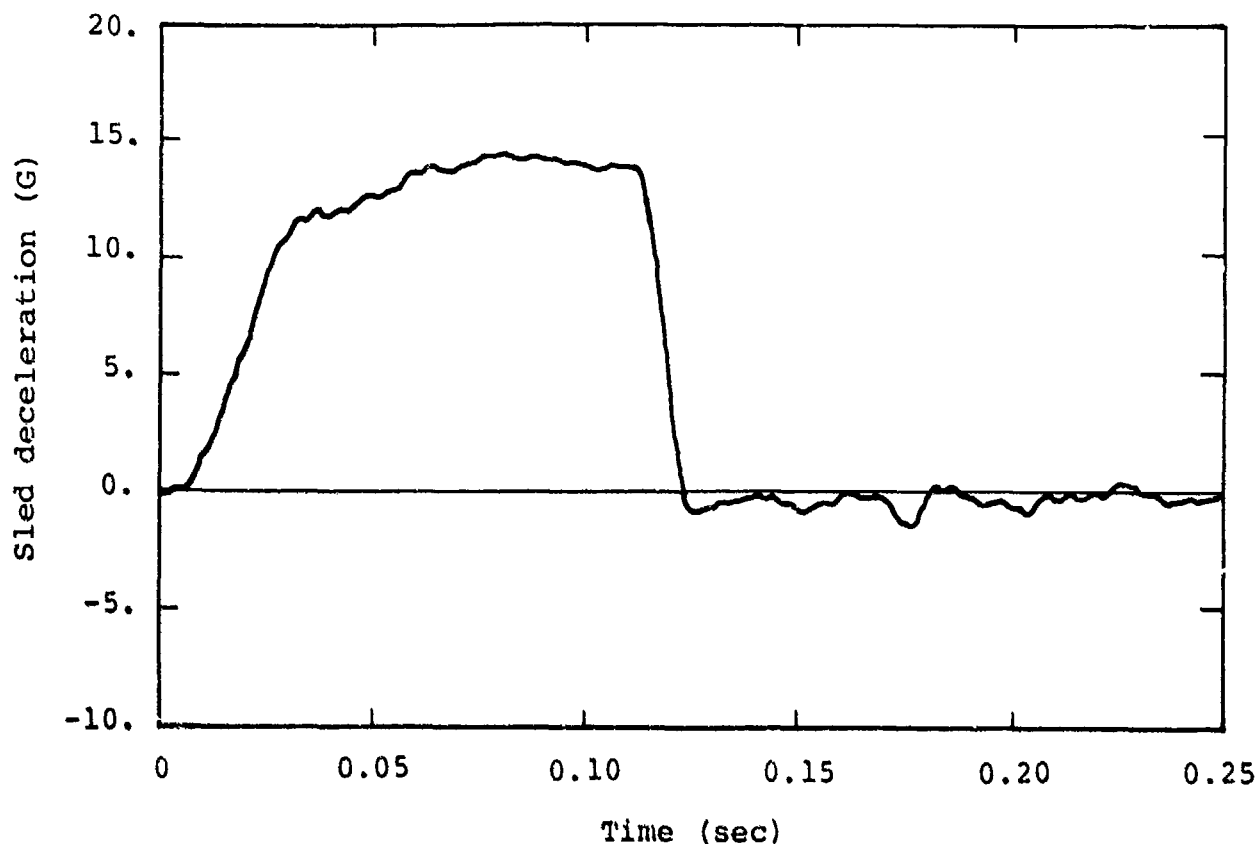


Figure 81. Sled deceleration, rigid seat test A80-026.

As listed in Table 18, three 50th-percentile dummies were compared, and three tests were conducted with each dummy. The peak dummy accelerations and seat pan force average for the three tests are presented in Table 18. For a given dummy, measured accelerations varied by a maximum of ± 1 G from the mean. The acceleration values presented in Table 18 indicate that for x-axis response in a vertical test, the Hybrid II and VIP-50 are similar. However, the elastomeric lumbar spine in the Hybrid II appears to significantly alter the z-axis response. The peak z-axis accelerations measured for the Hybrid II exhibit variations for the pelvis,

TABLE 18. AVERAGE PEAK ACCELERATIONS AND SEAT PAN LOADS FOR RIGID SEAT COMPARISON TESTS OF 50TH-PERCENTILE DUMMIES (AVERAGE OF THREE TESTS)

Dummy Description	Peak Acceleration (G)						Seat Pan z Force (lb)
	Pelvis x	Pelvis z	Chest x	Chest z	Head x	Head z	
Hybrid II ¹	9.6	42.9	6.6	26.2	12.0	33.4	2710
Alderson VIP-50 ²	10.0	35.3	5.3	37.4	14.7	39.0	2960
Alderson CG-50 ³	16.9	39.9	14.3	41.3	56.6	46.8	5500

Notes: 1. Tests A80-025, A80-026, and A80-027.
2. Tests A80-022, A80-023, and A80-024.
3. Tests A80-032, A80-033, and A80-034.

chest, and head, while the essentially incompressible column of the VIP-50 maintains a fairly uniform acceleration level throughout the body. Response of the older design CG-50 is significantly different from the other two dummy types, particularly in the head acceleration and the load transmitted to the seat pan (as shown in Figure 82).

A second series of tests for comparison of dummy types used three 95th-percentile dummies commonly used for dynamic qualification tests of energy-absorbing seats: the VIP-95 (with elastomeric spine), the CG-95, and the Sierra 292-895. These tests were conducted with the Black Hawk seat in the baseline test configuration. Results of these tests, presented in Table 19, are inconclusive due to the lack of complete data sets and small sample size. However, the seat pan response appears to be consistent among the three dummies. Results from the two VIP-95 dummies cannot be directly compared since dummy 4a (Test A81-123) had been reworked to include an Ensolite pad in the buttocks area, not present in dummy 4b. Also, dummy 4a had been modified to include load cells in the lumbar and neck regions.

6.1.7 Dummy Percentile Series

Evaluation of seat and occupant performance as functions of dummy percentile was complicated by the lack of similar anthropomorphic test dummies. Two sets of baseline configuration tests were run with a Hybrid II 50th-percentile dummy and a VIP-95 dummy with an elastomeric spine similar to the Hybrid II configuration. Results of the test series are presented in Table 20. In the final test

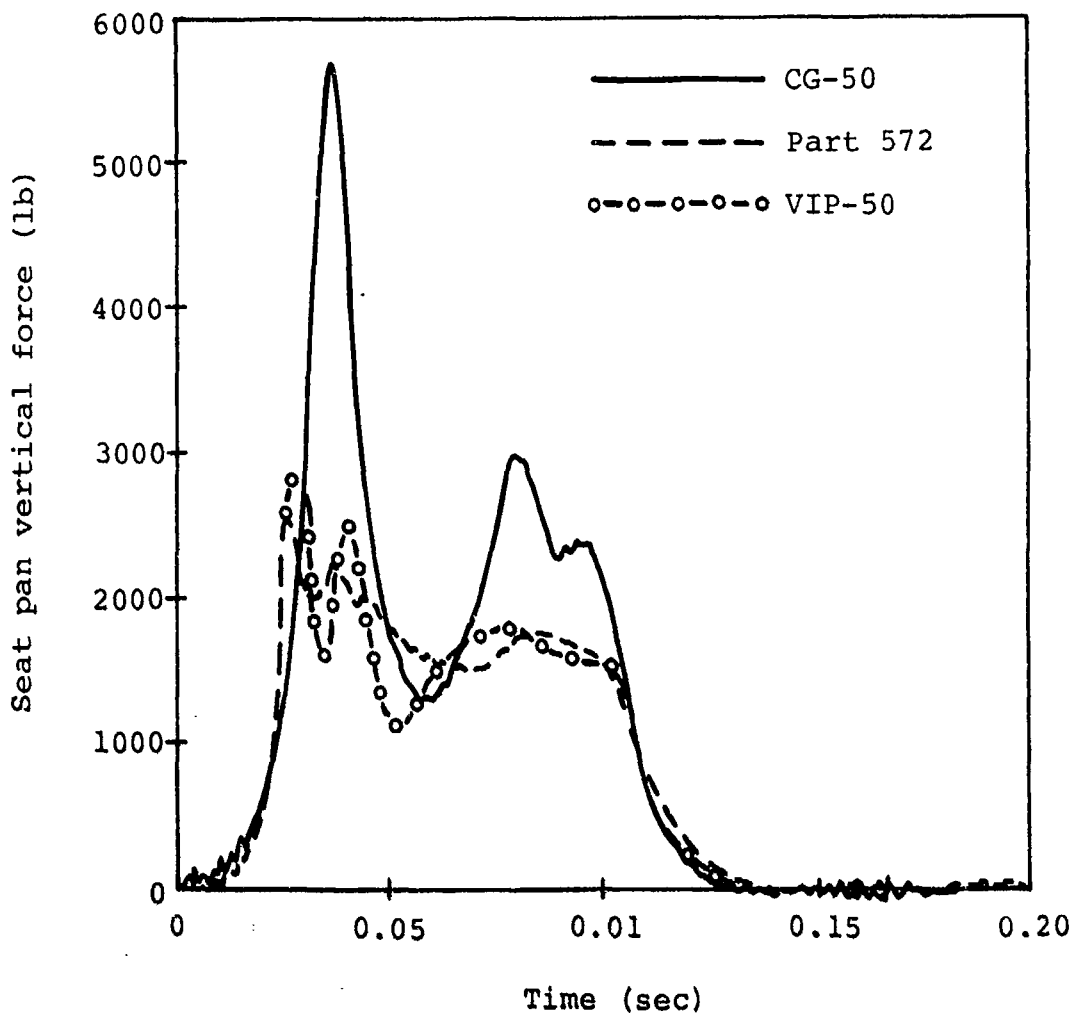


Figure 82. Comparison of seat pan force measured in rigid seat tests with three 50th-percentile dummies.

TABLE 19. COMPARISON OF RESPONSE FOR 95TH-PERCENTILE DUMMIES IN THE BASELINE TEST CONFIGURATION

Dummy Description	Test No.	Seat Stroke (in.)	Peak Acceleration (G)								Duration of Seat Pan z Acceleration at 23 G (sec)	DRI
			Seat Pan x	Seat Pan z	Pelvis x	Pelvis z	Chest x	Chest z	Head x	Head z		
Alderson VIP-95	A81-123 ^{1,3} A80-073 ^{2,3}	13.2 12.0	29.6 29.3	28.1 25.1	24.8 21.8	35.0 41.2	41.5 15.4	26.8 29.8	N/M ⁴ 53.6	N/M 32.2	0.012 0.005	17.2 19.7
Alderson CG-95	A81-125	13.1	28.4	29.6	N/M	N/M	57.0	34.2	N/M	N/M	0.012	18.3
Sierra 292-895	A81-126	11.0	29.8	31.9	22.8	63.3	N/M	N/M	N/M	N/M	0.010	20.0

Notes: 1. Dummy 4a (consolidate pad under pelvis, as noted in Table 4) with lumbar and neck load cells.
2. Dummy 4b.
3. With elastomeric spine.
4. Not measured.

TABLE 20. SUMMARY OF THE EFFECT OF ANTHROPOMORPHIC DUMMY PERCENTILE ON PEAK ACCELERATION VALUES

Dummy Percentile	CAMI Test No.	Seat Stroke (in.)	Peak Acceleration (G)								Duration of Seat Pan z Acceleration at 23 G (sec)	DRI
			Seat Pan x	Seat Pan z	Pelvis x	Pelvis z	Chest x	Chest z	Head x	Head z		
50th Percentile	A80-053	10.6	25.1	26.4	30.5	30.5	18.1	30.4	31.5	36.5	0.007	21.0
	A80-054	10.5	26.8	29.4	25.1	30.8	24.1	25.8	38.5	36.5	0.016	19.7
	A81-124 ¹	11.4	32.3	26.0	22.2	28.5	35.5	28.1	32.5	28.5	0.006	19.4
95th Percentile	A80-073 ²	12.0	29.3	25.1	21.8	41.2	15.4	29.8	53.6	32.2	0.005	18.0
	A81-123 ³	13.2	29.6	28.1	24.8	34.5	41.5	26.8	N/A	N/A	0.012	17.2

Notes: 1. Load cell in lumbar region.
2. Dummy 4b.
3. Dummy 4a, Ensolite pad in buttocks, load cells in lumbar spine and neck.

of each series (test numbers A81-124 and A81-123) the anthropomorphic test dummies were modified by the addition of a six-axis load cell at the base of the lumbar spine which was used to obtain load and moment data. Measured load and moment data for these two tests are presented in Table 21.

TABLE 21. SUMMARY OF THE EFFECT OF ANTHROPOMORPHIC DUMMY PERCENTILE ON SPINAL LOADS AND MOMENTS

Dummy Percentile	Test No.	Peak Lumbar Load (lb)				Peak Lumbar Moment (in.-lb)			
		x	y	z	Resultant	x	y	z	Resultant
50th Percentile	A81-124	360	60	1220	1220	360	1250	93	1260
95th Percentile	A81-123	593	153	1230	1260	653	1500	107	1510

When a 95th-percentile dummy is used in place of the 50th-percentile device, the increase in seat stroke of approximately 2 in. is predictable by the increase in vertical effective weight. However, one might also assume that there would be a general decrease in acceleration for the 95th-percentile dummy, although this is not readily apparent from the peak values presented in Table 20. The explanation is that the peak values, due to dynamic overshoot, are not strongly affected by the occupant size,

while the average acceleration during the crash sequence is lower for a heavier occupant (provided that the energy-absorbing limit load is fixed). This is evident from the seat pan DRI, which shows a definite trend of lower values for increasing occupant size.

Loads and moments presented in Table 21 are intended for use in validation of computer models and correlation with injury criteria, and are not intended for use as a quantitative measure of spinal damage based on known vertebral segment strength distributions. The data presented indicate that axial spinal force (z-axis) is not a function of occupant size, while the moment associated with forward rotation of the body (y-axis) does show an increasing trend with body size. However, these data should be used with caution because the chest x-axis acceleration measured in tests with the modified dummies shows a substantial increase in peak value. This is possibly an indication that the installation of the load cell may have altered the rotational stiffness of the torso. Also, as noted in Section 5.6, a second load path carries part of the axial force and bending moment in the torso, perhaps a greater percentage in the dummy than in a human, where the abdominal region is not as stiff.

6.1.8 Cadavers Versus Anthropomorphic Dummies

A series of tests is being conducted to establish decelerative spinal fracture loads for occupants of energy-absorbing seats, as discussed in Chapter 2. That program has not yet been completed, and the test data have not yet been analyzed in detail. However, enough tests have been completed to determine characteristic responses of cadavers in the Black Hawk seat and to justify the use of the Part 572 dummy as a human surrogate for seat testing. Although not specifically part of the sensitivity analysis being discussed in this chapter, the cadaver test program has significant implications on the development of more rigorous seat criteria. A comparison of cadaver and dummy test results is presented here.

The cadaver test series is being conducted at Wayne State University under the baseline test conditions. Similar tests were conducted at WSU with the Part 572 dummy that was instrumented to measure spinal forces and moments. Results of comparable cadaver and dummy tests are shown in Table 22. Resultant peak body accelerations are presented for comparison because the accelerometer orientation in the cadaver did not necessarily correspond to the standard dummy coordinate system.

Required seat stroke values presented in Tables 22 and 23 indicate that, in general, the Part 572 dummy requires slightly less stroke distance than does the cadaver. The seat pan vertical accelerations, presented in Figures 83 and 84 for the vertical and combined tests, respectively, show that the interaction between the

TABLE 22. COMPARISON OF SEAT AND OCCUPANT RESPONSE
FOR DUMMIES AND CADAVERS

	Seat Stroke (in.)	Peak Acceleration (G)					Duration of Seat Pan z Acceleration at 23 G (sec)	DRI
		Seat Pan x	Seat Pan z	Pelvis Resultant	Chest Resultant	Head Resultant		
Dummy, Vertical	6.3	15.3	28.9	40.3	43.4	41.7	0.011	18.4
Cadaver, Vertical	7.6	17.5	26.5	33.9	N/A	49.7	0.004	21.8
Dummy, Combined	4.5	27.8	23.9	35.2	31.6	46.9	0.004	17.8
Cadaver, Combined	4.5	37.3	25.4	22.8	N/A	59.6	0.004	22.2
	5.5	40.5	21.0	44.4*	N/A	97.3*	0.	19.3

*Impact between mouth-mount accelerometer and thigh.

TABLE 23. COMPARISON OF SEAT STROKE FOR CADAVERS
AND DUMMIES IN THE UH-60A CREWSEAT

Test Description	Cadaver Tests		Dummy Tests	
	Occupant Weight (lb)	Seat Stroke (in.)	50th* Hybrid II	
			Occupant Weight (lb)	Seat Stroke (in.)
14.5-G E/A, Vertical Orientation, 42-45 G Peak Input Acceleration	166	7.6	164	6.3
	160	7.4	164	7.0
	140	7.1		
	148	7.1		
14.5-G E/A, Combined Orientation, 42-45 G Peak Input Acceleration	166	5.5	164	4.5
	140	4.5		
11.5-G E/A, Combined Orientation, 42-45 G Peak Input Acceleration	218	9.4	164	6.5
	141	7.0		
	160	9.0		
8.5-G E/A, Combined Orientation, 42-45 G Peak Input Acceleration	200	13.1		
	143	9.7		
	165	8.9		

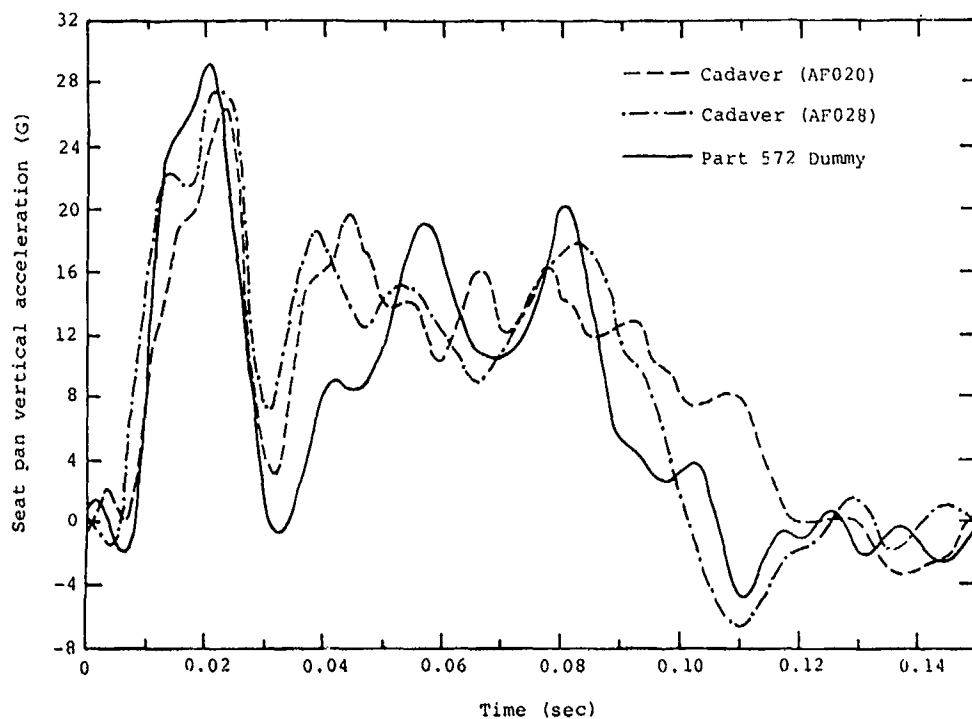


Figure 83. Seat pan vertical acceleration for a Part 572 dummy and two cadavers measured in vertical mode tests with 14.5-G energy absorbers.

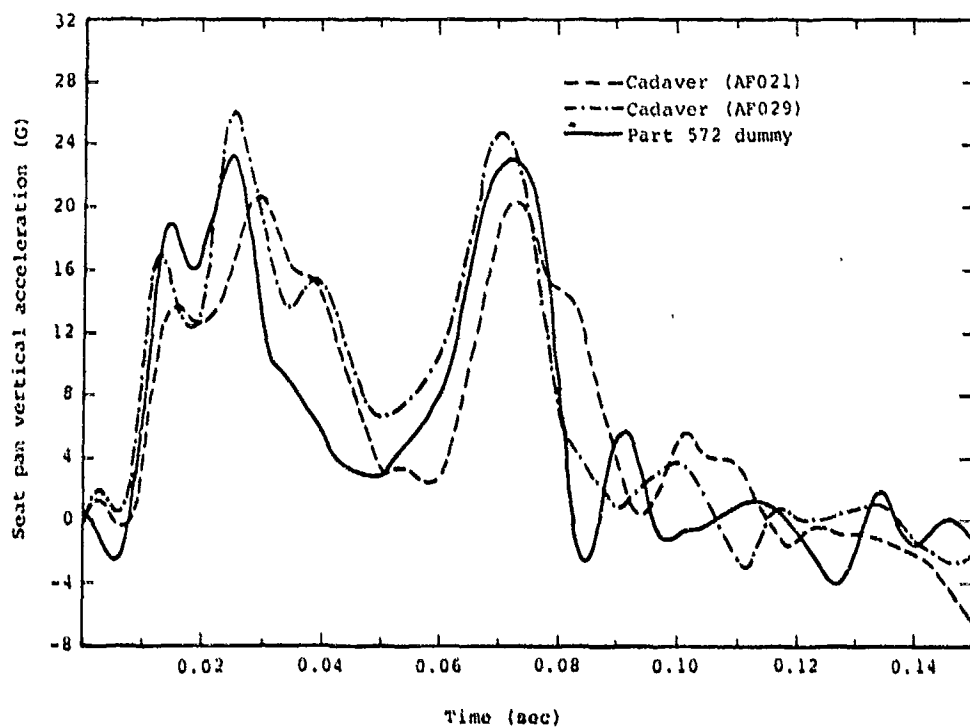


Figure 84. Seat pan vertical acceleration for a Part 572 dummy and two cadavers measured in combined mode tests with 14.5-G energy absorbers.

Part 572 dummy and seat pan is very similar to the response measured with human cadavers. Also, a comparison of the required seat stroke for cadavers and dummies, shown in Figure 85, indicates that the occupant type has little effect on this parameter. The limit load for the cadavers in Figure 85 is normalized by the cadaver weight; that is, the effective limit load is equal to the measured energy absorber load divided by the effective vertical weight of the seat and occupant. The comparison between body accelerations for the dummy and cadaver does not show a good correlation.

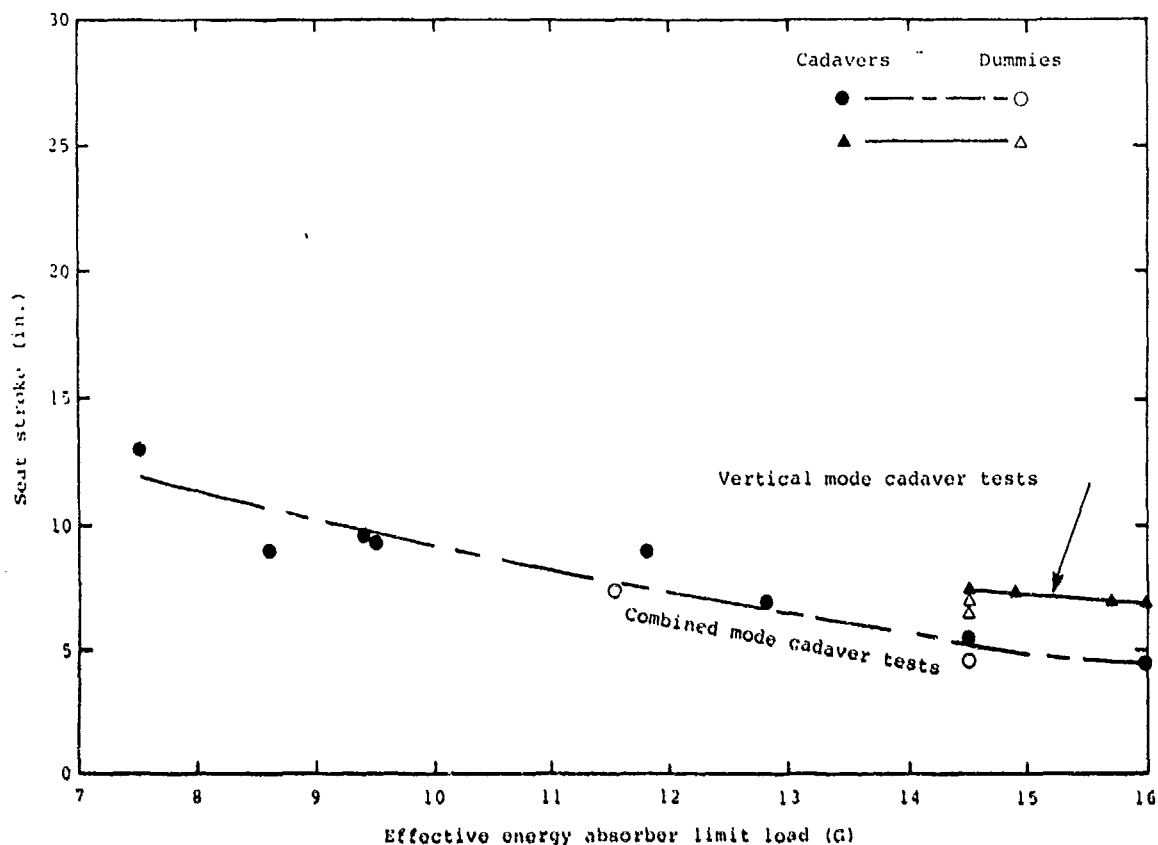


Figure 85. Comparison of normalized seat stroke for cadavers and dummies tested with the Wayne State University input pulse shape.

Results of this limited comparison between occupant types indicate that seat performance criteria based on seat pan acceleration may not be as sensitive to occupant type as a criterion based on body segment acceleration. However, it may also indicate that injury mechanisms within the body, e.g., spinal deformation, cannot be reliably predicted from seat pan acceleration, as internal body response can vary significantly for various occupant types with similar inputs from the seats.

6.1.9 Seat Orientation Series

In order to investigate the effect of aircraft (i.e., seat) orientation on seat and occupant response, tests were conducted with both rigid and energy-absorbing seats. The baseline rigid seat tests at CAMI were conducted with the seat vertical axis (and seat back) parallel to the impact velocity vector. Tests were also conducted with the seat vertical axis pitched forward 30 degrees and rolled 10 degrees. Results are compared in Table 24 for both the Hybrid II and VIP-95 dummies. The input conditions, in terms of sled velocity and deceleration, were held fairly constant as the orientation was changed. Both the seat pan force and resultant pelvis acceleration were essentially unaffected by the change in orientation. However, the resultant accelerations of the chest and/or head increased considerably in the pitched and rolled configuration, tending to indicate the increased severity of the environment.

TABLE 24. COMPARISON TEST RESULTS FOR SEAT ORIENTATION SERIES, RIGID SEAT

Seat Pitch/ Roll (deg)	Test No.	Dummy Percentile	Peak Sled Accel (G)	Initial Velocity (ft/sec)	Pelvis x	Pelvis z	Pelvis Resultant	Chest x	Chest z	Chest Resultant	Head x	Head z	Head Resultant	Seat Pan z-force (lb)
0/0	A80-026	50	14.4	42.1	8.22	42.1	42.9	6.04	25.7	26.4	12.1	32.2	34.4	2,650
0/0	A80-027	50	14.4	41.9	6.11	43.3	43.7	7.05	26.7	27.6	11.8	34.0	36.0	2,550
30/10	A80-038	50	15.6	42.6	15.8	38.4	41.5	29.2	24.8	38.3	18.6	31.4	36.5	2,580
0/0	A80-031	95	14.1	42.1	3.70	30.9	31.1	7.4	25.1	26.2	10.4	26.4	28.4	2,880
30/10	A80-037	95	14.7	42.3	17.5	25.2	30.7	20.2	22.5	30.2	23.1	25.8	34.6	2,850

Orientation of the energy-absorbing seat was also varied; two orientations were used at CAMI and three at NADC. Results for this series are summarized in Table 25. At CAMI, Test A80-078 maintained the same resultant sled acceleration and velocity as the baseline case, while Test A80-081 increased the resultant to maintain the same vertical components. In both cases, x- and z-accelerations were increased above the levels measured in the baseline configuration. At NADC, the drop height and, thus, the impact velocity and acceleration were held constant while the seat orientation was changed. There, as at CAMI, measured accelerations increased with increasing pitch angle, indicating an environment increasingly severe to the occupant. The same trend was not observed for the DRI or duration of seat pan acceleration above 23 G.

As shown in Table 25 and in Figure 86, the effect of orientation on seat stroke is evident. In Figure 86, results of those tests with similar resultant sled impact conditions are plotted. The reduced seat stroke with increasing aircraft pitch is expected as the vertical component of input acceleration is reduced, and probably accounts for increased seat and dummy accelerations.

TABLE 25. COMPARISON OF TEST RESULTS FOR SEAT ORIENTATION SERIES WITH ENERGY-ABSORBING SEAT

Seat Pitch/ Roll (deg)	Test No.	Peak Input Decel (G)	Velocity Change (ft/sec)	Total Seat Stroke (in.)	Peak Deceleration (G)								Duration of Seat Pan z Acceleration at 23 G (sec)	DRI
					Seat Pan x	Seat Pan z	Pelvis x	Pelvis z	Chest x	Chest z	Head x	Head z		
17/0	A80-053	40.7	44.8	10.6	25.3	26.4	17.1	30.5	18.1	30.4	31.5	36.5	0.007	21.0
17/0	A80-054	40.2	45.2	10.5	22.1	29.4	10.1	30.8	24.1	25.8	38.5	28.2	0.016	19.7
34/10	A80-078	39.9	44.0	6.7	30.2	34.1	30.5	49.9	37.2	40.2	29.8	50.4	0.010	18.7
34/10	A80-081	45.2	53.0	9.0	29.4	41.8	36.9	50.9	59.6	36.2	100.	46.8	0.015	20.6
0/0	N-195	42.7	41.0	12.1	18.1	34.5	17.7	34.4	4.67	33.7	15.4	37.7	0.006	21.1
13/0	N-189	44.9	40.4	10.8	16.6	36.3	15.0	38.8	10.1	36.1	24.7	40.8	0.006	20.8
13/0	N-190	45.0	40.5	11.6	16.8	34.6	18.7	40.1	14.7	37.4	22.7	42.8	0.007	20.7
30/10	N-196	46.7	41.3	7.3	28.8	35.5	18.7	43.1	26.8	40.8	33.1	44.8	0.014	20.3

Seat Pitch/Roll Angle	Test No.	Peak EA Load (lb)		Peak Lap Belt Load (lb)		Peak Shoulder Belt Load (lb)		Peak -G Strap Load (lb)	Peak Footrest Load (lb)	
		Right	Left	Right	Left	Right	Left		x	z
17/0	A80-053	1380.	1590.	373.	213.	200.	147.	593.	1760.	2200.
17/0	A80-054	1449.	1550.	300.	233.	87.	250.	560.	1900.	2120.
34/10	A80-078	1330.	1400.	200.	887.	620.	413.	613.	1930.	2120.
34/10	A80-081	1370.	1430.	707.	1550.	400.	540.	773.	2020.	2470.
0/0	N-195	1410.	1420.	348.	462.	26.8	40.2	610.	1740.	2330.
13/0	N-189	1449.	1457.	342.	335.	188.	221.	476.	1670.	2310.
13/0	N-190	1370.	1415.	361.	508.	181.	355.	515.	1890.	2410.
30/10	N-196	1480.	1530.	180.	616.	N/M*	107.	449.	1650.	2250.

*Not measured.

The effect of orientation on spinal loads is shown in Table 26, where results of two CAMI tests with the modified 50th-percentile dummy are presented. Note that in Table 26 "flexion" refers to forward bending of the torso which causes the chest to approach the knees. "Extension," on the other hand is a backward bending so that the distance between the chest and the knees is increased. Although the vertical component of input velocity and acceleration remained approximately the same, the axial compressive load in the lumbar spine increased by 43 percent. With the greater horizontal input, the maximum lumbar moment was increased by 84 percent.

6.1.10 Ramped Energy Absorber Series

Tests were conducted at both CAMI and NADC using energy absorbers of "ramped" design, whose loads increased linearly with stroke.

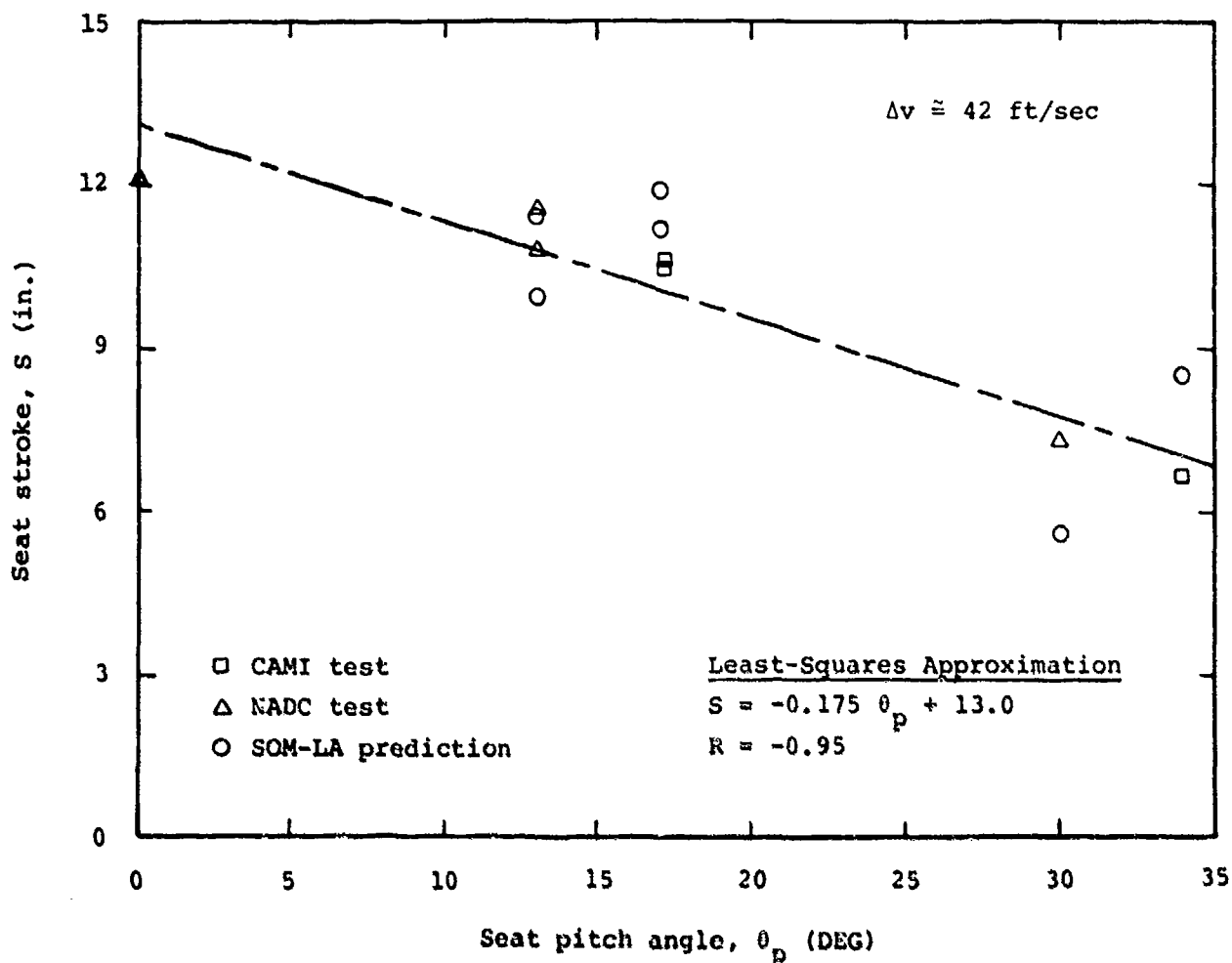


Figure 86. Seat orientation series, maximum seat stroke.

TABLE 26. EFFECT OF SEAT ORIENTATION ON LUMBAR FORCES AND MOMENTS

Seat Pitch/ Roll (deg)	Test No.	Impact Velocity (ft/sec)			Input Acceleration (G)			Maximum Axial Force (lb)	Maximum Shear Force (lb)	Maximum Flexion Moment (in.-lb)	Maximum Extension Moment (in.-lb)
		Resultant	Floor V_x	Floor V_z	Resultant	Floor x	Floor z				
17/0	A81-124	45.0	13.2	-43.0	41.3	-12.1	39.5	1220	360	1255	843
34/10	A81-127	52.4	28.9	-42.8	48.0	-26.4	39.2	1740	577	2307	1395

As illustrated in Figure 18, the load for the Type 1 device increased from a load factor of 9.5 G to 19.5 G through approximately 12 in. of stroke. The steeper slope of the Type 2 device increased from 7.25 G to 21.7 G in 12 in. of stroke. The energy absorber force-time histories measured in the CAMI tests are compared in Figure 87 with that for the baseline vertical test.

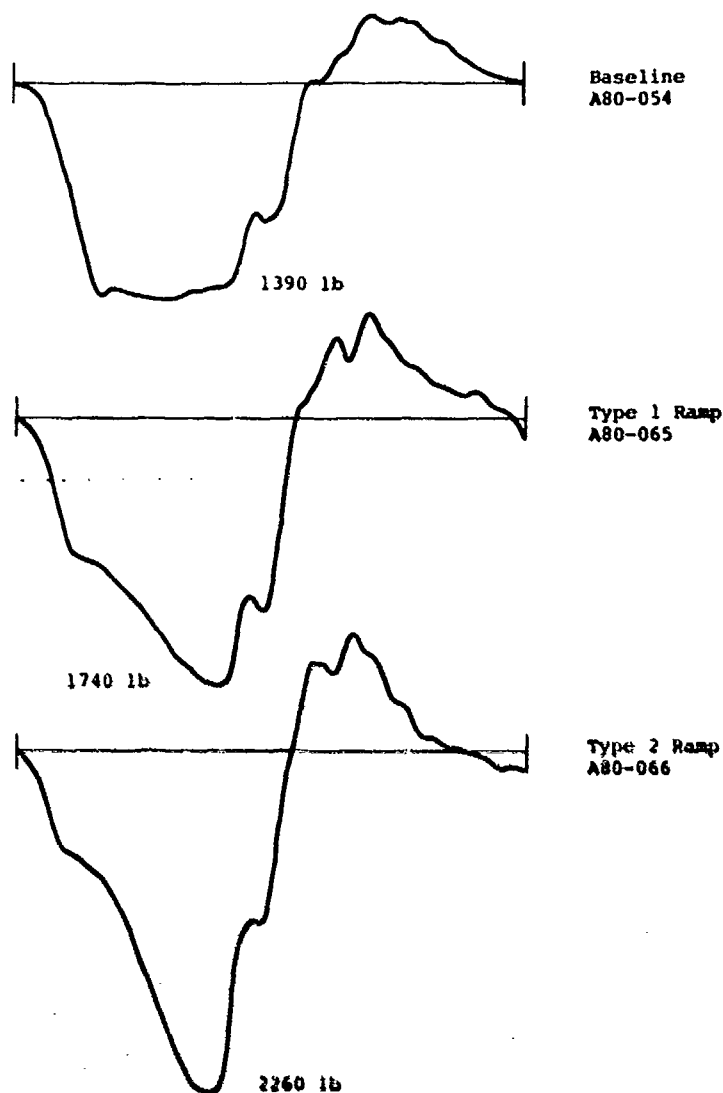


Figure 87. Comparison of energy absorber force-time histories for ramped E/A series.

Although the load-deflection characteristics of the two ramped devices were different, the trends in test results were similar. As shown by the data in Table 27, these special devices performed less efficiently than the standard square-wave type device. The ramped devices caused the Part 572 dummy to utilize more than 1.5 in. additional stroke, while the measured accelerations and calculated DRIs were actually higher.

6.1.11 Movable Seat Weight Series

The seat weight variable was included in the parametric test series because of the effect it has in performance of several production seats. Crewseat qualification tests for the Army UH-60A and AH-64A helicopters and Navy SH-60B helicopter indicated that the maximum seat pan z-axis acceleration was a function of seat

TABLE 27. COMPARISON OF RESULTS FOR RAMPED ENERGY ABSORBER LOAD SERIES

Energy Absorber Plastic Slope	Test No.	Peak Input Accel (G)	Total Velocity Change (ft/sec)	Seat Stroke (in.)	Peak Acceleration (G)								Duration of Seat Pan z Acceleration at 23 G (sec)	DRI
					Seat Pan x	Seat Pan z	Pelvis x	Pelvis z	Chest x	Chest z	Head x	Head z		
Type 2*	A80-066	41.9	43.7	12.3	27.9	34.8	19.4	48.8	19.7	34.8	26.8	24.8	0.018	27.4
Type 1*	A80-065	40.9	43.4	12.0	24.2	32.3	18.7	43.5	31.4	26.8	36.1	20.1	0.009	23.7
	N-194	46.6	41.4	11.8	13.4	28.5	16.4	30.8	13.0	28.4	24.7	20.1	0.027	27.0
Baseline*	A80-053	40.7	44.8	10.6	25.3	26.4	17.1	30.5	18.1	30.4	31.5	36.5	0.007	21.0
	A80-054	40.2	44.2	10.5	22.1	29.4	10.1	30.8	24.1	24.8	38.5	28.2	0.016	19.7

Test Parameter	Test No.	Peak E/A Load (lb)		Peak Lap Belt Load (lb)		Peak Shoulder Belt Load (lb)		Peak -G Strap Load (lb)	Peak Footrest Load (lb)	
		Right	Left	Right	Left	Right	Left		x	z
Type 1	A80-066	1960.	2260.	415.	449.	261.	147.	744.	1940.	2360.
Type 2	A80-065	1730.	1740.	321.	401.	254.	114.	562.	1900.	2340.
	N-194	1770.	1910.	599.	563.	188.	180.	610.	1390.	2220.
Baseline	A80-053	1380.	1590.	373.	213.	200.	147.	593.	1760.	2200.
	A80-054	1420.	1550.	300.	233.	87.	250.	560.	1900.	2120.

*See accompanying load/deflection curves.

bucket inertial and stiffness properties. These properties play a major role in the interaction between the occupant and seat pan which influences the body dynamics.

The ideal parametric test series for this variable would have included a seat bucket in which the weight and stiffness could be varied independently, and energy absorber loads could be adjusted to maintain a constant energy absorber limit load factor as seat weight was changed. Unfortunately, constraints placed on this research program made it prohibitive to adjust seat stiffness or to design energy absorbers with the correct inversion loads to maintain a constant limit load factor of 14.5 G. Therefore, in this test series, the effect of seat bucket stiffness on performance was not investigated. Movable seat weight was modified by adding steel plates to the Kevlar portion of the UH-60A production seat from which the armor had been removed. Seat weights for this series were 35.0, 60.6, and 120.0 lb, with 35.0 lb being the unmodified weight of the Kevlar bucket and 60.6 lb corresponding to the weight of the production armored UH-60A seat. The energy absorbers for this series all had the same nominal load corresponding to 14.5 G for the 60.6-lb seat. The effective limit-load factor varied in this series from 16.6 G for the 35-lb bucket to 11.2 G for the 120-lb bucket. Therefore, the measured test results for this series included the effects of two variables: the movable seat weight and the energy absorber limit-load factor. The sensitivity analysis for this series was conducted by plotting trend lines for the test data and also showing the expected

sensitivity due to the change in E/A limit-load factor which was deduced from the curves presented in Section 6.1.4 for the energy absorber limit-load series. It was assumed that any differences in the trend lines must be attributable to the effect that the movable mass of the seat bucket has on seat and occupant interaction.

The test values for this series are compared in Table 28, and sensitivity curves are shown in Figures 88 through 92. The seat stroke curves shown in Figure 88 indicate that the trend is entirely due to the effect of energy absorber limit load and not seat weight. Therefore, if the energy absorber loads had been modified to maintain a constant limit-load factor, then similar stroke distances would have been achieved. This may appear to be an obvious conclusion; however, there was uncertainty at the beginning of this effort concerning the effect that body dynamics might have on stroke.

TABLE 28. COMPARISON OF TEST RESULTS FOR SEAT MOVABLE WEIGHT SERIES

Movable Weight (lb)	Test No.	Peak Input Accel (G)	Total Velocity Change (ft/sec)	Effect L _L Factor (G)	Peak Acceleration (G)								Duration of Seat Pan z Acceleration at 23 G (sec)	DRI
					Seat Pan x	Seat Pan z	Pelvis x	Pelvis z	Chest x	Chest z	Head x	Head z		
35.0	ABO-060	41.5	44.5	16.6	35.1	29.6	24.0	42.8	25.7	26.8	37.8	28.9	0.012	21.9
60.6	ABO-053	40.7	44.4	14.5	25.3	25.4	17.1	30.5	18.1	30.4	31.5	36.5	0.007	21.0
60.6	ABO-054	40.7	44.2	14.5	22.1	29.4	10.1	30.8	24.1	25.8	38.5	28.2	0.016	19.7
120.0	ABO-061	40.7	43.8	11.2	23.4	22.9	17.1	32.8	38.5	21.1	43.5	22.4	0.	16.4

Movable Weight (lb)	Test No.	Seat Stroke (in.)	Peak E/A Load (lb)		Peak Lap Belt Load (lb)		Peak Shoulder Belt Load (lb)		Peak -G Strap Load (lb)	Peak Footrest Load (lb)	
			Right	Left	Right	Left	Right	Left		x	z
35.0	ABO-060	8.6	1400.	1450.	255.	389.	181.	147.	482.	1930.	2520.
60.6	ABO-053	10.6	1380.	1590.	373.	213.	200.	147.	593.	1760.	2200.
60.6	ABO-054	10.5	1420.	1550.	300.	233.	87.	250.	560.	1900.	2120.
120.0	ABO-061	14.0	1370.	1430.	523.	389.	255.	255.	791.	1720.	2450.

The next two parameters, maximum seat pan z-axis acceleration and Dynamic Response Index (DRI) (shown in Figures 89 and 90), are both based on the performance parameter, seat pan acceleration, used in the current criterion. The trend seen in recent qualification testing that additional weight in the seat bucket acts to reduce the oscillations of the seat pan is present in the parametric test series. This is exhibited by the fact that the two sensitivity lines diverge as weight increases, indicating that the reduction in vertical seat pan acceleration cannot be entirely explained by the reduction in energy absorber limit-load factor. The seat weight does appear to play a significant role in reducing accelerations measured on the seat. However, the final two graphs

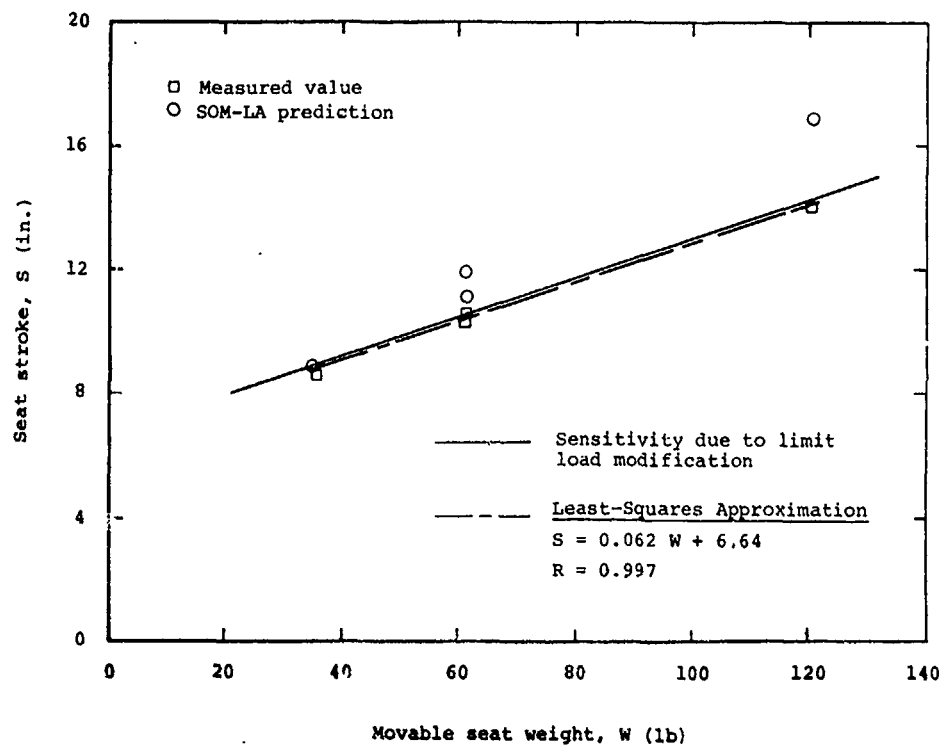


Figure 88. Movable seat weight series, maximum seat stroke.

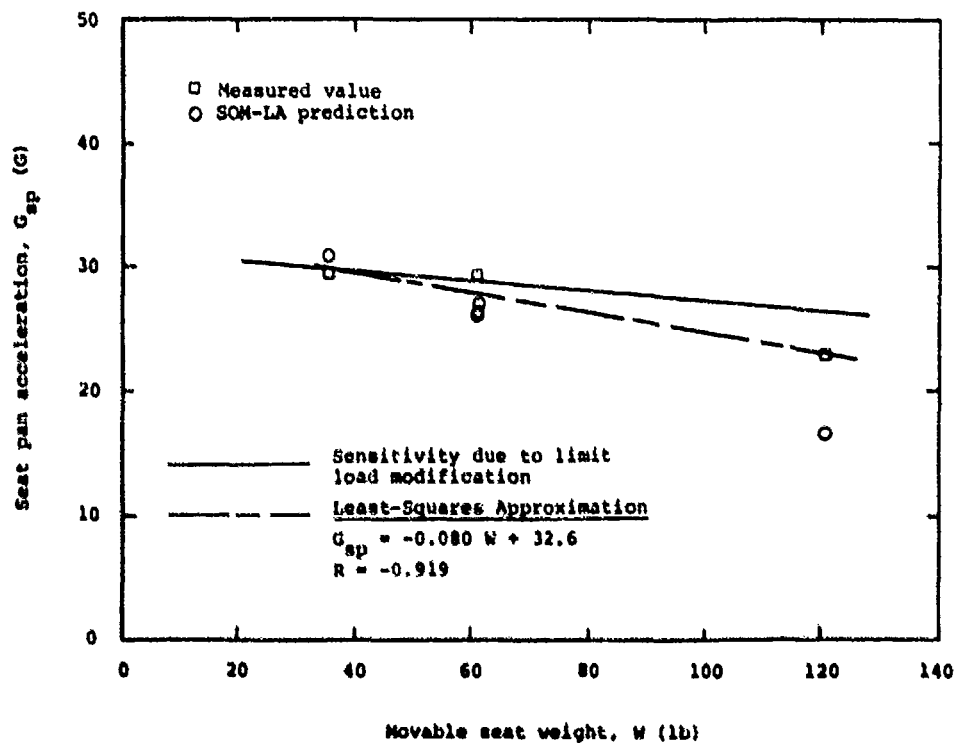


Figure 89. Movable seat weight series, maximum seat pan z-axis acceleration.

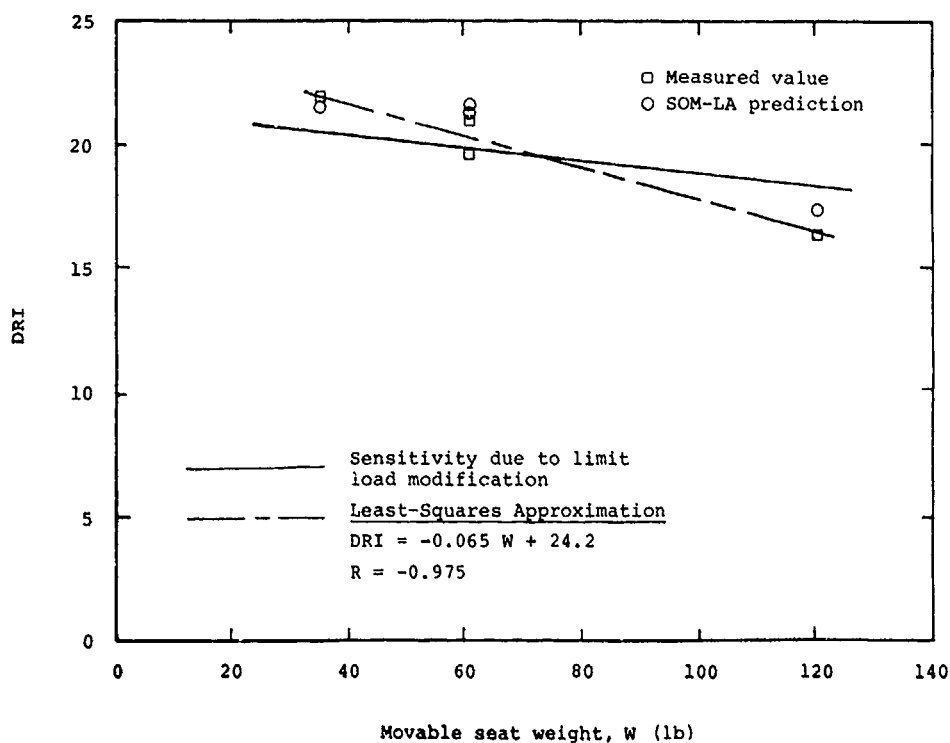


Figure 90. Movable seat weight series, Dynamic Response Index.

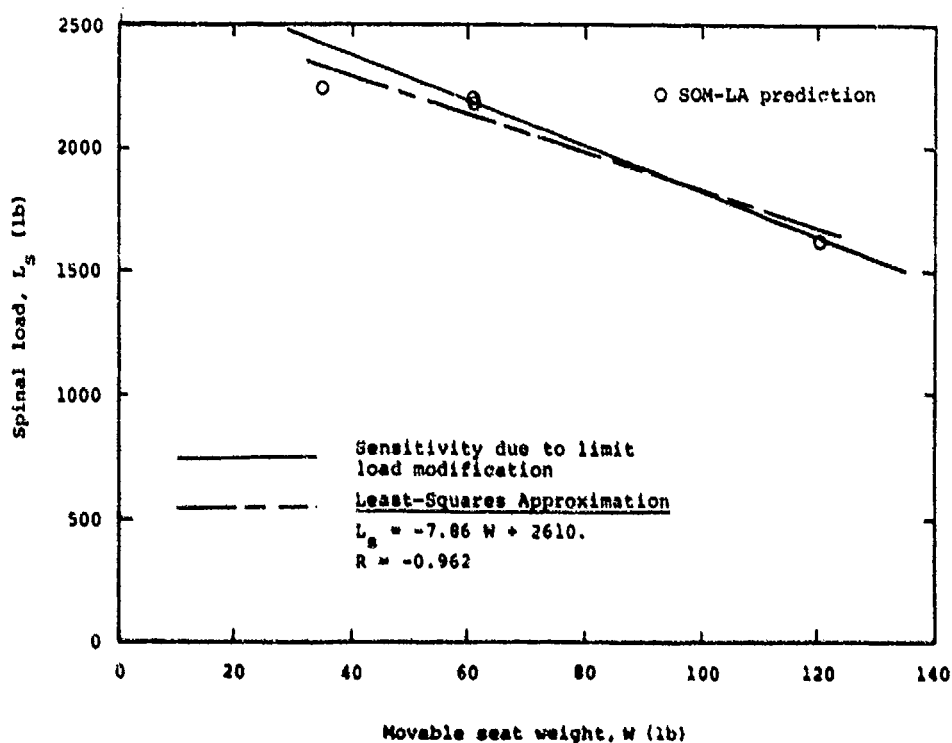


Figure 91. Movable seat weight series, maximum lumbar spine axial load (compression).

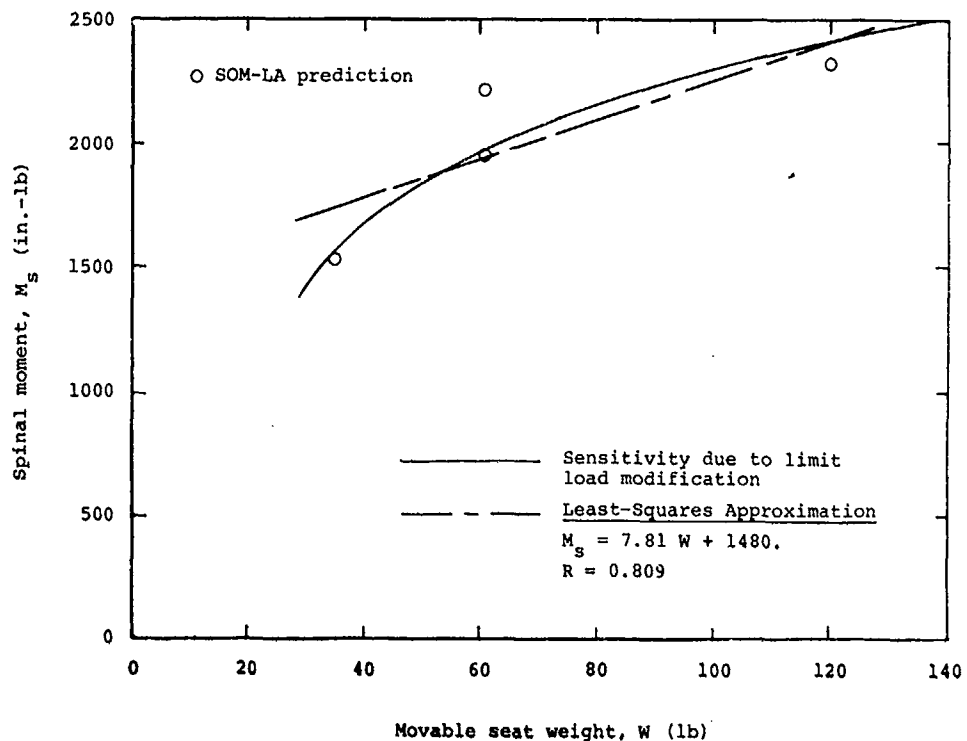


Figure 92. Movable seat weight series, maximum lumbar spine moment (flexion).

presented in this section for spinal loads and moments indicate that the apparent reduction in seat pan acceleration is not passed on in the form of reduced spinal loading. The trends seen in these curves can be almost entirely attributed to the change in energy absorber limit load.

There are two conclusions to be drawn from this series. First, the results of this series support the theory that the maximum seat pan accelerations occur because the occupant is not fully coupled to the seat pan, and these accelerations actually have little effect on the maximum loads to which the body is subjected. The second conclusion is that the practice of using the measured seat pan accelerations for determining hazard potential is inaccurate. This indicator is sensitive to localized conditions which are a function of bucket mass, and possibly also stiffness. Loads and moments measured in the spine are not sensitive to these localized, design-dependent conditions.

6.1.12 Seat Frame Spring Rate Series

For one test at CAMI, the top of the Black Hawk seat frame was secured rigidly to the sled with steel brackets, as illustrated in Figure 93. The intention of this test was to isolate the effect of longitudinal seat elasticity on seat and dummy response by comparison of results with those for the baseline configuration.

OCCUPANT ACCELEROMETERS

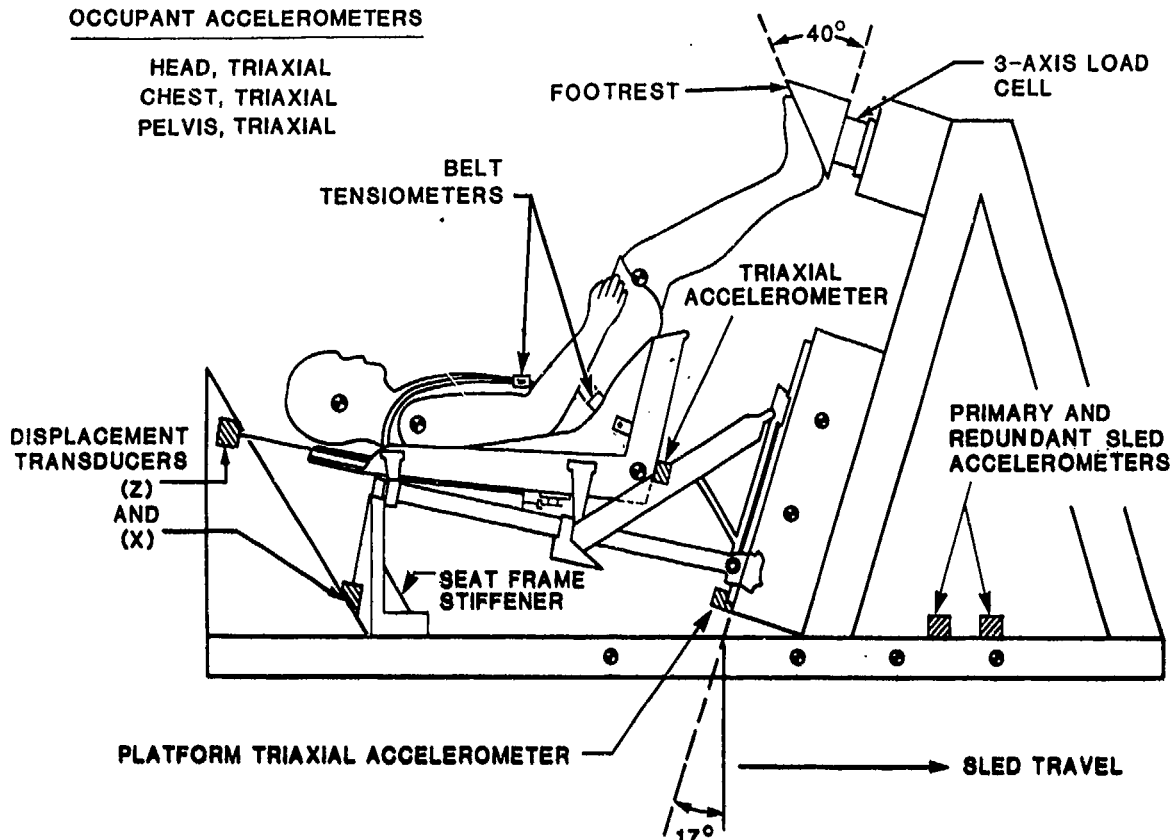


Figure 93. Test configuration (for stiffened seat frame test).

Results are summarized in Table 29, where it appears that seat stroke and DRI were essentially not affected by the frame modification. However, x-components of dummy pelvis and chest acceleration were reduced, as shown in Figure 94, while z-components were increased.

The results of this test are not conclusive because, although the frame was stiffened, seat bucket elasticity remained a factor.

6.1.13 Seat Cushion Stiffness Series

Two tests were conducted to determine the effect of seat cushion stiffness. For one CAMI test (A80-068) a block of rigid plastic foam was contoured to cushion shape; for another, layers of soft upholstery foam were used. In designing the cushions, an effort was made to achieve a thickness that would seat the dummy in the same position as in the baseline case. Force-deflection characteristics for each of the cushions were determined by compression under the VIP-95 dummy lower torso segment, as shown in Figure 95. Load-deflection characteristics for the two cushions are compared in Figure 96 with the baseline configuration, the production UH-60A Black Hawk cushion.

TABLE 29. COMPARISON OF TEST RESULTS FOR STIFFENED SEAT FRAME SERIES

Seat Frame Stiffness	Test No.	Peak Input Decel (G)	Total Velocity Change (ft/sec)	Seat Stroke (in.)	Peak Deceleration (G)								Duration of Seat Pan z Acceleration at 23 G (sec)	DRI
					Seat Pan x	Seat Pan z	Pelvis x	Pelvis z	Chest x	Chest z	Head x	Head z		
Baseline	A80-053	40.7	44.8	10.6	25.3	26.4	17.1	30.5	18.1	30.4	31.5	36.5	0.007	21.0
	A80-054	40.2	44.2	10.5	22.1	29.4	10.1	30.8	24.1	25.8	38.5	28.2	0.016	19.7
Stiffened	A80-059	40.4	43.7	10.4	28.1	32.2	21.1	37.5	11.4	34.2	20.1	36.8	0.013	19.4

Seat Frame Stiffness	Test No.	Peak E/A Load (lb)		Peak Lap Belt Load (lb)		Peak Shoulder Belt Load (lb)		Peak -G Strap Load (lb)	Peak Footrest Load (lb)		Forward Displ. at top of Guide Tube
		Right	Left	Right	Left	Right	Left		x	z	
Baseline	A80-053	1380.	1590.	373.	213.	200.	147.	593.	1760.	2200.	1.40
	A80-054	1420.	1550.	300.	233.	87.	250.	560.	1900.	2120.	1.51
Stiffened	A80-059	1390.	1470.	570.	429.	141.	248.	717.	1850.	2230.	0.00

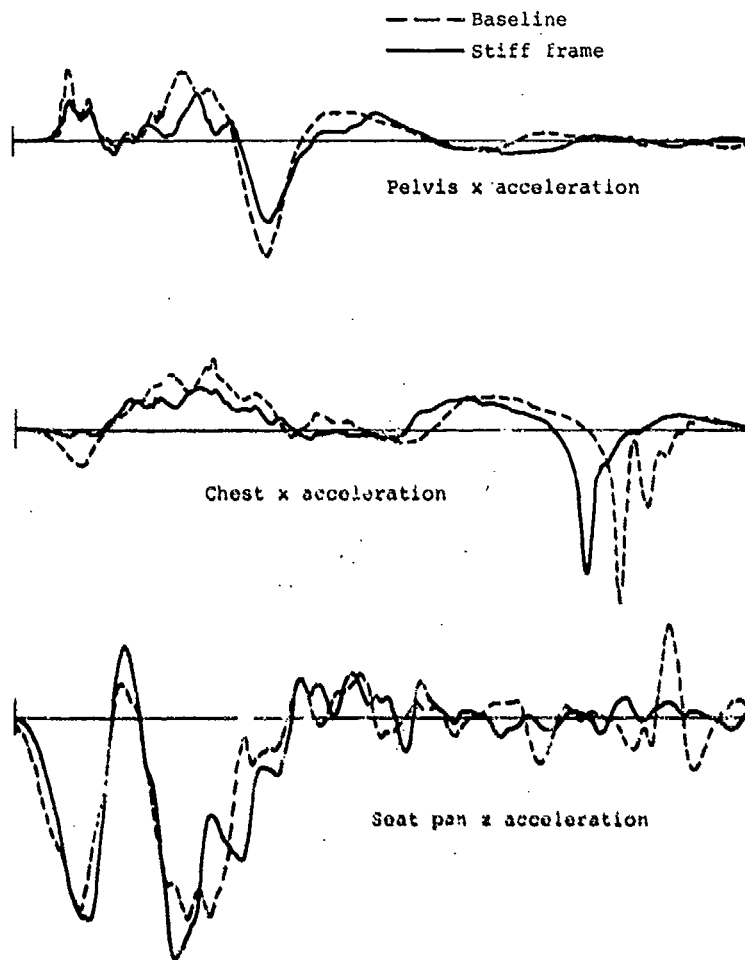


Figure 94. Comparison of response with stiffened seat frame.



Figure 95. Measurement of seat cushion force-deflection characteristics.

Results for the cushion series are compared in Table 30, where no variation in seat stroke or DRI from the baseline case is apparent. The rigid cushion increased the natural frequency of the system, so that acceleration waveforms exhibited both higher frequency and greater magnitudes, as shown in Figure 97 for the seat pan and Figure 98 for the pelvis. Also, the soft cushion permitted the dummy to reach a significantly higher velocity relative to the seat before bottoming out on the seat pan. The result was an increased pelvic acceleration, as shown in Figure 98.

Although only one actual seat cushion was compared with two extremes of stiffness, comparison of pelvic acceleration data indicates that the baseline cushion performs significantly better than one that is either very rigid or very soft.

6.2 ADDITIONAL PERFORMANCE VARIABLES

This section presents an examination of six variables that, although not originally conceived as part of the test program, would

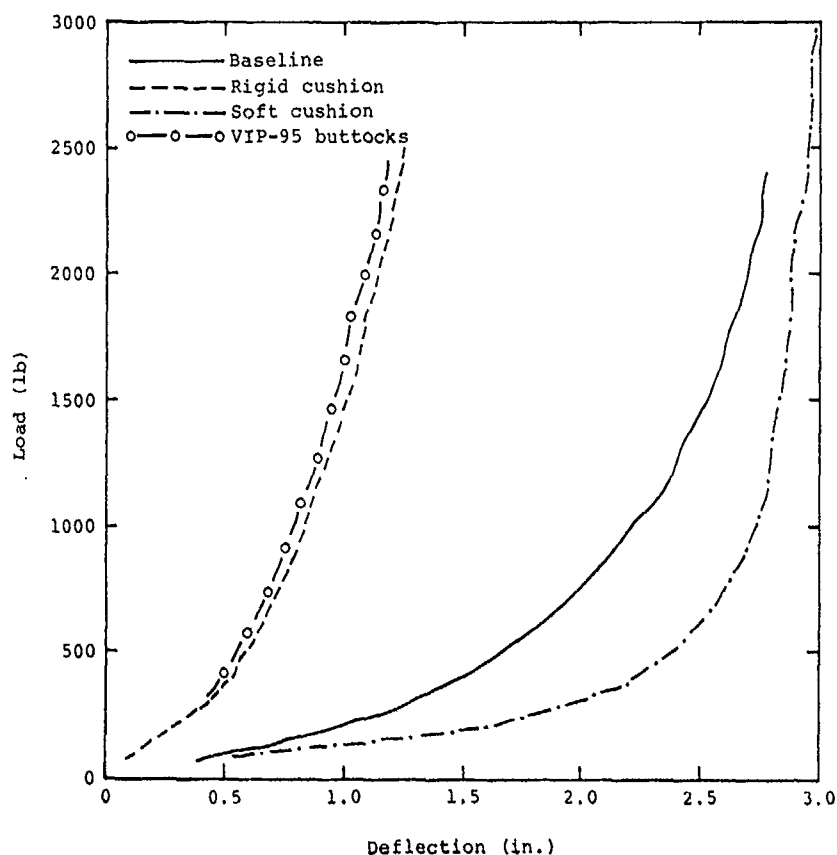
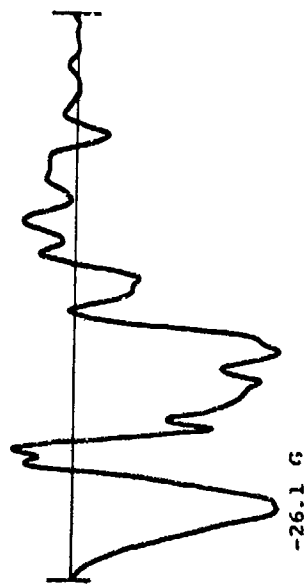


Figure 96. Load-deflection curves for cushions used in cushion spring rate series.

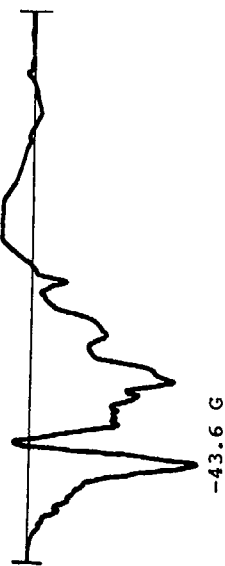
TABLE 30. COMPARISON OF TEST RESULTS FOR CUSHION SPRING RATE SERIES

Cushion Stiffness	Test No.	Peak Input Decel (g)	Total Velocity Change (ft/sec)	Seat Stroke (in.)	Peak Deceleration (G)								Duration of Seat Pan z Acceleration at 23 G (sec)	DRI
					Seat Pan x	Seat Pan z	Pelvis x	Pelvis z	Chest x	Chest z	Head x	Head z		
Soft	ABO-067	41.2	44.0	10.5	28.8	26.1	13.7	43.6	25.1	32.5	30.2	46.9	0.008	19.5
Baseline	ABO-053	40.7	44.8	10.6	25.3	26.4	17.1	30.5	18.1	30.4	31.5	36.5	0.007	21.0
	ABO-054	40.2	44.2	10.5	22.1	29.4	10.1	30.8	24.1	25.8	38.5	28.2	0.016	19.7
Rigid	ABO-068	41.2	44.1	10.6	29.3	29.0	25.4	49.2	26.8	31.8	28.5	28.2	0.008	20.4

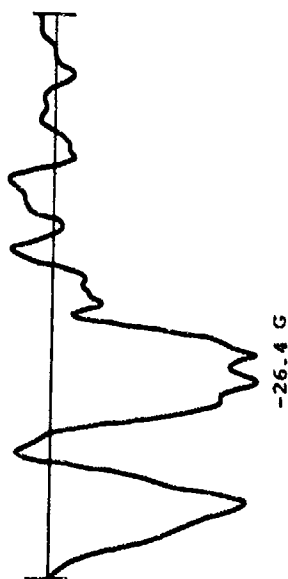
Cushion Stiffness	Test No.	Peak E/A Load (lb)		Peak Lap Belt Load (lb)		Peak Shoulder Belt Load (lb)		Peak -G Strap Load (lb)	Peak Footrest Load (lb)	
		Right	Left	Right	Left	Right	Left		x	z
Soft	ABO-067	1520.	1570.	374.	174.	261.	187.	555.	1810.	2320.
Baseline	ABO-053	1380.	1590.	373.	213.	200.	147.	593.	1760.	2200.
	ABO-054	1420.	1550.	300.	233.	87.	250.	560.	1900.	2120.
Rigid	ABO-068	1380.	1460.	509.	389.	322.	355.	750.	1970.	2260.



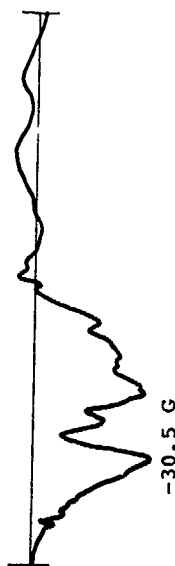
Soft Cushion
A80-067



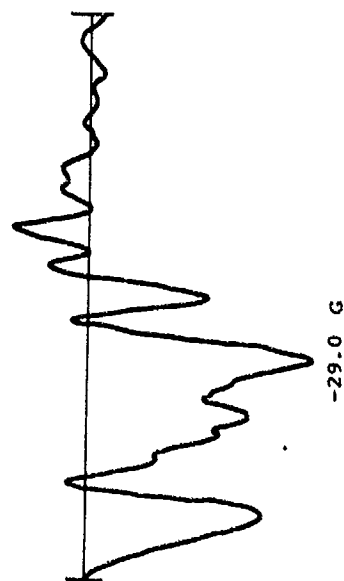
Soft Cushion
A80-067



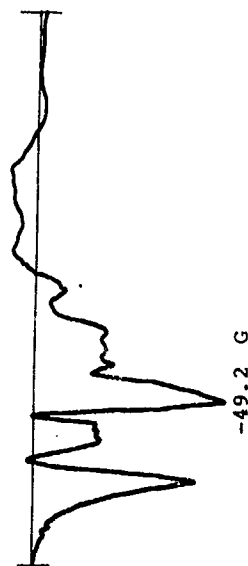
Baseline Cushion
A80-053



Baseline Cushion
A80-053



Rigid Cushion
A80-068



Rigid Cushion
A80-068

Figure 97. Comparison of seat pan z-acceleration for various cushion stiffnesses.

Figure 98. Comparison of pelvic z-acceleration for various stiffnesses.

be significant in developing a new seat performance specification. The degradation of dummy performance after repeated testing was determined by examining comparable tests at various intervals in the test program. Program SOM-LA was used to provide a simulated parametric test matrix for four of the parameters. In the final section, a comparison of calibration techniques for accelerometers is presented with an example showing the magnitude of performance differences that can occur.

6.2.1 Dummy Performance Degradation

The performance repeatability of the Hybrid II dummy, S/N 870, was examined by conducting rigid seat baseline tests with this dummy at intervals in the test program. The tests were designed to ensure that multiple tests would not degrade the performance to such an extent that the results of the parametric test matrix would be suspect. Figures 99 and 100 show a comparison of the force applied to the seat pan by the dummy buttocks and the resultant pelvic acceleration for tests conducted at three periods in the program. Test A80-025 was the first test in the research effort with the Hybrid II dummy. Twenty-two tests were subsequently conducted at CAMI with this dummy, followed by three tests (beginning with A80-083) repeating the conditions of A80-025 to compare performance. The final tests in this series, beginning with A81-004, were conducted following the 12 NADC and Simula energy-absorbing seat tests.

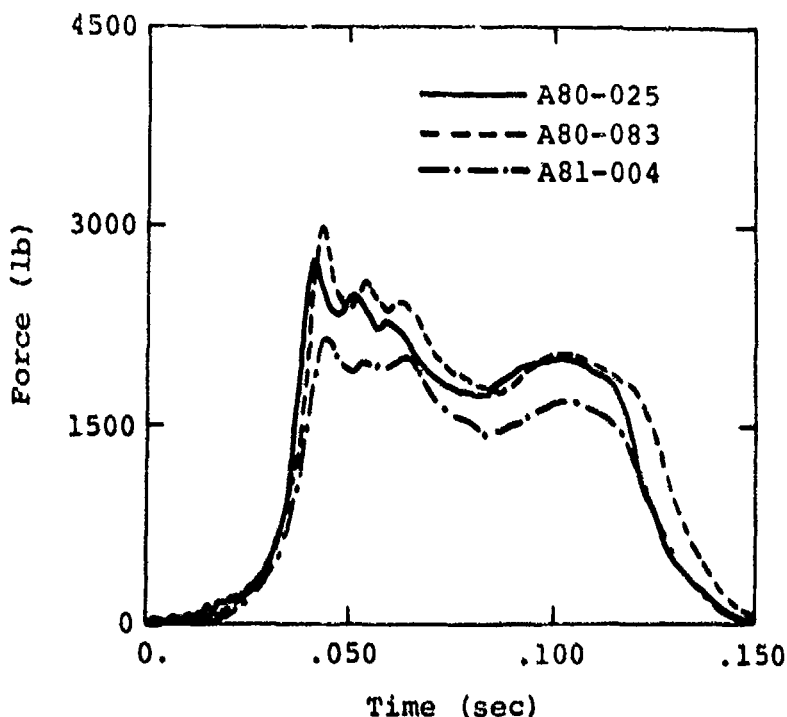


Figure 99. Comparison of seat pan z-axis force for dummy performance degradation tests.

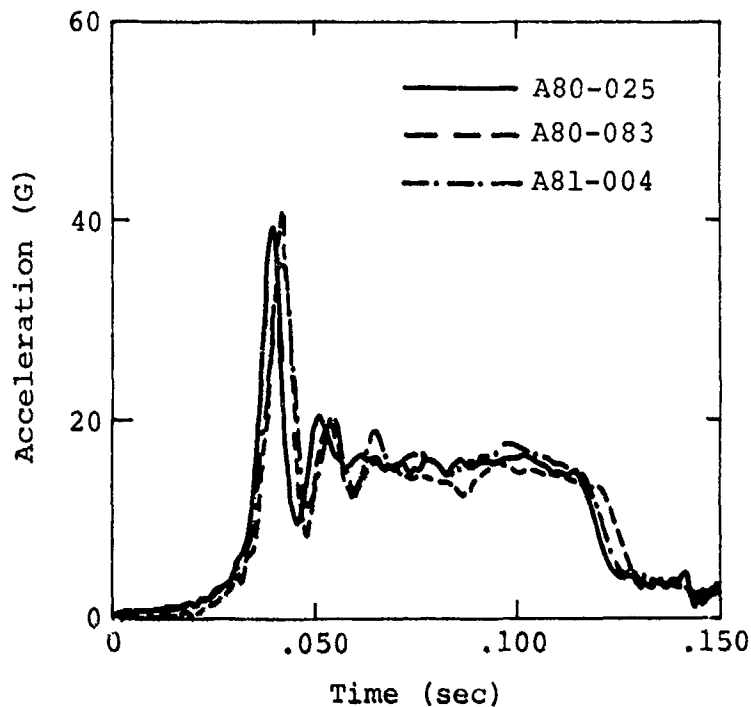


Figure 100. Comparison of pelvic resultant acceleration for dummy performance degradation tests.

Physical degradation in the form of a decrease in buttock cushioning properties did occur by Test A81-004. It was theorized that this reduction in cushioning might result in a large dynamic overshoot in the rigid seat test; therefore, the restraint system was given more preload in Test A81-004 than in the previous rigid seat tests. The result of this modified test procedure was a decrease in the measured seat pan force for Test A81-004. However, the accelerations recorded in the dummy pelvis do not vary notably in any of the three tests illustrated in Figure 100.

It was concluded from this series that performance of this dummy was not significantly altered by repeated testing. A standardized, instrumented dummy based on the Part 572 specification should be capable of providing repeatable results for many qualification tests. However, it is suggested that a periodic examination of the dummy be conducted followed by replacement of degraded components.

6.2.2 Footrest Location and Angle

It was noted during the cadaver test program that the loads measured on the footrest varied considerably depending on occupant anthropometry. This indicated that the load path through the legs reacting vertical and longitudinal inertial forces could be altered by the relative angles of the leg segments. A series of

six SOM-LA simulations was used to examine the effect of footrest location and angle on seat and occupant response. Conditions for these simulations are shown in Figure 101, and a comparison of results is presented in Table 31.

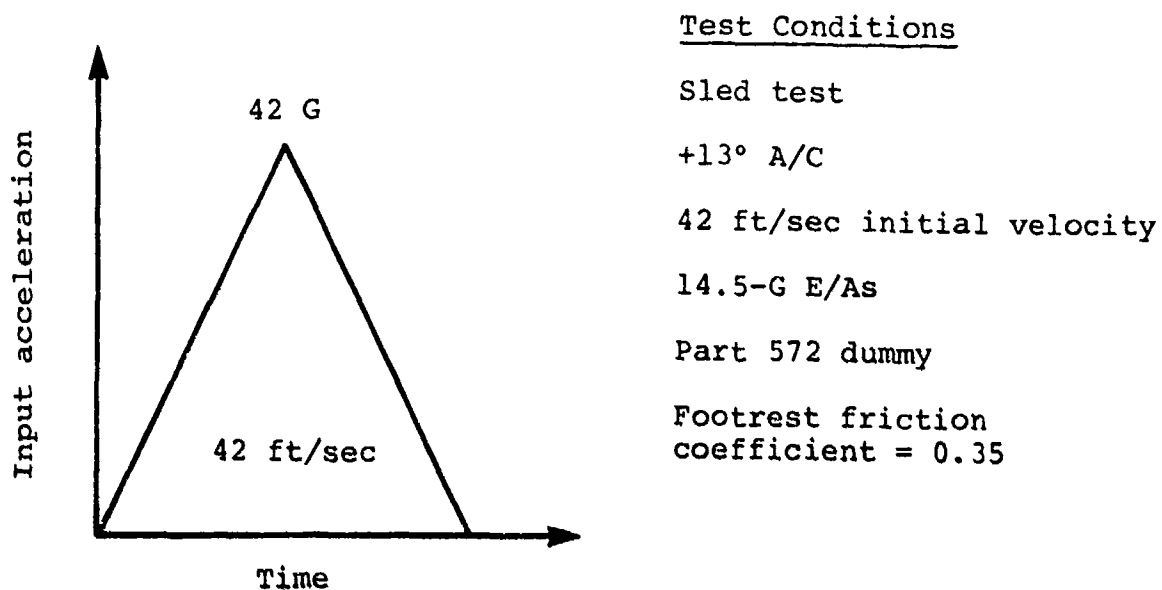


Figure 101. Test conditions for SOM-LA simulations to determine the effect of footrest angle and location.

TABLE 31. COMPARISON OF SOM-LA SIMULATIONS TO DETERMINE THE EFFECT OF FOOTREST ANGLE AND LOCATION ON SEAT AND OCCUPANT RESPONSE

Footrest Angle (Deg)	Location of SRP (in.)	Seat Stroke (in.)	Peak Seat Pan z-Accel (G)	Peak Pelvic z-Accel (G)	Peak Chest z-Accel (G)	Peak Lumbar Load (lb)	Peak Lumbar Moment (in.-lb)
40	33	10.8	30.2	26.5	36.0	2350.	1474.
20	33	10.0	30.3	24.3	36.7	2396.	1264.
0	33	11.5	30.3	26.6	33.8	2297.	1633.
40	26	9.2	30.6	26.6	35.4	2327.	2498.
0	26	9.8	30.4	25.3	35.8	2349.	2131.
0	19	7.6	30.1	26.1	29.9	2014.	2660.

The SOM-LA simulations indicate that the footrest plays an important role in determining how the loads are transmitted to the body. For example, the predicted lumbar spine moment increased by 110 percent when the feet were positioned 14 in. farther away from the seat on a footrest set at an angle of 20 degrees above the plane of the floor. The maximum seat stroke varied by as much as 3.9 in., which implies that the legs are bypassing the energy-absorption mechanism and transmitting crash loads directly to the body, thus reducing the required seat stroke.

The objective of this series was not to infer that the feet can be positioned to minimize load, although the great variation in results indicates that this may be possible. Rather, the goal was to show that there can be a significant effect on response due to foot positioning. Future qualification testing specifications must contain provisions for attaining repeatable foot constraints. It is recommended that footrest angle and position correspond to expected foot position at impact. Also, in the parametric test series the dummy's feet were taped securely to the footrest, probably affecting system response. As mentioned in Section 7.1.4, future qualification test specifications should address the question of whether to tape the feet.

6.2.3 Landing Gear Acceleration Ramp

Recent qualification test specifications of energy-absorbing seats have not been consistent in reducing the energy-absorption capability of the aircraft landing gear in the input acceleration pulse. The qualification test for the AH-64A Apache, which has energy-absorbing landing gear that absorb a significant amount of crash energy, did include a 5.35-G acceleration plateau for approximately 100 msec prior to the main impact pulse. However, the test pulse for the UH-60A crewseat qualification test was the nominal, triangular pulse described in MIL-S-58095(AV). Hearon, et al., (Reference 15) have shown that a very short duration, low level acceleration just prior to the main impact can have a very significant protective effect by minimizing dynamic overshoot. The simulations presented here are designed to show what effect the landing gear acceleration ramp has on seat and occupant response.

Three input acceleration pulses are shown in Figure 102: the AH-64A crewseat qualification test pulse, the main segment of this pulse without the landing gear acceleration ramp and with a correspondingly reduced velocity change, and a modified principal pulse that includes the entire 50 ft/sec velocity change of the 95th-percentile accident. Simulations for the first two input pulses presented in Table 32 compare the conditions when the seat and occupant encounter the main impact pulse (corresponding to fuselage impact) at the same velocities with and without the benefit of preload. In the second simulation, without the benefit of preload, the seat requires an additional 0.8 in. of stroke distance and the vertical accelerations and spinal load increase by at least 30 percent. Only the lumbar spine moment appears to be

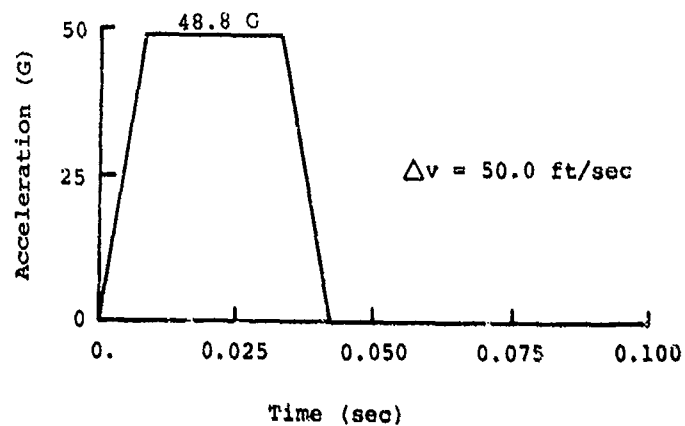
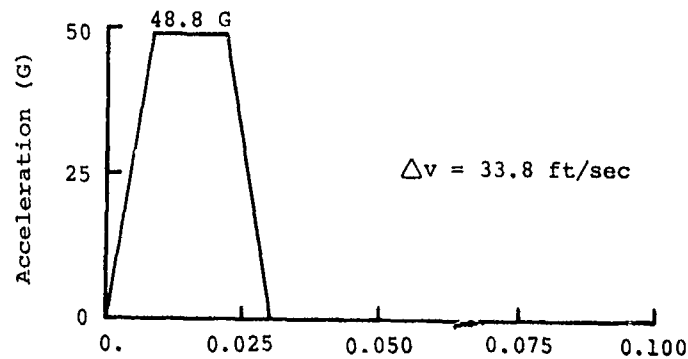
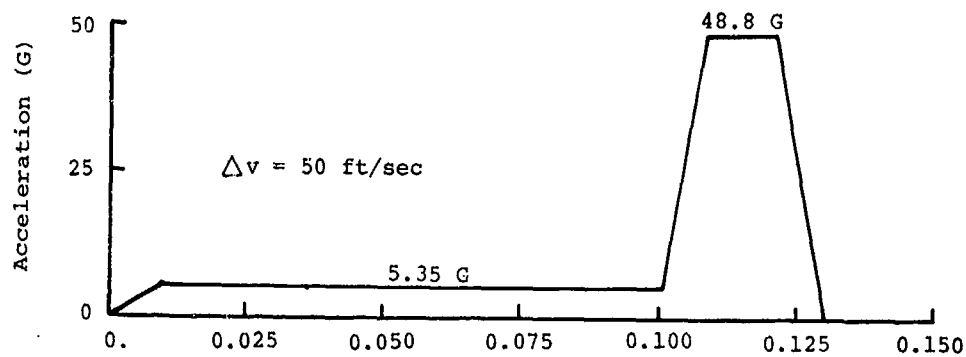


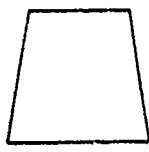


Figure 102. Input acceleration pulses for simulations examining the effect of landing gear acceleration on seat and occupant response.

less hazardous without preloading, possibly due to the duration of the applied acceleration. The third simulation shows the effect on seat and occupant response if the fuselage were required to absorb the entire impact pulse. The results show an increase in seat stroke of 12 in. when the simulation is performed without the effect of the landing gear. Body segment accelerations and spinal load are very similar for the second and third cases, indicating that they are a result of the initial dynamic overshoot

TABLE 32. COMPARISON OF PREDICTED SEAT AND OCCUPANT RESPONSE FOR INPUT DECELERATION PULSES WITH AND WITHOUT LANDING GEAR RAMP

Input Pulse Shape	Δv (ft/sec)	Seat Stroke (in.)	Peak Seat Pan z-Accel (G)	Peak Pelvic z-Accel (G)	Peak Chest z-Accel (G)	Peak Lumbar Load (lb)	Peak Lumbar Moment (in.-lb)
	50.0	9.2	24.9	21.6	25.3	1742.	1801.
	33.8	10.0	34.8	28.9	36.6	2441.	732.
	50.0	21.2	34.8	28.6	33.2	2263.	2404.

due to lack of preload and not necessarily a function of crash energy. However, the spinal moment does show a large increase between the two cases.

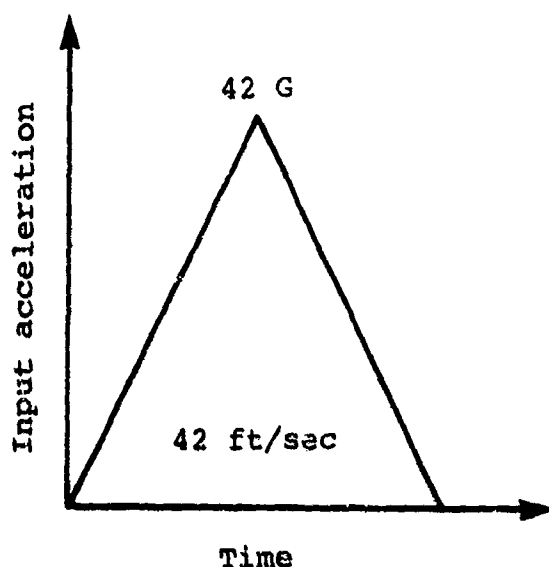
Results presented in this section indicate that the preload due to landing gear acceleration can have a significant effect on reducing injury potential. Future specifications must account for this effect in a consistent manner for qualification testing.

6.2.4 Test Orientation to Gravity Vector

The facilities test variable discussed in Section 6.1.5 actually included the influence of two variables: the input pulse shape and the orientation of the decelerator mechanism to the gravity vector. It was known prior to conducting the parametric test series that gravity can influence occupant response. For a horizontal decelerator conducting a "vertical" impact test, gravity acts to resist flexion of the upper torso. In this orientation, the gravity vector is equal to about 10 percent of the component of the impact acceleration that it opposes. Making the same comparison for a vertical decelerator, gravity opposes the main input

acceleration pulse for which it is equivalent to only about 2.5 percent. An attempt was made to adjust the test conditions to counteract the effect of gravity by adding additional seat pitch for the horizontal decelerator test conditions. The two simulations presented in this section were conducted to determine whether the vertical and modified horizontal decelerator test conditions were equivalent.

Test conditions for each of the simulations, shown in Figure 103, were identical with the exception of seat orientation to gravity. For the vertical test condition, seat pitch was +13 degrees, which oriented the seat back plane at zero degrees to the gravity vector. The horizontal condition had a seat pitch of +17 degrees resulting in a 73-degree angle between the seat z-axis and the gravity vector. Results of the simulations for these two test conditions are shown in Table 33.



Test Conditions

42 ft/sec initial velocity

14.5-G E/As

Part 572 dummy

Figure 103. Conditions for aircraft orientation simulation.

TABLE 33. COMPARISON OF SEAT AND OCCUPANT RESONSE FOR VERTICAL AND HORIZONTAL TEST CONDITION SIMULATIONS

Decelerator Test Condition	Seat Pitch (deg)	Seat Stroke (in.)	Peak Seat Pan z-Accel (G)	Peak Pelvic z-Accel (G)	Peak Chest z-Accel (G)	Peak Lumbar Load (lb)	Peak Lumbar Moment (in.-lb)
Horizontal	17	9.8	30.2	26.5	36.0	2350.	1474.
Vertical	13	11.3	29.7	26.8	34.6	2332.	1937.

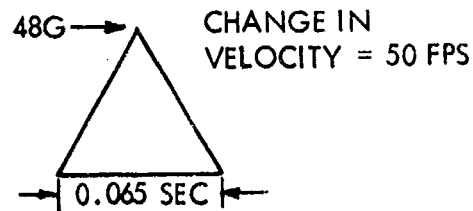
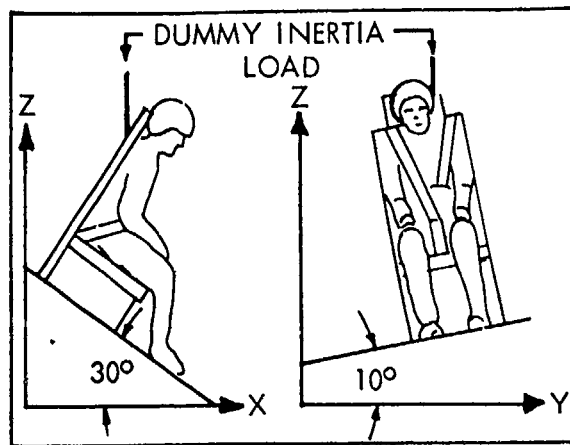
There does not appear to be a significant difference in the z-axis accelerations or axial spinal load for the two test conditions. However, SOM-LA predicts a difference in seat stroke of 1.5 in. and a 31 percent increase in lumbar moment for the vertical decelerator test condition. It appears that the additional seat pitch added to the horizontal test condition was not sufficient to produce similar flexion in the upper torso as measured by the lumbar moment. If additional seat pitch was used to overcome gravity, then the disparity in seat stroke would be even greater. Obviously, the vertical and horizontal test conditions used in the simulations did not result in predictions of identical response. Additional work needs to be conducted with simulations to identify comparable test conditions, followed by dynamic tests to verify equivalency. Also, because SOM-LA applies a 1-G force to initially seat the occupant in the cushions, it does not truly simulate the free-fall conditions of a vertical drop test. This factor would have to be taken into account in future simulations, perhaps modifying the computer program for simulating a drop test.

6.2.5 Tolerances on Input Deceleration Pulse Allowed by MIL-S-58095(AV)

Dynamic test requirements for Test No. 1 of MIL-S-58095(AV), shown in Figure 104, allow the rise time of the impact acceleration pulse to vary between 0.4 and 0.8 of the total pulse duration. Program SOM-LA was used to conduct a parametric matrix of simulations for the two limits on the rate of onset with 50th- and 95th-percentile occupants and 11.5- and 14.5-G energy absorbers (based on a 50th-percentile occupant). The nominal and actual input pulses used for the simulations are shown in Figures 105 and 106, respectively. The eight cases comprising the parametric series are described in Table 34, with results listed in Tables 35 and 36 for the 14.5- and 11.5-G series, respectively.

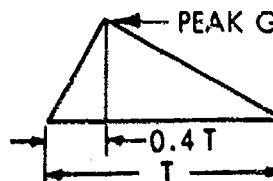
In each of the four series comparing the minimum and maximum rate of onset cases, the minimum rate of onset case was always less severe. There is a minimum of 1-in. difference in seat stroke, and seat pan and chest z-axis accelerations are greatly reduced. Maximum lumbar spine load is also decreased significantly for the minimum rate of onset cases, while the lumbar moment is not affected to a large degree.

Results of the rate of onset test series, described in Section 6.1.3, did not demonstrate this significant effect of rate of onset on system response, and when those tests were simulated with SOM-LA, the accelerations did not exhibit any significant variation, thus agreeing with the test data. Seat stroke, on the other hand, was 1.5 in. greater for the simulation of the higher-rate-of-onset test (A80-058) than for the baseline tests (A80-053 and A80-054). The analysis of pulse tolerances described here are not intended to be used quantitatively but only to determine possible significance of variables that should be investigated in greater detail by further testing.

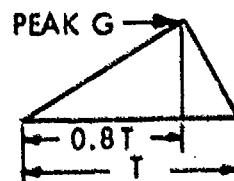


Nominal test pulse

The rise time for the nominal pulse may vary between the two values illustrated (T = time)



Maximum rate of onset pulse



Minimum rate of onset pulse

Figure 104. Dynamic test requirements for Test No. 1 of MIL-S-58095(AV).

6.2.6 Method of Transducer Calibration

At all test facilities the input (sled or drop cage) acceleration was measured using two accelerometers in order to ensure acquisition of that important parameter. The same NADC-owned strain-gage-type accelerometer was used as the primary transducer in all tests

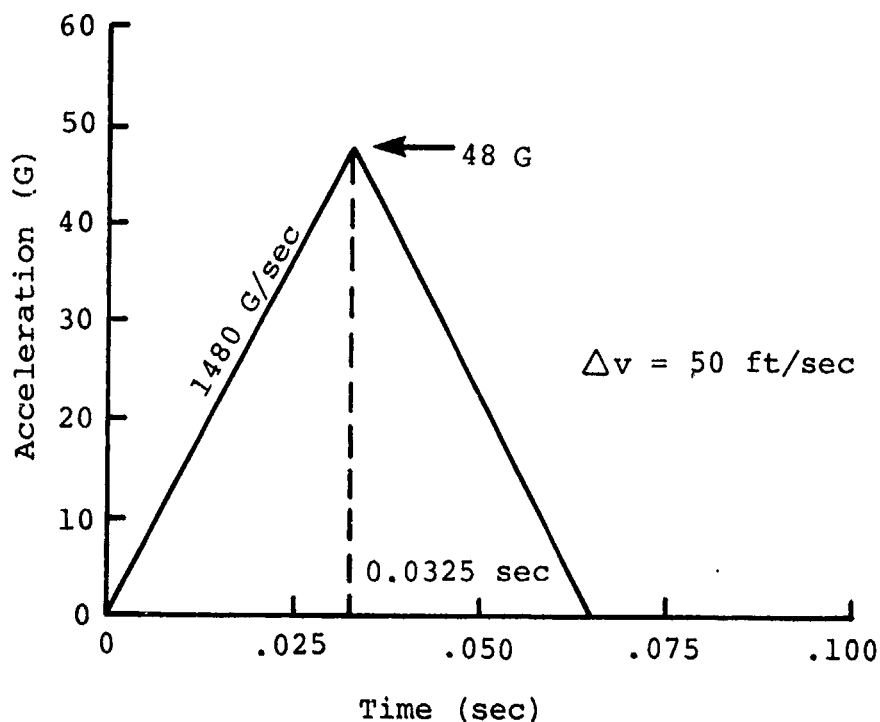


Figure 105. Nominal acceleration pulse for Test No. 1, MIL-S-58095(AV).

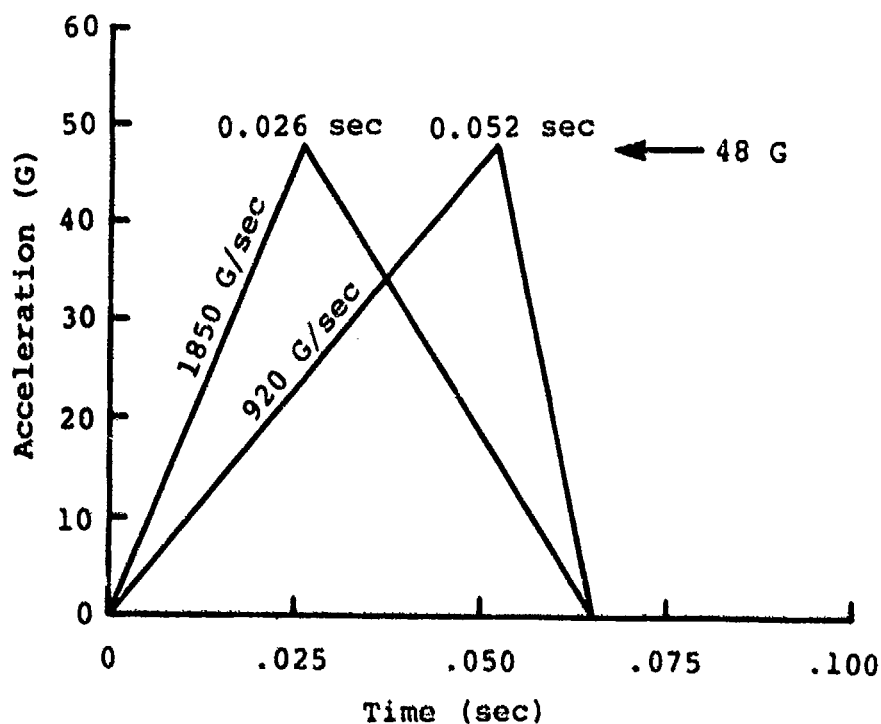


Figure 106. Minimum and maximum rate of onset conditions for simulations of Test No. 1, MIL-S-58095(AV).

TABLE 34. MATRIX OF SOM-LA SIMULATIONS FOR EVALUATION OF SENSITIVITY TO TEST PULSE TOLERANCES AT 11.5- AND 14.5-G ENERGY ABSORBER LIMIT LOAD SETTINGS

Minimum Rate of Onset 920 G/sec		Occupant Percentile	Maximum Rate of Onset 1850 G/sec	
11.5 G	14.5 G		11.5 G	14.5 G
11.5 G	14.5 G	50	11.5 G	14.5 G
11.5 G	14.5 G	95	11.5 G	14.5 G

TABLE 35. COMPARISON OF PREDICTED SEAT AND OCCUPANT RESPONSE TO MIL-S-58095(AV) DYNAMIC TEST 1 WITH 14.5-G E/A LIMIT LOAD

Input Pulse	Occupant Percen- tile	Seat Stroke (in.)	Peak Seat Pan z-Accel (G)	Peak Pelvic z-Accel (G)	Peak Chest z-Accel (G)	Peak Lumbar Load (lb)	Peak Lumbar Moment (in.-lb)
Max RO	50	12.5	33.2	27.4	39.0	2770.	4153.
Min RO	50	11.4	22.0	27.2	30.9	2350.	4424.
Max RO	95	14.9	32.3	26.2	31.5	3010.	6100.
Min RO	95	13.8	20.8	25.0	24.5	2460.	6160.

TABLE 36. COMPARISON OF PREDICTED SEAT AND OCCUPANT RESPONSE TO MIL-S-58095(AV) DYNAMIC TEST 1 WITH 11.5-G E/A LIMIT LOAD

Input Pulse	Occupant Percen- tile	Seat Stroke (in.)	Peak Seat Pan z-Accel (G)	Peak Pelvic z-Accel (G)	Peak Chest z-Accel (G)	Peak Lumbar Load (lb)	Peak Lumbar Moment (in.-lb)
Max RO	50	18.6	28.3	23.4	30.6	2363.	4170.
Min RO	50	17.0	21.8	24.3	25.0	1970.	4130.
Max RO	95	20.7	27.1	22.6	25.4	2560.	5800.
Min RO	95	19.3	20.9	22.4	19.3	2230.	5910.

at all facilities, and the redundant transducer was furnished by the individual facility performing the test. At Simula, where a different method of calibration was used for accelerometers, a significant difference was observed between primary and redundant accelerometer measurements. For example, in Simula Test SEAC-1, the primary and redundant accelerometers (both Bell and Howell 4-202-0001) produced peak values of 35.4 and 40.1 G, respectively. The pulses were of identical shape, but the difference in magnitudes produced a difference in computed velocity change, 38.8 versus 42.5 ft/sec. (The actual impact velocity was 31.1 ft/sec, and the remainder of the velocity change resulted from the rebound, which was significant).

The primary accelerometer was calibrated statically at NADC, using a centrifuge, whereas the redundant Simula transducer was dynamically calibrated in a frequency regime comparable to that expected in the testing: 10-2000 Hz. Although CAMI and NADC both employ centrifuge calibrations, they use different techniques to compensate for lead resistance. In an attempt to understand the differences in results, prior to their dummy verification tests (A81-004 through -006), CAMI recalibrated the NADC and Simula accelerometers using their centrifuge. Using the calibration resistance (R_c) value from NADC, their accelerometer produced an output that was 3.75 G low at 100 G. Simula's accelerometer, using their R_c value, was 5.0 G high at 100 G. When these two transducers were mounted side by side with a CAMI accelerometer for tests A81-004 through -006, using the CAMI calibration, all three produced identical results.

It should also be noted that each facility used signal conditioning equipment with different characteristics. This means that the control accelerometer was placed into a resistive balancing network which varied at each test facility. Full bridge-type transducers are susceptible to balance circuit errors because shunt-type balancing is essential. This follows because the bridge circuit is usually enclosed within the transducer. Errors from this requirement arise when a transducer is calibrated in a system which uses a given value of balancing resistor, but is then operated in the test with a signal conditioner having completely different balancing circuit characteristics. This error is normally eliminated by the system (end-to-end) calibration method practiced by the test facility.

The static/centrifuge method can be performed more readily in a number of laboratories, while the dynamic/shaker method requires more complex apparatus. However, the dynamic method considers the response characteristics of the transducer in an environment which may more closely resemble that experienced in the test. The results here demonstrate the need for specifying calibration methods in revised test specifications.

7.0 DISCUSSION OF RESULTS

This chapter presents conclusions drawn from results of the parametric test series and sensitivity analysis as applied to the overall goal of developing more efficient energy-absorbing seating systems. The U.S. Army's four-part research effort will ultimately lead to an improved, comprehensive specification for these systems that will ensure procurement of optimal designs.

7.1 INPUT ACCELERATION PULSE

The shape of the acceleration pulse used as input for crash testing has a significant influence on seat and occupant response. Each facility used for testing will have a characteristic pulse shape dependent on the type of decelerator mechanism used, as illustrated by the results of the test facility series described in Section 6.1.5. Any of the test pulses may resemble the acceleration environment that might be experienced in an aircraft accident. However, some facilities are able to provide a much better approximation of the nominal triangular pulse shape.

It was found that seat and occupant response to a specific input acceleration pulse was very sensitive to the peak acceleration and velocity change. The rate of onset of the acceleration pulse appears to have a secondary influence on response compared with the above two variables. However, computer simulations presented in Section 6.2.5 show that the tolerances allowed for rate of onset of the input pulse for Dynamic Test No. 1 of MIL-S-58095(AV) are large enough to allow significant variations in response. Orientation of the test facility decelerator mechanism to the gravity vector was also shown to have a marked influence on stroke for the seat orientations used in this program.

Simulations with Program SOM-LA indicated that the low-level acceleration provided by stroking landing gear can create a protective effect by causing a preload in the seat and body that minimizes dynamic overshoot.

7.2 PERFORMANCE CRITERION

The current criterion in MIL-S-58095(AV) for evaluation of energy-absorbing seat performance is based on acceleration measured in the vertical direction on the seat pan. Knowledge concerning the dynamics of impact and the interaction between the seat and occupant, and the typical injury-causing mechanisms has been greatly expanded since this specification was written. For example, it is now known that maximum seat pan acceleration does not occur concurrently with maximum vertical loads on the body; and that the typical lower spine injuries, anterior wedge fractures, are as much a function of torso flexion as axial loading along the spine. Vertical seat pan acceleration is unrelated to bending that occurs in the spine, and it is also very sensitive to localized seat pan properties that do not influence injury potential as was shown in the movable seat weight series.

Another parameter investigated for correlation with injury potential, the Dynamic Response Index, does have the advantage of accounting for the cumulative, time-dependent effects of acceleration. The DRI, therefore, can provide a measure of test severity that considers the effects of multiple acceleration peaks on occupant response. However, it suffers from some of the same disadvantages as the direct use of the maximum seat pan acceleration because it must be calculated using measured seat pan acceleration as input to a simple dynamic model; and it is also unrelated to moment generated in the spine due to bending during the significant torso rotations likely to occur in helicopter accidents.

The only parameters investigated that provided predictable trends in the injury-causing mechanisms were actual measurements of lumbar spine load and moment. The feasibility of this technique was demonstrated in this study by modifying two Alderson anthropomorphic dummies, a 50th-percentile Hybrid II and a 95th-percentile VIP-95, and repeating several key tests from the parametric test matrix. Although results from the modified dummy test series indicated some differences in performance with the load cell installation, it was apparent that the concept was sound. The occupant model in Program SOM-LA was correlated to the modified dummy response characteristics and was able to show important trends in the spinal injury-causing mechanism for all of the series in the parametric test matrix.

7.3 SEAT DESIGN PARAMETERS

The energy absorber limit load plays a very important role in determining the efficiency of a seat design. For any given stroke distance and maximum force, a constant-force (square-wave) type device can absorb the greatest amount of energy. The design problem becomes one of selecting a limit load as high as possible while not exerting injurious forces on the occupant. The actual limit load setting that provides optimal protection from spinal injury was not examined in the parametric study; however, results of the related cadaver and human volunteer test series combined with accident injury data should supply this information when completed. The energy absorber limit-load series conducted in the parametric program determined the sensitivity of seat performance to limit-load setting. It was determined that the relationship between seat stroke and limit load is not linear; i.e., required stroke distance increases more rapidly than the reduction in limit load would indicate.

In terms of occupant response, the spinal load decreases proportionally with a reduction in energy absorber limit load. Unexpectedly, however, predicted spinal y-axis moment increases with decreasing limit load. It appears that the moment is being influenced by the magnitude of seat stroke, which, due to the kinematics of the constrained legs, causes rotation of the lower torso. This trend may not be realized if the feet were not tied to the footrest as the test procedures in this program specified.

Although it was once believed that ramped limit-load energy absorbers would provide a less injurious environment compared with constant load devices, results showed that they produced a more severe occupant loading. Also, the ramped E/A's that were tested are less efficient, thereby requiring a greater stroke distance and increasing the hazard of "bottoming out."

It was determined that movable seat weight was not a factor influencing the potential for injury as measured by spinal loads and moments. However, vertical seat pan acceleration was a function of seat weight, possibly due to dynamic overshoot of the structure that occurs when the occupant motion is not strongly coupled to the seat pan. This series reinforced the conclusion that seat pan acceleration is not a good indicator of test severity. The effect of seat bucket stiffness on occupant response was not examined and may be a significant influence on seat and occupant interaction.

7.4 TESTING PROCEDURES

Procedures were developed in the parametric test program to prepare the seat and occupant for testing. These procedures were very important in obtaining repeatable test conditions, particularly pretest measurement of body segment targets and the small, repeatable initial tension given to the restraint system. It is recommended that these or similar procedures be adopted as a standard for qualification testing. However, one procedure that will require further analysis is placement of the feet. In the parametric test series it appeared that taping the feet to the footrest was an unrealistic constraint and possibly altered the kinematics of the body during the crash sequence. Simulations with Program SOM-LA indicated that footrest location and angle can influence seat and occupant response to the impact by altering the load path between the seat and the floor.

Response of various types of anthropomorphic dummies currently used for qualification testing was found to be dissimilar enough to prohibit interchangeable use in testing. The one standardized test device, the Hybrid II, conforming to the Part 572 specification, was found to provide repeatable test results without sustaining significant degradation after use in 36 dynamic tests. This model dummy was also found to be capable of being modified to allow measurement of spinal loads and moments with the addition of a six-axis load cell at the base of the spine. The elastomeric spine in the Hybrid II was designed to approximate human response in flexion. It would be desirable to develop a spine optimized to replicate combined axial and flexural response with an integral load and moment measuring capability.

The discussion presented on instrumentation calibration in Section 6.2.6 is critically important in terms of qualification testing. When the instrumentation is responsible for providing data used to assess compliance with the procurement specification, it is important to ensure its repeatability and its calibration for

the regime in which it will be required to operate. A further examination of calibration methods may be required. Data filtering is also an important area requiring additional analysis. Current Army specifications do not require a standardized filtering procedure, such as SAE J211 (Reference 25), although this recommended procedure is followed by many laboratories. However, it is not clear whether the tolerances allowed in this specification are too great; also, it has been suggested by participants in this program that SAE J211 does not make use of the performance abilities of digital filters.

-
25. Society of Automotive Engineers, Instrumentation for Impact Tests, SAE Recommended Practice SAE J211 JUN80, Transactions, SAE Handbook, Society of Automotive Engineers, Inc., Warrendale, Pennsylvania, 1981.

8.0 CONCLUSIONS

Based on the results of this program, the following conclusions can be drawn:

1. The shape of the input acceleration pulse has a significant effect on seat and occupant response.
2. Different test facilities will produce different results in terms of seat and occupant response. Differences can be attributed to test orientation, i.e., horizontal or vertical, as well as to the characteristic pulse shape.
3. Measurement of spinal force and moment provides the most reliable means of relating test performance to spinal injury. Seat pan acceleration, on the other hand, is not a good indicator of test severity or injury potential.
4. Stroke distance and energy-absorber limit load are not linearly related; i.e., required stroke distance increases more rapidly than a reduction in limit load would indicate.
5. Increasing ramp energy absorbers are less efficient than constant load (square-wave) devices and potentially more hazardous to the occupant.
6. Simulations of crash tests indicate that placement of the dummy feet can significantly influence seat and occupant response in a dynamic test.
7. The Part 572 dummy provides repeatable results, and extensive testing produced no measurable degradation of performance. However, it is not certain that the elastomeric spine of this dummy provides a response similar to that of a human spine.
8. Simulations indicate that low-level acceleration provided by the landing gear portion of the crash pulse can reduce the magnitude of dynamic overshoot, hence lowering the peak accelerations and loads in the body.

9.0 RECOMMENDATIONS

9.1 FOLLOW-ON RESEARCH

The results of the parametric test program and sensitivity analysis presented in this report constitute a tremendous step in attaining the goals of the Army's research efforts in energy-absorbing seating. However, there are several important, unanswered questions that must be examined. Those areas requiring additional work are discussed below.

9.1.1 Energy Absorber Limit-Load Threshold

The threshold, or upper limit, of energy absorber load that prevents a significant portion of spinal fracture injuries is being investigated in the cadaver and human volunteer testing programs discussed in the Introduction. However, it is equally important to maintain an on-going effort to monitor injury data in accidents involving current, production energy-absorbing seats. The accident conditions and aviator population involved can never be duplicated in laboratory conditions. It may be desirable to use a statistical approach to minimize the total number or the severity of injuries by combining the statistical distributions of spinal strengths and accident severities with the sensitivity curves presented here to set an optimal energy absorber load level.

9.1.2 Standardized Test Dummy

A standard test dummy for energy-absorbing seat testing needs to be developed. Results of the study to determine anthropometry for the military aviator population can be incorporated with methods developed in the instrumented dummy research effort to produce a standardized device. If funding constraints should prohibit development of a new dummy, then an economical alternative would be to modify the spinal properties of the Part 572 design to meet vertical testing requirements. The spine must be instrumented to provide a measure of forces and moments. The optimum location for force and moment measurement is not known, and should be determined if a new lumbar spine is designed. In the existing Part 572 system, the base of the spine is the only practical location for a transducer. Also, it may be necessary to scale the design of the 50th-percentile dummy to develop 95th- and 5th-percentile versions for testing the occupant size range for variable load energy absorber systems now under development.

The ultimate goal of the standardized dummy development will be to provide a means for quantitative assessment of injury potential rather than just a comparison of relative test severity. Achieving this end will require conducting a matrix of dynamic tests with the standardized dummy, replicating cadaver and human volunteer experiments, as well as performing a number of the sensitivity tests conducted in this program. The purpose would be

to develop actual spinal load and moment measurements that represent the spinal injury threshold for the aircraft crash environment. An adjunct to this effort would be to correlate Program SOM-LA to the new dummy response characteristics to minimize the number of dynamic tests required for future parametric studies.

9.1.3 Refinement of Qualification Test Methods

An analysis of the tolerances allowable on the input acceleration pulse needs to be conducted. This would require the development of a set of reasonable seat/occupant response variations and then the use of the sensitivity analysis presented in this report to define the allowable deviations from the desired test pulse for parameters such as peak acceleration, velocity change, and rate of onset. It would then be desirable to conduct dynamic tests with the new standardized test dummy to verify predicted performance variations and explore the range of spinal loads and moments that these variations produce.

An effort should be undertaken to determine if an equivalent test condition can be achieved for vertical and horizontal decelerator test facilities. The best approach for accomplishing this would be the use of SOM-LA simulations, followed by a set of dynamic tests to verify the results. If equivalent test conditions cannot be produced, then it must be decided whether the resulting performance variations exceed the tolerable limits thus requiring one decelerator mechanism type or orientation.

The final area requiring additional research in order to develop an improved specification is calibration of transducers, along with data processing. A comparison needs to be made of transducers to be used for determination of performance compliance and their available calibration techniques. The type of transducers to be examined would include accelerometers for input acceleration and load cells for measuring spinal load and moments. Procedures for signal conditioning and filtering must be explored to develop a set consistent with the magnitude of allowable errors.

9.2 SUGGESTED MODIFICATIONS TO CURRENT ENERGY-ABSORBING SEAT SPECIFICATIONS

The following areas have been identified as requiring modification in MIL-S-58095(AV), MIL-STD-1290(AV), and possibly the Aircraft Crash Survival Design Guide, TR-79-22, to achieve the Army's goals of improved energy-absorbing seating systems:

- Define closer tolerances on the input deceleration pulse and provide definitions for each prescribed variable.
- Specify equivalent test conditions for horizontal and vertical test facilities and types of decelerator mechanisms.

- Require the use of the standardized test dummy with applicable instrumentation.
- Possibly modify the required test matrix to include tests at the limits of occupant size range, i.e., 95th and 5th percentile, possibly including female occupants.
- Specify required energy absorber limit-load factor.
- Add performance assessment criteria based on maximum allowable spinal load and moment values for the standardized test dummy.
- Provide a standard procedure for test dummy positioning and seat preparation prior to qualification testing.
- In addition to testing of the seat itself, require an evaluation of equipment and structural interfaces applicable to specific aircraft that will affect seat performance. Floor structure and attachment should be as close as possible to actual aircraft structure for the seat qualification test, and procedures for providing floor deformation should be specifically defined. Then such equipment as helmet, instrumentation consoles, and sights should be included in an additional test to evaluate crew station safety performance.
- Footrest location for testing should be required in system specification, but default position can be included in more general seat specifications.
- Standardize calibration procedures for transducers used for assessing compliance with specification requirements.
- Specify data filtering procedures and filter characteristics.

10.0 REFERENCES

1. Singley, G. T., III, and Desjardins, S. P., "Crashworthy Helicopter Seats and Occupant Restraint Systems," in Operational Helicopter Aviation Medicine, AGARD Conference Proceedings No. 255, North Atlantic Treaty Organization, Advisory Group for Aerospace Research and Development, Neuilly sur Seine, France, May 1978.
2. Crash Survival Design Guide, Dynamic Science, A Division of Marshall Industries, USAAMRDL Technical Report 71-22, Eustis Directorate, U.S. Army Air Mobility Research and Development Laboratory, Fort Eustis, Virginia, 1971, AD 733358.
3. Military Standards, MIL-STD-1290(AV), Light Fixed - Rotary-Wing Aircraft Crashworthiness, Department of Defense, Washington, D.C., 25 January 1974.
4. Military Specification, MIL-S-58095(AV), Seat System: Crashworthy, Non-Ejection, Aircrew, General Specification For, Department of Defense, Washington, D.C., 27 August 1971.
5. Desjardins, S. P., and Harrison, H., The Design, Fabrication, and Testing of an Integrally Armored Crashworthy Crewseat, Dynamic Science, Division of Marshall Industries; USAAMRDL Technical Report 71-54, Eustis Directorate, U.S. Army Air Mobility Research and Development Laboratory, Fort Eustis, Virginia, January 1972, AD 7421733.
6. Desjardins, S. P., and Laananen, D. H., Aircraft Crash Survival Design Guide, Volume IV - Aircraft Seats, Restraints, Litters, and Padding, Simula Inc., USARTL-TR-79-22D, Applied Technology Laboratory, U.S. Army Research and Technology Laboratories (AVRADCOM), Fort Eustis, Virginia, June 1980, AD A088441.
7. Laananen, D. H., Aircraft Crash Survival Design Guide, Volume II - Aircraft Crash Environment and Human Tolerance, Simula Inc., USARTL-TR-79-22B, Applied Technology Laboratory, U.S. Army Research and Technology Laboratories (AVRADCOM), Fort Eustis, Virginia, January 1980, AD A082512.
8. Eiband, A. M., Human Tolerance to Rapidly Applied Accelerations: A Summary of the Literature, NASA Memorandum 5-19-59E, National Aeronautics and Space Administration, Washington, D.C., June 1959.
9. Brinkley, J. W., Weis, E. B., Clarke, N. P., and Temple, W. E., A Study of the Effect of Five Orientations of the Acceleration Vector on Human Response, AMRL Memo M-28, Aerospace Medical Research Laboratory, Wright-Patterson Air Force Base, Ohio, 1963.

10. Reader, D. C., The Restraint Afforded by the USAF and Proposed RAF IAM Seat Harnesses for the F-111 Under High Forward and Lateral Decelerations, IAM Report 421, Institute of Aviation Medicine, Farnborough, Hampshire, United Kingdom, 1967.
11. Crash Survival Design Guide, Dynamic Science, A Division of Marshall Industries, USAAMRDL Technical Report 70-22, Eustis Directorate, U.S. Army Air Mobility Research and Development Laboratory, Fort Eustis, Virginia, 1970, AD 695648.
12. Domzalski, L., and Singley, G. T., III, Joint Army/Navy Test Program for Black Hawk Seat Systems, Report NADC-79229-60 (Draft), Naval Air Development Center, Warminster, Pennsylvania, 1979.
13. Dummer, R. J., Qualification Test Report, 613-1787 C00L Qualification Testing of Armored Crashworthy Aircrew Seat, RA-305252-1, for Sikorsky Aircraft Contract 576344, Norton Company, Worcester, Massachusetts, October 1978.
14. Chandler, R. F., Dynamic Test of Joint Army/Navy Crashworthy Armored Crewseat, Protection and Survival Laboratory, Memorandum Report AAC-119-80-2, Civil Aeromedical Institute, Mike Monroney Aeronautical Center, Federal Aviation Administration, Oklahoma City, Oklahoma, 25 April 1980.
15. Hearon, B. F., Raddin, J. H., and Brinkley, J. W., "Guidance for the Utilization of Dynamic Preload in Impact Injury Prevention," in Impact Injury: Mechanisms, Prevention and Cost, North Atlantic Treaty Organization, Advisory Group of Aerospace Research and Development, Neuilly sur Seine, France, April 1982.
16. Applied Technology Laboratory, U.S. Army Research and Technology Laboratory (AVRADCOM), Contract DAAK51-C-0016, "Provide Hardware, Test Support and Engineering Services" Contracted with Simula Inc., Tempe, AZ, May 1979.
17. Laananen, D. H., and Coltman, J. W., Measurement of Spinal Loads in Two Modified Anthropomorphic Dummies, Simula Inc. TR-82405, Final Report, Contract DAMD17-81-C-1175, U.S. Army Aeromedical Research Laboratory, Fort Rucker, Alabama, May 1982.
18. Desjardins, S. P., et al., Crashworthy Armored Crewseat for the UH-60A Black Hawk, paper presented at 35th Annual National Forum of the American Helicopter Society, Washington, D.C., May 1979.
19. Code of Federal Regulations, "Anthropomorphic Test Dummy," Title 49, Chapter 5, Part 572, Federal Register, Vol. 38, No. 62, April 2, 1973, pp. 8455-8458.

20. Military Specification, MIL-S-9479, Seat System Upward Ejection, Aircraft, General Specification for, Department of Defense, Washington, D.C.
21. Stech, E. L., and Payne, P. R., Dynamic Models of the Human Body, Frost Engineering Development Corp. AMRL Technical Report 66-157, Aerospace Medical Research Laboratory, Wright-Patterson Air Force Base, Ohio, November 1969, AD 701383.
22. Brinkley, J. W., and Shaffer, J. T., Dynamic Simulation Techniques for the Design of Escape Systems: Current Applications and Future Air Force Requirements, AMRL Technical Report 71-29-2, Aerospace Medical Research Laboratory; Wright-Patterson Air Force Base, Ohio, December 1971, AD 740439.
23. Laananen, D. H., Bolukbasi, A. O., and Coltman, J. W., Computer Simulation of an Aircraft Seat and Occupant in a Crash Environment, Volume I - Technical Report, TR-82401, Simula Inc., DOT/FAA/CT-82/33-I, Federal Aviation Administration Technical Center, Atlantic City Airport, New Jersey, September 1982.
24. Laananen, D. H., Coltman, J. W., and Bolukbasi, A. O., Computer Simulation of an Aircraft Seat and Occupant in a Crash Environment, Volume II - Program SOM-LA User Manual, TR-81415, Simula Inc., DOT/FAA/CT-82/33-I, Federal Aviation Administration Technical Center, Atlantic City Airport, New Jersey, September 1982.
25. Society of Automotive Engineers, Instrumentation for Impact Tests, SAE Recommended Practice SAE J211 JUN80, Transactions, SAE Handbook, Society of Automotive Engineers, Inc., Warrendale, Pennsylvania, 1981.

APPENDIX A

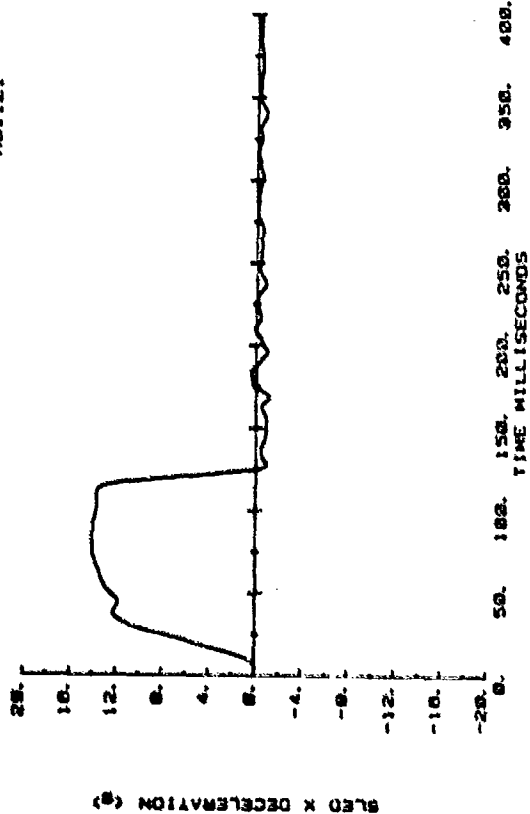
CAMI TEST A81-121

Rigid Seat
50th-Percentile Dummy
(modified for spinal load measurement)

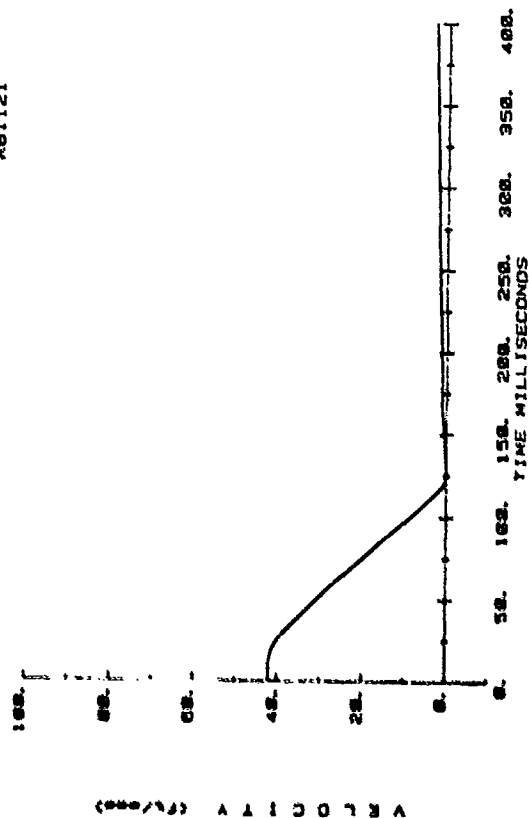
$$\Delta v = 42.4 \text{ ft/sec}$$

$$G_{\text{peak}} = 14.1$$

CAMI SLED TEST
A81121

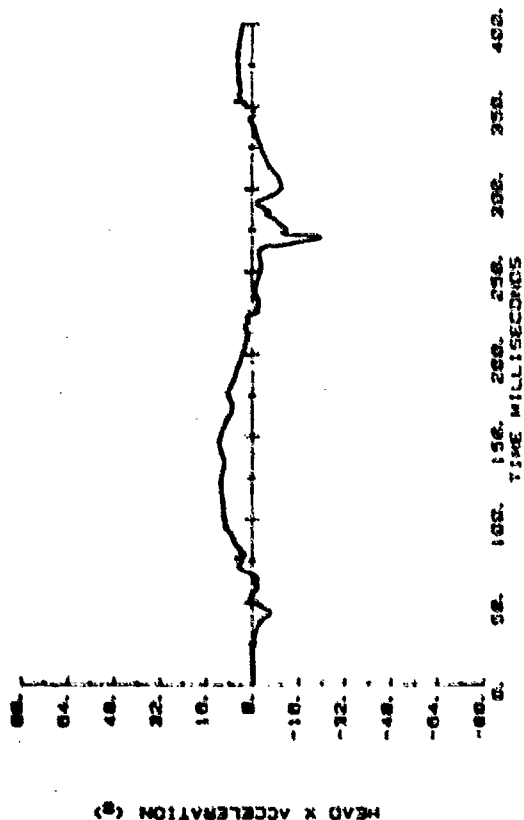


CAMI SLED TEST
A81121

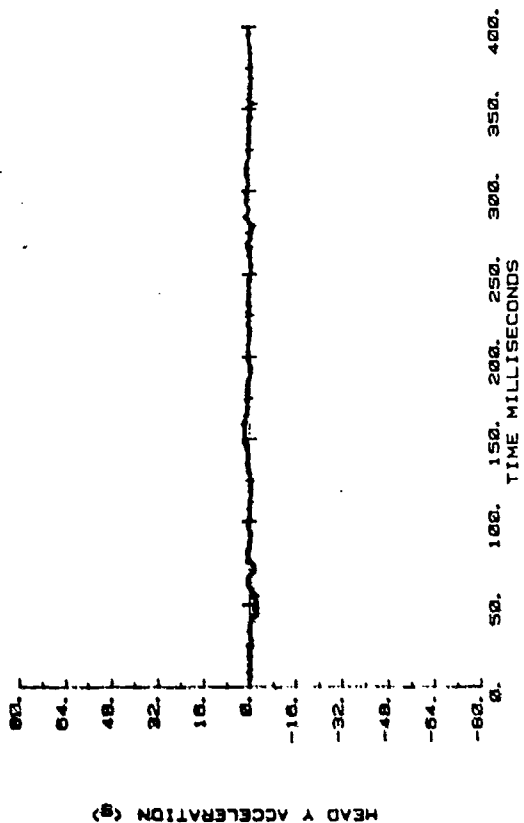


Sled Deceleration and Velocity

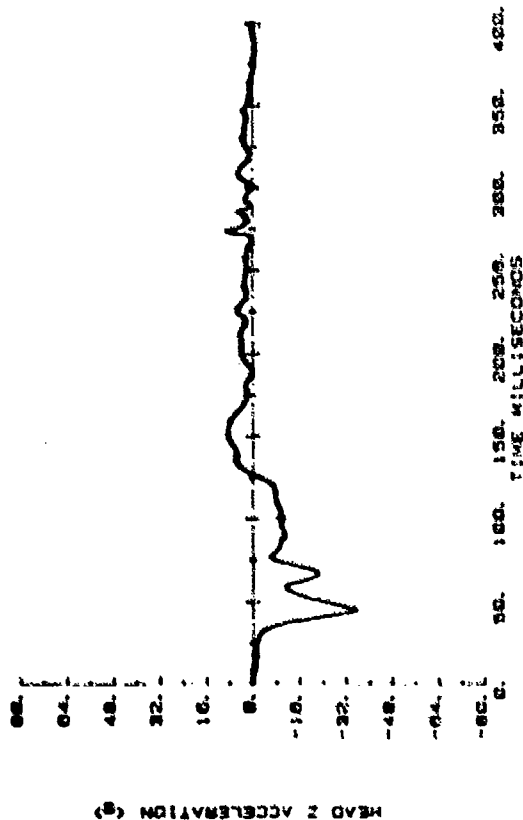
CAMI SLED TEST
AB1121



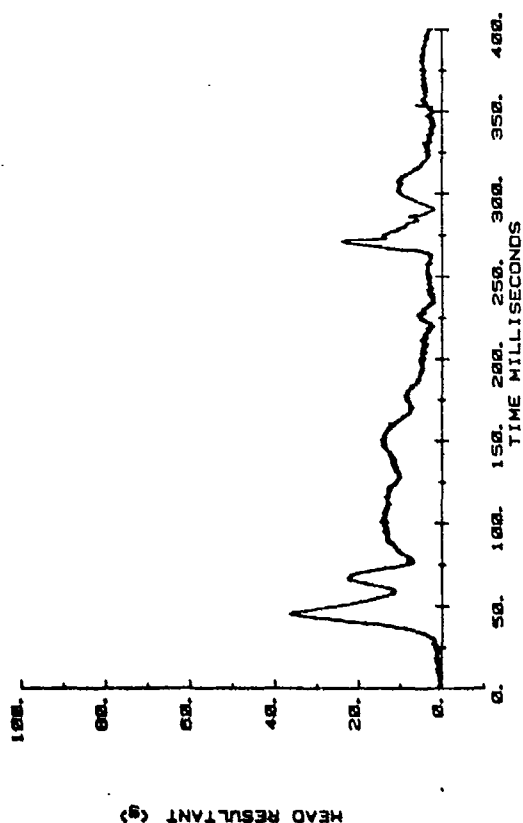
CAMI SLED TEST
AB1121



CAMI SLED TEST
AB1121

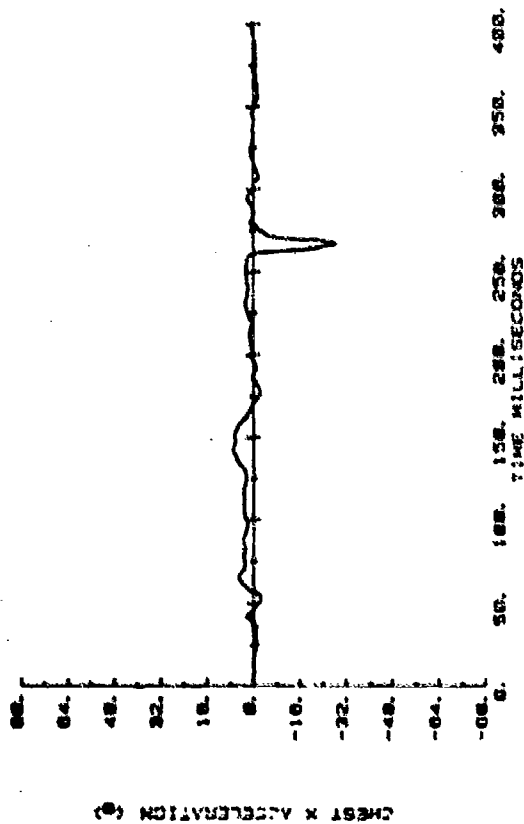


CAMI SLED TEST
AB1121

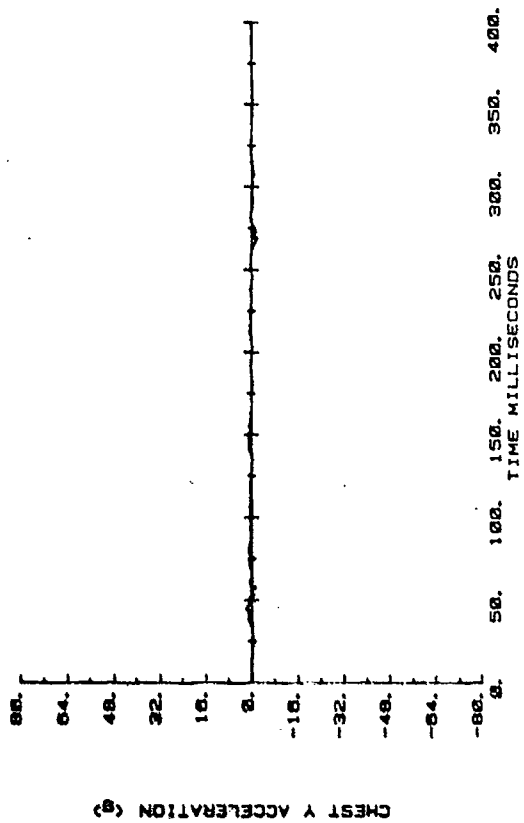


Head Acceleration

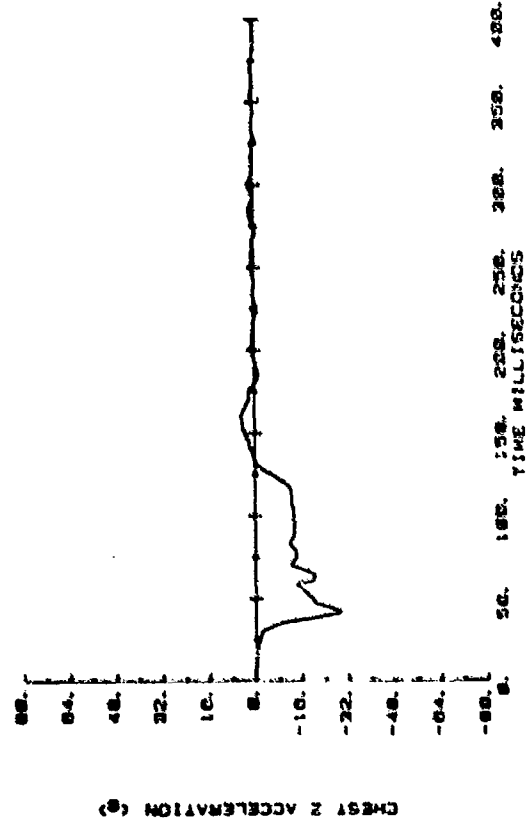
CAMI SLED TEST
A81121



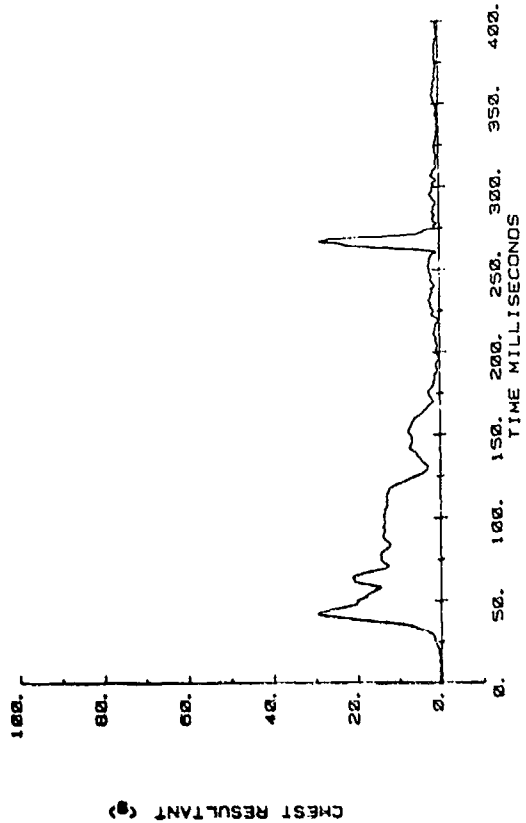
CAMI SLED TEST
A81121



CAMI SLED TEST
A81121

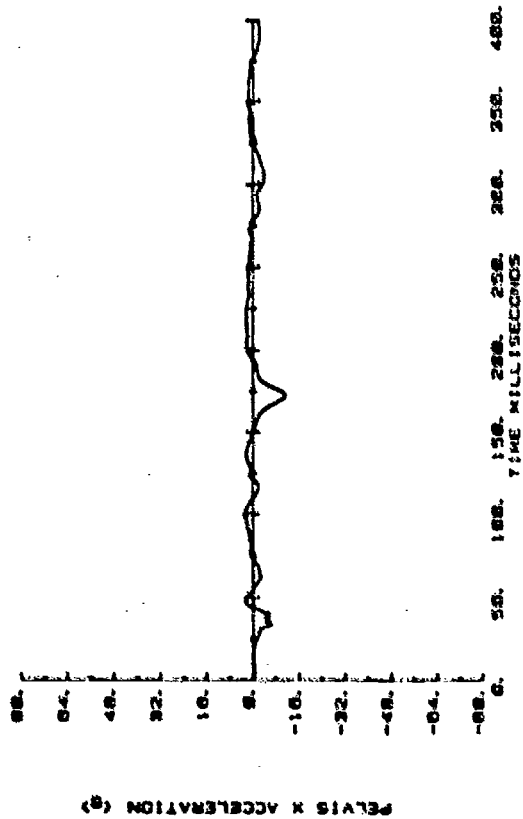


CAMI SLED TEST
A81121

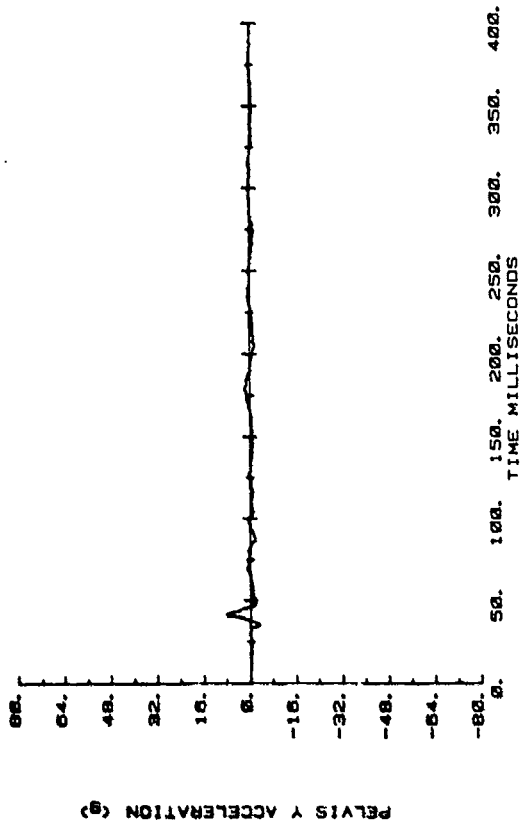


Chest Acceleration

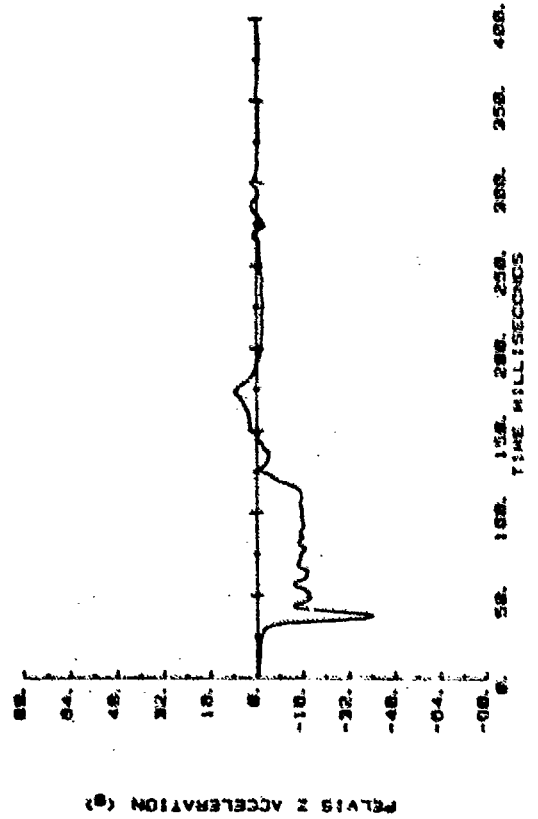
CAMI SLED TEST
AB1121



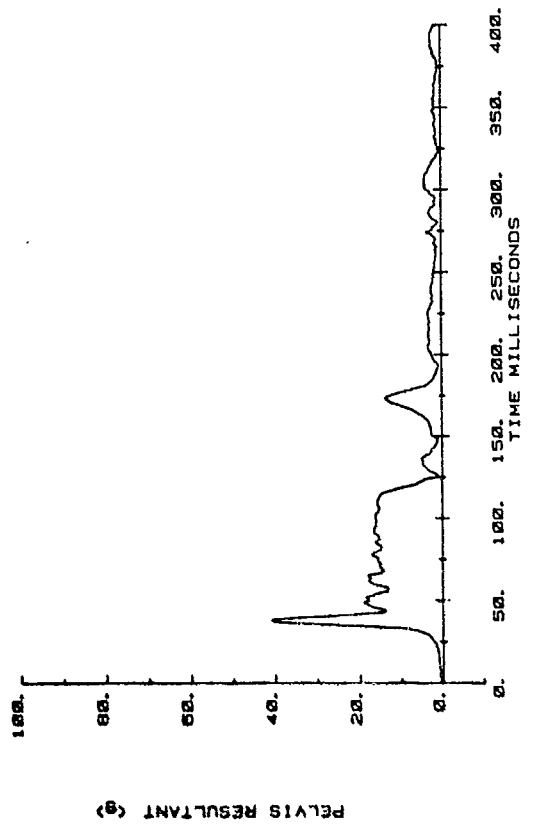
CAMI SLED TEST
AB1121



CAMI SLED TEST
AB1121

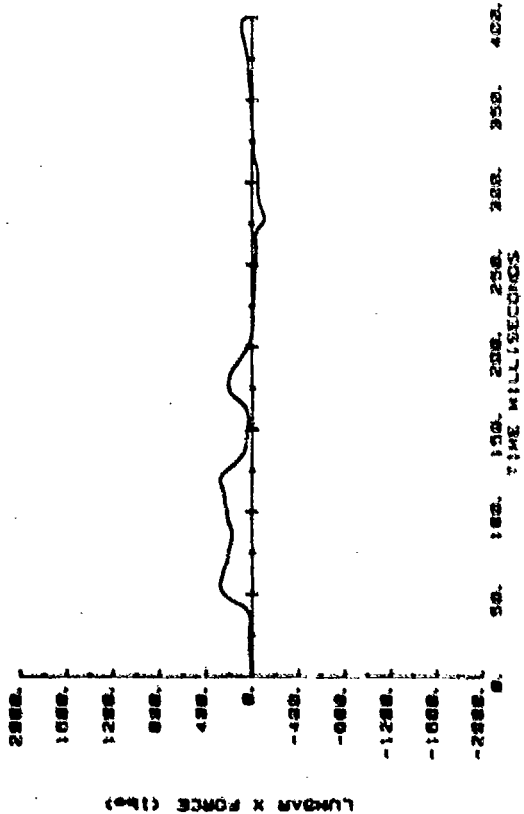


CAMI SLED TEST
AB1121

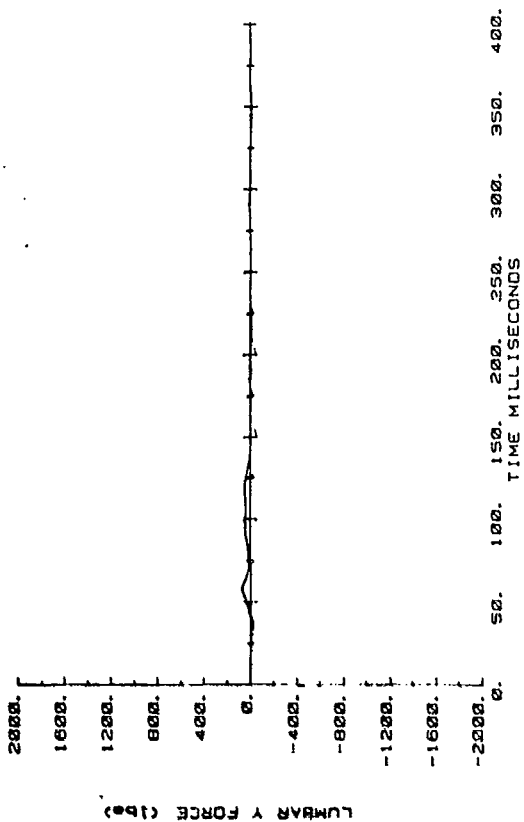


Pelvis Acceleration

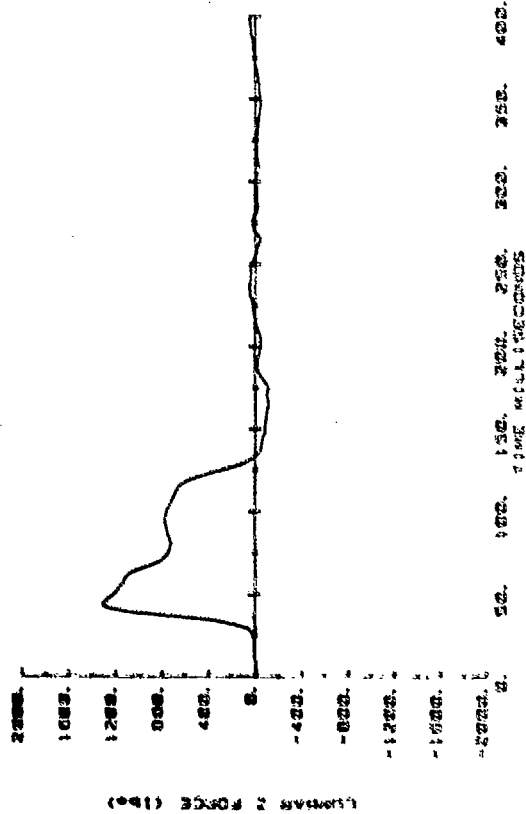
CAMI SLED TEST
AB1121



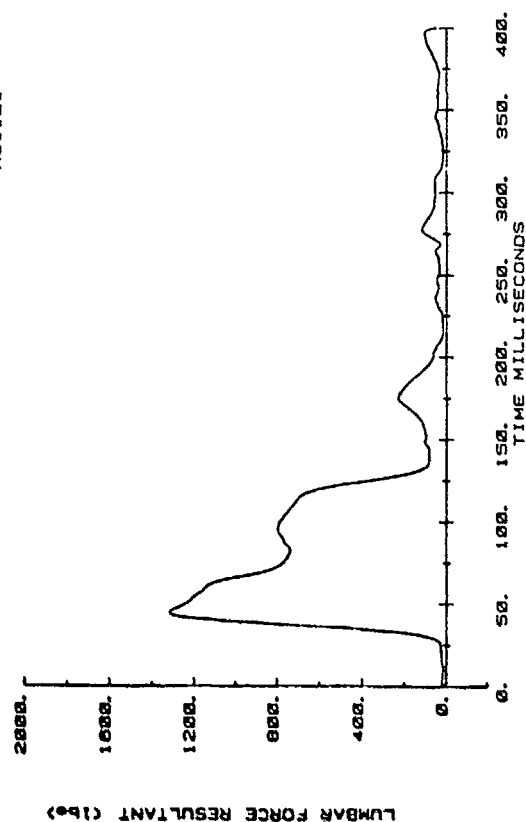
CAMI SLED TEST
AB1121



CAMI SLED TEST
AB1121

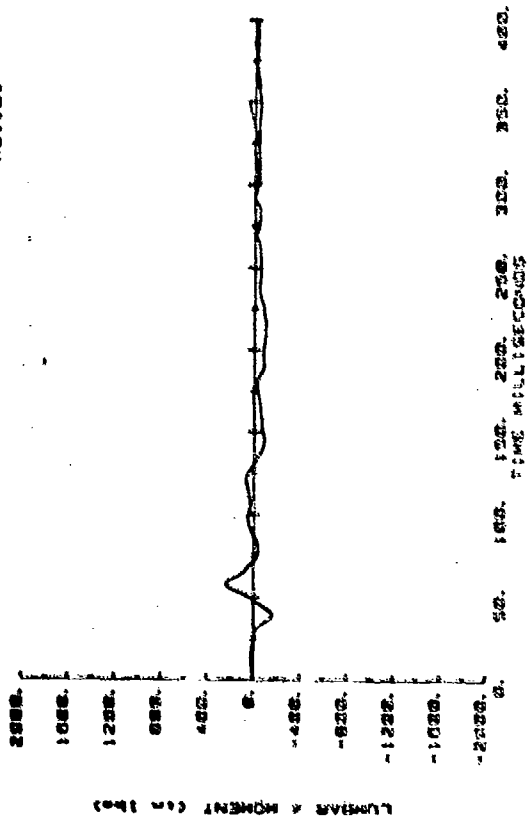


CAMI SLED TEST
AB1121

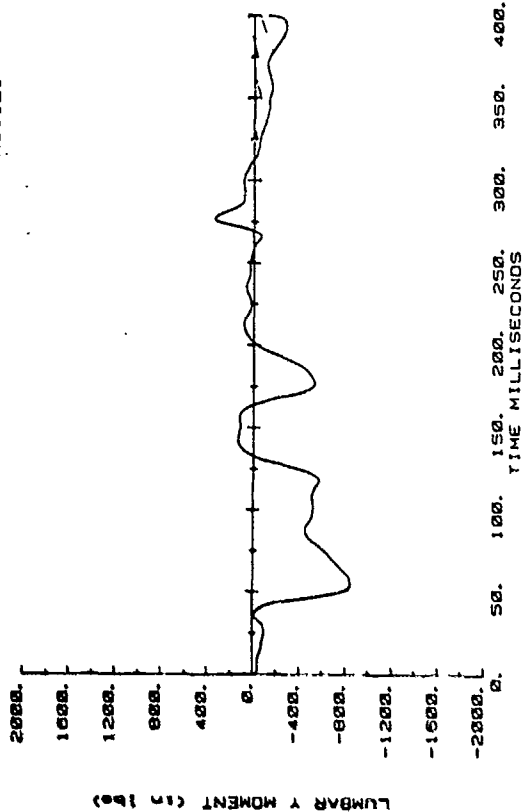


Lumbar Force

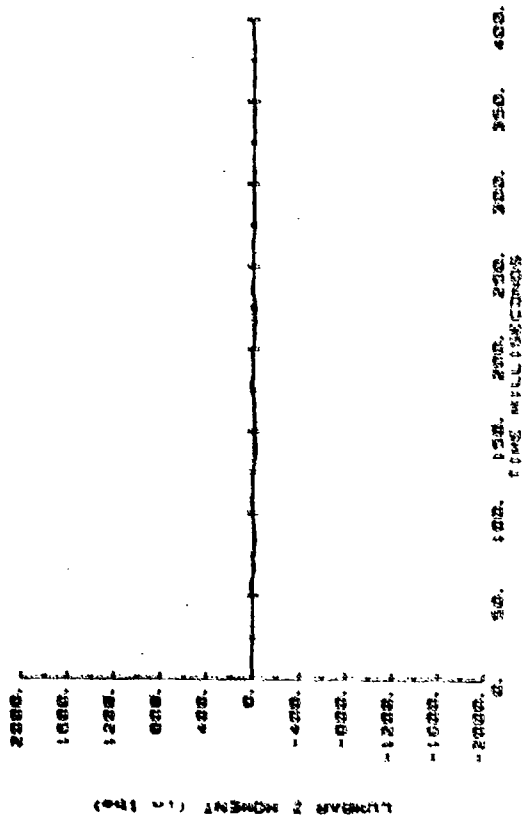
CAMI SLED TEST
A81121



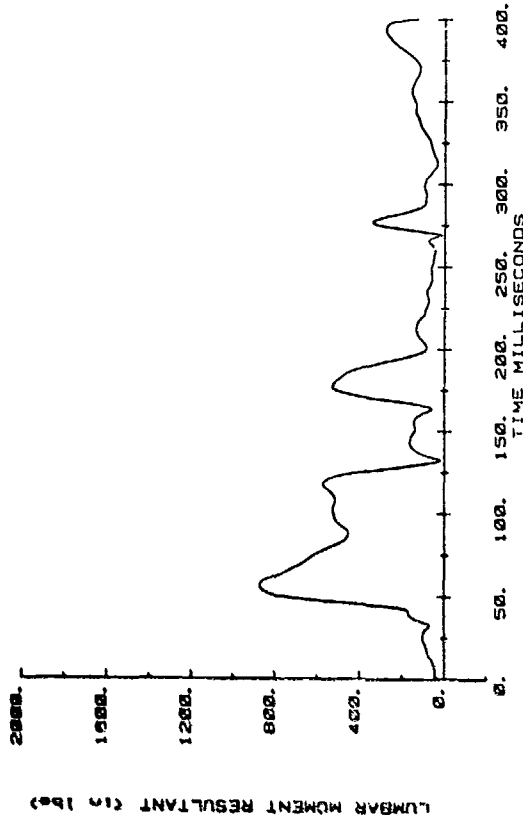
CAMI SLED TEST
A81121



CAMI SLED TEST
A81121

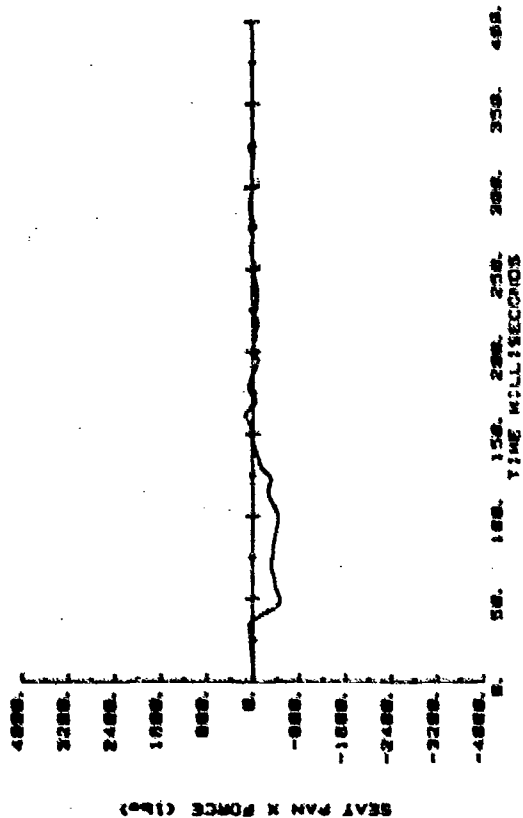


CAMI SLED TEST
A81121



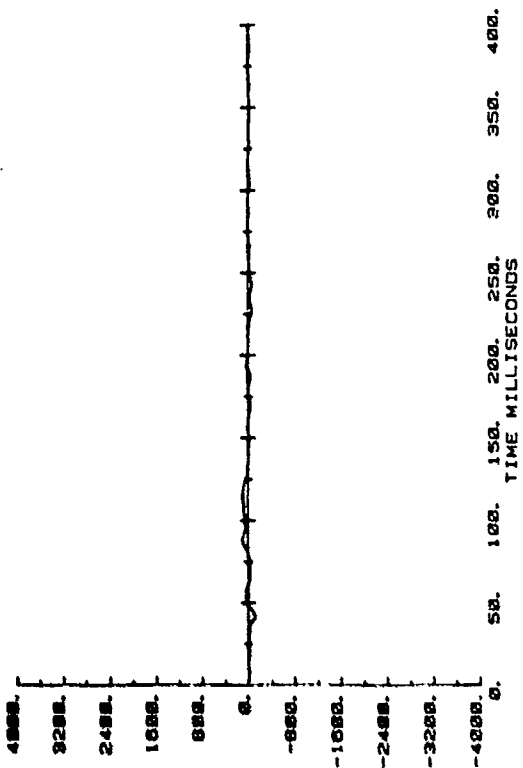
Lumbar Moment

CAMI SLED TEST
A81121



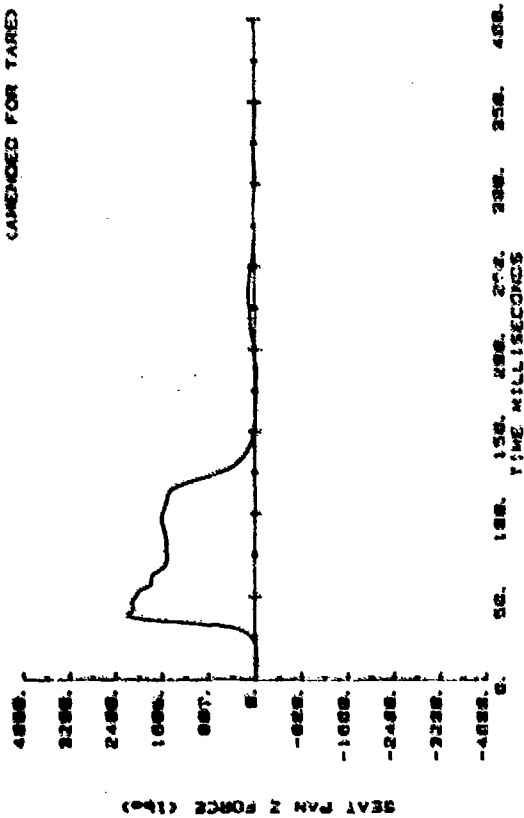
50. 100. 150. 200. 250. 300. 350. 400.
TIME (MILLISECONDS)

SEAT PAN Y FORCE (lbs)



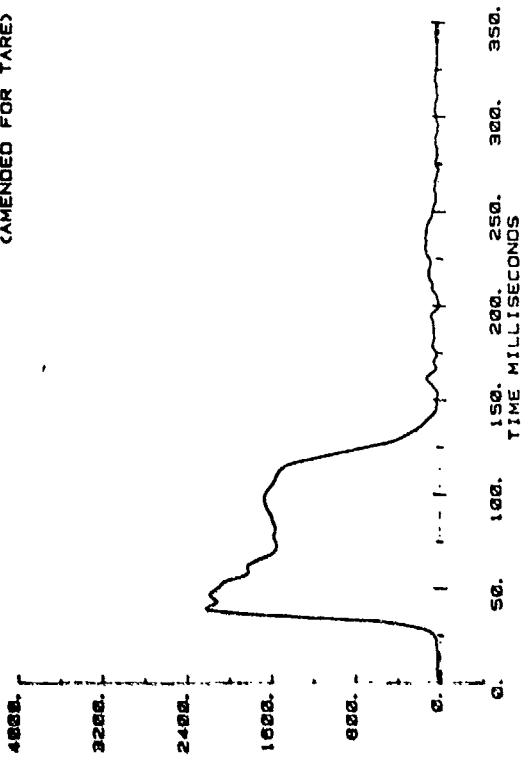
50. 100. 150. 200. 250. 300. 350. 400.
TIME (MILLISECONDS)

CAMI SLED TEST
A81121
(AMENDED FOR TARE)



50. 100. 150. 200. 250. 300. 350. 400.
TIME (MILLISECONDS)

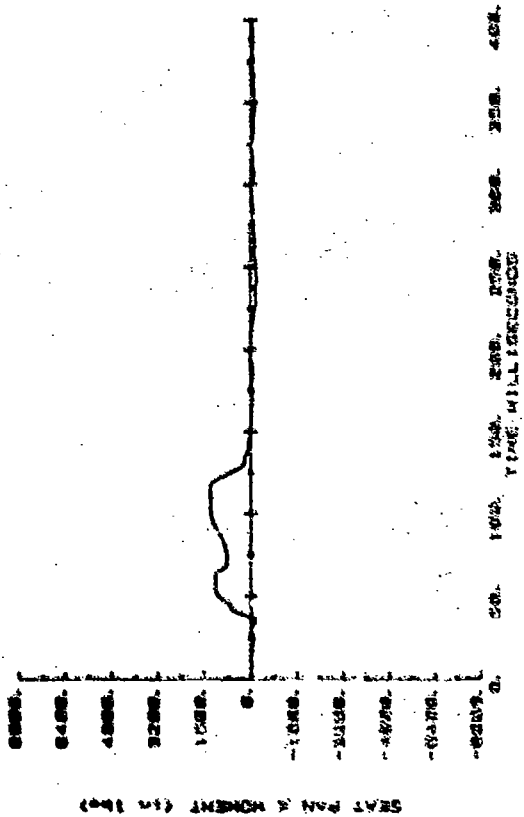
SEAT PAN FORCE RESULTANT (lbs)



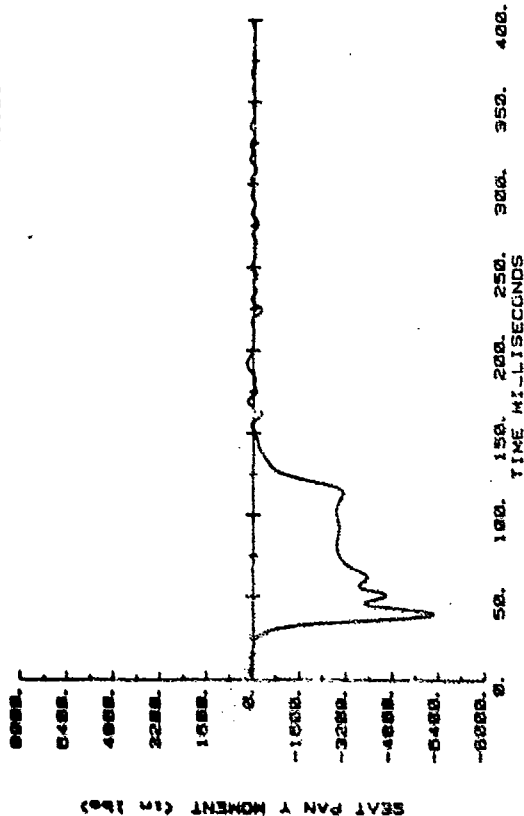
50. 100. 150. 200. 250. 300. 350.
TIME (MILLISECONDS)

Seat Pan Force

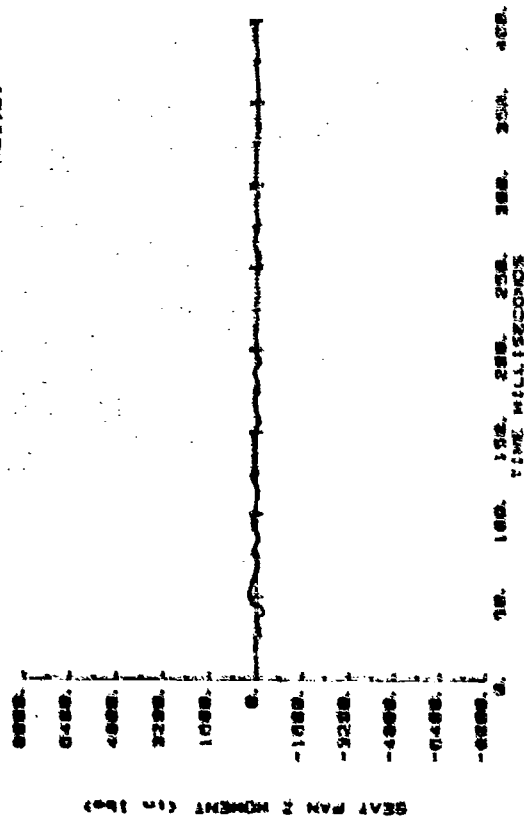
CAMI SLED TEST
AB1121



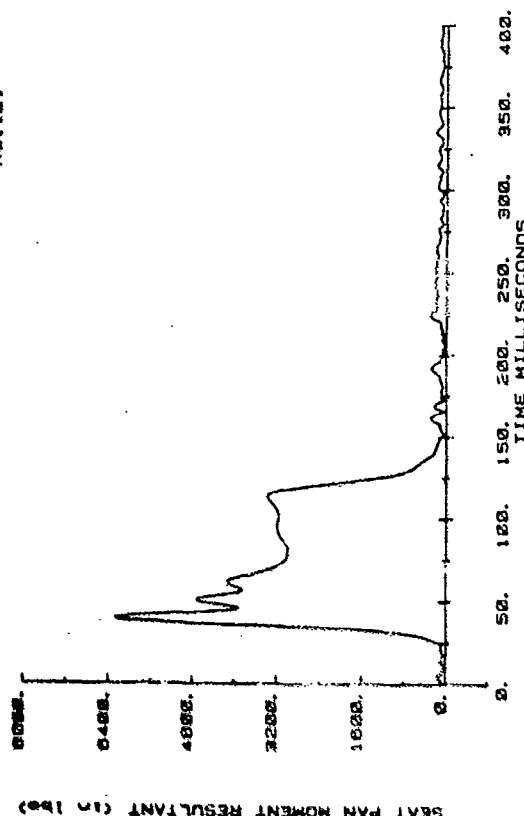
CAMI SLED TEST
AB1121



CAMI SLED TEST
AB1121

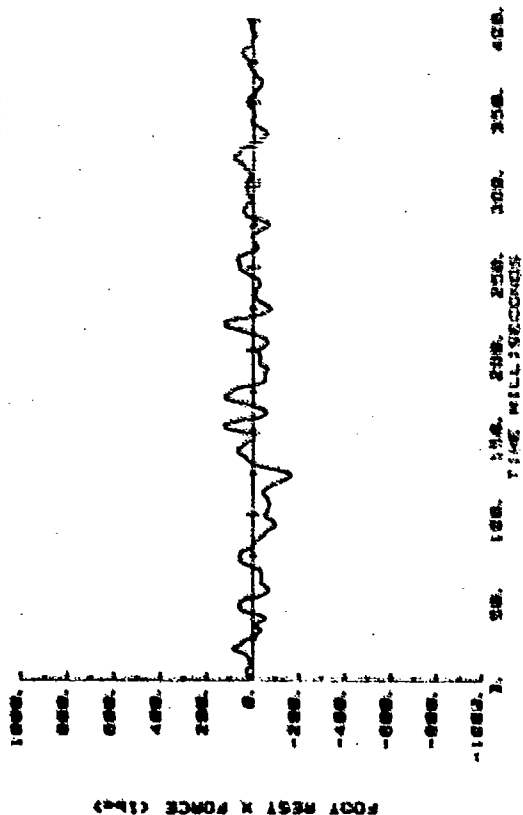


CAMI SLED TEST
AB1121

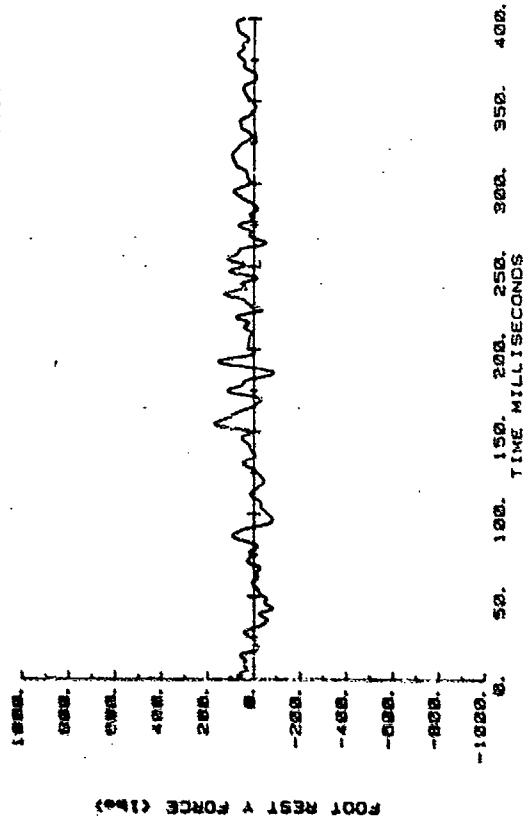


Seat Pan Moment

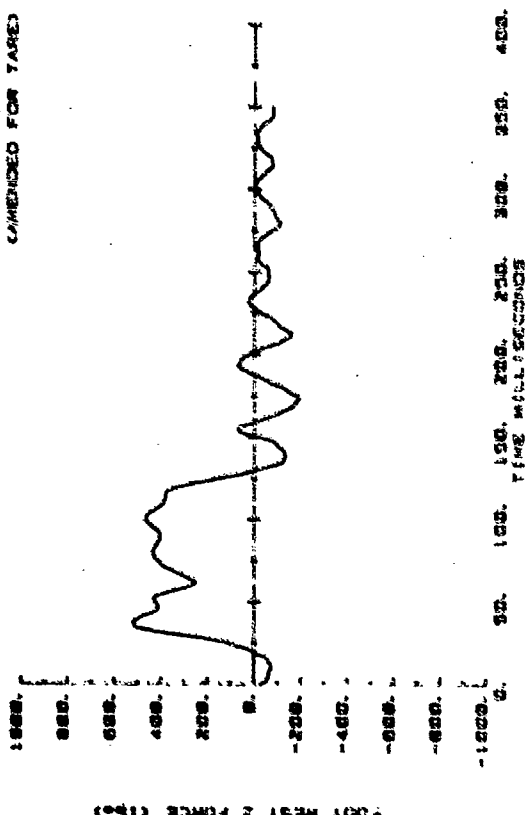
CAMI SLED TEST
A81121



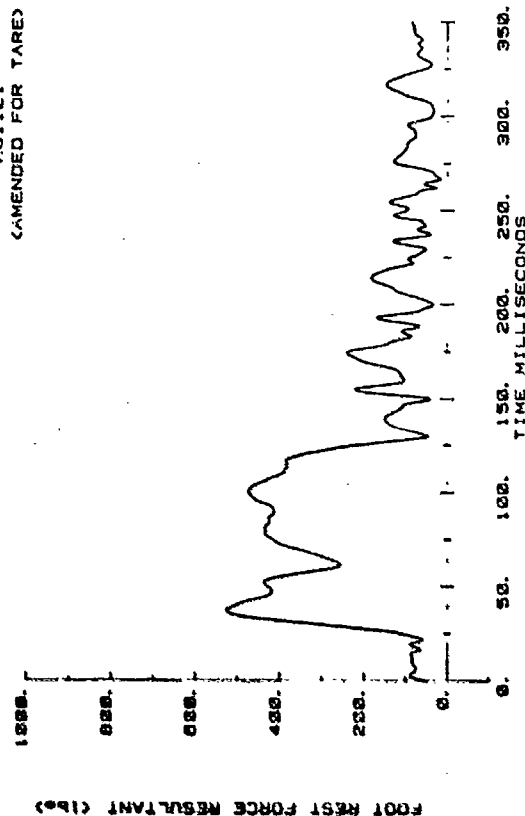
CAMI SLED TEST
A81121



CAMI SLED TEST
A81121
(AMENDED FOR TARE)



CAMI SLED TEST
A81121
(AMENDED FOR TARE)



Footrest Force

APPENDIX B

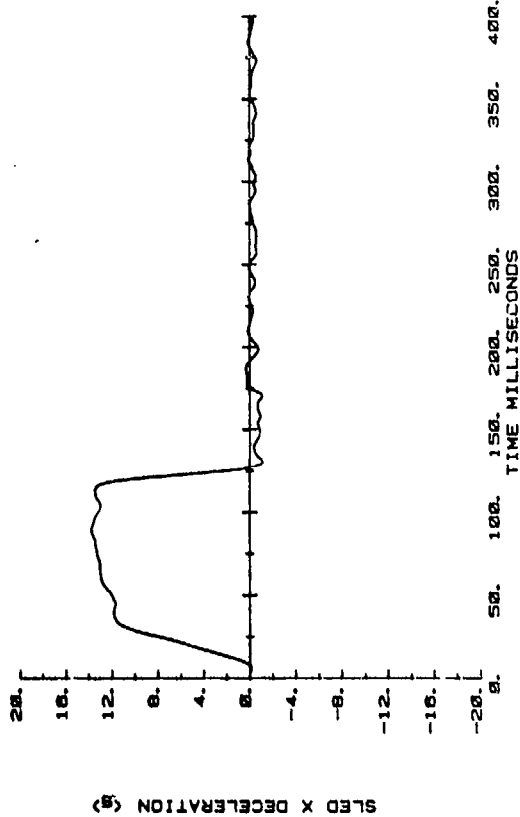
CAMI TEST A81-122

Rigid Seat
95th-Percentile Dummy
(modified for spinal load measurement)

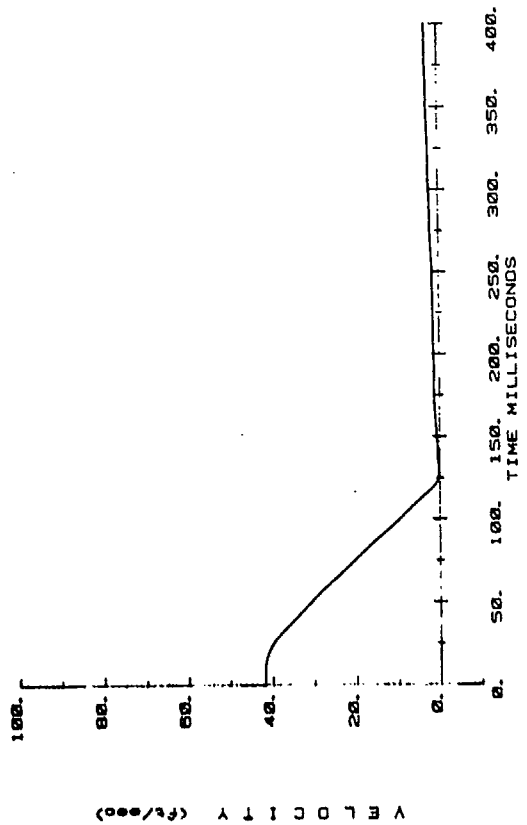
$$\Delta v = 42.5 \text{ ft/sec}$$

$$G_{\text{peak}} = 13.8$$

CAMI SLED TEST
A81122

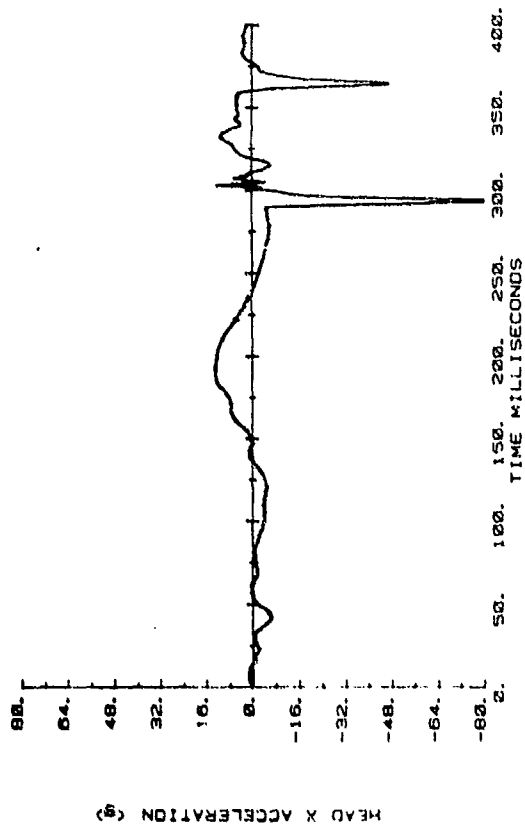


CAMI SLED TEST
A81122

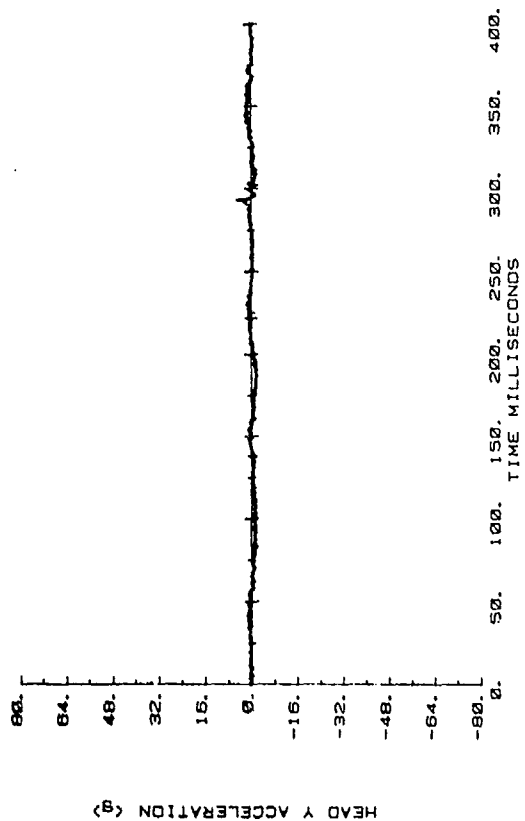


Sled Deceleration and Velocity

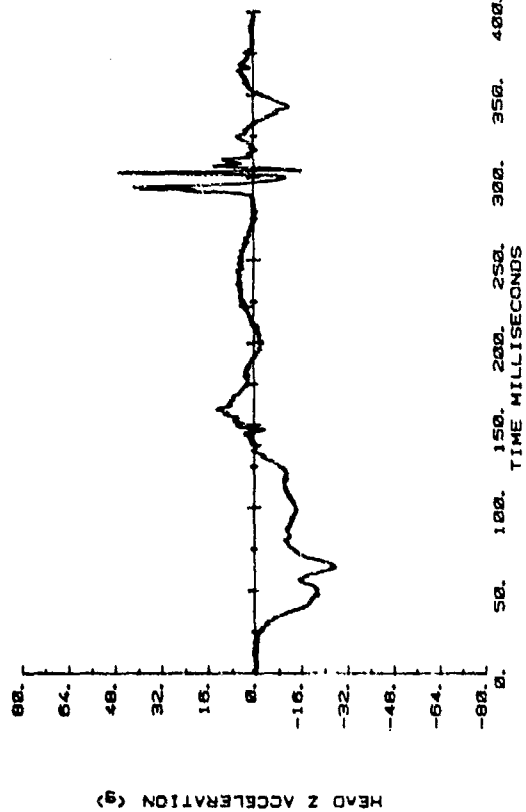
CAMI SLED TEST
AB1122



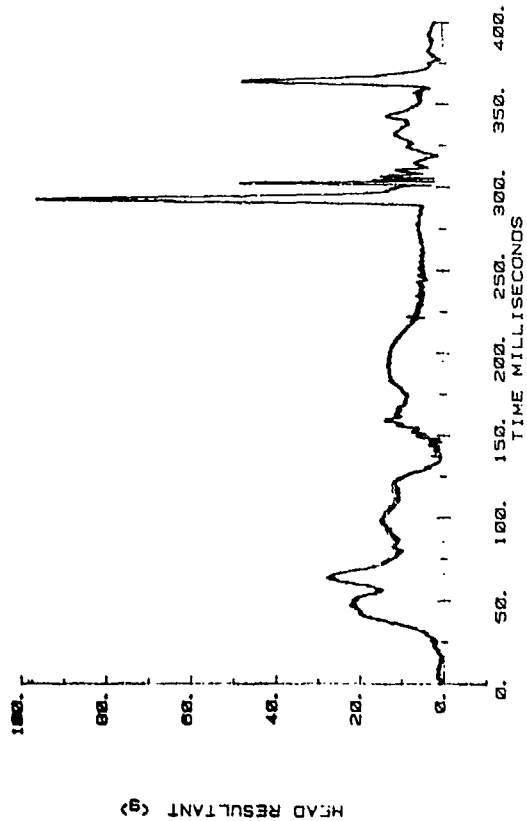
CAMI SLED TEST
AB1122



CAMI SLED TEST
AB1122

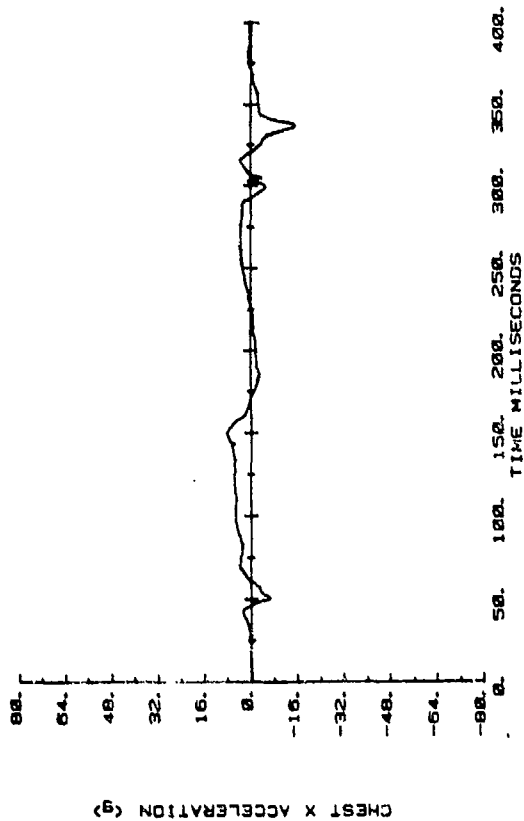


CAMI SLED TEST
AB1122

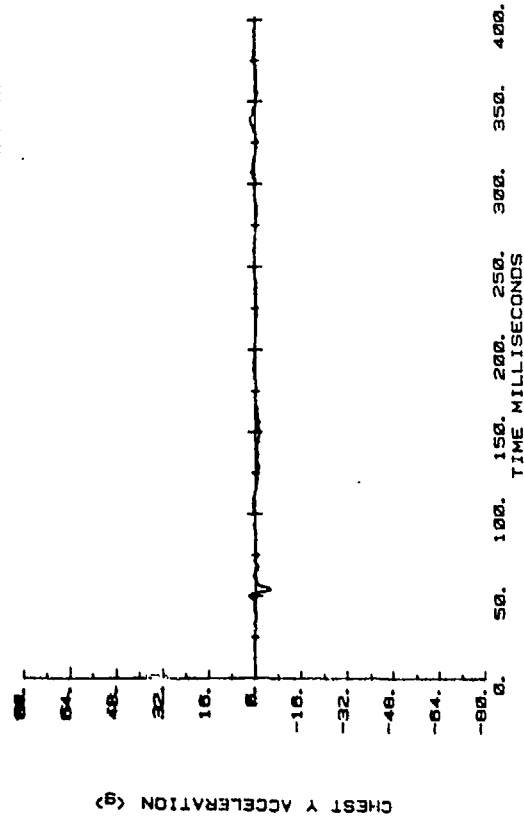


Head Acceleration

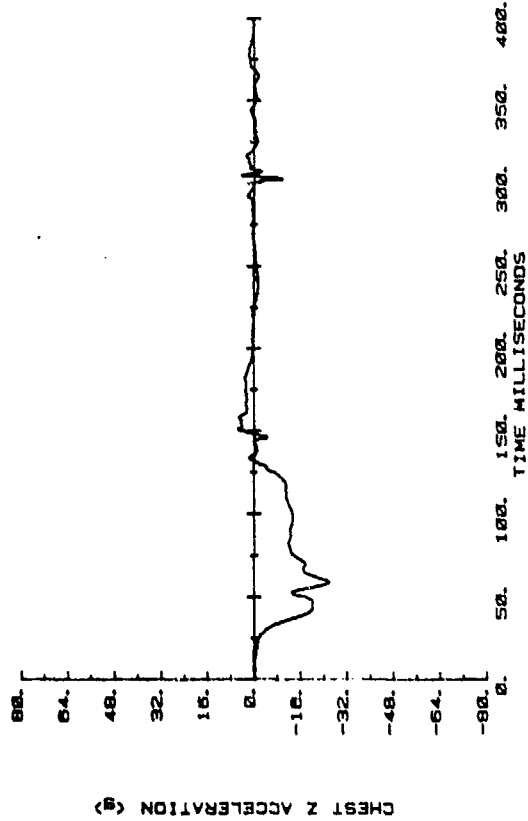
CAMI SLED TEST
AB1122



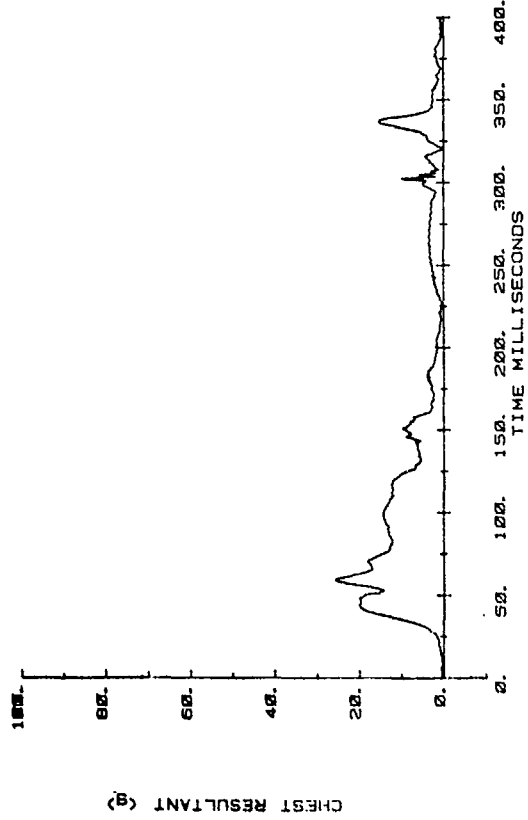
CAMI SLED TEST
AB1122



CAMI SLED TEST
AB1122

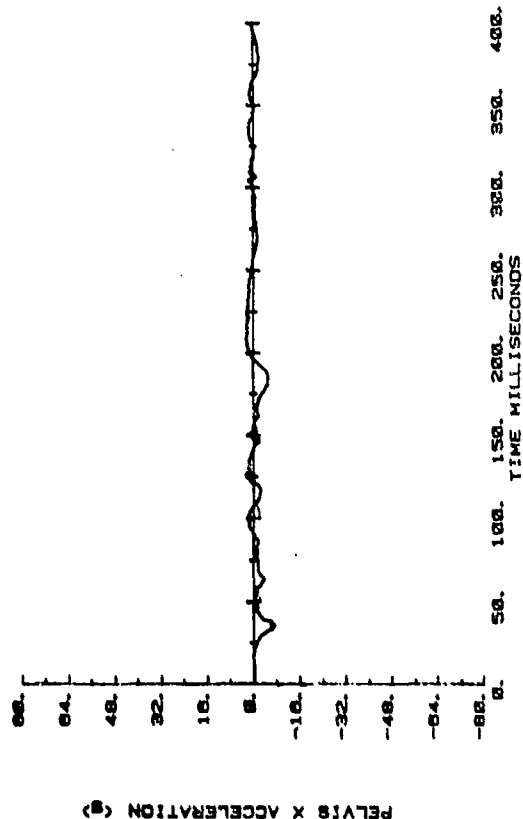


CAMI SLED TEST
AB1122

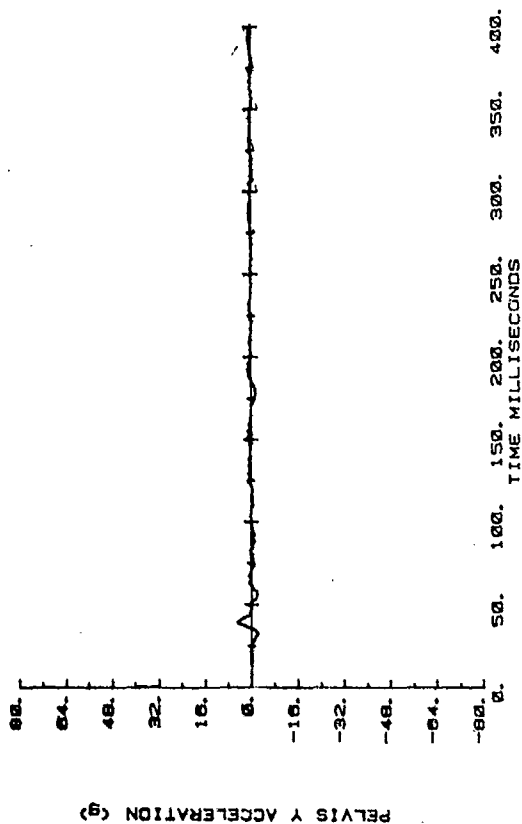


Chest Acceleration

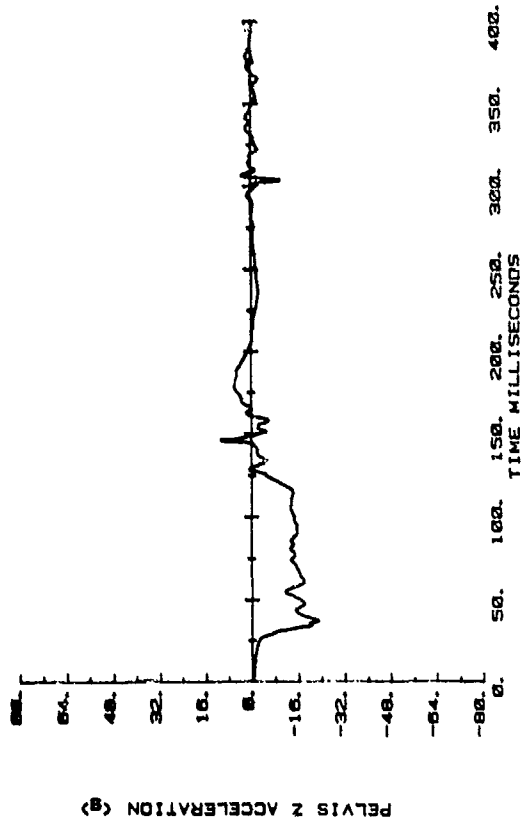
CAMI SLED TEST
A81122



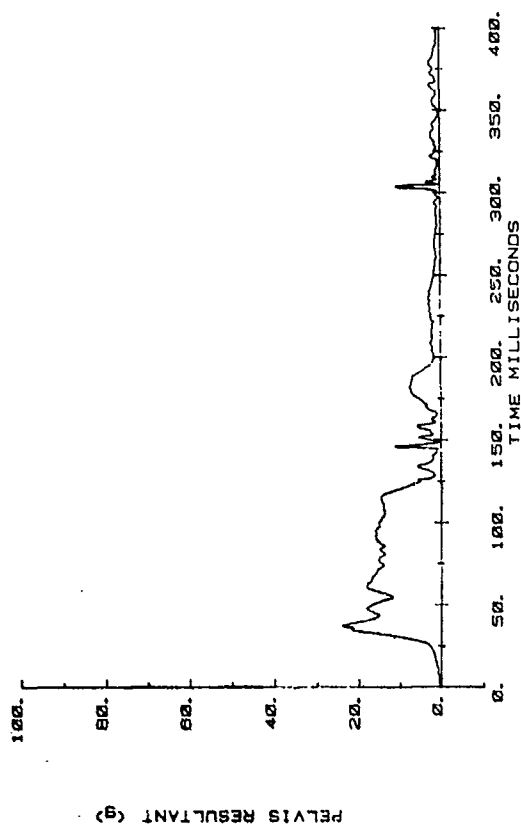
CAMI SLED TEST
A81122



CAMI SLED TEST
A81122

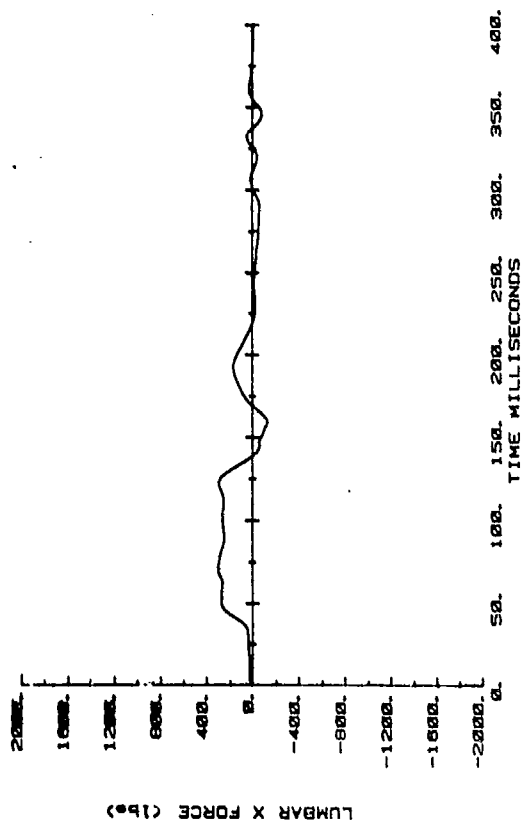


CAMI SLED TEST
A81122

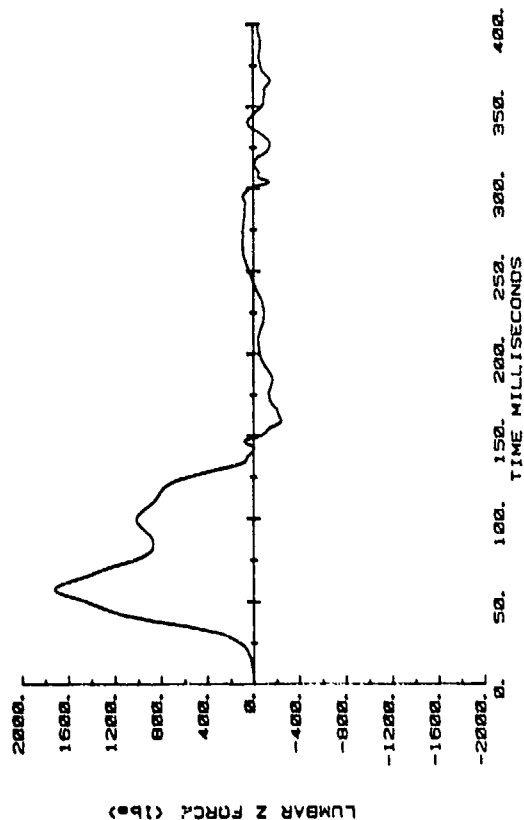


Pelvis Acceleration

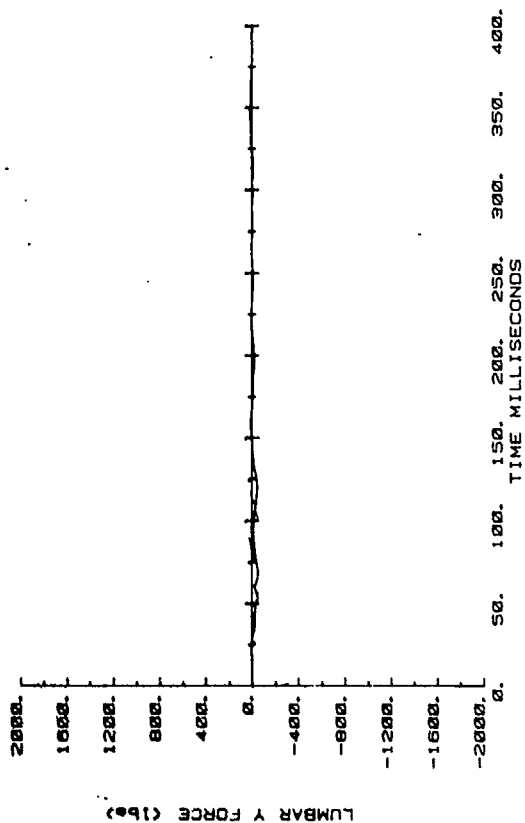
CAMI SLED TEST
AB1122



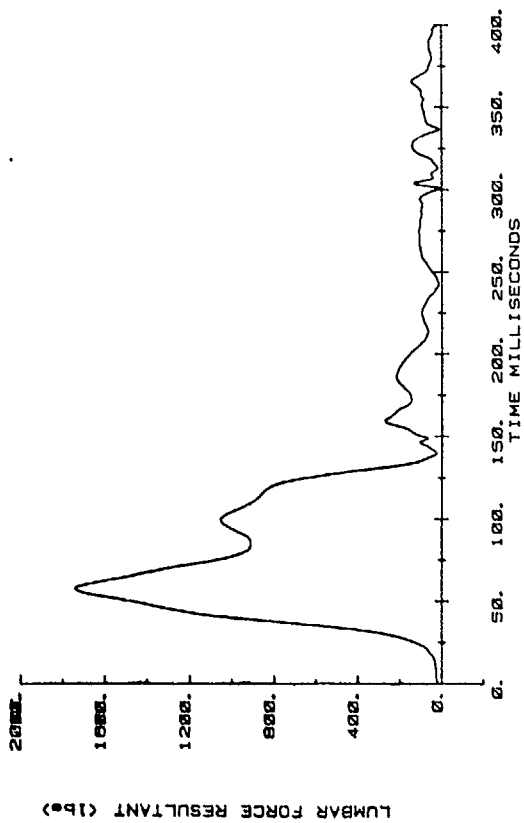
CAMI SLED TEST
AB1122



CAMI SLED TEST
AB1122

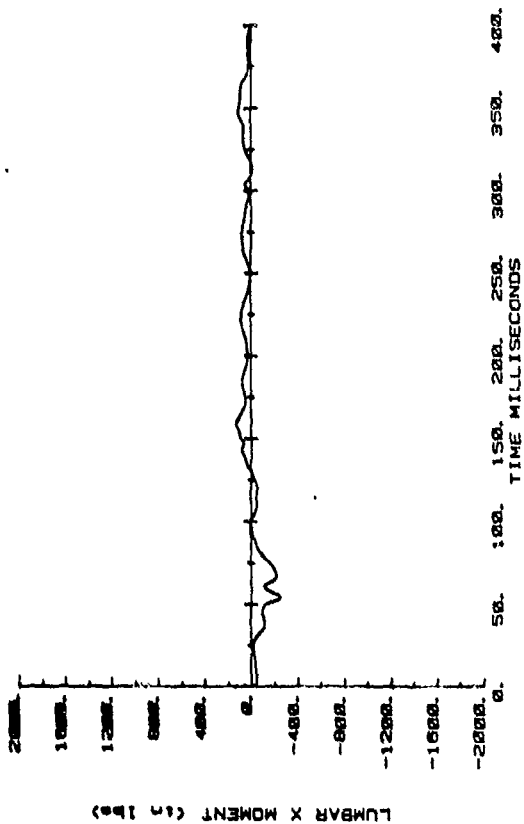


CAMI SLED TEST
AB1122

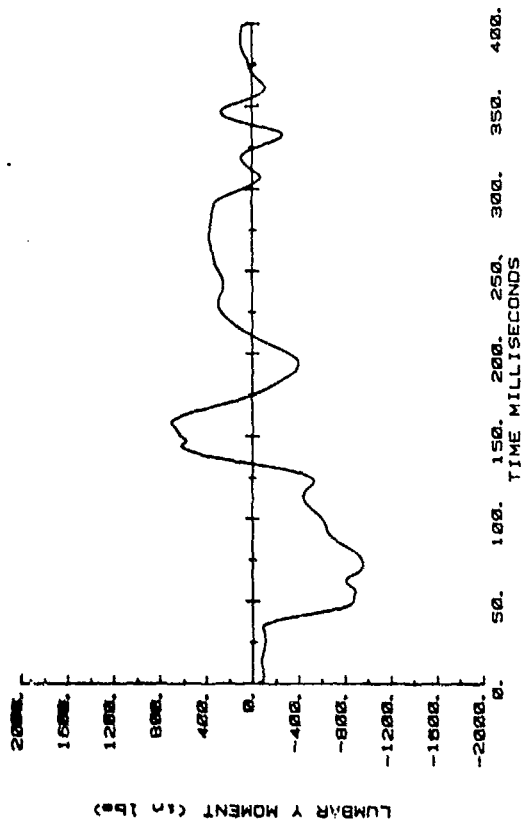


Lumbar Force

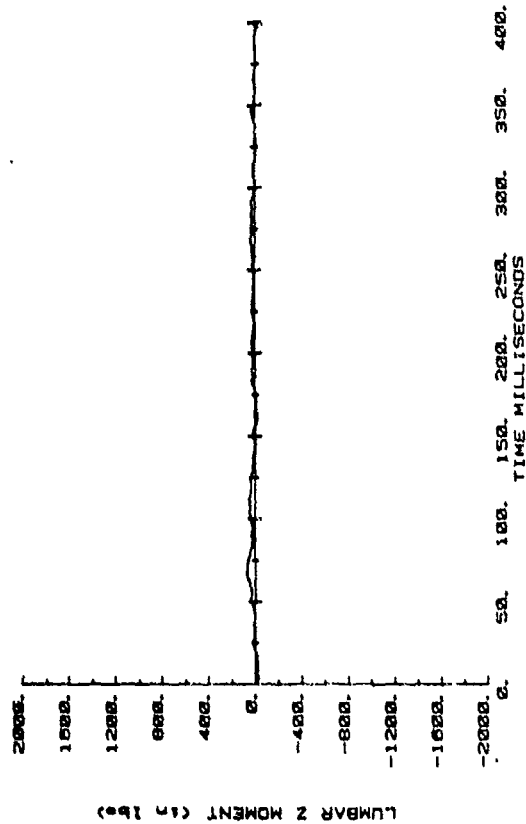
CAMI SLED TEST
AB1122



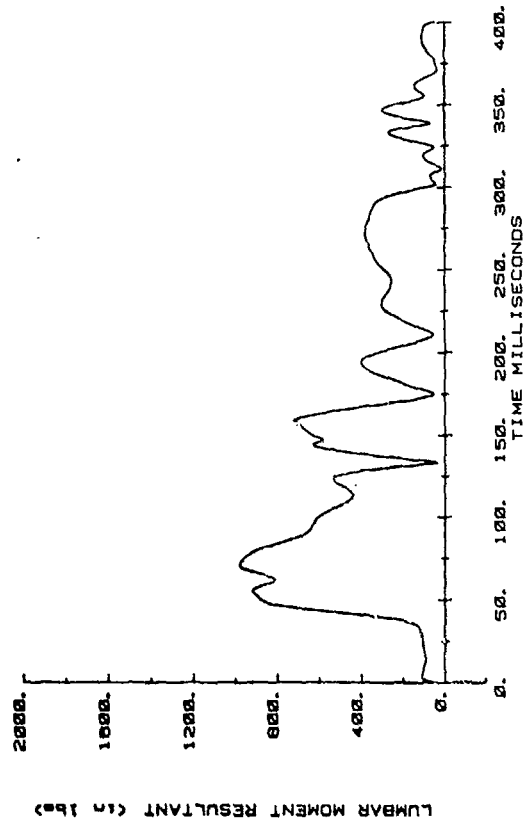
CAMI SLED TEST
AB1122



CAMI SLED TEST
AB1122

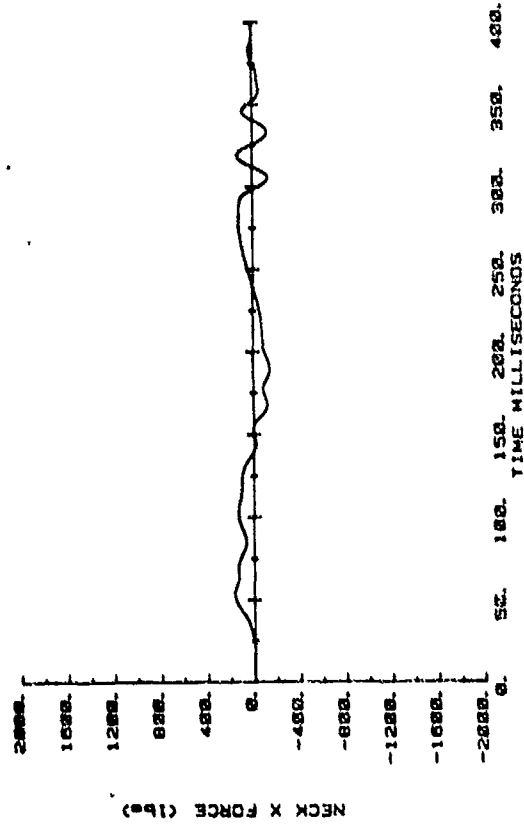


CAMI SLED TEST
AB1122

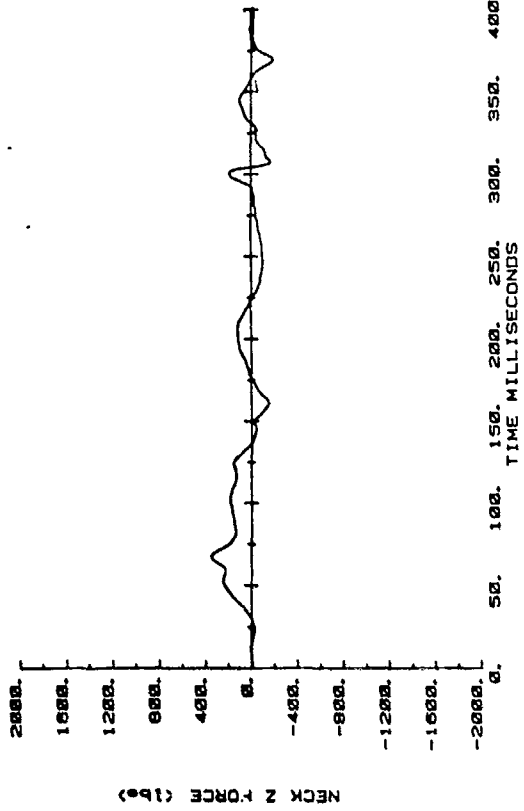


Lumbar Moment

CAMI SLED TEST
A81122

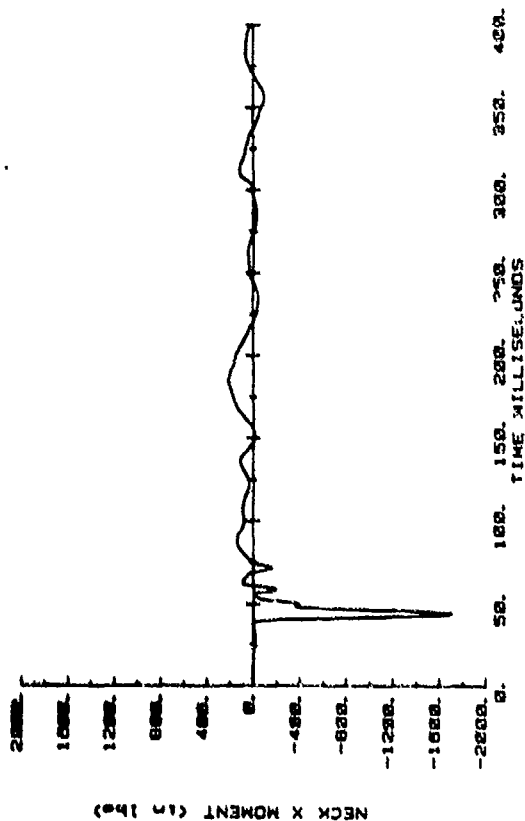


CAMI SLED TEST
A81122

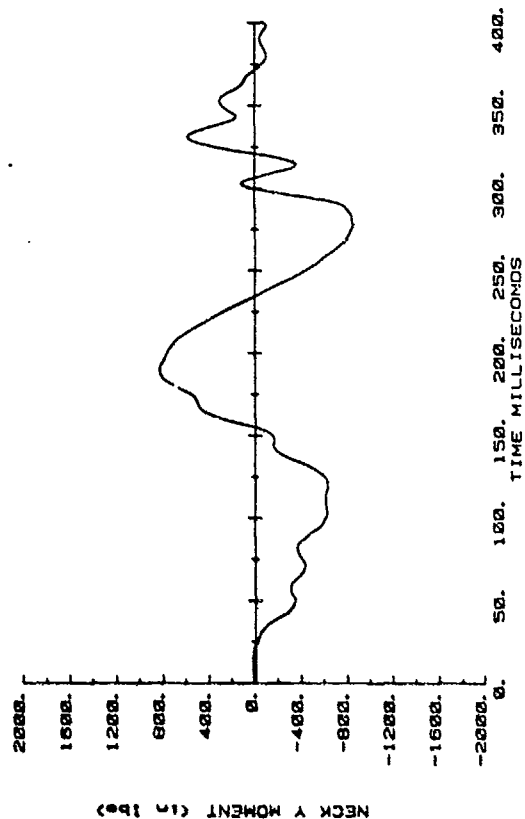


Neck Force

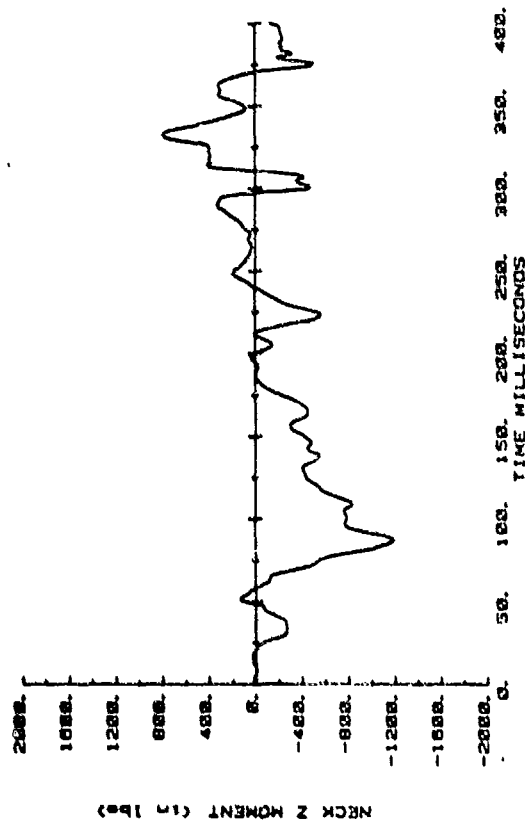
CAMI SLED TEST
A81122



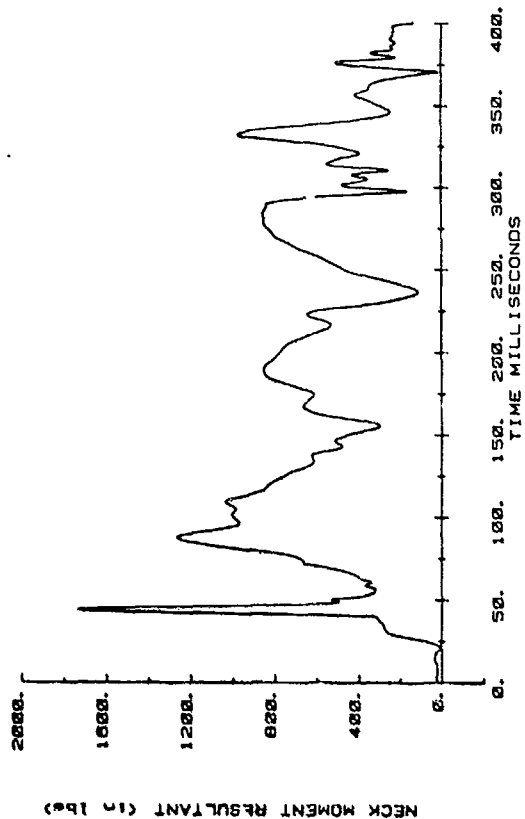
CAMI SLED TEST
A81122



CAMI SLED TEST
A81122

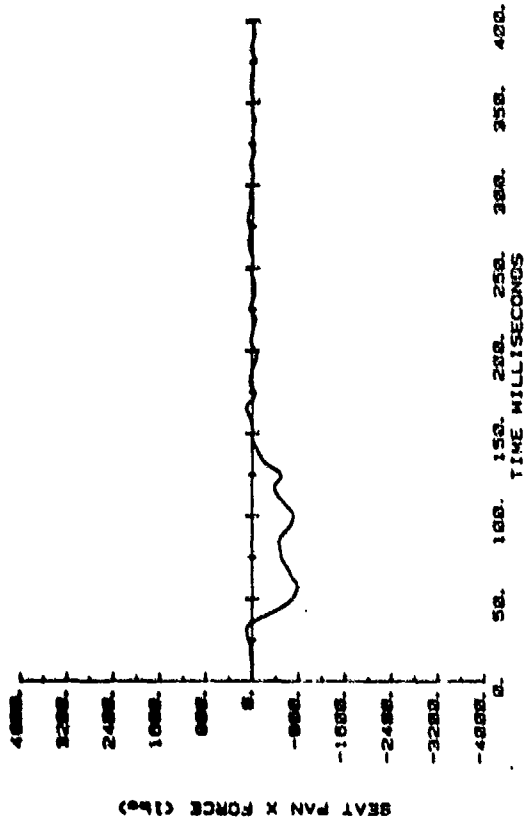


CAMI SLED TEST
A81122

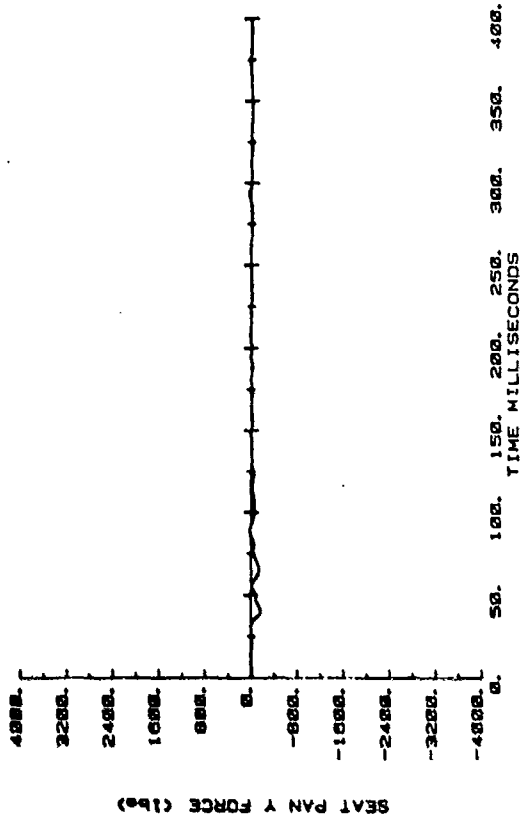


Neck Moment

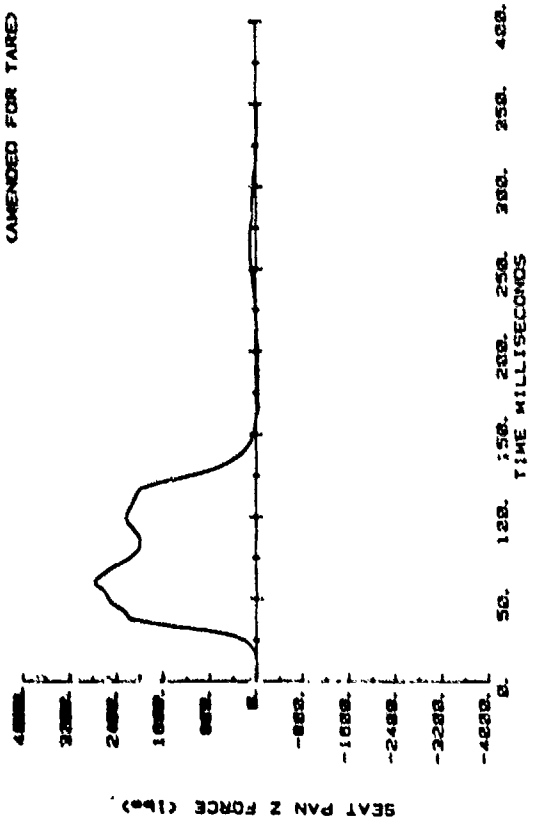
CAMI SLED TEST
AB1122



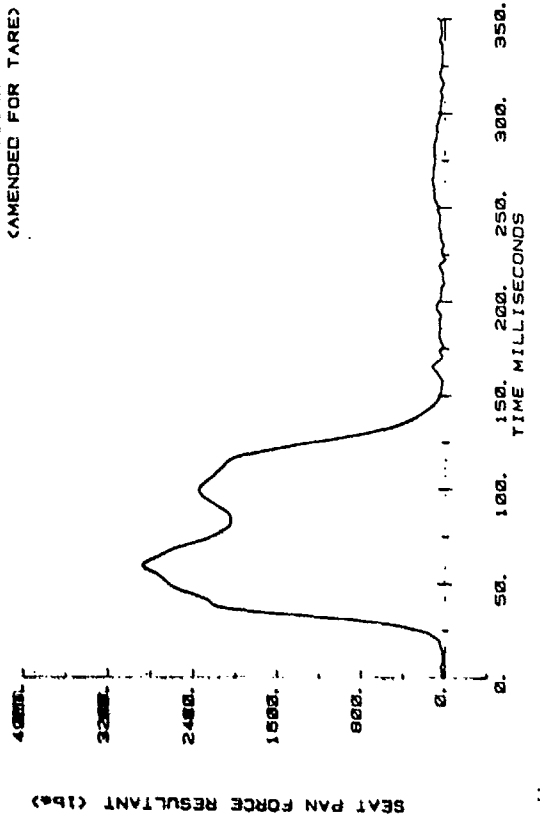
CAMI SLED TEST
AB1122



CAMI SLED TEST
AB1122
(AMENDED FOR TARE)

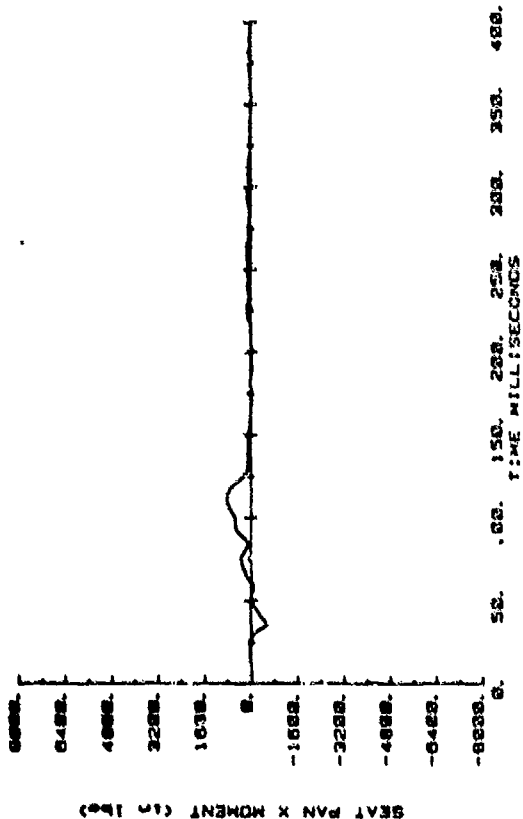


CAMI SLED TEST
AB1122
(AMENDED FOR TARE)

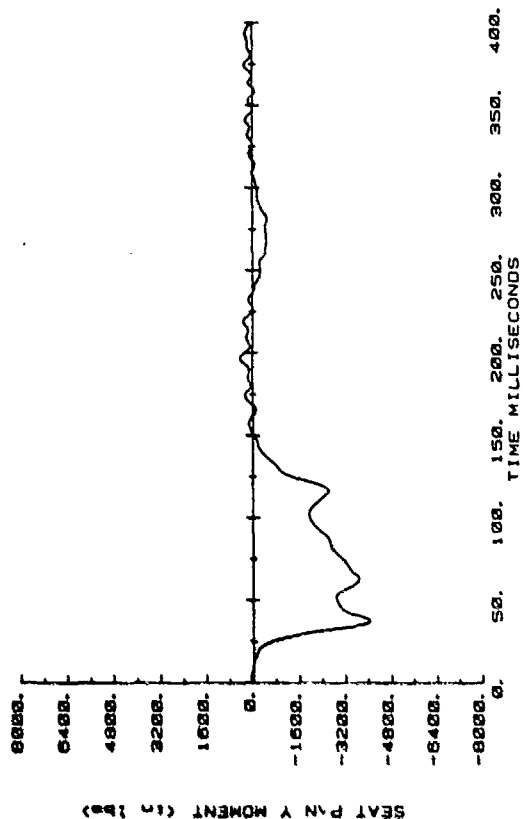


Seat Pan Force

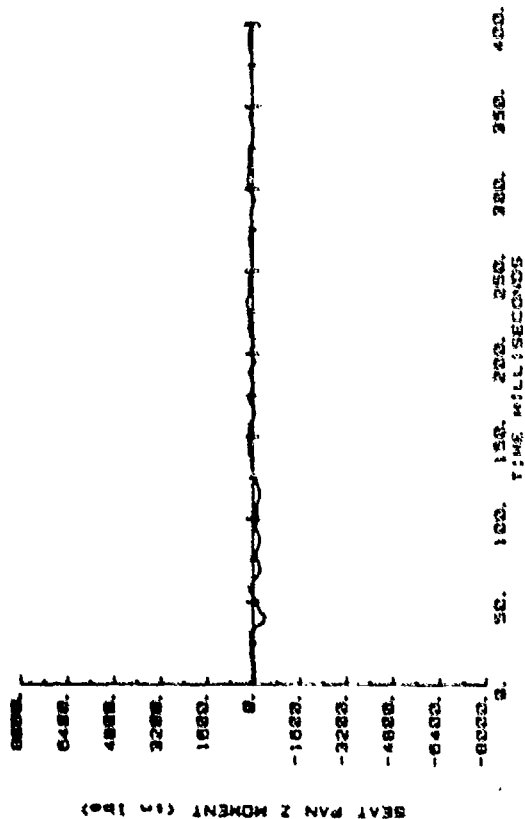
CAMI SLED TEST
AB1122



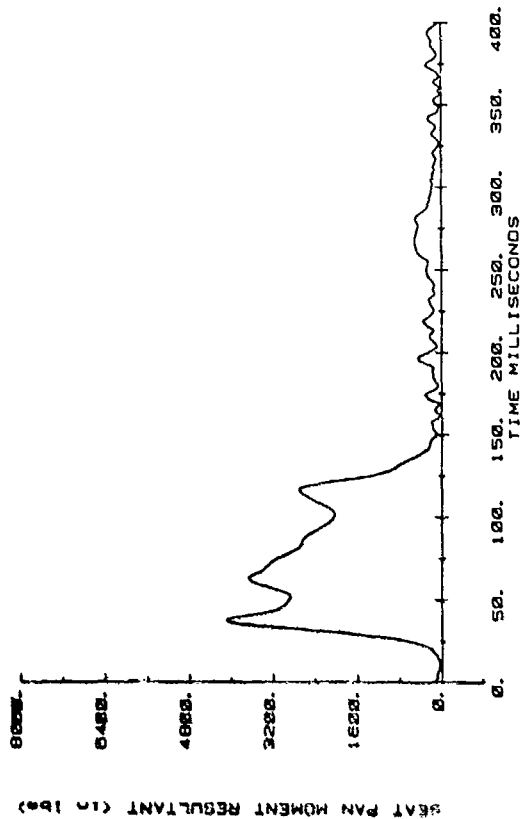
CAMI SLED TEST
AB1122



CAMI SLED TEST
AB1122

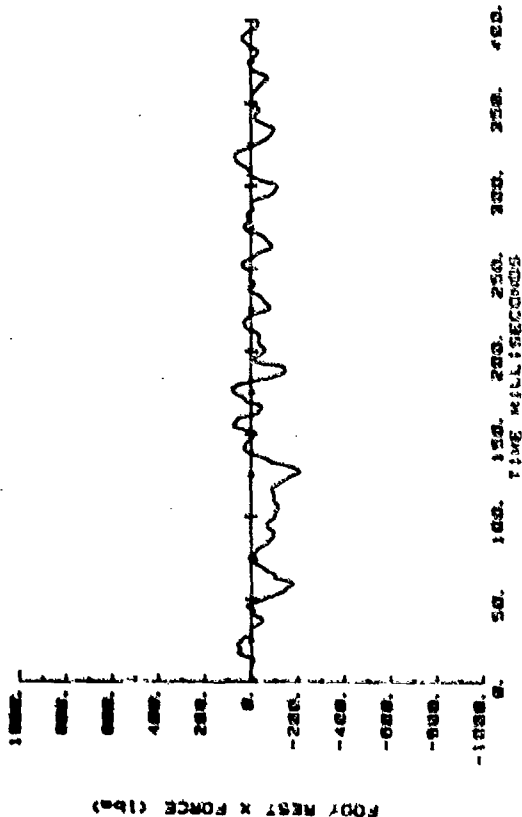


CAMI SLED TEST
AB1122

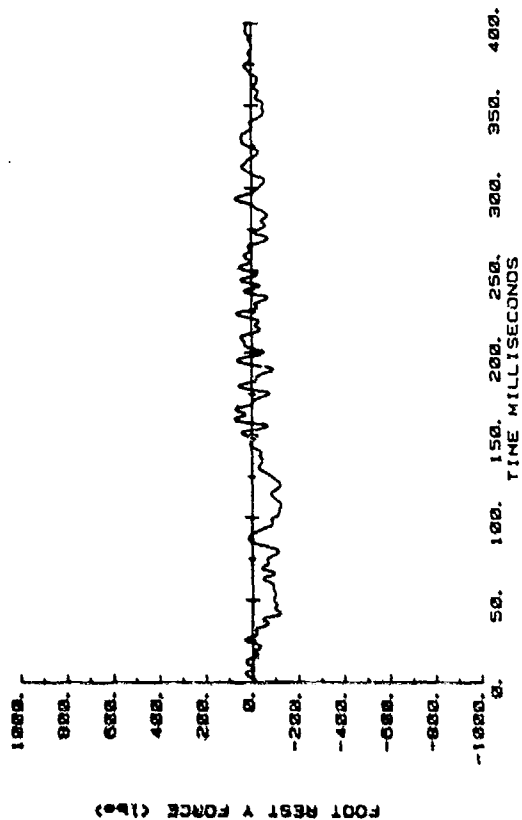


Seat Pan Moment

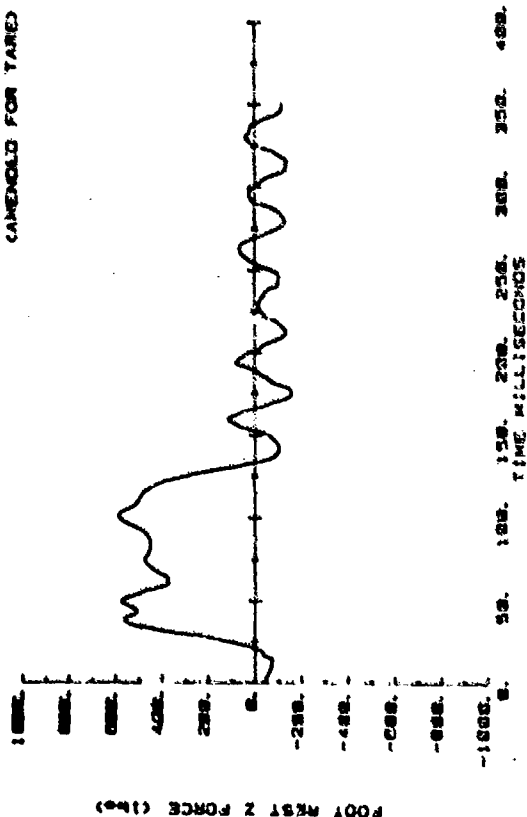
CAMI SLED TEST
A81122



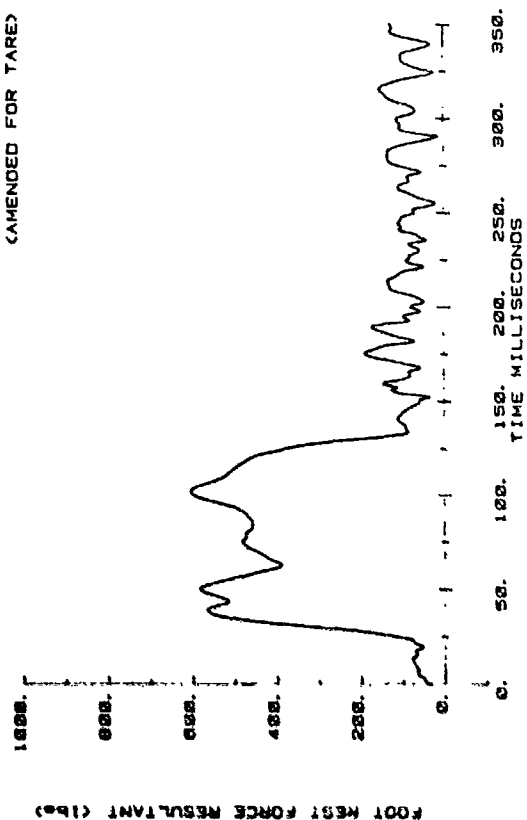
CAMI SLED TEST
A81122



CAMI SLED TEST
A81122
(AMENDED FOR TARE)



CAMI SLED TEST
A81122
(AMENDED FOR TARE)



Footrest Force

APPENDIX C

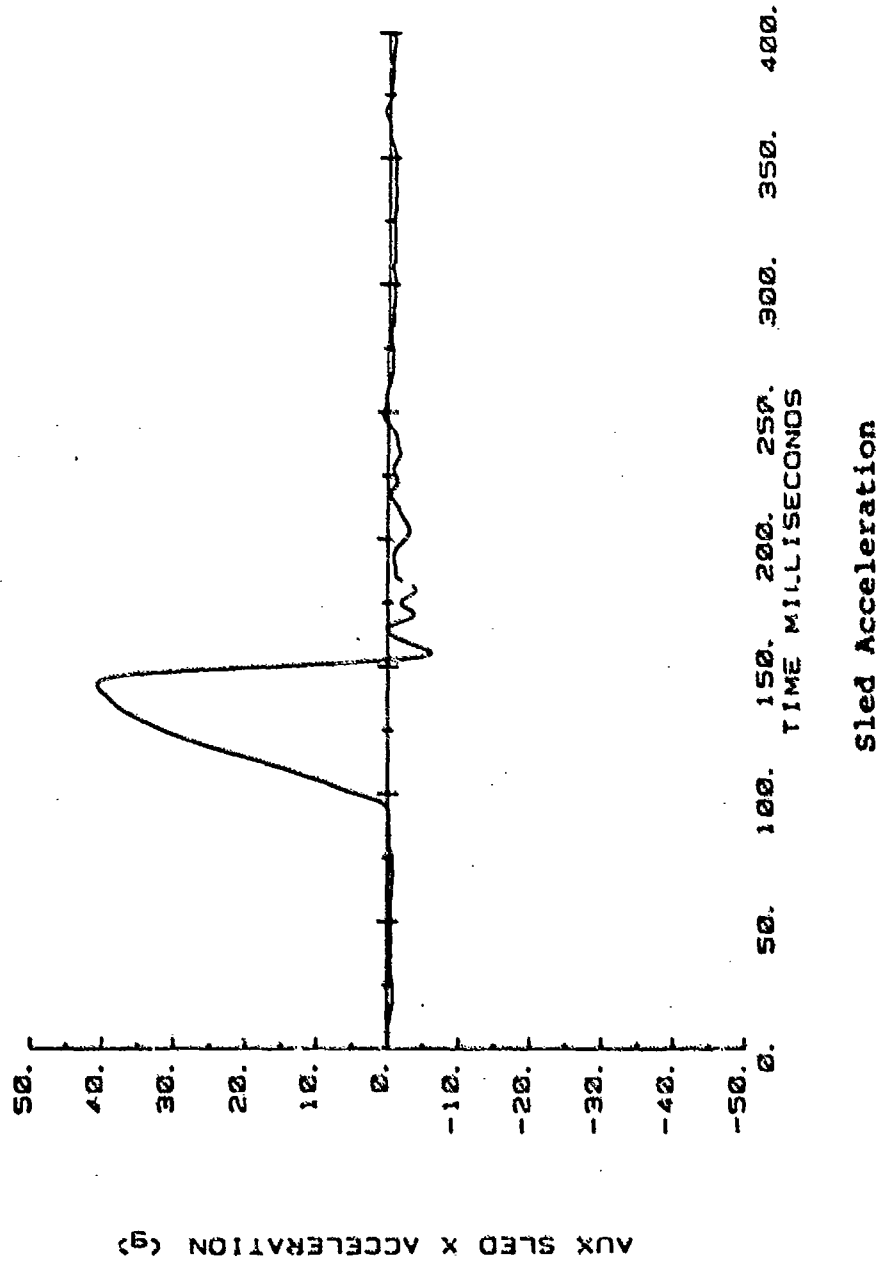
CAMI BASELINE TEST A80-053

Energy-Absorbing Seat
50th-Percentile Dummy

$$\Delta v = 44.8 \text{ ft/sec}$$

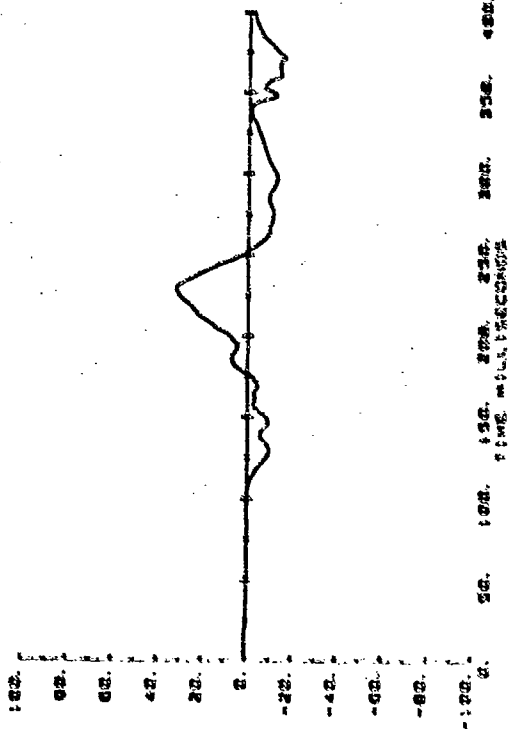
$$G_{\text{peak}} = 40.7$$

CAMI SLED TEST
A80053

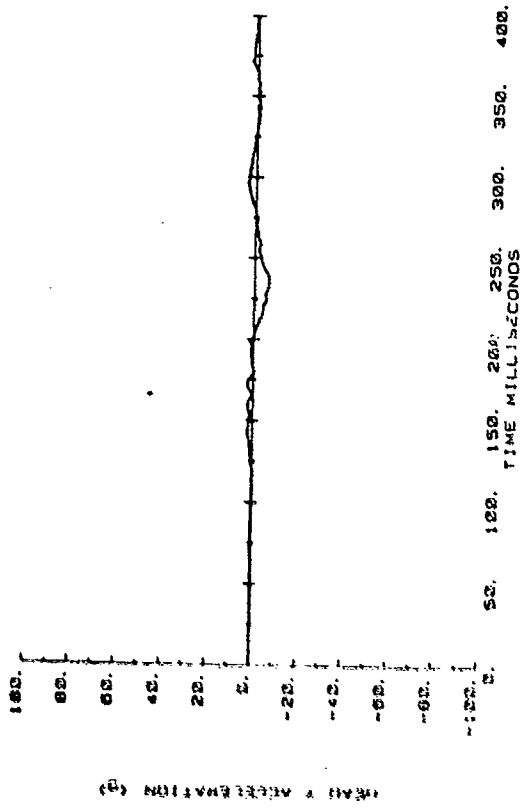


AUX SLED X ACCELERATION (g)

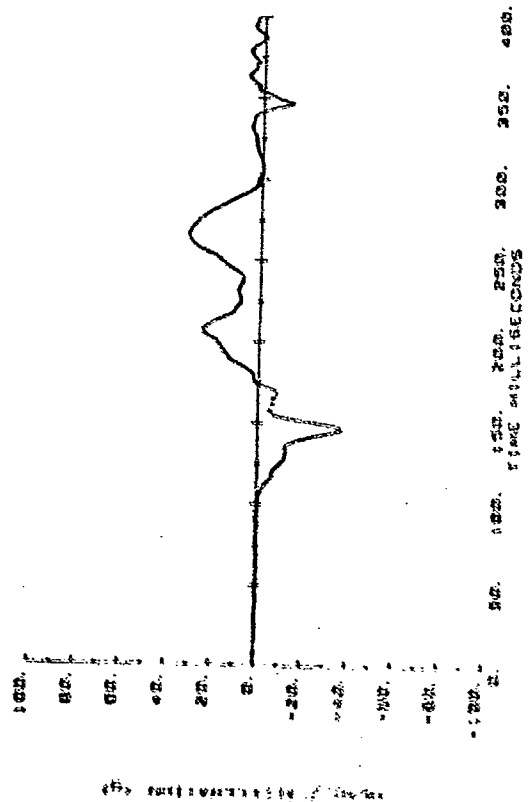
CAM: SLED TEST
AB0053



CAM: SLED TEST
AB0053

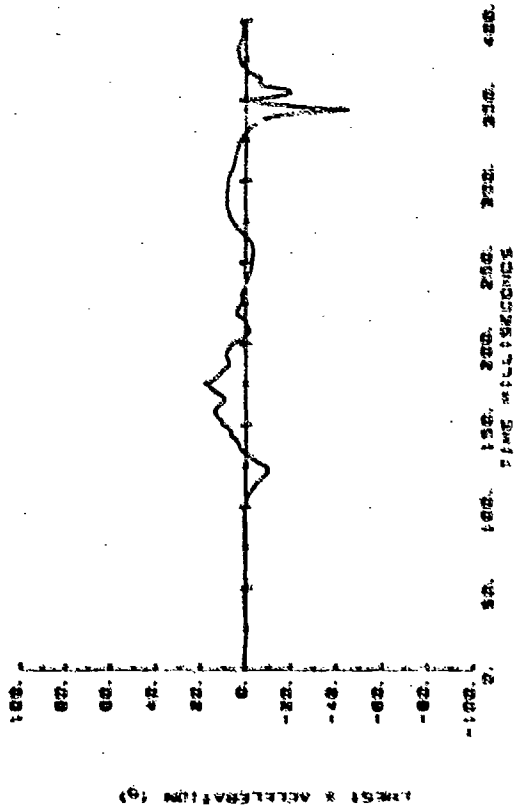


CAM: SLED TEST
AB0053

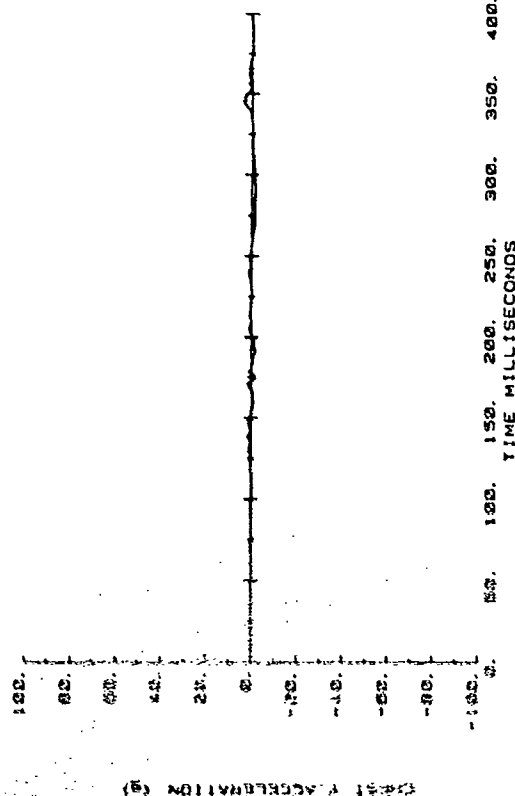


Head Acceleration

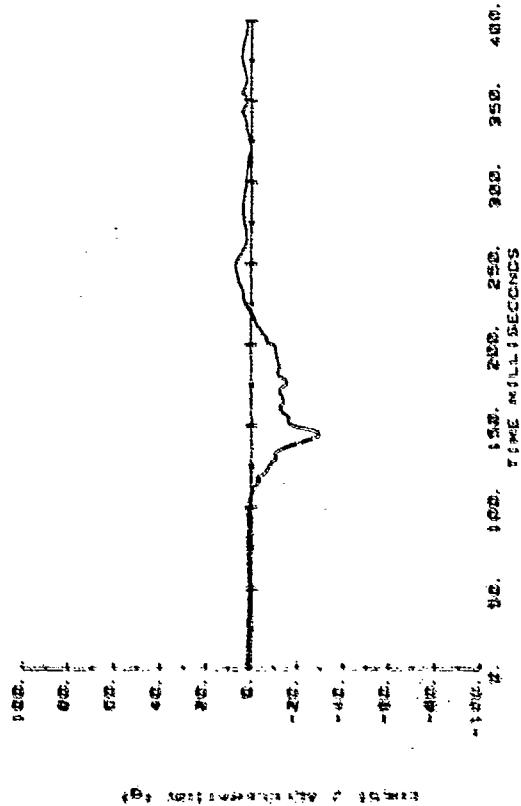
CAM: SLED TEST
A80053



CAM: SLED TEST
A80053

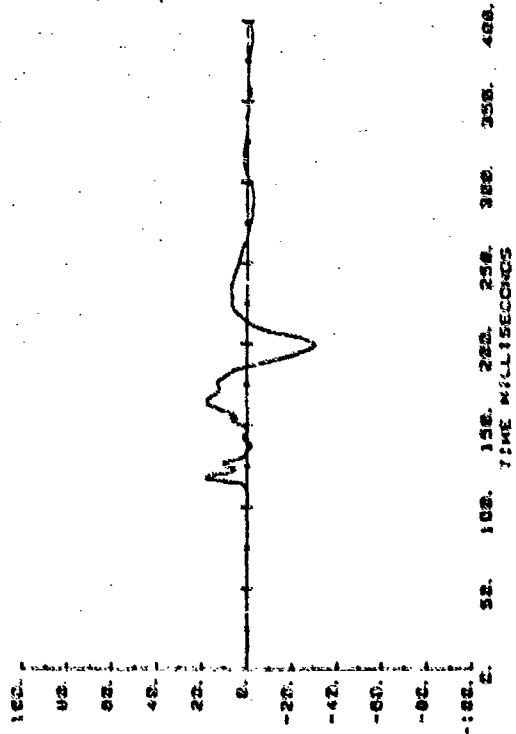


CAM: SLED TEST
A80053

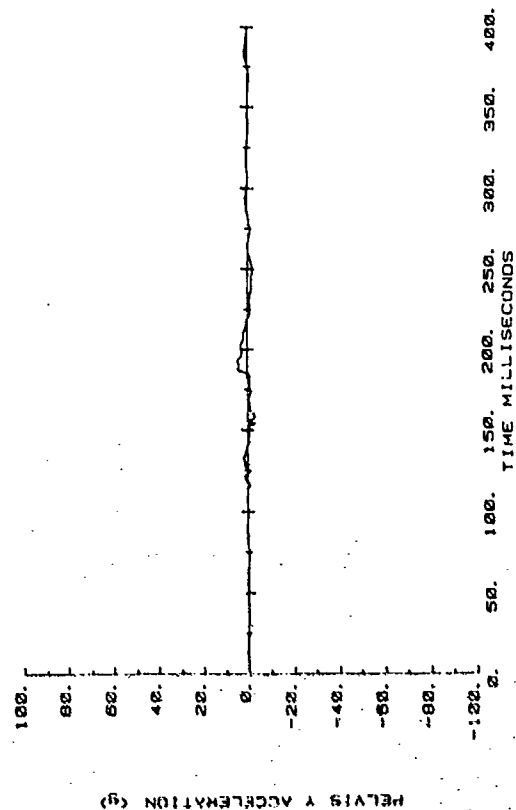


Chest Acceleration

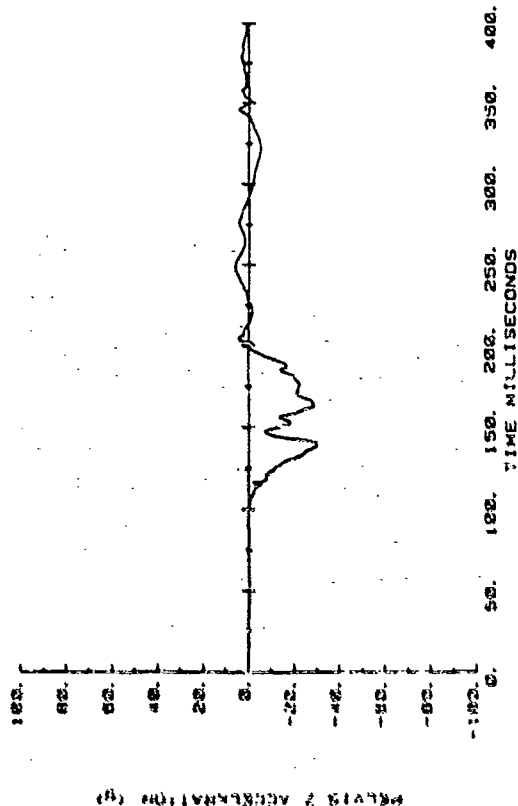
CAMI SLED TEST
A88053



CAMI SLED TEST
A88053

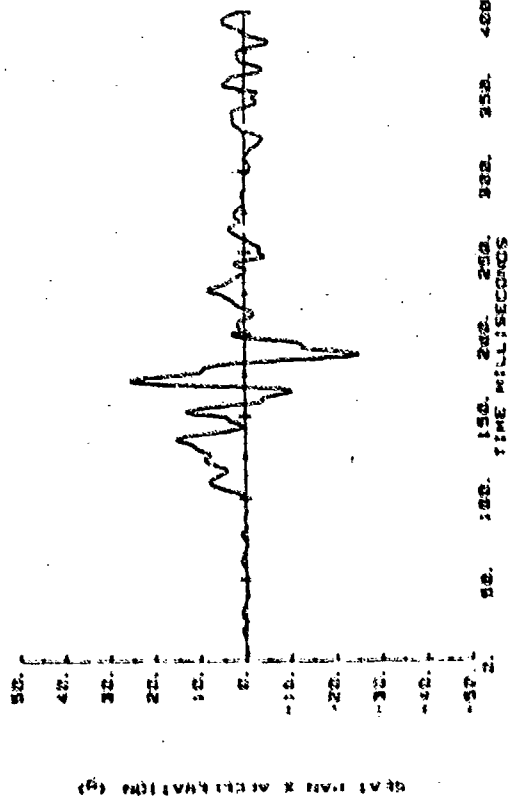


CAMI SLED TEST
A88053



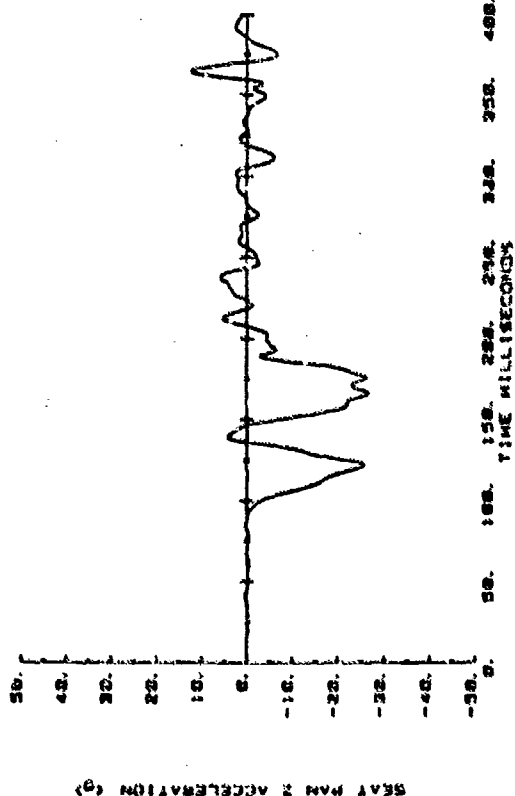
Pelvis Acceleration

CAMI SLED TEST
A80053



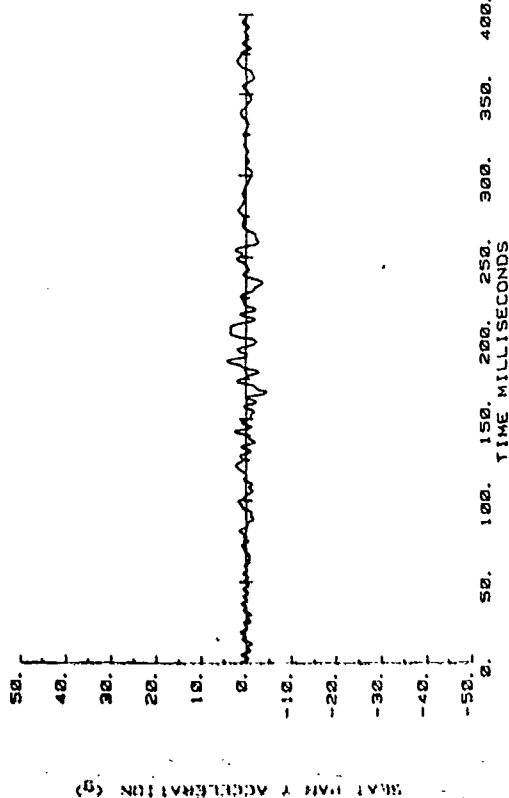
50. 100. 150. 200. 250. 300. 350. 400.

CAMI SLED TEST
A80053



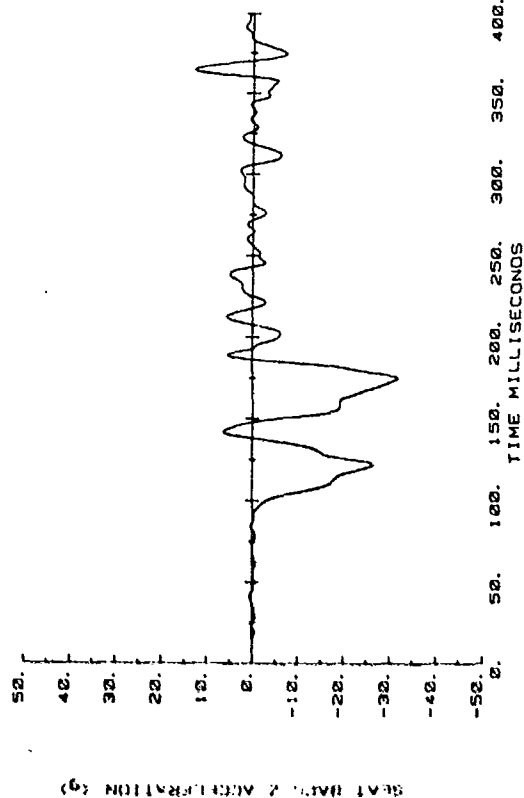
50. 100. 150. 200. 250. 300. 350. 400.

CAMI SLED TEST
A80053



50. 100. 150. 200. 250. 300. 350. 400.

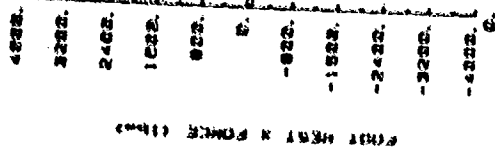
CAMI SLED TEST
A80053



50. 100. 150. 200. 250. 300. 350. 400.

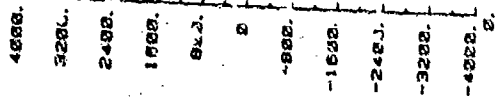
Seat Pan and Seat Back Acceleration

CAMI SLED TEST
A88853



FOOT REST FORCE (lb)

50. 100. 150. 200. 250. 300. 350. 400.
TIME (MILLISECONDS)

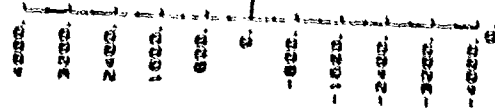


FOOT REST FORCE (lb)

50. 100. 150. 200. 250. 300. 350. 400.
TIME (MILLISECONDS)

CAMI SLED TEST
A88853

CAMI SLED TEST
A88853

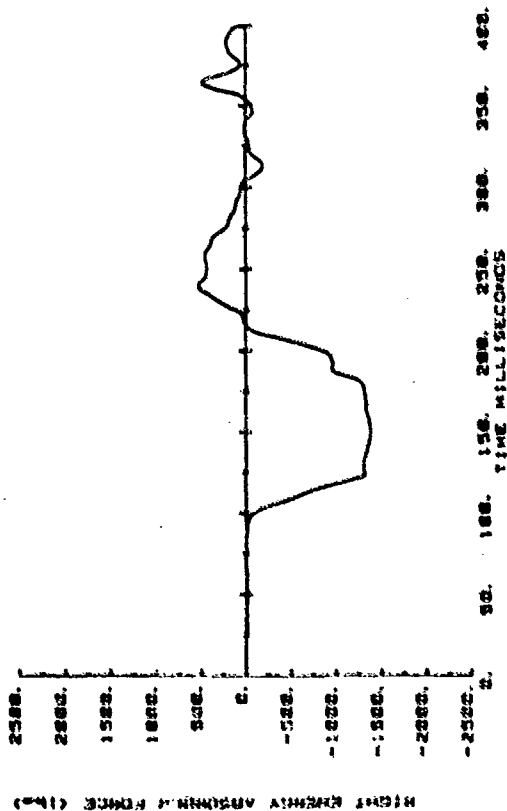


FOOT REST FORCE (lb)

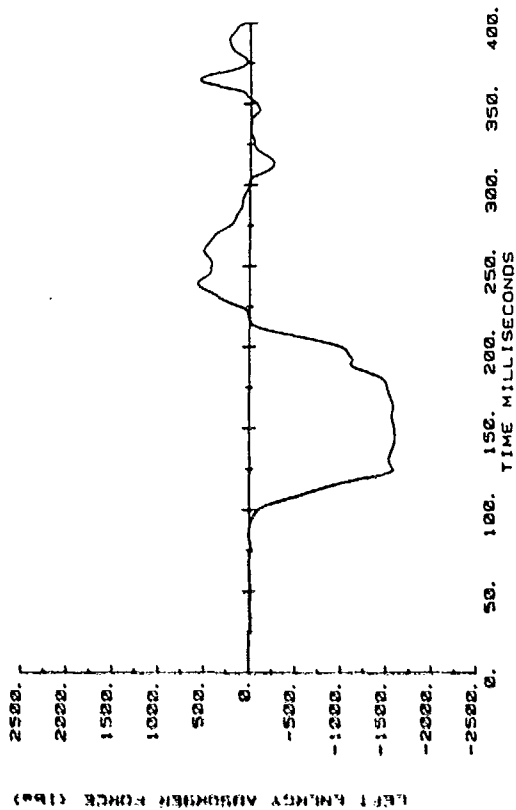
50. 100. 150. 200. 250. 300. 350. 400.
TIME (MILLISECONDS)

Footrest Force

CAMI SLED TEST
A80053

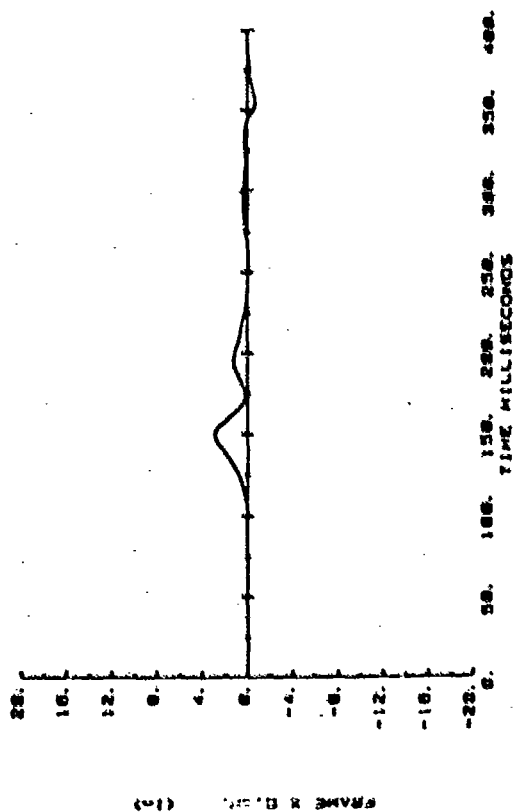


CAMI SLED TEST
A80053

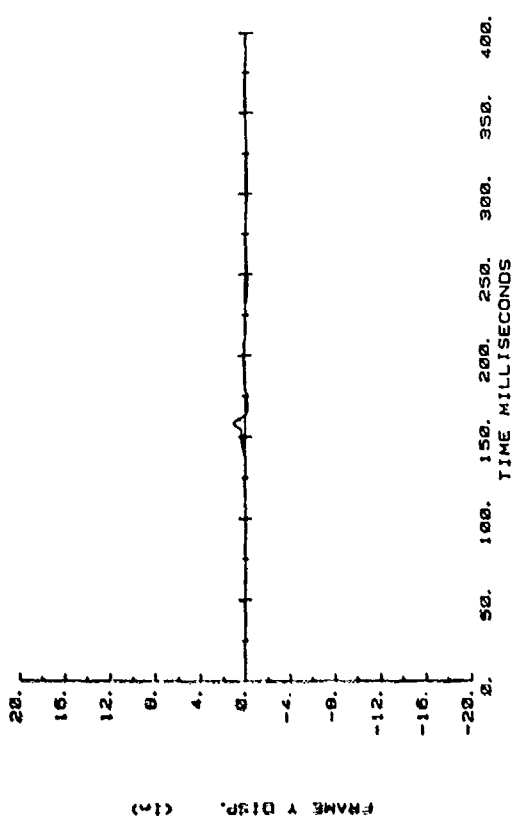


Energy Absorber Force

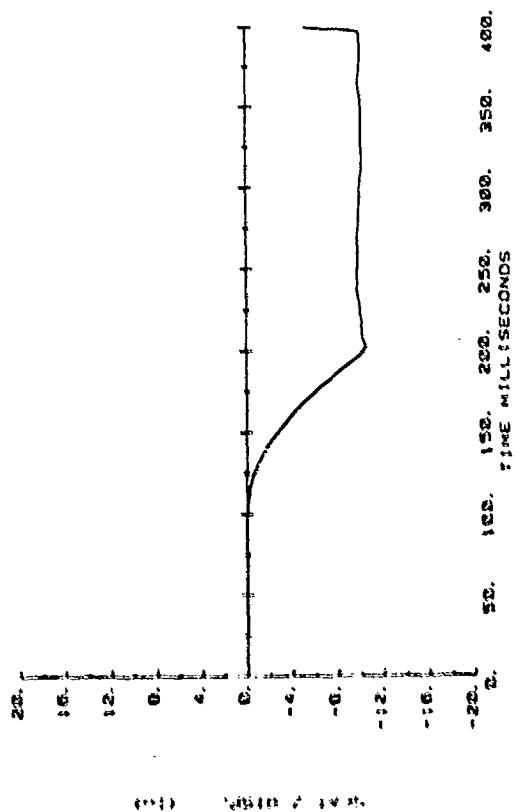
CAMI SLED TEST
AB0053



CAMI SLED TEST
AB0053

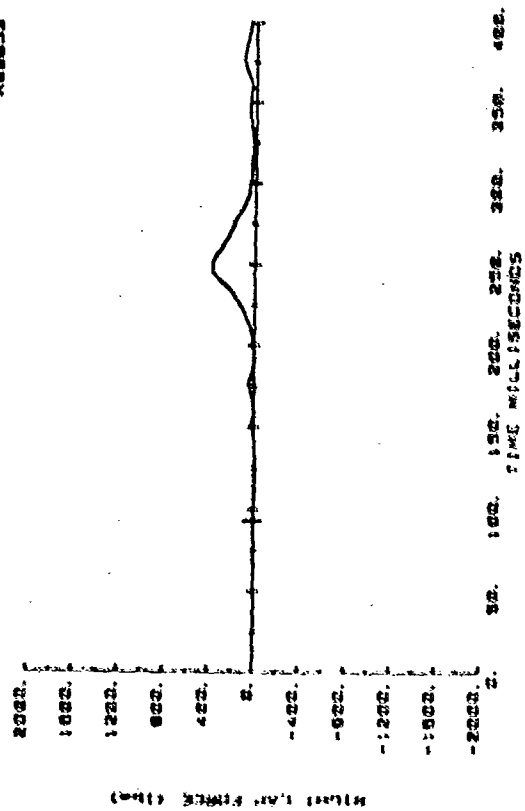


CAMI SLED TEST
AB0053

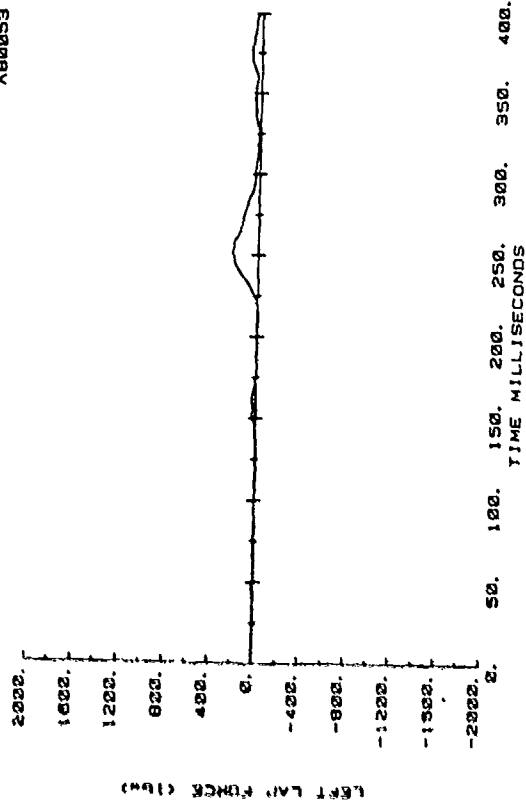


Frame Displacement and Seat Stroke

CAMI SLED TEST
AB0053

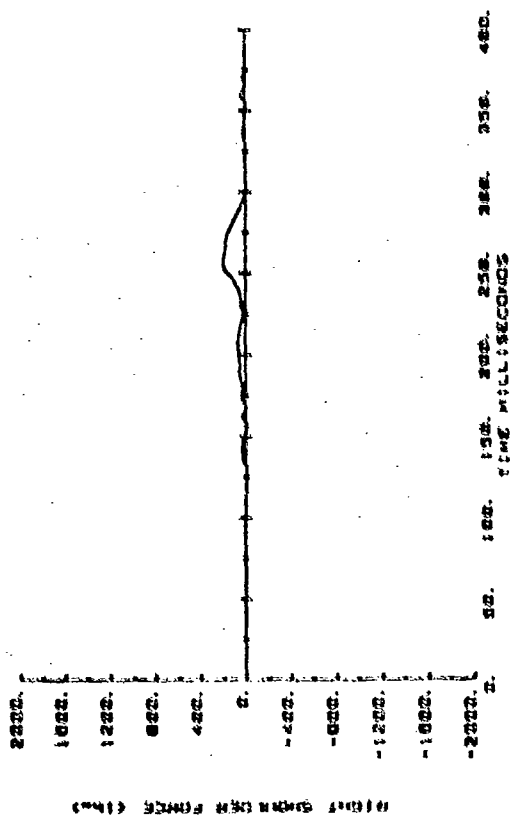


CAMI SLED TEST
AB0053

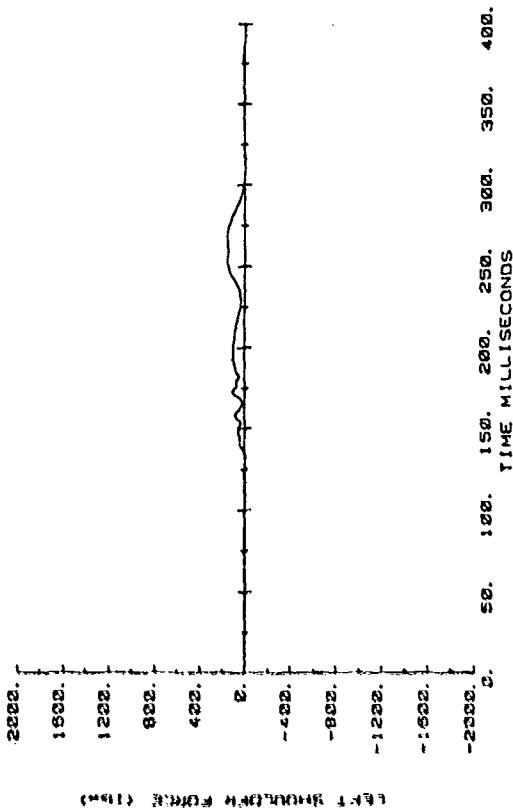


Lap Belt Force

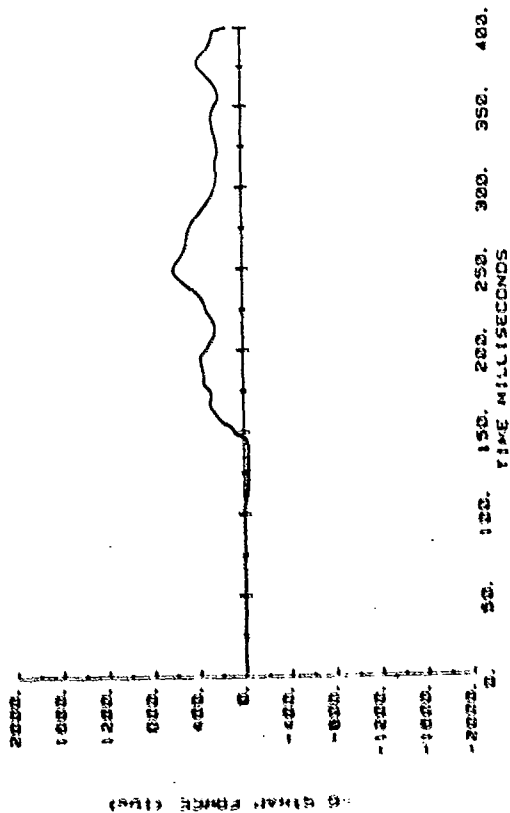
CAMI SLED TEST
A88053



CAMI SLED TEST
A88053

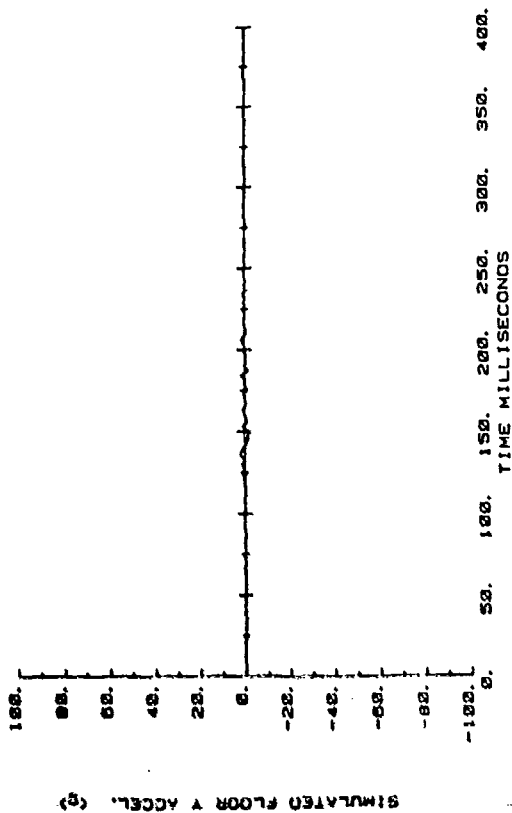


CAMI SLED TEST
A88053

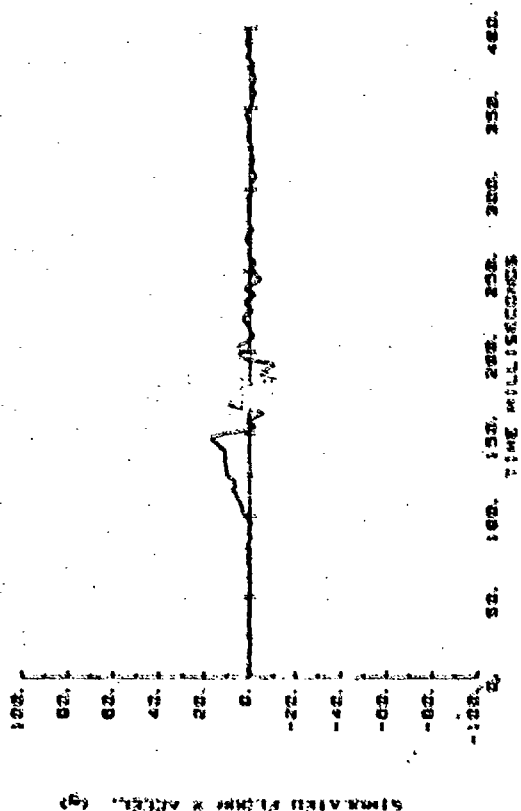


Shoulder Belt and -G Strap Force

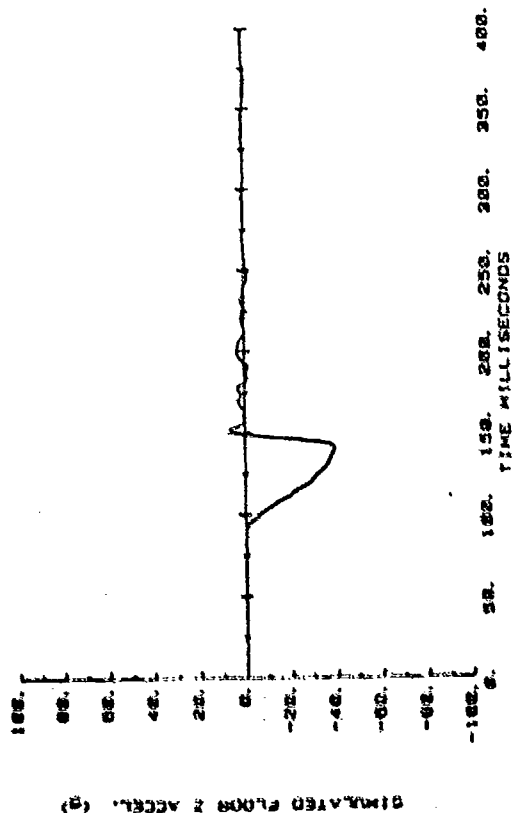
CAMI SLED TEST
A88853



CAMI SLED TEST
A88853



CAMI SLED TEST
A88853



Floor Acceleration

APPENDIX D

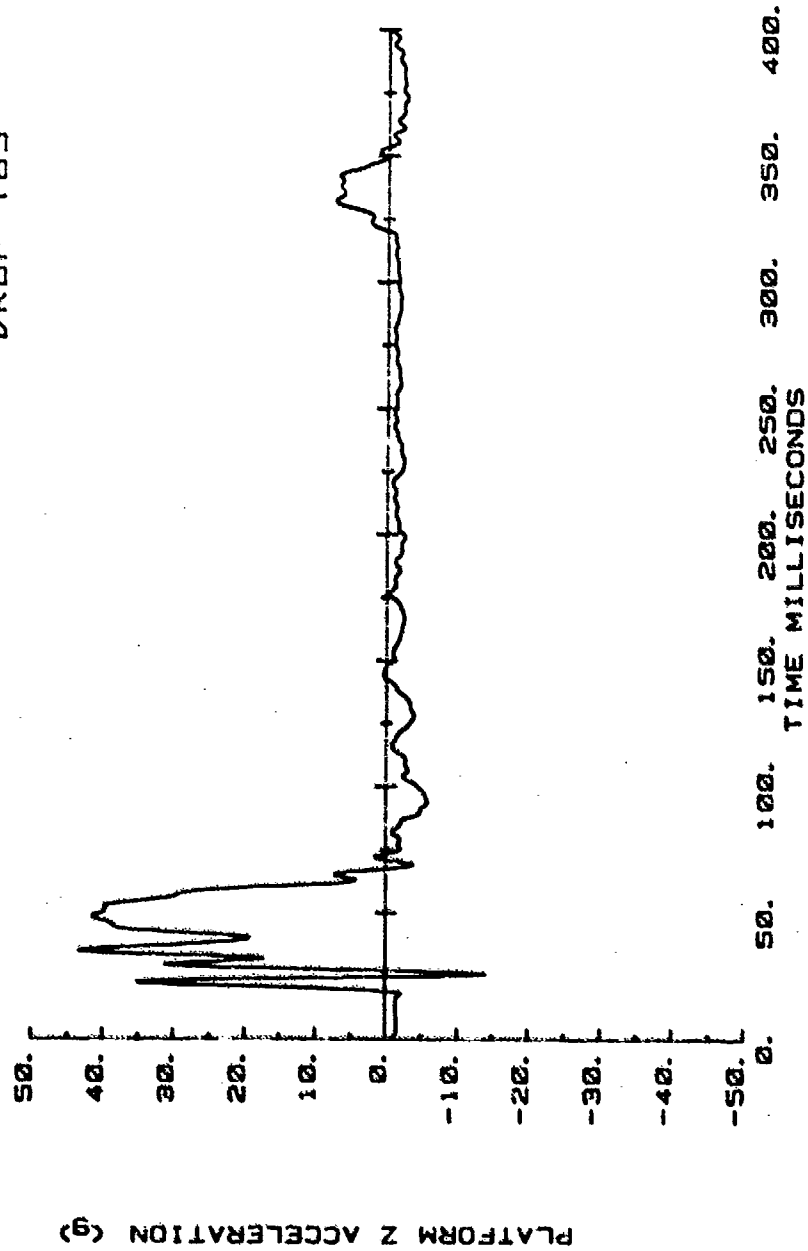
NADC BASELINE TEST N-189

Energy-Absorbing Seat
50th-Percentile Dummy

$$\Delta v = 40.4 \text{ ft/sec}$$

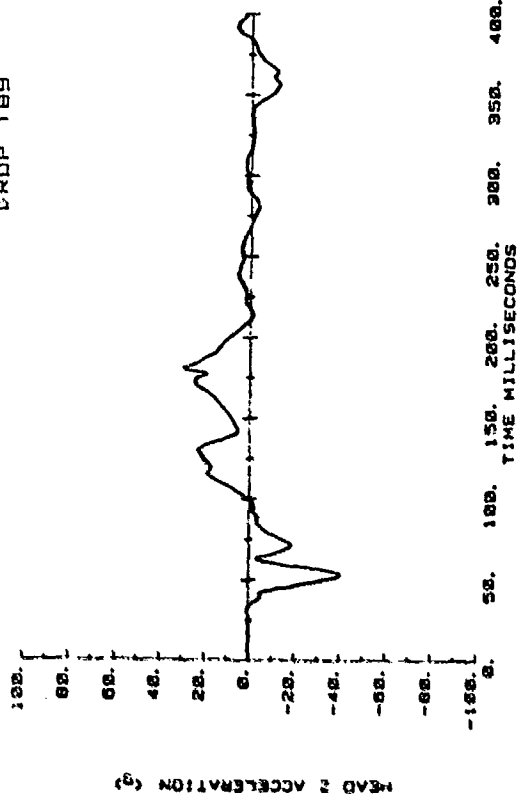
$$G_{\text{peak}} = 44.9$$

NADC TEST 2
DROP 189

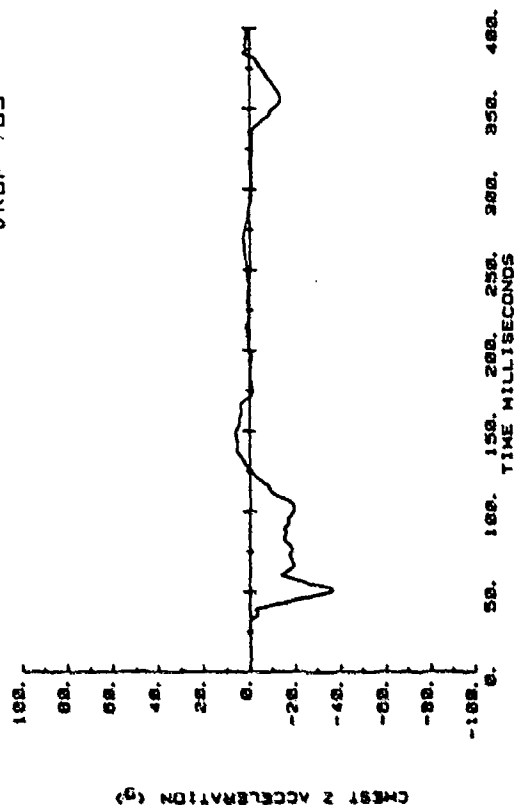


Platform (Input) Acceleration

NRDC TEST 2
DROP 189

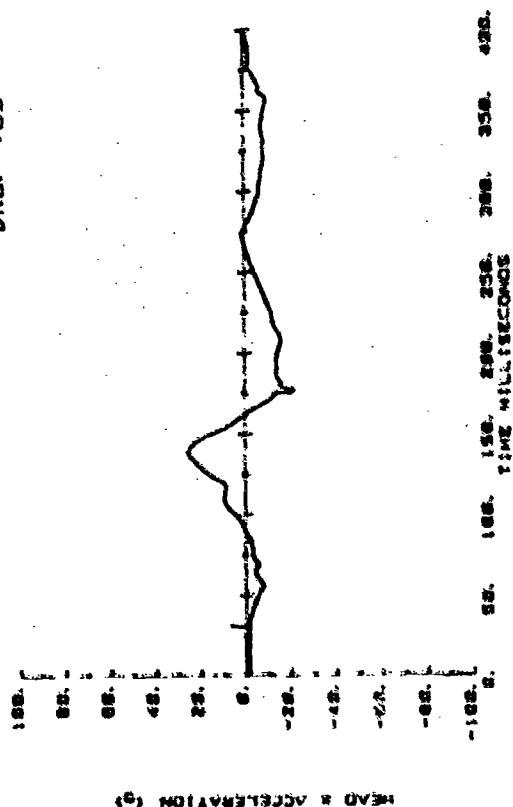


NRDC TEST 2
DROP 189

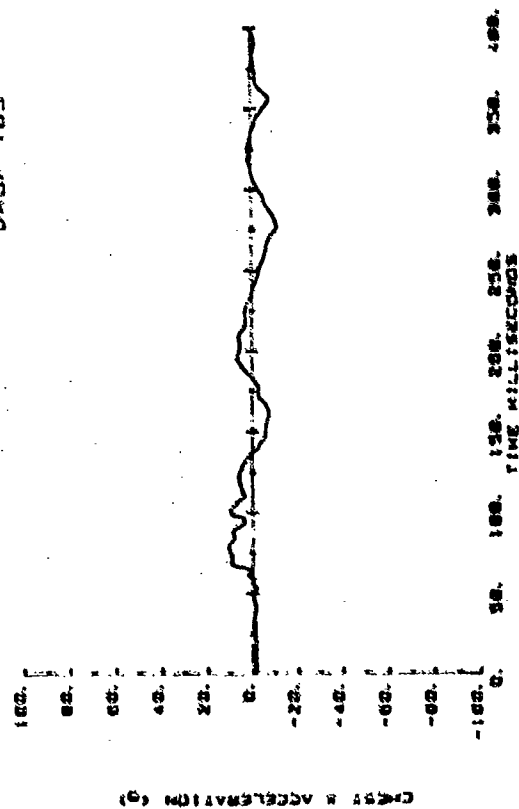


Head and Chest Acceleration

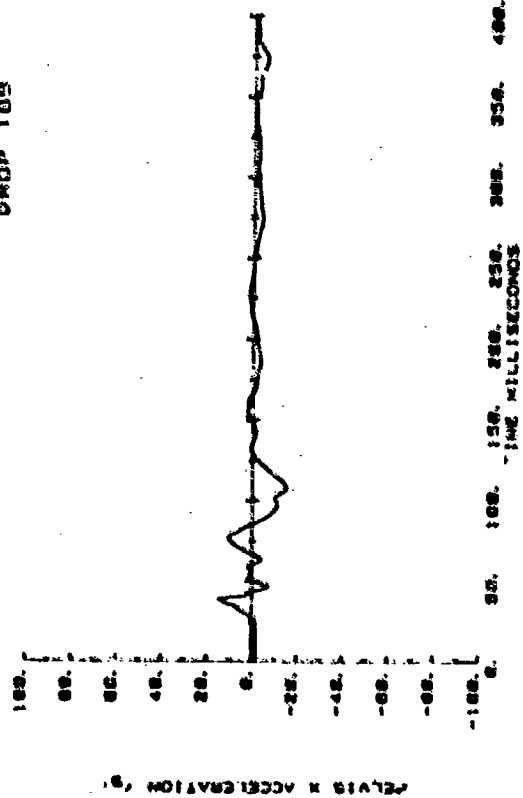
NRDC TEST 2
DROP 189



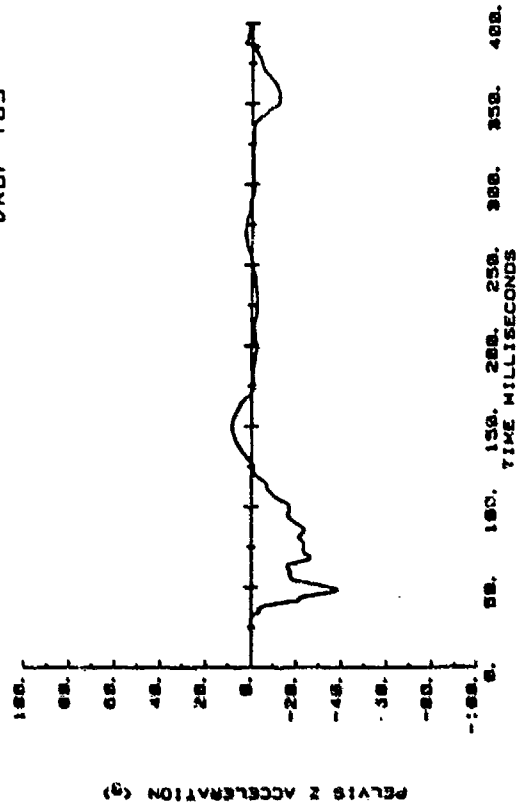
NRDC TEST 2
DROP 189



NRDC TEST 2
DROP 109

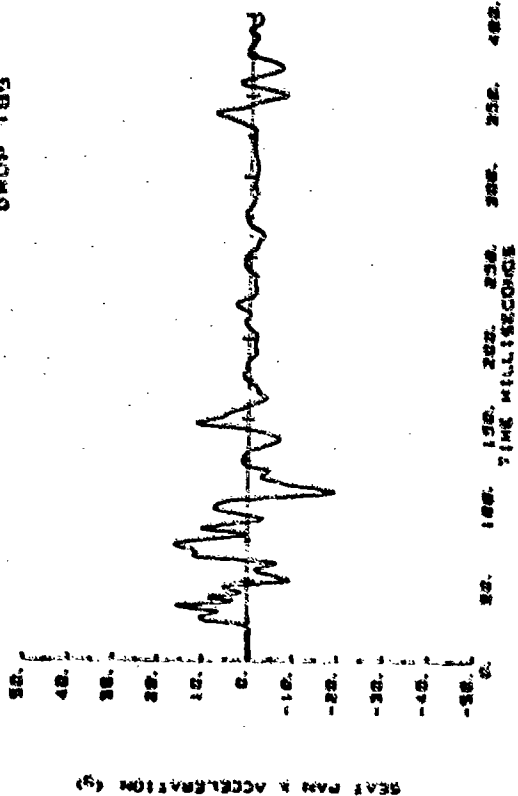


NRDC TEST 2
DROP 189

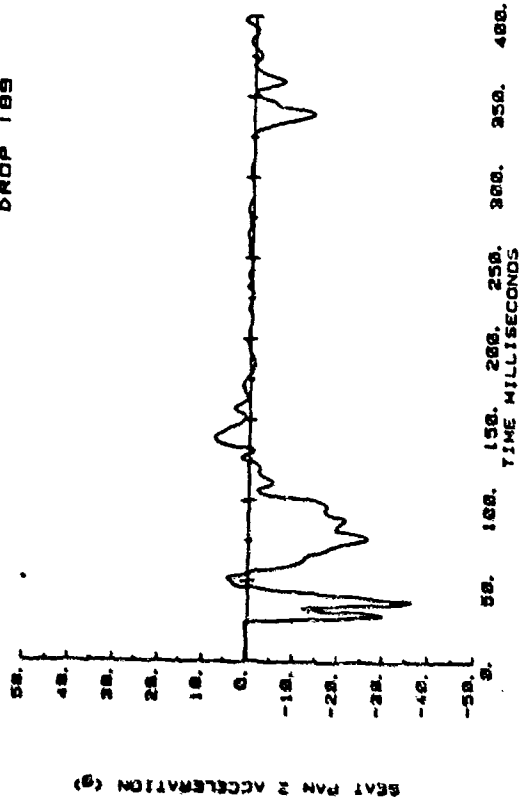


Pelvis Acceleration

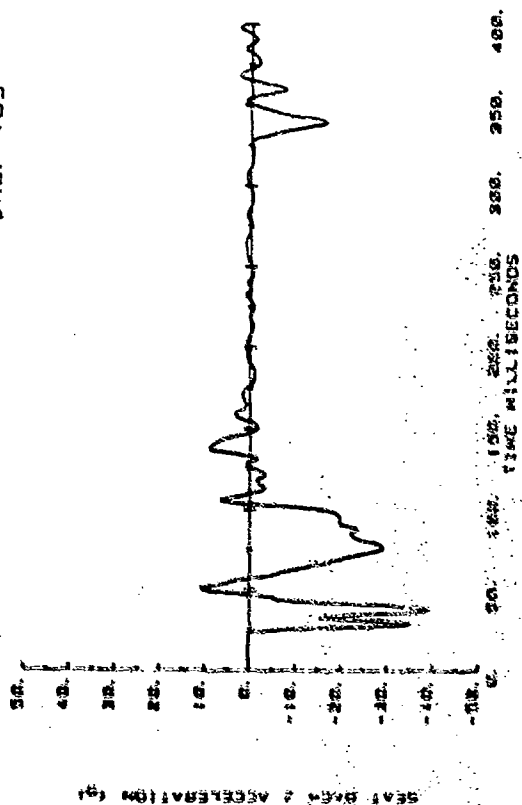
NRDC TEST 2
DROP 183



NRDC TEST 2
DROP 189

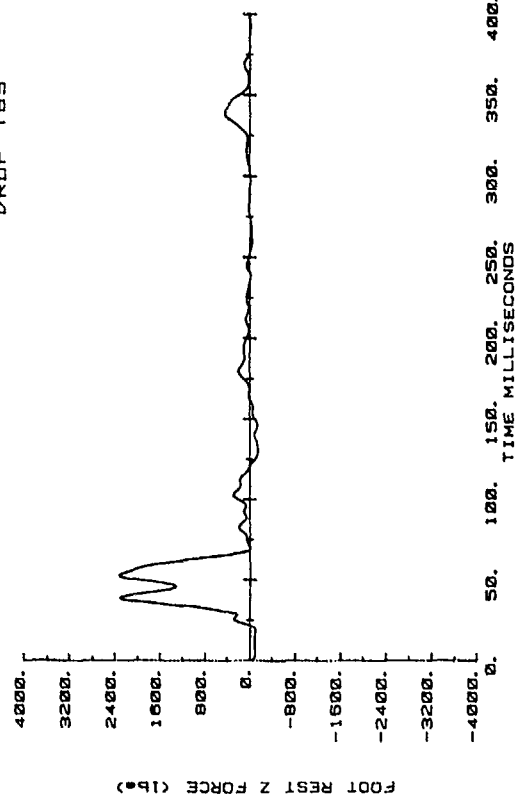


NRDC TEST 2
DROP 189

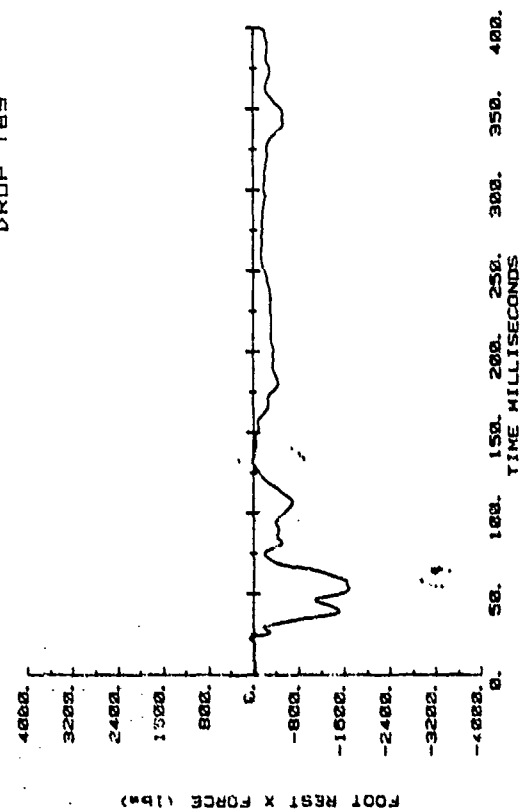


SEAT PAN and SEAT BACK Acceleration

NADC TEST 2
DROP 189

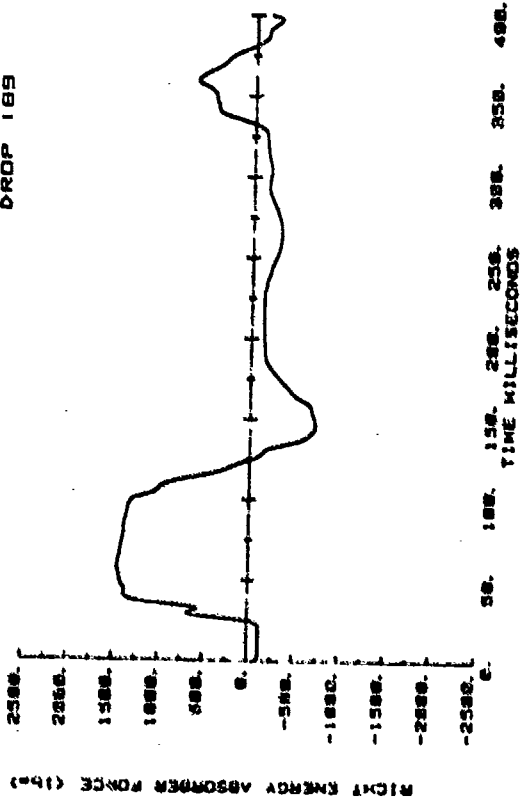


NADC TEST 2
DROP 189

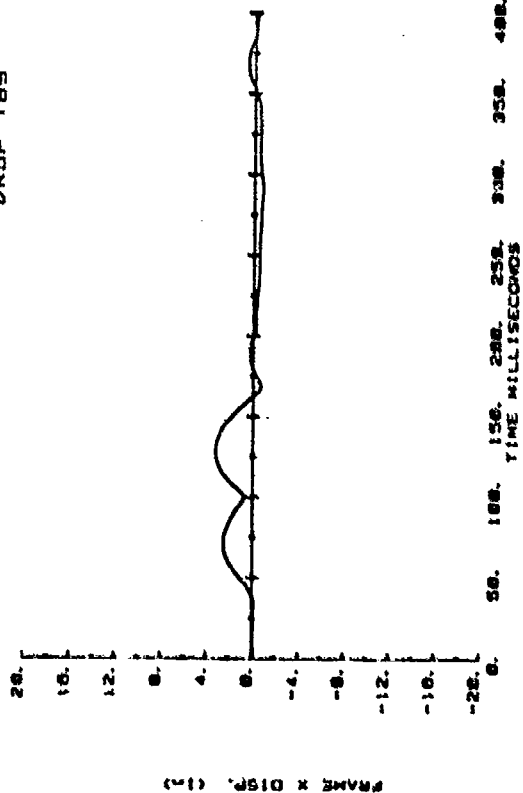


Footrest Force

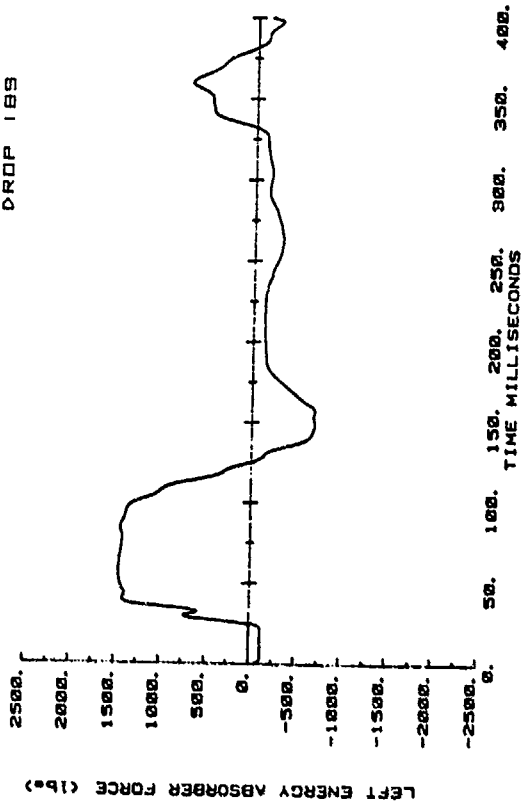
NADC TEST 2
DROP 189



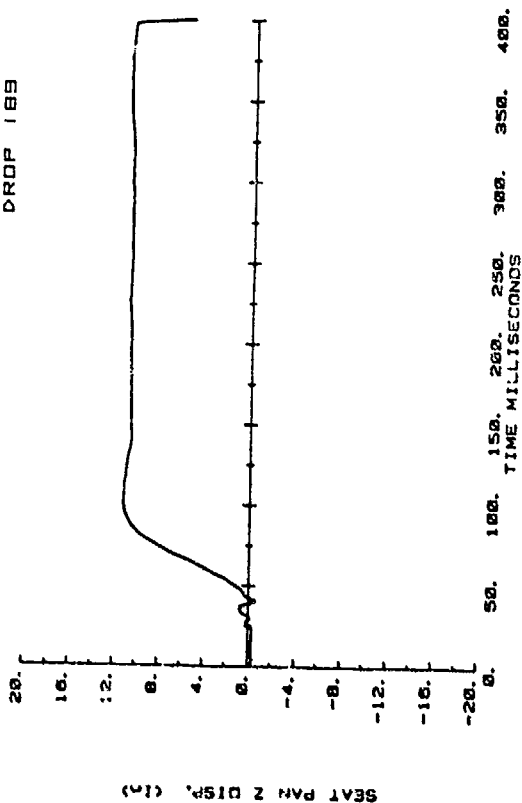
NADC TEST 2
DROP 189



NADC TEST 2
DROP 189

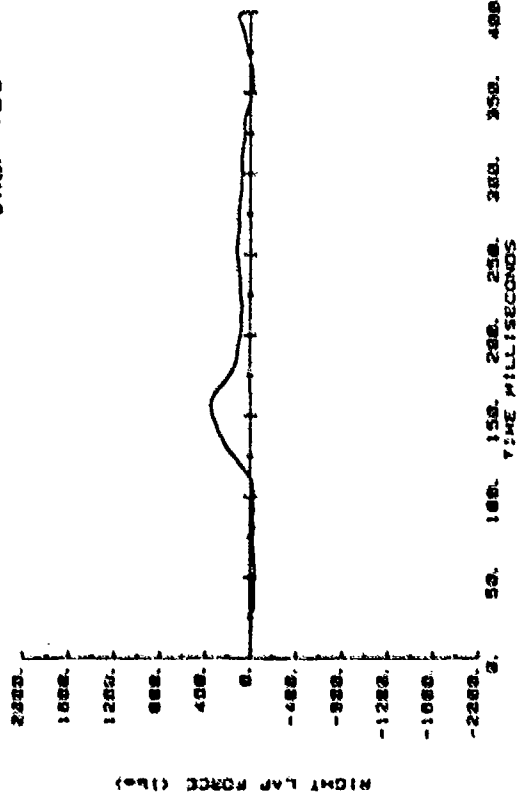


NADC TEST 2
DROP 189

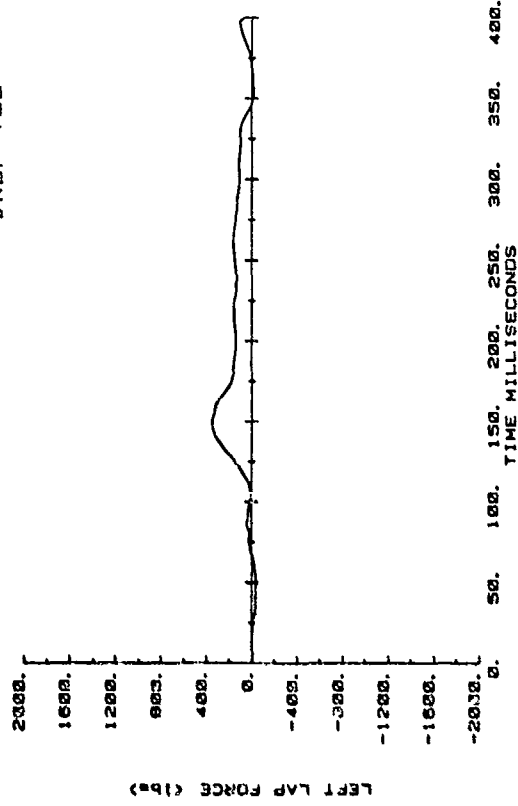


Energy Absorber Force and Seat Displacement

NRDC TEST 2
DROP 189

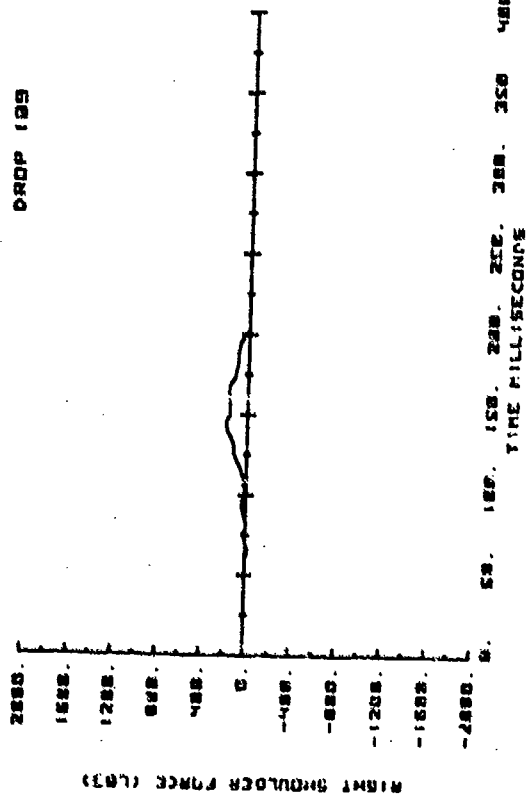


NRDC TEST 2
DROP 189

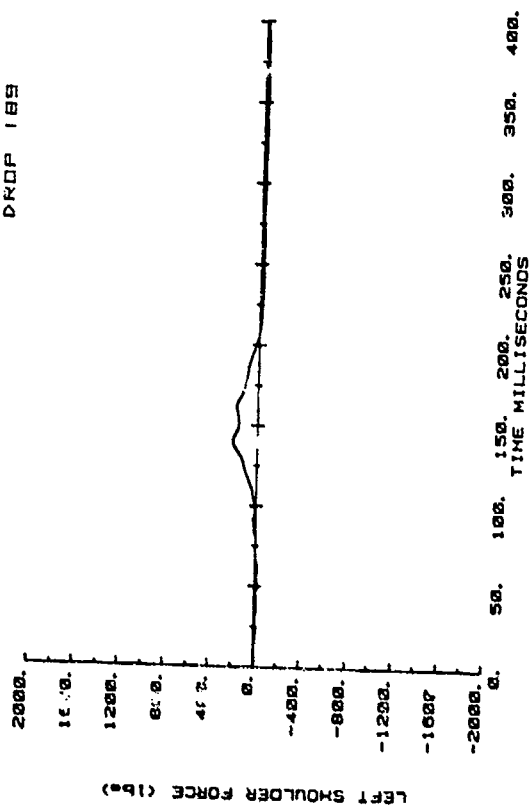


Lap Belt Force

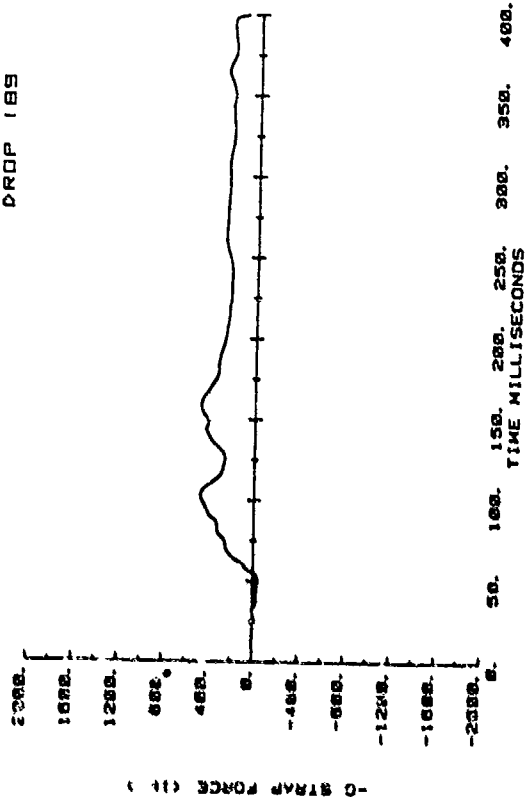
NRDC TEST 2
DROP 189



NRDC TEST 2
DROP 189

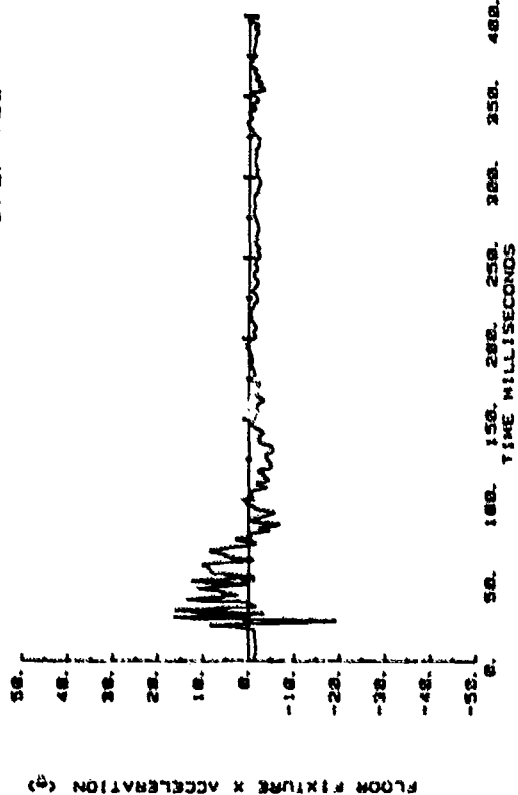


NRDC TEST 2
DROP 189

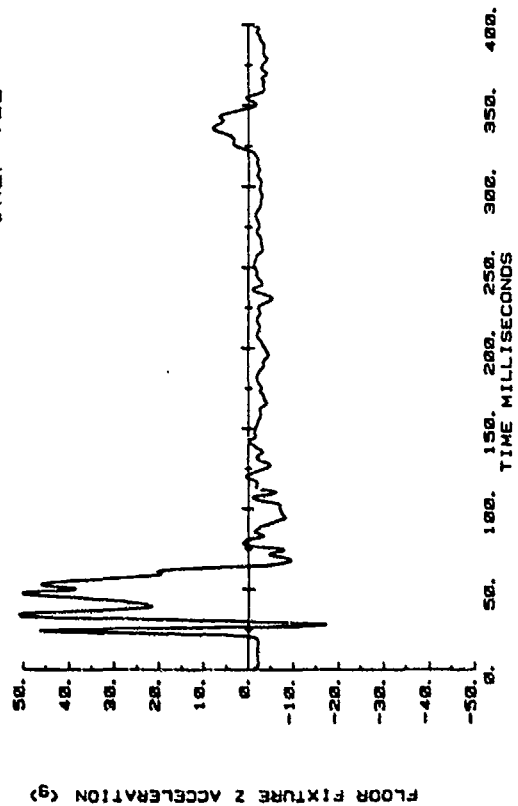


Shoulder Belt and -G Strap Force

NRDC TEST 2
DROP 189



NRDC TEST 2
DROP 189



Floor Acceleration

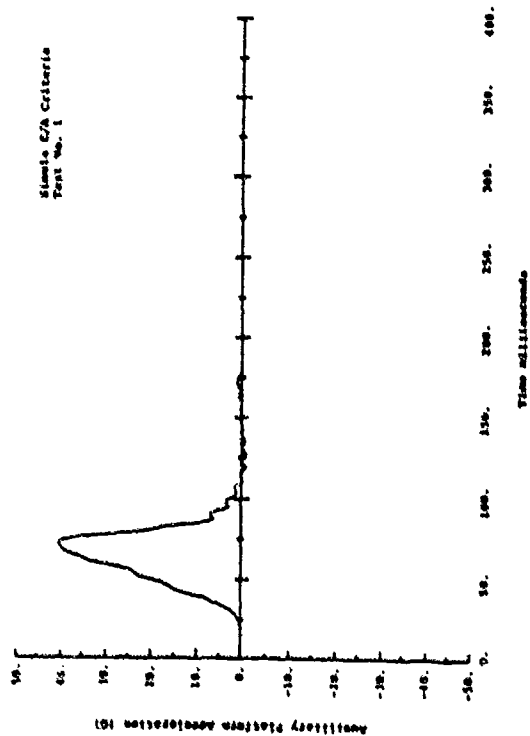
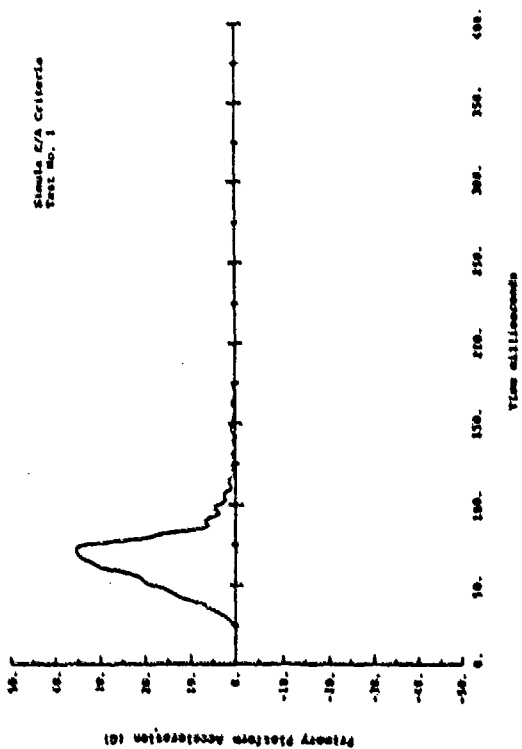
APPENDIX E

SIMULA BASELINE TEST SEAC-1

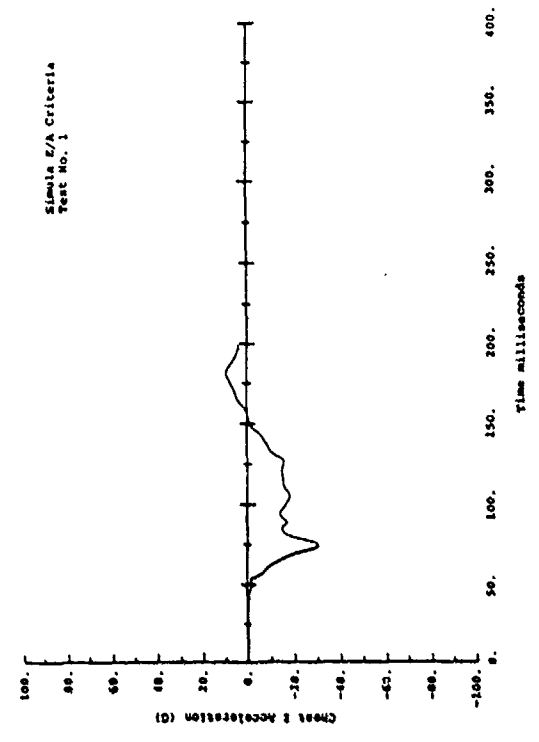
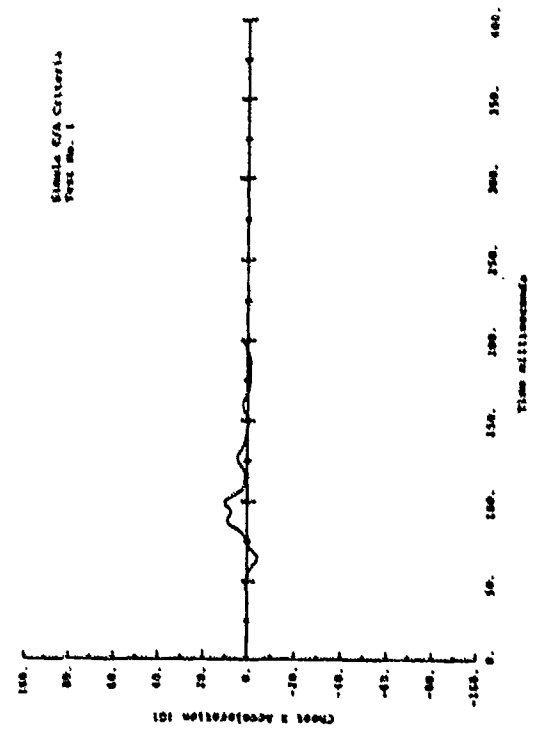
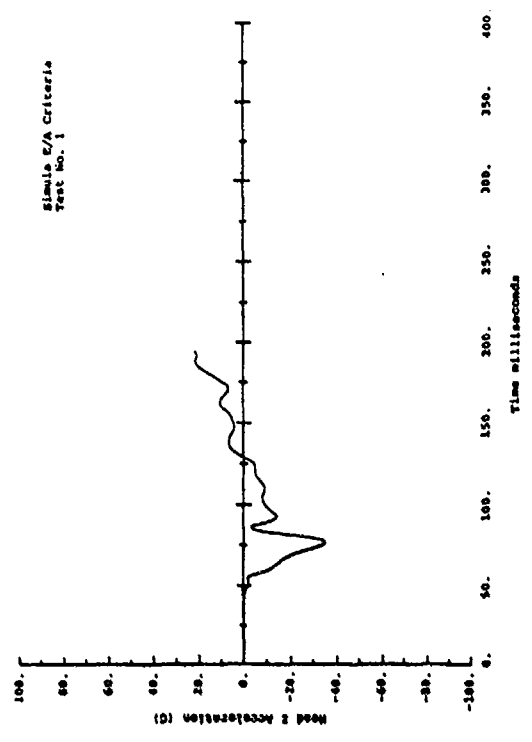
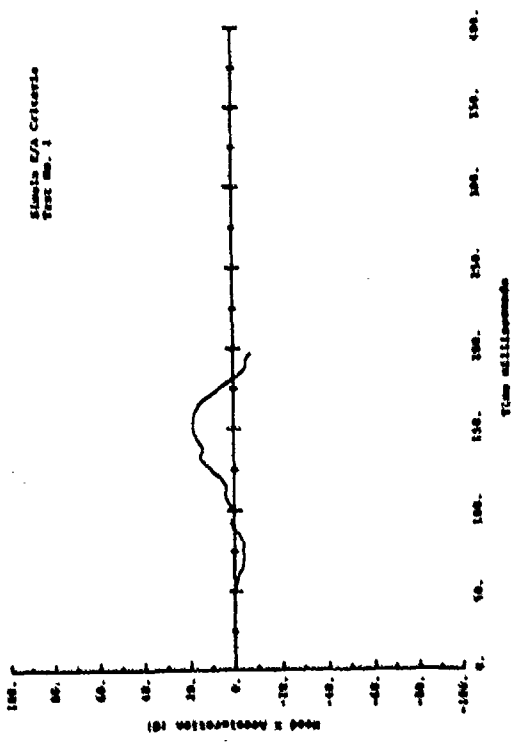
Energy-Absorbing Seat
50th-Percentile Dummy

$$\Delta v = 38.8 \text{ ft/sec}$$

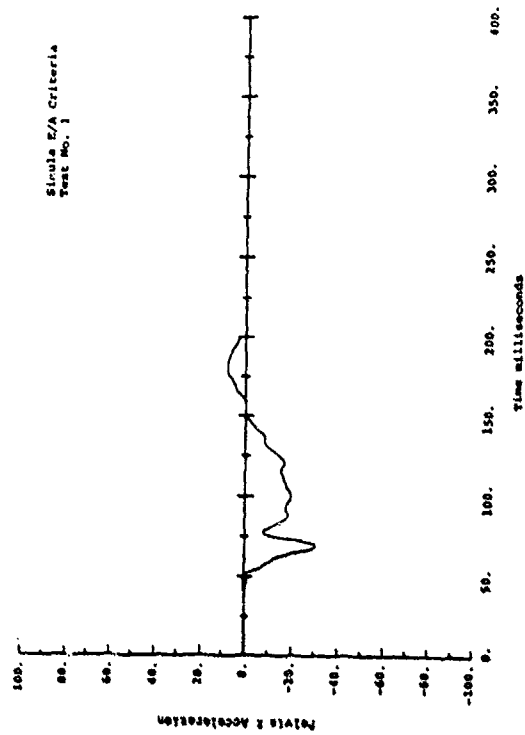
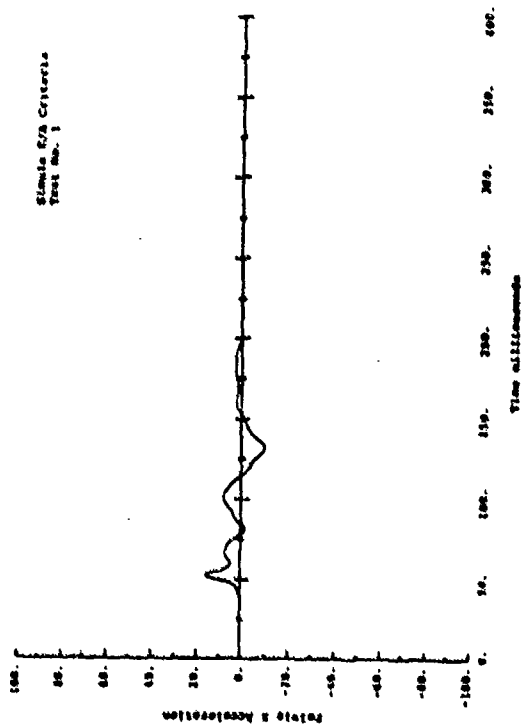
$$G_{\text{peak}} = 39.8$$



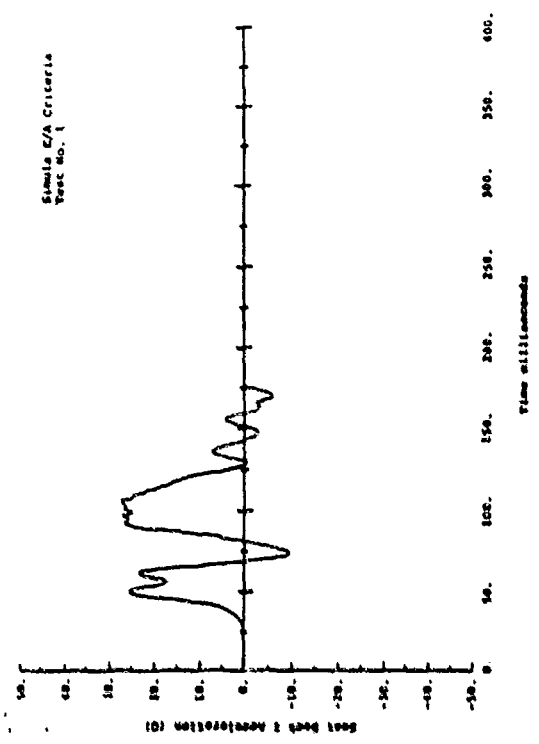
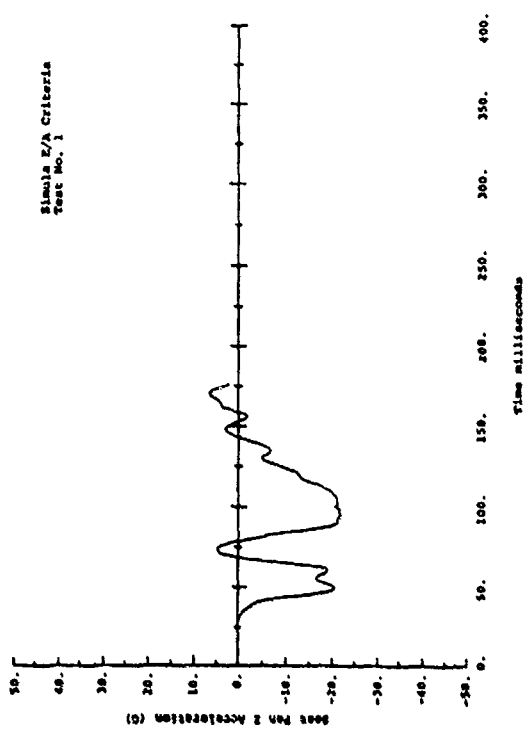
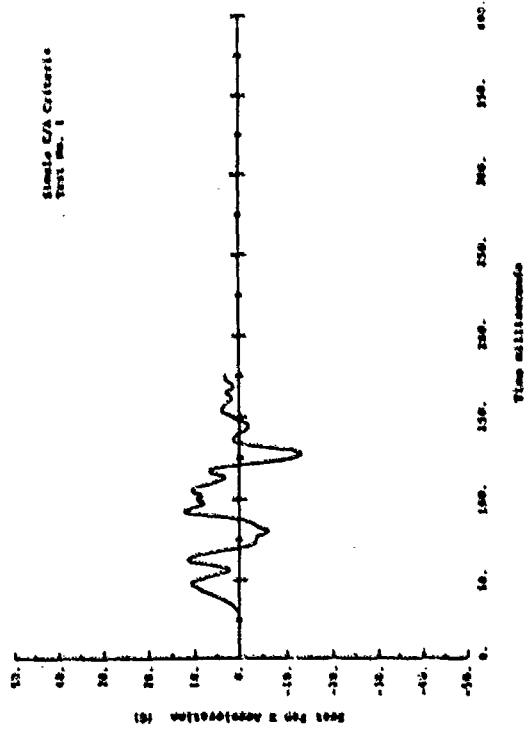
Platform Acceleration



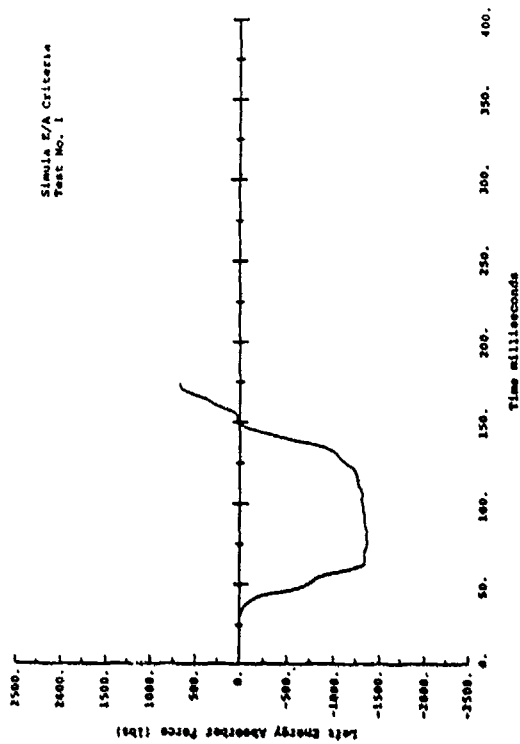
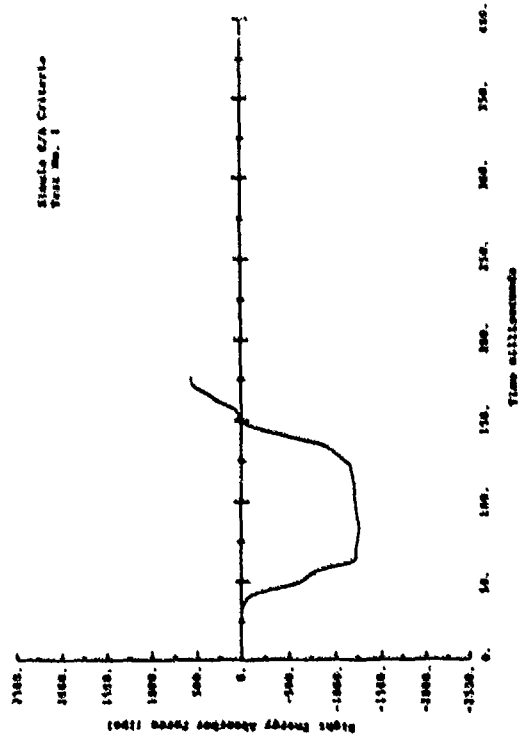
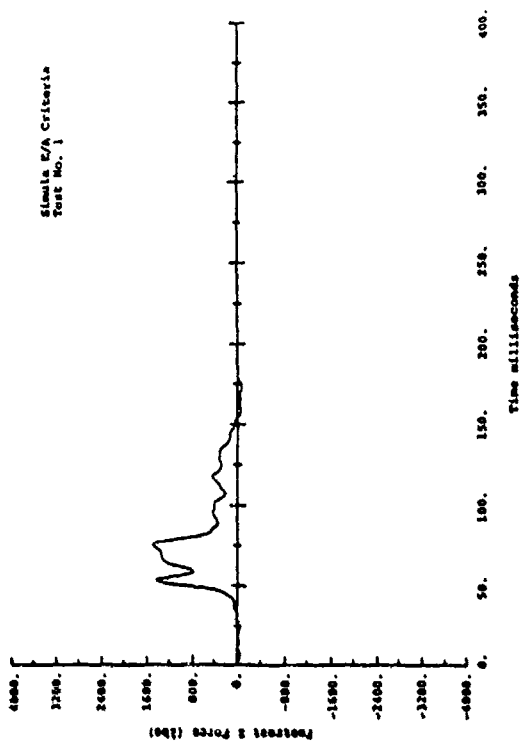
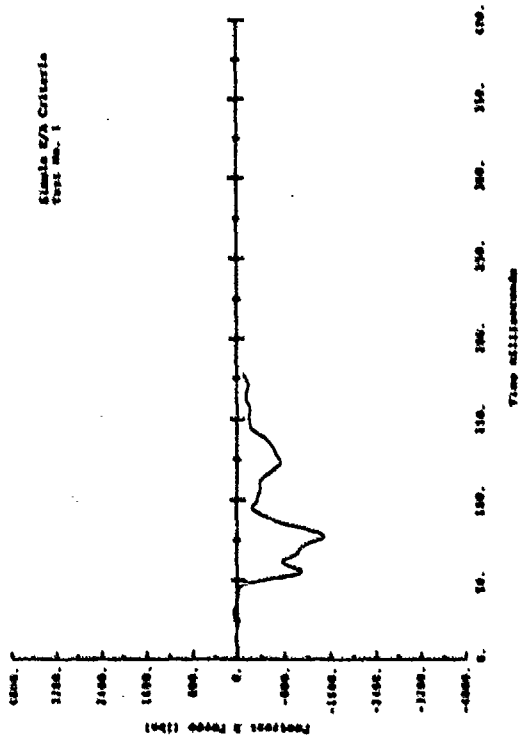
Head and Chest Acceleration



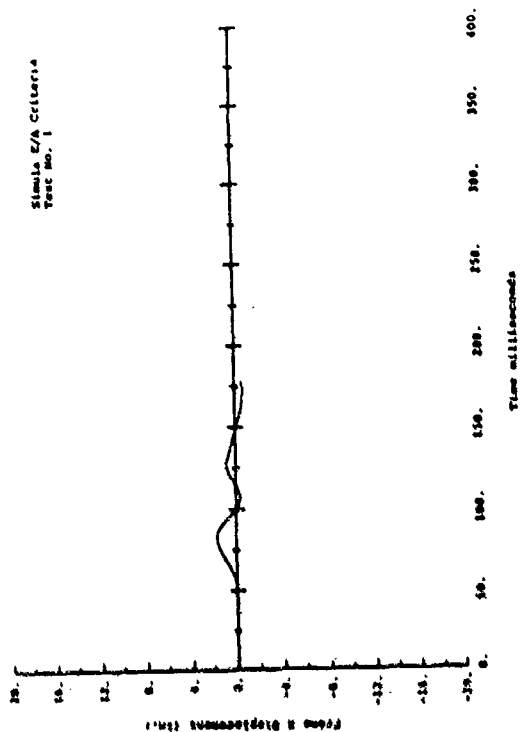
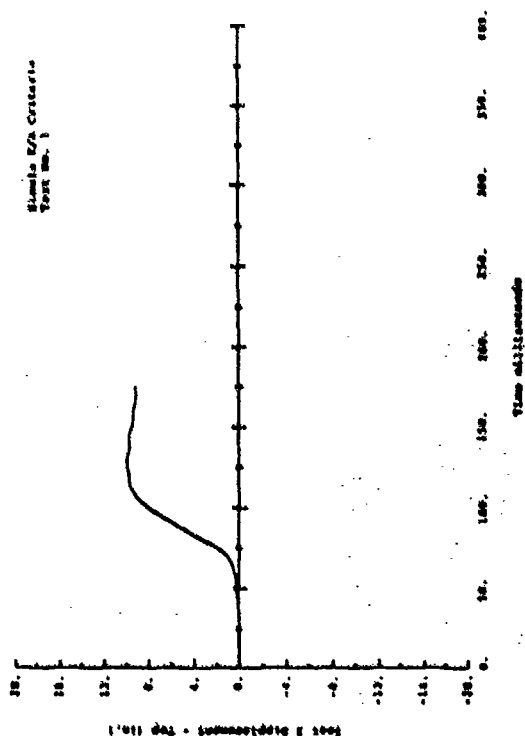
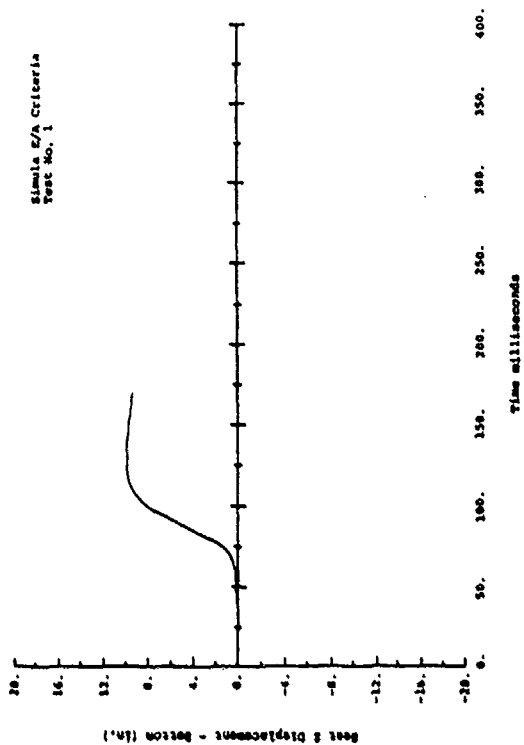
Pelvis Acceleration



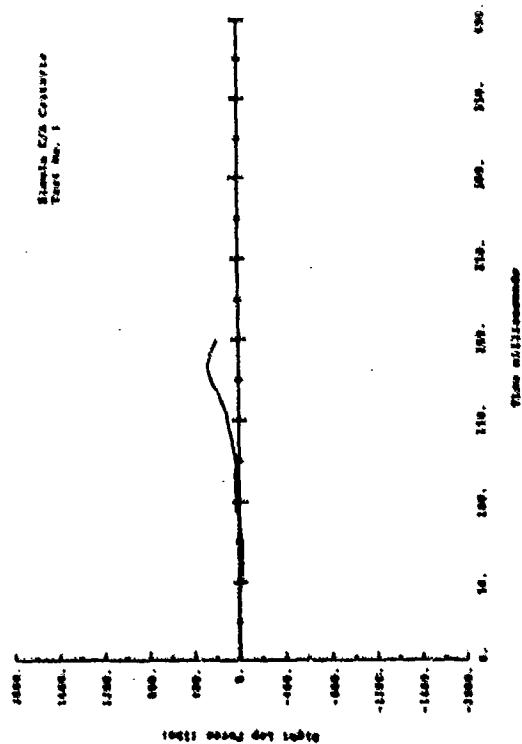
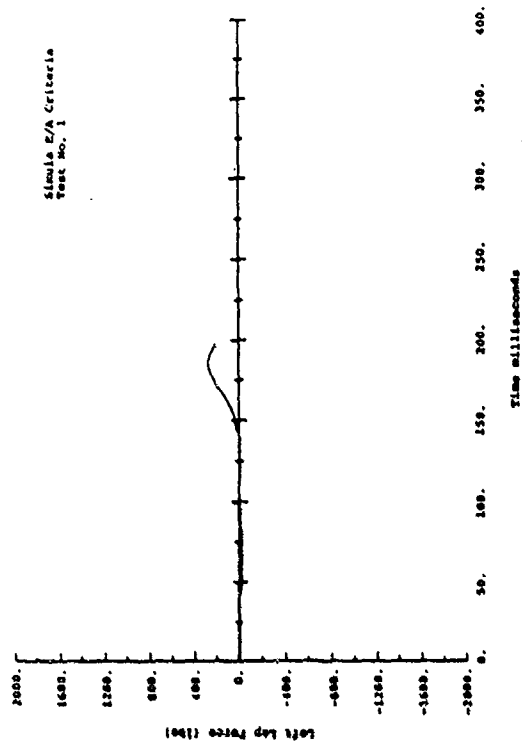
Seat Pan and Seat Back Acceleration



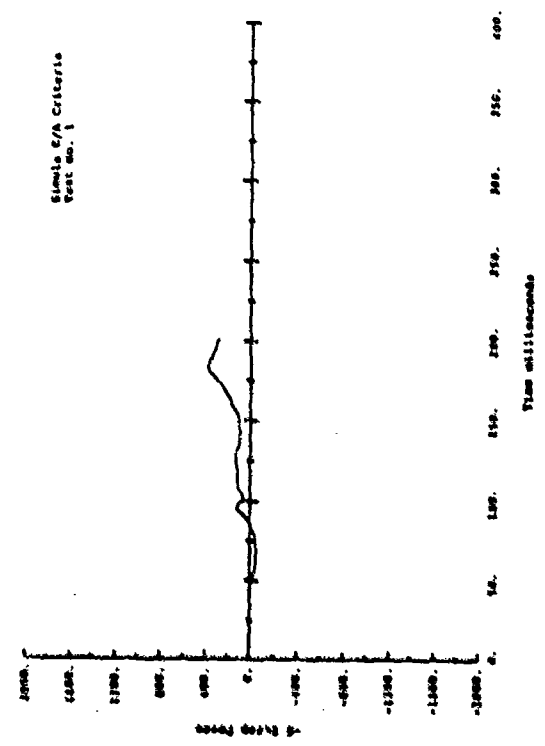
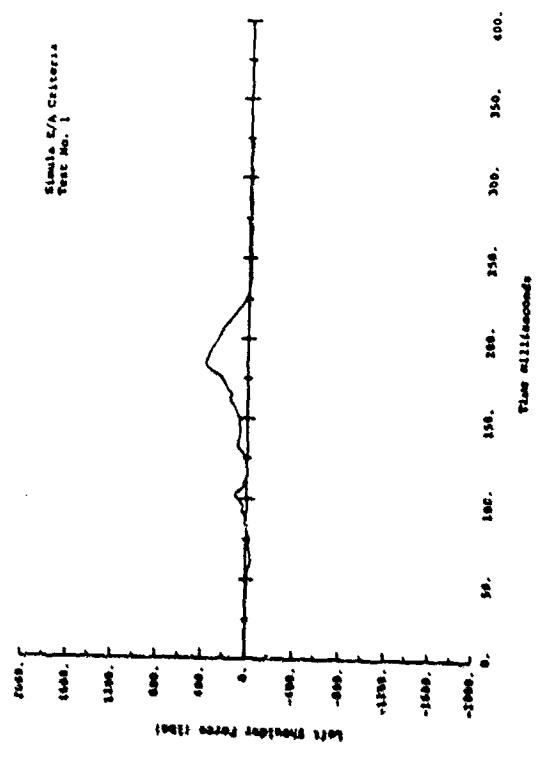
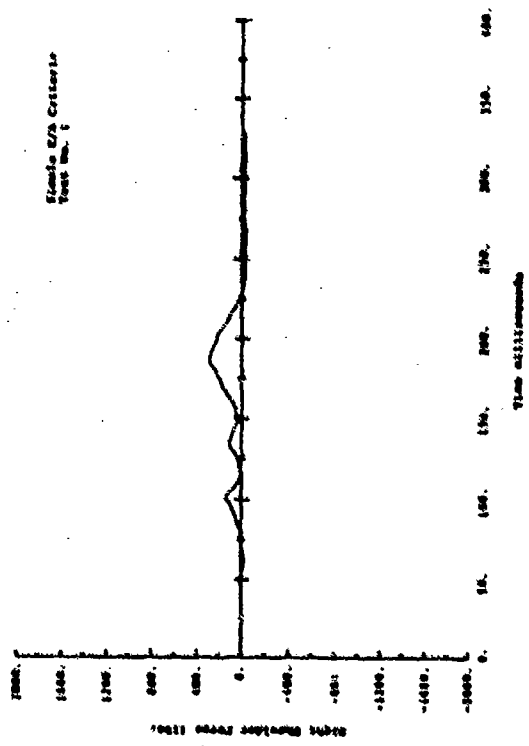
Footrest Force and Energy Absorber Force



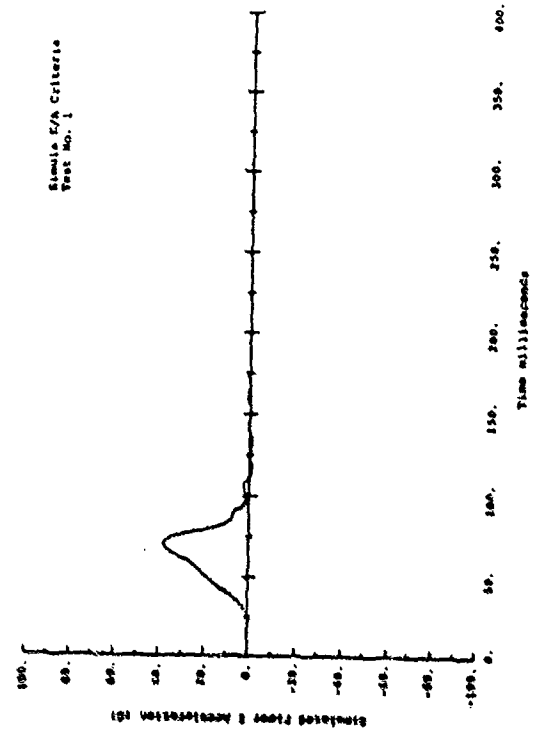
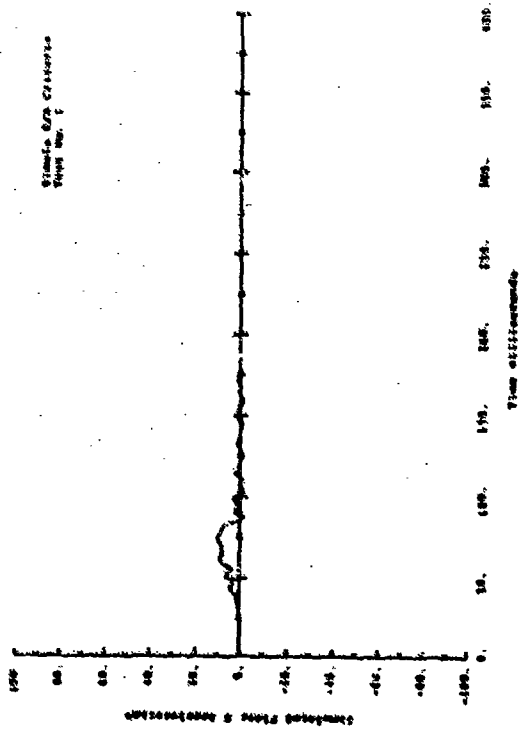
Frame Displacement and Seat Stroke



Lap Belt Force



Shoulder Belt and -G Strap Force



Floor Acceleration

APPENDIX F

WAYNE STATE UNIVERSITY TEST 159

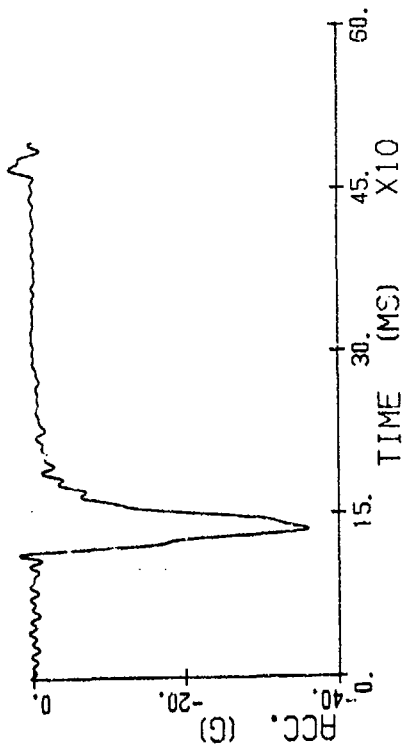
Energy-Absorbing Seat
50th-Percentile Dummy
(modified for spinal load measurement)

$$\Delta v = 41.1 \text{ ft/sec}$$

$$G_{\text{peak}} = 35.7$$

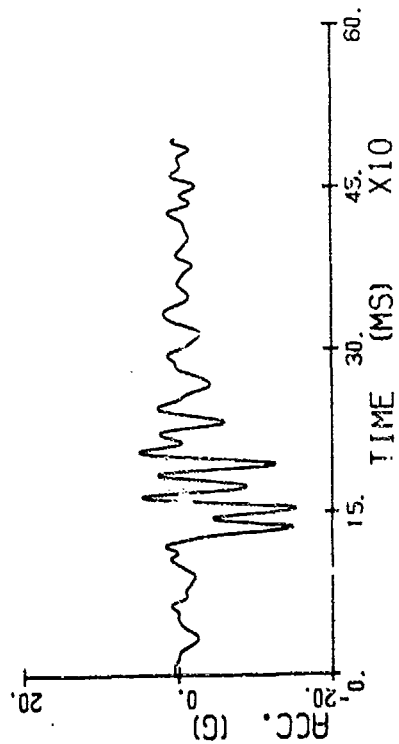
SLED

SIMULR 04.1



SEAT X

SIMULR 04.1



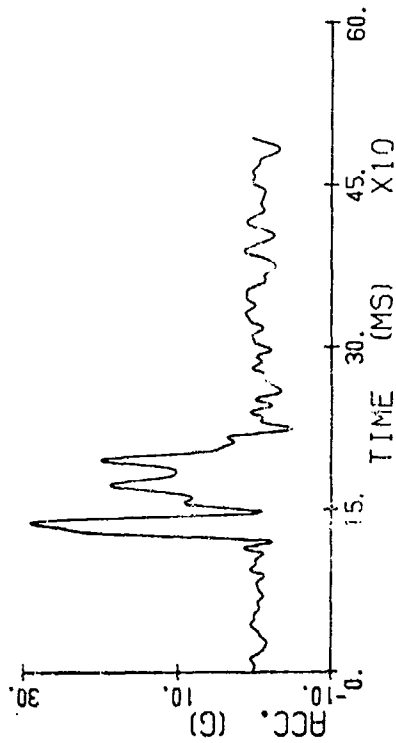
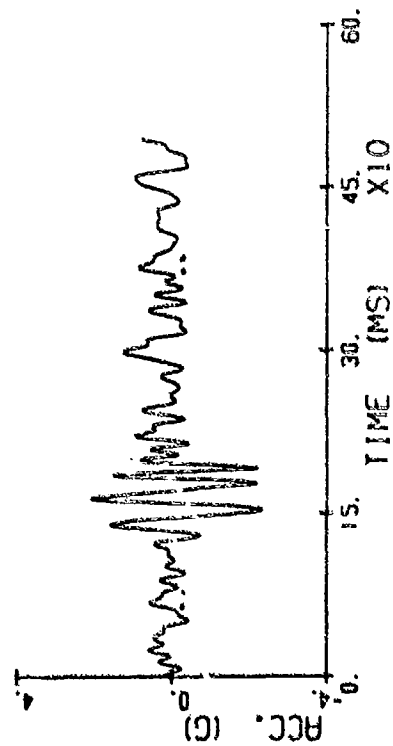
Sled and Seat Pan Accelerations

SIMULA 04.1

SERT Y

SIMULA 04.1

SERT Z



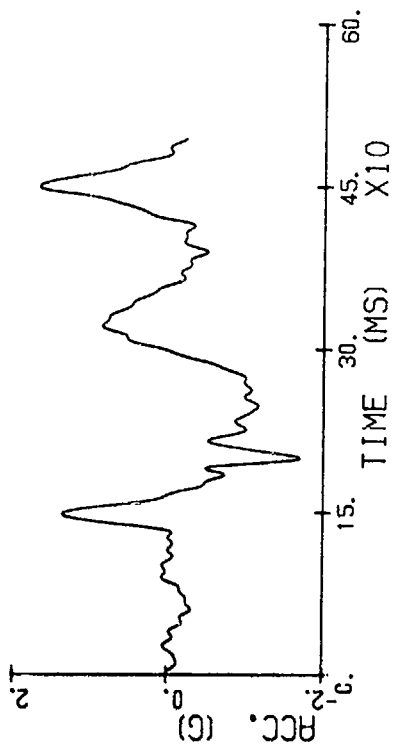
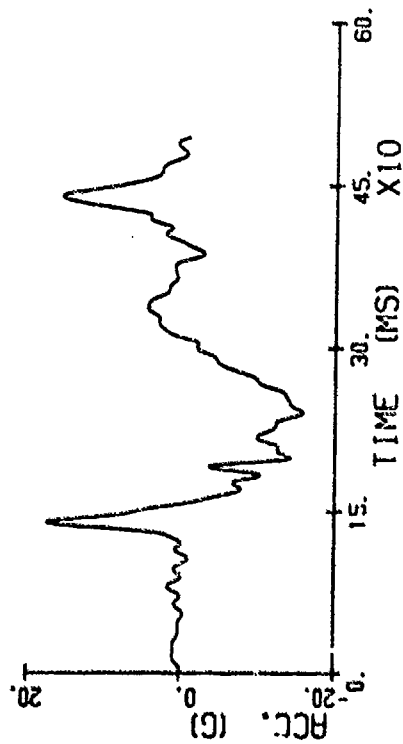
Sled and Seat Pan Accelerations (continued)

SIMULA 05. 2

HEAD X

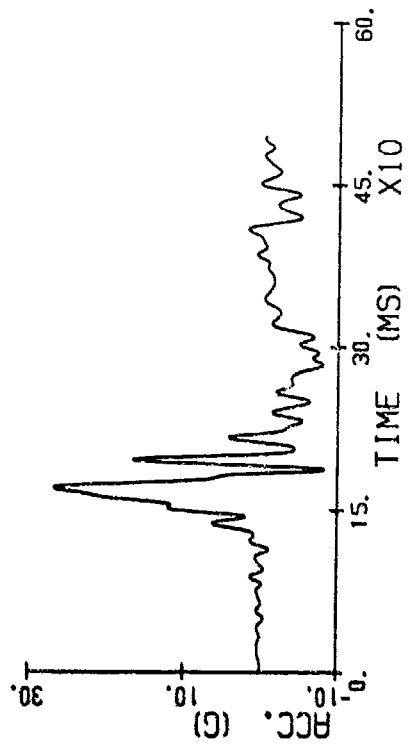
SIMULA 05. 2

HEAD Y



SIMULA 05. 2

HEAD Z



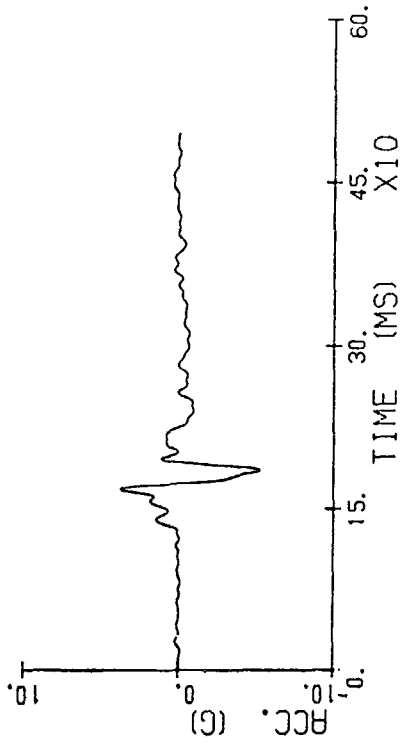
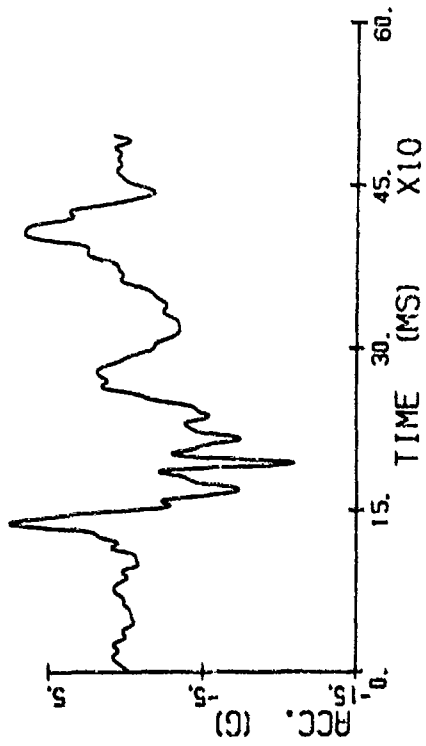
Head Acceleration

SIMULR: 05. 2

CHEST X

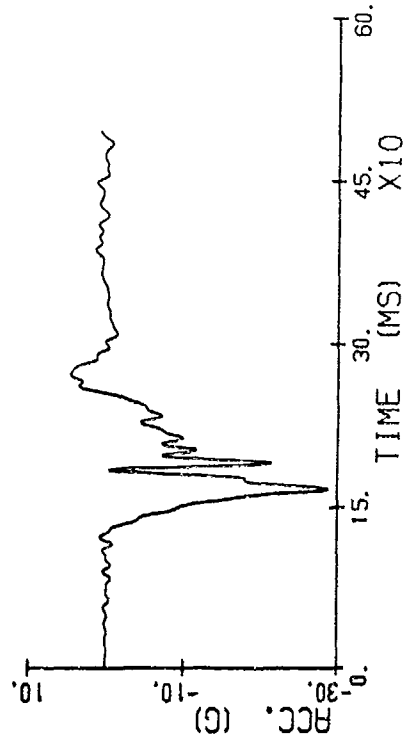
SIMULR: 05. 2

CHEST Y



SIMULR: 05. 2

CHEST Z



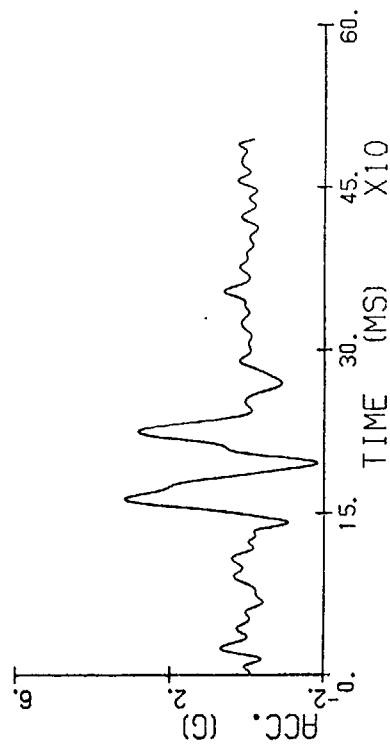
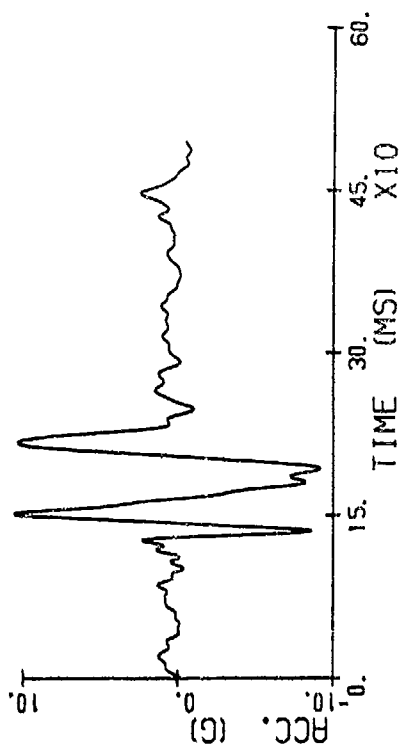
Chest Acceleration

SIMULA: 05. 2

PELVIC X

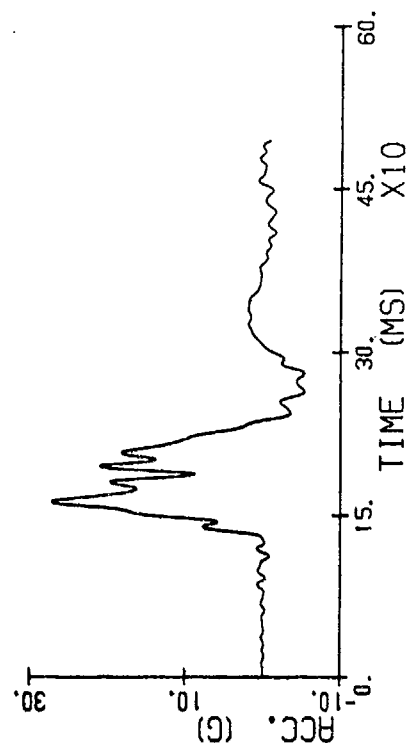
SIMULA: 05. 2

PELVIC Y



SIMULA: 05. 2

PELVIC Z

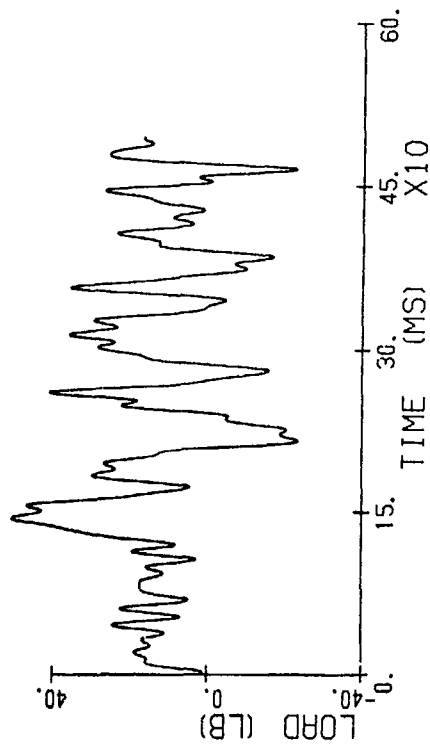
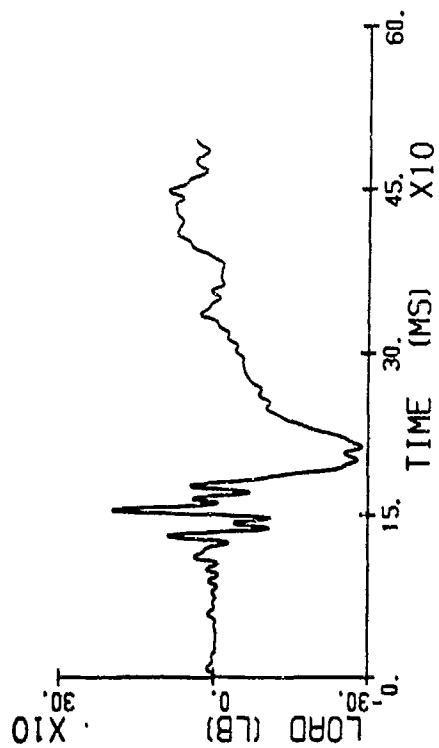


Pelvis Acceleration

SPINE X

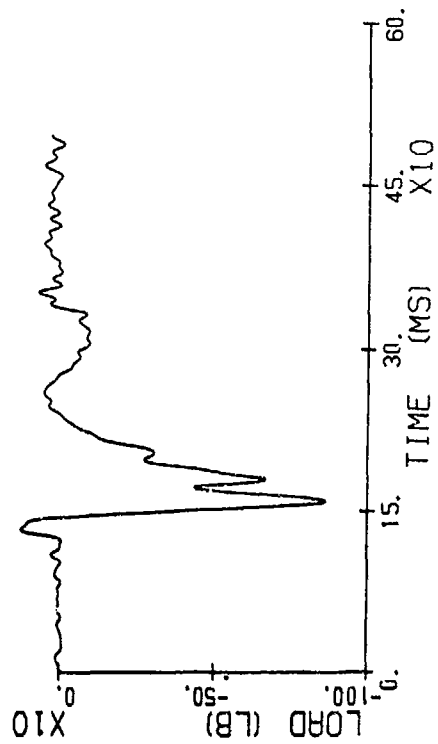
SIMULR 04.1

SPINE Y



SPINE Z

SIMULR 04.1



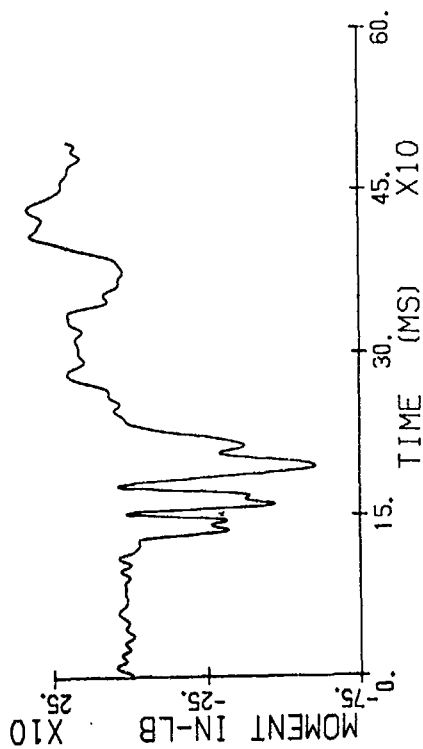
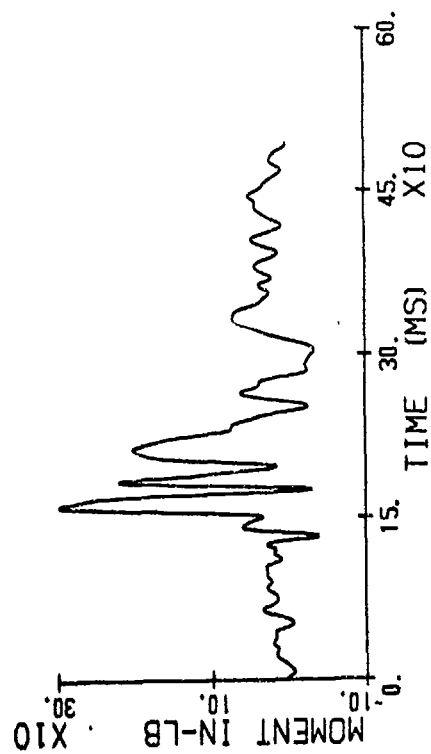
Lumbar Force

SPINE X

SIMULR: 04.1

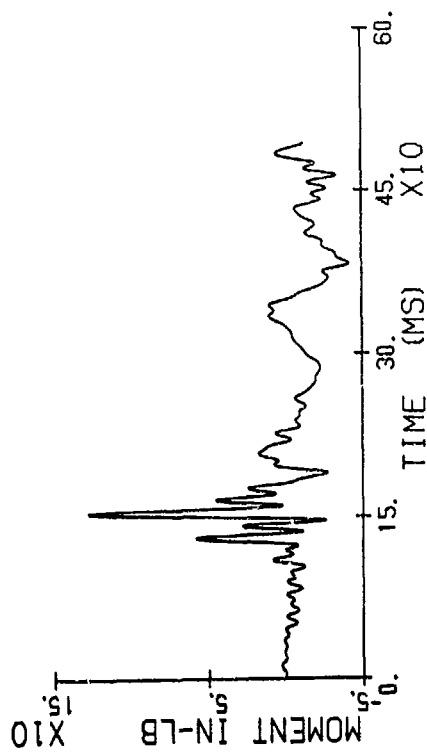
SPINE Y

SIMULR: 04.1



SIMULR: 04.1

SPINE Z

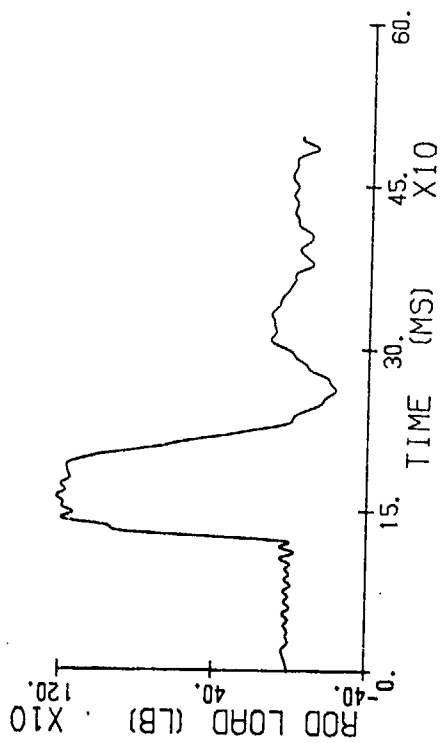
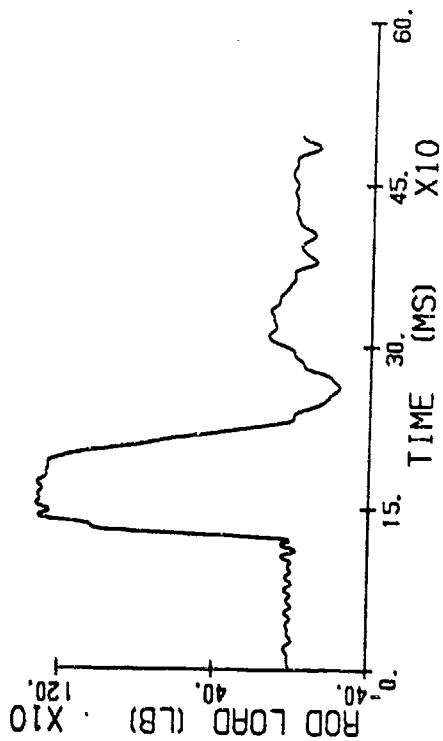


Lumbar Moment

SIMULA: 04.4

RT. END

LT. END



SIMULA: 04.4

FRONT

REAR



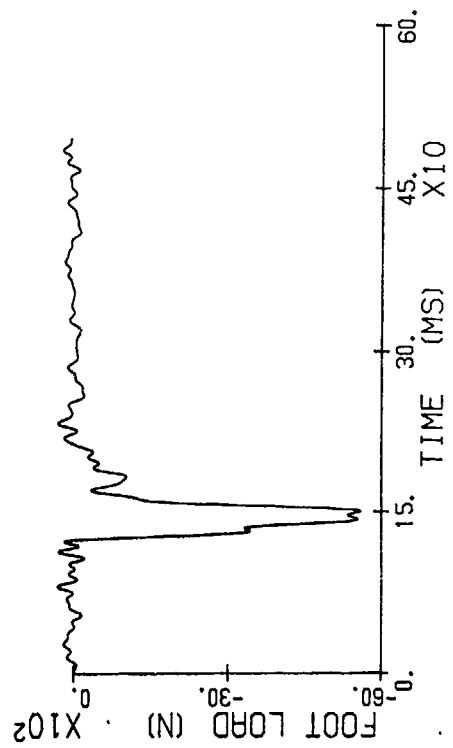
SIMULA: 04.4



Energy Absorber Force and Stroke

RIGHT Z

SIMULR: 04.3



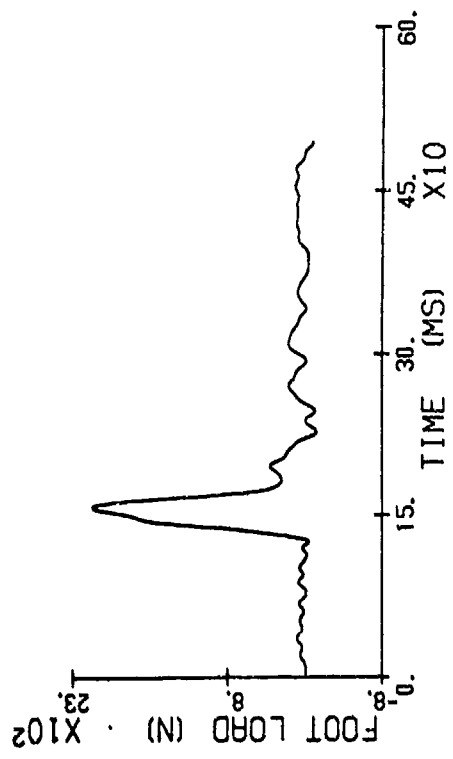
LEFT Z

SIMULR: 04.3



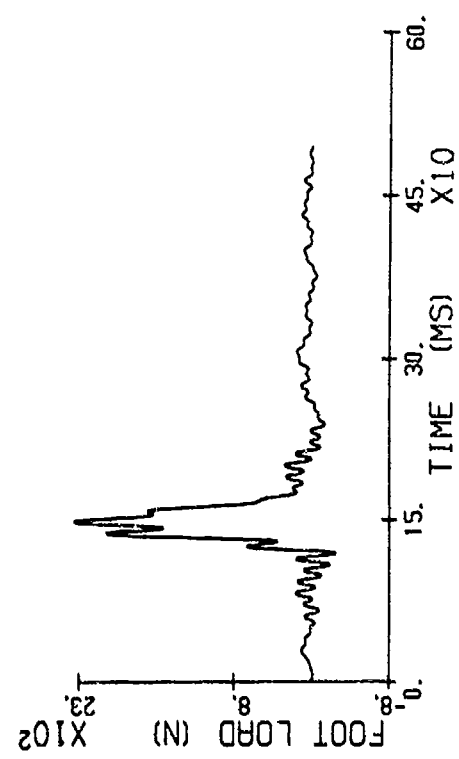
RIGHT X

SIMULR: 04.3



LEFT X

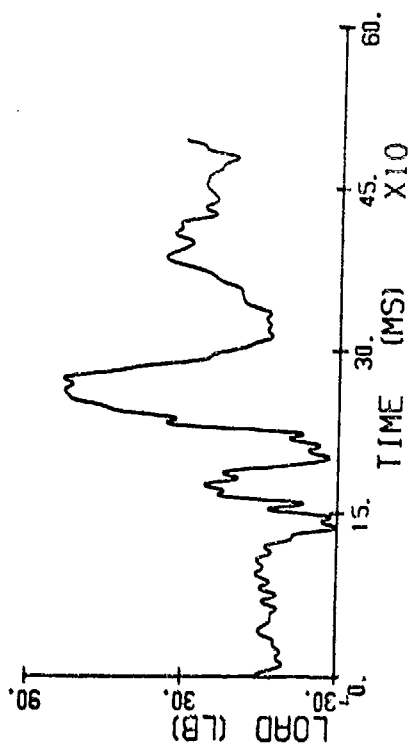
SIMULR: 04.3



Footrest Force

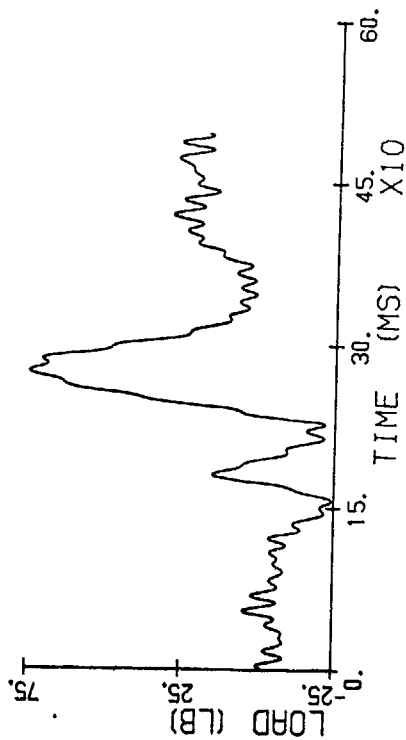
SIMULR: 04.3

RT LAP



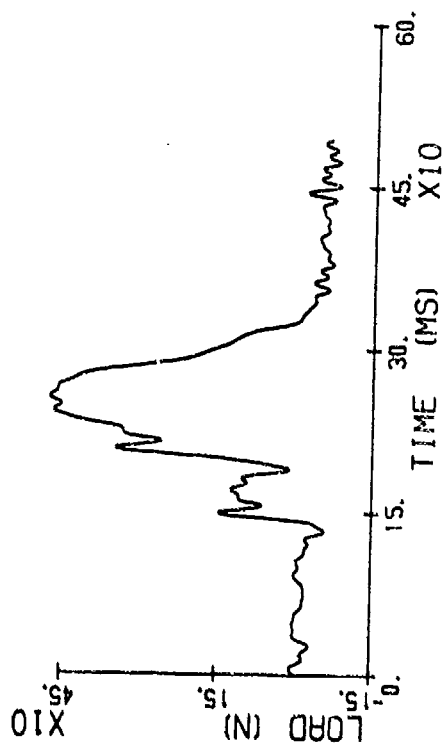
SIMULR: 04.3

LT LAP



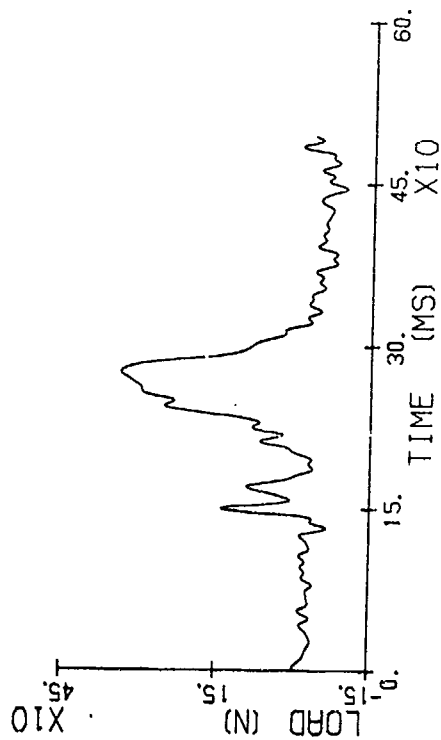
SIMULR: 04.3

RT SHLDR



SIMULR: 04.3

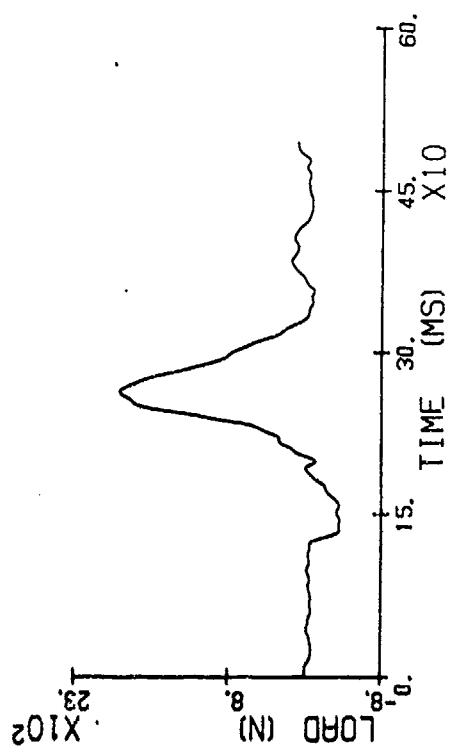
LT SHLDR



Lap and Shoulder Belt Forces

STIMUL: 04.3

TIE DOWN



Tiedown Strap